REPUBLIQUE DU CAMEROUN
Paix – Travail – Patrie
****
UNIVERSITE DE YAOUNDE I
FACULTE DES SCIENCES
DEPARTEMENT DE PHYSIQUE
****
CENTRE DE RECHERCHE ET DE FORMATION DOCTORALE EN SCIENCES, TECHNOLOGIES ET GEOSCIENCES
Laboratoire de Mécanique,Matériaux et Structures

REPUBLIC OF CAMEROUN
Peace – Work – Fatherland
****
UNIVERSITY OF YAOUNDE I
FACULTY OF SCIENCE
DEPARTMENT OF PHYSICS
****
POSTGRADUATE SCHOOL OF SCIENCES,TECHNOLOGY AND GEOSCIENCES
Laboratory of Mechanics, Materials and Structures

TRANSPORT PROPERTIES AND DIFFUSION OF BROWNIAN PARTICLES IN THE DEFORMABLE POTENTIAL

Thesis submitted in partial fulfillment of the requirements for the awardof the degree of Doctor of Philosophy (Ph.D.) in Physics

Par : **KEPNANG PEBEU Maxime Fabrice**
Master of Science in Physics

Sous la direction de
WOULACHE Rosalie Laure
Senior Lecturer
University of Yaounde I
KOFANE Timoléon Crépin
Professor
University of Yaounde I

Année Académique : 2020

UNIVERSITE DE YAOUNDE I
UNIVERSITY OF YAOUNDE I

FACULTE DES SCIENCES
FACULTY OF SCIENCE

DEPARTEMENT DE PHYSIQUE
DEPARTMENT OF PHYSICS

ATTESTATION DE CORRECTION DE LA THESE DE DOCTORAT/Ph.D

Nous, Professeur **DJUIDJE KENMOE Germaine** et Professeur **FEWO SERGE Ibraïd**, Examinateurs, et Professeur **WOAFO Paul**, Président du Jury de la Thèse de Doctorat/Ph.D de Monsieur **KEPNANG PEBEU Maxime Fabrice**, Matricule **10W1537**, préparée sous la direction du Docteur **WOULACHE Rosalie Laure** et sous la supervision du Professeur **KOFANE Timoléon Crépin,** intitulée : « **Transport properties and diffusion of Brownian particles in the deformable potential**», soutenue le **Lundi, 24 Aout 2020**, en vue de l'obtention du grade de Docteur/Ph.D en Physique, Spécialité **Mécanique fondamentale et systèmes complexes**, attestons que toutes les corrections demandées par le Jury de soutenance ont été effectuées.

En foi de quoi, la présente attestation lui est délivrée pour servir et valoir ce que de droit.

Fait à Yaoundé le 11 SEP 2020

Les Examinateurs | **Le Président du Jury**

Pr. DJUIDJE KENMOE Germaine

Pr. FEWO Serge Ibraïd

Pr. WOAFO PAUL

Le Chef de Département de Physique

UNIVERSITE DE YAOUNDE I
FACULTE DES SCIENCES
Le Chef de Département
DEPARTEMENT DE PHYSIQUE

Ndjaka Jean-Marie
Bienvenu
Professeur

University of Yaoundé I

Faculty of Sciences

Department of Physics

Transport properties and diffusion of Brownian particles in the deformable potential

Submitted and defended in Fulfillment of the Requirements for the Degree of Doctor of Philosophy/PhD in Physics
Option: Fundamental Mechanics and Complex Systems

By

KEPNANG PEBEU Maxime Fabrice
Registration number: 10W1537
Master in Physics

Director
Dr. WOULACHE Rosalie Laure
Senior Lecturer, University of Yaoundé I (Cameroon)

Supervisor
Prof. KOFANE Timoleon Crepin
Professor, University of Yaoundé I (Cameroon)

Laboratory of Mechanics, Materials and Structures

Dedications

✠ *To almighty God for all he has done for me.*

✠ *To my mother for his love and support.*

Acknowledgements

The accomplishment of this thesis would not be possible without the assistance and the help of numerous individuals and institutions.

★ First of all, I would like to express my deepest thankfulness to my supervisor, Professor **KOFANE Timoleon Crepin**, for giving me the opportunity to complete successfully this thesis. His expertise, his vast knowledge in both nonequilibrium physics and coherent structures and his unique scientific feeling considerably shaped my current interest and experience in theoretical physics.

★ A very special acknowledgment goes out to my director, Doctor **WOULACHE Rosalie Laure** for his guidance and help during the entire course of this work. His tremendous physical insight and unreserved willingness to share his understanding of physics with others have made this project very enjoyable and instructive. I owe her a debt of gratitude and respect.

★ I am very grateful to thank Professor **Hugo Touchette** of the Stellenbosch University, for his advices, orientations about the stochastic systems, also to have accepted to supervise me during my visit at the Stellenbosch University.

★ I gratefully thank Professor **TABI Bertrand Conrad** for his help during the preparation of different papers of this thesis.

★ I would like to acknowledge Professor **Jean-Marie Bienvenu NDJAKA**, the head of Department of Physics at the Faculty of Science at the University of Yaoundé I, for receiving me in his Department.

★ I would like to acknowledge the European commission through the "Pafroid" project, which gave me the opportunity to perform a part of this thesis at the Stellenbosch University.

★ I would like to thank the coordinators team of "Pafroid" project for being friendly, welcoming and having great patience with me and taking the time to explain things to me in an understandable way.

★ I am grateful to Professor **WOAFO Paul**, Chairman of the Cameroon Physical Society for his teaching specially in numerical methods.

★ I would like to thank the various members of the Jury who agreed to participate in this thesis defense. Professor **WOAFO Paul** who, despite his various occupations, has accepted to lead this Jury. I would like to thank Professor **YAMAPI Réné** from the University of Douala for having accepted to participate in this Jury as an examiner. I also thank Professor **DJUIDJE KENMOE Germaine** and Professor **FEWO Serge Ibraïd** who have accepted to play the role of examiners within this Jury. Finally, I would like to thank Professor **KOFANE Timoleon Crepin** and Doctor **WOULACHE Rosalie Laure** for having accepted, despite their occupations, to write the report of this thesis defense.

★ It would be very pleasing to recognize trade and constructive discussions combined with great moments of sharing with all the teachers of the Department of Physics in general and of the laboratory of Mechanics, Materials and Structures in particular. I have named Professor **ZEKENG Serge**, Professor **TCHAWOUA Clement**, Professor **DJUIDJE Germaine**, Professor **NANA NBENDJO Blaise Roméo**, Professor **FEWO Serge**, Professor **VONDOU Derbetini**.

★ Special thanks to **NDJOMATCHOUA Thomas Frank**, **DJOMO MBONG Thierry Landry Michel**, **GNINZANLONG Carlos**, **MOKEM FOKOU Igor Simplice**, **FOPOSSI MBEMMO André Marie**, **Cassidy BITANG A ZIEM**, **MUNDY Schatz**, **WADOP NGOUONGO Yannick Joel**, **ZANGA Dieudonné**, **Cedric TAKOUTSING**, **FOKOUENG WOUEMBE Francis**, and **DJOKO Martin** for the multitude exchanges and helps.

★ I express my eternal gratefulness to my parents, **PEBEU Christophe** and **KEJOUPIEU Helene**, without whose support and love throughout my entire life, I would not have started and finished this thesis. I also thank the permanent support provided by my dears aunt and uncle: **POUENI Aline**, **POUENI Simon**, **YOSSA Thaddée**.

★ I am feelingly grateful to members of my familly, for the crucial role they have played in my life through their love, patience and all the great moments that we have shared during this time.

★ Special thank goes to **TCHOKOKOUE Michael**, **POUENI Yolande**, **POUENI GAMO Gisele Grace**, **DJOMAGA Christian Wilfried**, and **PADJOUO NDOPNANG Boris**, for not only their moral and financial support, but also for all their prayers for me.

★ I cannot finish without thank the **International Center for Theoretical Physics** (ICTP), whose my participation to numerous schools over there has contributed to im-

prove my level in nonequilibrium physics and allowed me to feel comfortable when treating my subject.

• My sincere thanks go to the official editors and referees of **Physical Review E**, and **Physica A**, for their detailed review, constructive criticism and excellent advice during the preparation of my different publications.

Grants, fellowships and financial supports

1. August 2014: Laureate of the "Pafroid", project funded by the European Commission To perform a mobility Ph.D at the Stellenbosch University in South Africa.
2. 6^{th}-17^{th} July 2015: NIThePP Winter School on Computational Physics held at Stellenbosch University; Numerical Methods and Stochastic processes (Matlab).
3. 16^{th}-18^{th} September 2015: Short Course on Missing Data, Venue: Stellenbosch SACEMA.
4. 24^{th} April-20^{th} May 2016: Participation to the Spring College on the Physics of Complex Systems (courses and examination)
   Venue: ICTP (International Centre for Theoretical Physics), Trieste, Italy
   Subject: Conformal Field Theory, Machine Learning, Quantum of Non-Equilibrium Systems and Model Based-Inference in Epidemiological and ecological, statistical Mechanics of Cellular Motion
5. 19^{th} September-30^{th} September 2016: Ecole de Recherche CIMPA-CETIC 2016 "MODELISATION MATHEMATIQUE DANS LES SCIENCES DU VIVANT", ENSP YAOUNDE.
6. 08^{th} January-28^{th} January 2017: IBro-Simons "Computational Neuroscience" Muizenberg, Cape Town, South Africa (Presentation of project in Neuroscience)
   Subject: spiking neurons, networks and plasticity, dynamic systems, deep learning, unsupervised learning, multitaper spectral estimation, machine learning, statistical physics.
7. 31^{th} July-12^{th} August 2017: Hand-on Methods of Physics of Complex Systems, ICTP, Trieste, Italy (Oral-Presentation and Poster session)
   Subject: Molecular dynamic, computational fluid(Couette flow), chemical pattern, turbulence, diffusive wave, biology processes, Introduction to Matlab, Bacterial osmotic pressure.
8. 24^{th} June-16^{th} July 2018 July 2018: "African School of Fundamental Physics and Applications", University of Namibia-ICTP, Namibia (Oral-Presentation and Poster Session)

Subject: Particle Physics, Electronics, Astrophysics, Particle detector, Standard model, Cosmology, particle accelerator, gravitational waves

Contents

List of Figures

Abstract

In this thesis, we analyze the influence of the deformable potential on the dynamics of Brownian particles and the formation of localized modes in nonlinear deformable lattices.

Firstly, the directed transport in a one-dimensional overdamped, Brownian motor subjected to a travelling-wave potential with variable shape and exposed to an external bias is studied numerically. In the whole thesis, we focus our attention on the class of Remoissenet-Peyrard parametrized on-site potentials with slight modification, whose shape can be varied as a function of a parameter r, recovering the sine-Gordon shape as the special case. We demonstrate that in the presence of the travelling-wave potential the observed dynamical properties of the Brownian motor, which crucially depends on the travelling-wave speed, the intensity of the noise and the external load, respectively, is significantly influenced also by the geometry of the system. In particular, we notice that systems with broad wells and sharp barriers favour the transport under the influence of an applied load. The efficiency of the transport of Brownian motors in deformable systems remains equal to 1 (in the absence of an applied load) up to a critical value of the travelling wave speed greater than that of the pure sine-Gordon shape.

Secondly, using the Langevin-Monte-Carlo method, we show that the average velocity of Brownian particles is an increasing function of the shape parameter in the overdamped case, and a decreasing function of the shape parameter in the underdamped case. In the presence of the deformable travelling-wave potential, for negative as well as positive values of the shape parameter, the underdamped case favors the transport properties in the medium. The average velocity needed to cross the potential barriers is lowest in the underdamped case. Moreover, the effective diffusion coefficient in both cases exhibits peaks, and the diffusion process enhancement is discussed for some values of the shape parameter. The distribution of Brownian particles is also analyzed in the deformed system by using the Smoluchowski equation and the finite-element methods.

In the presence of an external load, the deformable potential tilts. Using the matrix continued fraction method, we compute the diffusion coefficient of Brownian particles via the dynamics factor structure at low temperature and intermediate values of friction coefficient. It is numerically found that the transport properties of Brownian particles such as the effective diffusion coefficient, the average velocity and the distri-

bution probability are sensitive to the shape parameter r of the modified nonsinusoidal Remoissenet-Peyrard deformable potential. The bistable behaviour and the distribution of velocity which also shed light on the diffusion anomalies are discussed for some values of the shape parameter. We show that for negative values of the shape parameter ($r < 0$), the average velocity versus the external tilting of Brownian particles is optimized, while for positive values ($r > 0$), the average velocity of Brownian particles collapses due to the geometry of the system combined with the friction. We find a power law for the effective diffusion coefficient in terms of the shape parameter r, and show that, it evolves as $D_{effmax} \sim r^2$.

Keywords: Brownian particles; Effective diffusion; Fokker-Planck equation; Travelling-wave deformable potential; external load; Matrix continued fraction method; Spectral method; Euler-Muyurama Method; Kasdin algorithm.

Résumé

Dans cette thèse, nous analysons l'influence du potentiel déformable sur la dynamique des particules Browniennes ainsi que la formation des modes localisés dans des réseaux déformables non linéaires.

Dans un premier temps, le transport dirigé des particules Browniennes, sur-amorties dans un potentiel déformable en mouvement et soumis à une action externe est étudié numériquement. Dans cette thèse, nous nous concentrons sur la classe des potentiels de site paramétrés et modifiés mis sur pieds au début des années 80 par Remoissenet et Peyrard, et dont la forme peut être modifiée en fonction d'un paramètre r, et prenant la forme du potentiel de sine-Gordon comme un cas particulier. Nous démontrons qu'en présence du potentiel déformable, les propriétés de transport des particules Browniennes, qui dépendent essentiellement de la vitesse du potentiel, de l'intensité du bruit et de la charge externe, sont également influencées de manière significative par la géométrie du système. En particulier, nous remarquons que les systèmes avec de larges puits et des barrières rétrécies favorisent le transport sous l'influence d'une action externe appliquée. Le rendement du transport des moteurs Browniens dans les systèmes déformables reste égale à 1 (en l'absence de toute action externe appliquée) jusqu'à une valeur critique de la vitesse du potentiel supérieure à celle de la forme sine-Gordon.

Deuxièmement, en utilisant la méthode de Langevin-Monte-Carlo, nous montrons que la vitesse moyenne des particules Browniennes est une fonction croissante du paramètre de déformabilité dans le cas sur-amorti et une fonction décroissante du paramètre de déformabilité dans le cas sous-amorti. En présence du potentiel déformable en mouvement, pour des valeurs négatives et positives du paramètre de déformabilité, le cas sous-amorti favorise les propriétés de transport dans le milieu. La vitesse moyenne des particules Browniennes nécessaire pour franchir les barrières de potentiel est plus faible dans le cas sous-amorti. En plus, le coefficient de diffusion effectif dans les deux cas présente des pics, et l'amélioration du processus de diffusion est discutée pour certaines valeurs du paramètre de déformabilité. La distribution des particules Browniennes est également analysée dans le système déformé en utilisant l'équation de Smoluchowski et la méthode des éléments finis.

En présence d'une charge externe, le potentiel déformable s'incline. Ainsi, en utilisant la méthode de decomposition en fraction de matrices continues, nous calculons le

coefficient de diffusion des particules Browniennes via le facteur dynamique de structure à basse température, et pour les valeurs intermédiaires du coefficient de frottement. Numériquement, les propriétés de transport des particules Browniennes telles que le coefficient de diffusion effectif, la vitesse moyenne et les distributions sont sensibles au paramètre de déformabilité r, du potentiel déformable. Le comportement bistable et les distributions de la vitesse instantanée qui prédisent également les anomalies de diffusion, sont discutés pour certaines valeurs du paramètre de déformabilité. Nous montrons que pour les valeurs négatives du paramètre de déformabilité ($r < 0$), la vitesse moyenne par rapport à la force externe appliquée aux particules Browniennes est optimisée, tandis que pour les valeurs positives ($r > 0$), la vitesse moyenne des particules Browniennes s'effondre en raison de la géométrie du système associée aux frottements. Nous trouvons en plus une loi de puissance pour le coefficient de diffusion effectif en fonction du paramètre de déformabilité r et montrons qu'il évolue selon la loi $D_{effmax} \sim r^2$.

Mots clés: Particules Browniennes; Diffusion effective; Equation de Fokker-Planck; Potentiels déformables en mouvement; Force externe; Méthode de la fraction continue matricielle; Méthode spectrale; Méthode de Euler-Muyurama; Algorithme de Kasdin.

General Introduction

Brownian motion is the seemingly random movement of a tracer particle suspended in a fluid. In fact, The phenomenon of Brownian motion was first observed by Jan Ingenhousz for coal dust particles on the surface of alcohol. However, Ingen-Housz provided a quite incorrect physical explanation of his observations by ascribing the effect to the evaporation of the suspension fluid. So, Brownian motion became more widely known only later on by the work of botanist Robert Brown in 1827, who reported vigorous irregular motion of small particles originating from pollen floating on water [1]. Puzzled by the phenomenon, he performed a number of further experiments, using different organic and inorganic objects, different surrounding fluids like water or alcohol and different microscopes, where he concluded that this kind of motion is caused by the bombardments by the small particles, which he calls "active molecules". His theory, however, has one weakness: He claimed that the motion of active molecules originates from the molecules themselves and not that it is caused by heat. Although Brown was not the first observer of this kind of motion, he was the pioneering experimentalist who made systematic investigations, trying to understand the origin of this random motion. His study showed that this kind of motion is universal and in particular not restricted to living matter. He turned the story of the neverending inanimate bodies dances in fluids from biology to a problem of physics. It is Albert Einstein who will come along later to give a plausible explanation of the Brownian motion through the molecular-kinetic description [2]. There, he states (freely translated from the German) "In this work, we show, by use of the kinetic theory of heat, that microscopic particles which are suspended in fluids undergo movements of such size that these can be easily detected with a microscope. It is possible that, these movements, to be investigated here, are identi-

cal with the so-called Brownian molecular motion; the information available to me on the latter, however, is so imprecise that I cannot make a judgement". Later, Jean Perrin made some breakthrough experimental results in 1908 and 1909 (published in Annales de Chimie et de Physique **18**, 1-114, (1909)). It was these results that finally convinced the general physics and chemistry community of the existence of atoms. Perrin said about Brownian motion, "Every particle situated in the liquid, instead of taking on, according to its density, a regular movement of falling or rising, is rather found animated by a completely irregular movement. It comes and goes, it stops, it starts again, it rises, it sinks, it rises again, without at all tending to immobility ... the odd phenomena discovered by Brown did not attract much attention. Rather, it was ignored for a long time by most physicists, and it can be supposed that those who had heard about it believed that it was analogous to the motion of dust motes that we see dancing in sunbeams under the action of weak air currents caused by slight differences in temperature." Nevertheless, the two founders of Brownian motion theory, Einstein and Smoluchowski [3], as well as their contemporaries, were also unaware of related, mathematical-statistical precursors of the phenomenon: Already in 1880, Thorvald Nicolai Thiele [4] proposed a model of Brownian motion while studying time series. Another important development is the work by the founder of modern Mathematical Finance, Louis Bachelier [5], who attempted to model the market noise of the Paris Bourse through a Gaussian process. Moreover, Lord Rayleigh [6] also did study a discrete, heavy random walker and performed a corresponding limiting procedure towards a heat equation which is augmented by a drift term for the statistical velocity.

Since then, the Brownian motion of particles in periodic structures have attracted the attention of many researchers due to their multidisciplinary applications and constitute an active field of research over recent years, being relevant for various applications in Condensed Matter Physics, Chemical Physics, Nanotechnology, and Molecular Biology [7-16]. Indeed, the subtle interplay of thermal noise, nonlinearity, asymmetry, and unbiased driving of either stochastic, or chaotic, or deterministic origin can indeed induce a rectification of the noise, resulting in directed motion of Brownian particles. So, in

biology, overdamped Brownian particles are molecular motors such as kinesins whose importance is known in living biological cells and which have led to a great number of theoretical and experimental works in recent years [17-21]. Particularly, many experimental studies such as modern microscopic techniques, have been performed recently in the domain of living cells and showed the emergence of the anomalous diffusion; the relevant behaviour in these works is that although the mean displacement of the tracking particle is not linear, but random, its resulting motion is directed ([19], and Refs therein). They moving along a periodic structure performing basic tasks in living organisms, and they do not necessarily need an external applied load to accomplish their task, that is, carrying a load across a viscous environment [22, 23]. Inspired by molecular motors in biology, Magnasco [24] and Prost et *al.* [15] proposed that such particle transport could be achieved with artificial Brownian motors (BMs) based on an asymmetric energy landscape and non-equilibrium fluctuations.

Similarly, Brownian particles have also been studied in detail in connection with superionic conductors, Josephson junctions, the dynamics of phase-locked loops [9,25-29]. The common feature of these latter cases is that they consist of species of high mobile particles considered to be Brownian particles moving on a periodic structure with diffusion coefficients comparable to those found in liquids [30-38]. In either case, Brownian particles are small machines that operate far from thermal equilibrium, using the thermal energy imbalance to perform mechanical work so as to generate the directed transport, with noise playing an important role in the process [39, 40]. Thus, the drift of particles is generated when conditions such as the presence of thermal noise, the anisotropy of the medium, and the time dependence are supplied by external variations of the constraints on the system [8, 41]. Moreover, the interactions of the Brownian particles with the surrounding bath may be considered statistically rather than treating each Brownian particle individually due to the fluctuating forces described only by their statistical properties [20,42-46].

In the present thesis, we study the transport properties and diffusion of Brownian particles in deformable potentials. The original study consists of two parts, in the first

part we investigate the transport properties of noninteracting Brownian particles in the overdamped limit, while in the second part the transport properties of Brownian particles are investigated in the underdamped limit.

Accordingly, to what is reported in the literature, it is clear that the deformability of sinusoidal potential can be a factor inducing deterministic chaos and instability in nonlinear systems [47, 48, 49, 50, 51, 52]. Thus, it was shown that the deformable potential can serve as a tool to integrate variable surface due to atomic friction force in nanotribology [53]. Moreover, Woafo et *al.* [54] used the deformable potential to explain the gaps existing in experimental measurements of mobility, the diffusion, and the Peierls-Nabarro barrier in the Frenkel-Kontorova lattice.

The thesis is structured in three parts described as follow:

In the first Chapter, we conducted a review of the scientific literature around the theme of this thesis. It presents the Brownian particles and their usefulness both in biology systems and in condensed matters physics. In Chapter 2, this thesis presents the approaches used to solve the problems mentioned in Chapter 1 and how they will be used in order to obtain the results. Among the techniques used, the Langevin equation is used to model the Brownian particles move along its track and the Fokker-Planck equation its equivalent, is used to describe the dynamics of the system. Indeed, the Fokker-Planck equation provides a powerful tool with which the effects of fluctuations close to transition points can be adequately treated and that the approaches based on the Fokker-Planck equation are superior to other approaches, e.g., based on Langevin equations. In the first part of the chapter, the dynamic properties of the overdamped Brownian particles are examined in the deformable travelling-wave potential. The Fokker-Planck equation is solved in order to compute the average velocity of Brownian particles which is perfectly sufficient to describe the dynamics of Brownian particles in a system as well as its transport properties. Meanwhile, the efficiency of Brownian particles to converting the energy introduced by perturbations into useful work [39,46-48] is computed analytically and numerically as a function of the shape parameter. In the second part of chapter, using the Langevin-Monte-Carlo method [55, 56], the dynamic proper-

ties of Brownian particles such as the average velocity, the diffusion, the distribution, and the Monte-Carlo Error are analyzed both in the underdamped and overdamped limits for several values of the shape of the system. Using the spectral method which is a semi-analytical method, the solution of the Fokker-Planck equation is approximated in the underdamped limit. Later on, the dynamic properties of Brownian particles is analyzed in presence of an external perturbation when they are submitted to a variable shape potential. The average and the distribution of the velocity is analyzed for some values of the shape parameter. It is found that, the transport properties of Brownian particles strongly depend on the form of the potential. Thus, using the matrix continued fraction method (MCFM), the diffusion of Brownian particle is derived as a function of the shape parameter. The Chapter 3 is devoted to the presentation of the key obtained results and their discussions. In fact, we show in this part that the shape of the system highly influences the performance of Brownian particles.

The document ends up by a general conclusion summarizing the main findings and provides the future directions.

CHAPTER I

LITERATURE REVIEW

I.1 Introduction

A great challenge for the burgeoning field of nanotechnology is to design and construction of microscopic motors that can use input energy to drive directed motion in the face of inescapable thermal and other noise. Driving such motion is what protein motors perfected over the course of millions of years by evolution do in every cell in our bodies [7,51-54]. Indeed, all materials at finite temperature store a substantial amount of energy in the form of kinetic energy of electrons, atoms or molecules. It is an old and tempting idea to convert this undirected, thermal motion (heat) into directed, useful motion (work) by rectifying the random motion of particles [57, 58].

In this Chapter, we present some generalities on Brownian particles and their applications in biology and technology. It is organized as follows: In Section II, molecular motors are presented with their modus operandi. In Section III, without being exhaustive, we describe some systems such as Josephson junction, superionic conductors that use the concept of Brownian particles in their modus operandi. The diffusion of Brownian particles as a mode of transport is briefly described in Section IV. Section V gives the motivation as well as the problematic of this thesis, whose eventual solutions are presented in the next Chapter. The Chapter ends with a conclusion.

I.2 Molecular motors

The tiny machines in a living cell that are responsible for transport processes other than pure diffusion are motors − molecular motors. Indeed, molecular motors are biological machine of only $0.01\mu m$ in size that for example, perform mechanical tasks such as in-

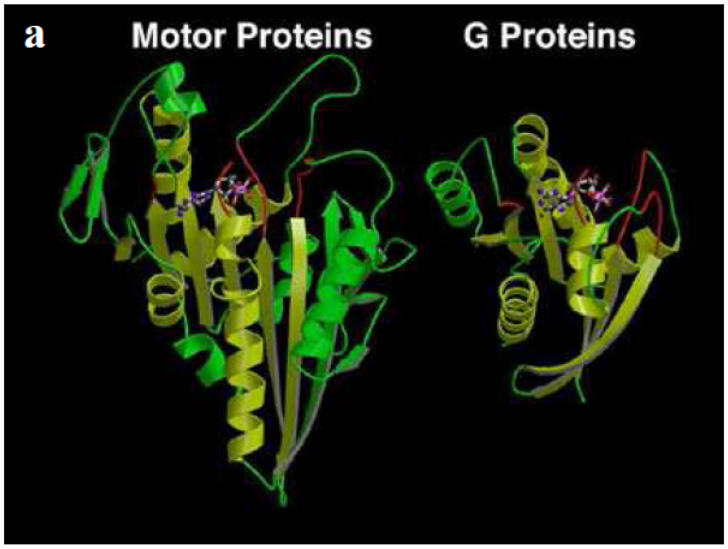

Figure 1: Image of two types of molecular motors [59].

tracellular transport, ion pumping, DNA replication and protein synthesis [59, 60, 61]. They can also generate a strength as well as play a role in cell mitosis. These are for example complex protein assemblies (protein engines, Figure 1-a) or enzymes. The driving force for a motor protein comes from a very important biochemical reaction, occurring inside the protein, called ATP hydrolysis: $ATP + H_2O \leftrightharpoons ADP + P_i$, where H_2O is water, ADP is adenosine diphosphate, and P_i is phosphate. These molecular engines are therefore capable to convert the chemical energy into mechanical work. Despite this similarity, molecular motors operate under conditions very different from artificial macroscopic motors. They operate in an noisy environment, where thermal fluctuations are significant and probably important for the operation of the particle. Indeed, because of frequent collisions with other surrounding molecules, protein engines are continuously subjected to substantial Brownian motion. This makes it impossible for a molecular engine to move forward in a deterministic and smooth manner, such as a car on the road. How Molecular Engines Treat Such a Noisy Environment? One model suggests that these engines use random Brownian motion to perform work [15, 62, 63, 64]. A physical model for how such a Brownian engine can work is the *ratchet*. Indeed, it is thought that some molecular motors in biological systems can use *ratchet* effects [65, 66].

For example, *ratchet flashing* has been proposed as a model for linear molecular motors, such as the *kinesin*, *Myosin* molecule transporters [63]. *Kinesin* is a protein molecule

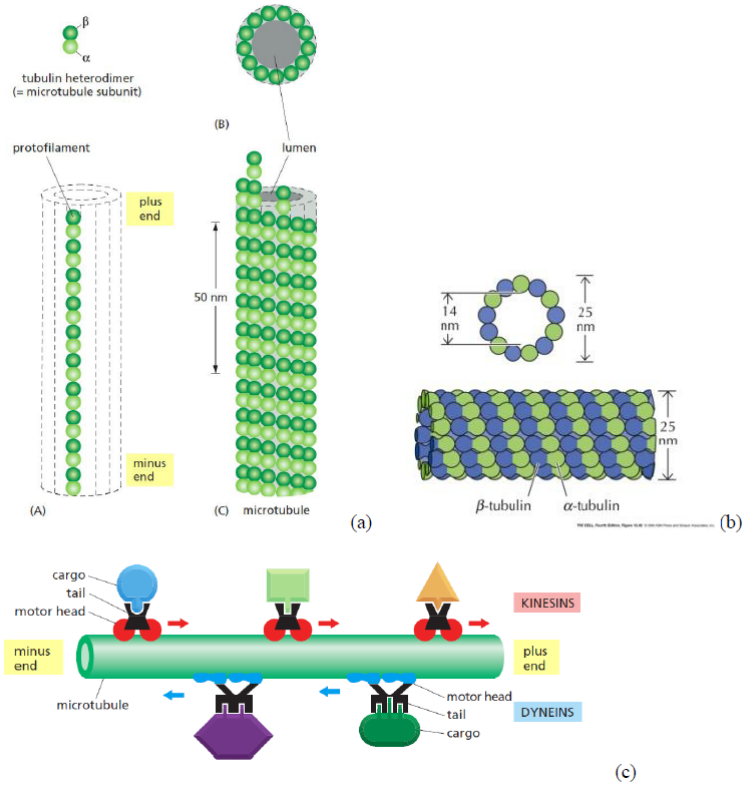

Figure 2: Representation of the structure of a Microtubules (MT). (a) Illustration of the hollow and cylindrical shape of a MT, (b) The size of a MT, (c) Illustration of a cellular organelles transport [67, 68].

that can "walk" along microtubules (Figure 2) [22, 23, 69, 70, 71] in living cells in the presence of an unbalanced concentration of ATP, and carries material (Figure 3). Single molecule *kinesin* takes 8 nm steps [14, 70] per ATP hydrolysis [71, 72] on a microtubule rail and generates $\simeq 7pN$ maximum force [72, 73, 74]. For example, the periodic polar microtubule may be interpreted as a *ratchet* potential, to which the *kinesin* engine binds closely during one step of the ATP cycle, while it remains much less bound, and capable to perform a one-dimensional diffusion along the microtubule, in another stage of the cycle. Another example is myosin, which is active when a muscle contracts. In a similar way, some enzymes (molecular motors) in living cells are able to move along the polymer filaments by the hydrolysis of ATP [64]. The interaction (chemical "affinity")

between the molecular motor and the filament is spatially periodic and asymmetric, and thermal fluctuations play an important role on these small scales. The result would be essentially a diffusion of a particle (like an ion or a polypeptide) whose net motion is strongly polarized in one direction.

Among the various families of kinesins and myosins, we find motors that work as monomers, dimers, trimers or tetramers, move to the plus end or the minus end of their track, and take just one or many steps before dissociating. The two heads of the kinesin dimer work in a coordinated manner to move along one of 13 protofilament tracks of the microtubule. Each protofilament consists of asymmetric α β-tubulin heterodimers. A heterodimer is about $8nm$ long and is asymmetric because it is composed of two globular subunits α-tubulin and β-tubulin which are joined together in a head-to-tail fashion so that the dimer has a translational symmetry. Because the α β-tubulin heterodimers are asymmetrical, the microtubule is polar and its ends are structurally different. One consequence of this polarity is that polymerization is faster at one end than the other. The fast-growing end is called the plus-end, whereas the slow-growing end is called the minus-end. The conventional kinesin moves towards the plus-end. There are other biomotors like e.g. ncd dimer. Despite this wide spectrum of behaviours, in all motors the initial events in the generation of movement are similar and can be explained by stepwise amplification [22, 23, 73, 74, 75]. Furthermore, it is not a surprising fact that most of the defects in motor-dependent transport are associated with a large range of diseases, including neurodegeneration, tumorigenesis and developmental defects. Thus, a unidirectional motion may be generated by allowing thermal fluctuations in the favored direction while blocking those in the opposite direction.

The two catalytic sites (heads) hydrolyze ATP in a "hand-over-hand" manner that mimics bipedal walking [76, 77, 78] by alternating its two heads in coordination with different nucleotide-microtubule binding states [79]. Kinesin shows backward steps occasionally at no load and frequently at high loads [76, 77, 78]. Recent experiments indicate that the biased unidirectional motion is achieved by regulating selective binding (unbinding) of the head to (from) the appropriate binding site [80, 81, 82, 83, 84]. In all

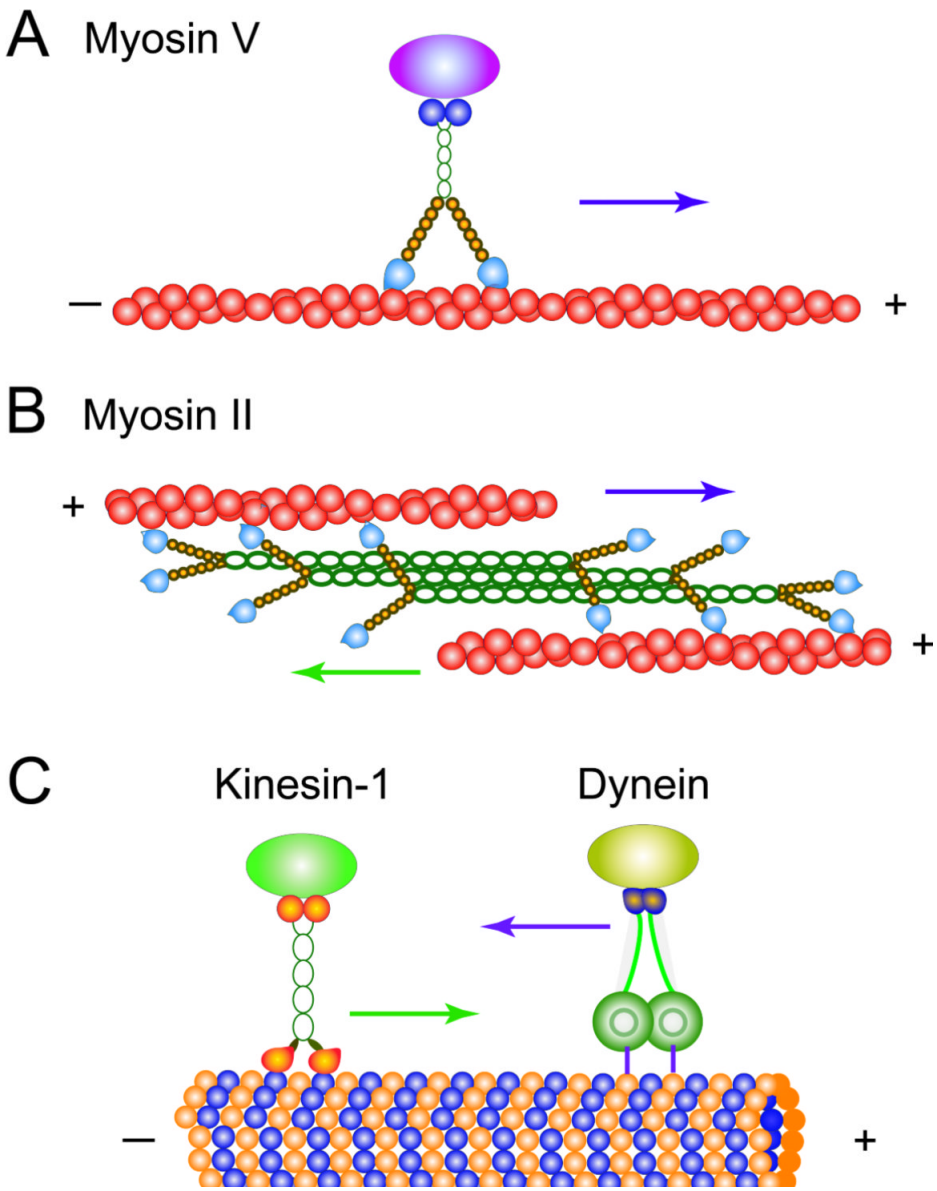

Figure 3: Schematic view of most important linearly translocating motor proteins. A) Dimeric MyosinV motor proteins step unidirectionally along actin cytoskeleton filaments. B) A group of monomeric myosin-II motor proteins combined in the filament can move together along several actin filaments. C) Conventional kinesin motor proteins translocate along the microtubules in the positive direction, while the dynein motors step along the microtubules in the opposite direction [85].

molecular motor classes, ATP hydrolysis causes a conformational change in a globular motor domain that is amplified and translated into movement with the aid of accessory structural motifs [86]. The conformational change associated with the movement of interspersed molecular motors can be exploited to reorganize a nematic liquid-crystal film and thus change its color, which is a macroscopic property. In fact, the conformational changes lead to changes in binding strength and catalytic activity for different possible ligands (ATP, ADP, P_i, and Mg^{2+}) [87], modifying also the interactions between the substrate and its surroundings while evaluating implicitly the interaction between the molecular motor and itself.

Brownian motors (or microscopic ratchets) are excellent models for understanding how machines can operate at the nanoscale in the presence of substantial thermal motion. It is for this reason that the Brownian motor concept is often used to model biological and molecular motors.

I.2.1 Mechanisms of molecular motors

At first, the mechanics of proteins may seem counterintuitive because their motions are dominated by Brownian motion, the name given to the frequent changes in velocity of a macromolecule as it is buffeted about by random thermal motions of surrounding water molecules. In addition to "smearing out" deterministic trajectories, Brownian motion serves as an effective "lubricant," allowing molecules to pass over high energy barriers that would arrest a deterministic system. More subtly, it makes possible "uphill" motions against an opposing force by "capturing" occasional large thermal fluctuations.

Generally, a Brownian motion or stochastic process refers to a random variable that evolves in time. An example is a one-dimenisonal coordinate, $x(t)$, locating a protein diffusing in an aqueous solution. The rationale for this is twofold. Discrete random variables are conceptually simpler than their continuous counterparts. The results for the discrete case are applicable when studying continuous random processes because continuous random variables represent limiting behavior of their discrete counterparts.

Our discussion is restricted to Markov processes. A Markov process is a mathematical idealization in which the future state of a protein is affected by its current state but is independent of its past. That is, the system has no memory of how it arrived at its current state. To a very good approximation, all systems consisting in Brownian motion in this thesis satisfy the Markov property. The mathematics involved with studying stochastic processes that are non-Markovian is considerably more complicated [88, 89, 90]. Indeed, motor protein kinesis is known to carry out intracellular vesicle transport along microtubules. Various polymerases are moving along their corresponding templates. All these processes are essential to a living cell. In a muscle cell, the motor protein is called myosin, and its designated track is called an actin filament. The actin filament has a periodic structure of $\sim 36nm$ [73, 74, 75, 91, 92]. In fact, the radius of a water molecule is about $0.1nm$, while proteins are two orders of magnitude larger, in the range $2 - 10nm$. This size difference suggests that we can view the fluid as a continuum. This will be subject of our investigations in the next chapter.

I.3 Artificial Brownian motors

Nanotechnology has been intricately linked with biological systems since its inception. Fascinated by the complexity and smallness of the cell, Feynman [93] challenged the scientific community to "make a thing very small which does what we want". In his visionary response, Drexler [94] proposed to focus on protein synthesis as a pathway for creating nanoscale devices. Both Feynman's and Drexler's propositions were met with much skepticism, as accurate manipulations at the nanoscale were deemed impossible. However, in view of the recent advances in systems biology [7, 95], cellular mechanisms are now being cited as the key proof of the nanotechnological viability of devices with atomic precision. In spite of their established complementarity, a fundamental difference between systems biology and nanotechnology is their ultimate goal. Systems biology aims to uncover the fundamental operations of the cell in an effort to predict the exact response to specific stimuli and genetic variations, whereas nanotechnology is chiefly

concerned with useful design.

I.3.1 Josephson junction (JJ)

For several decades, there has been intense interest in the effect of noise on the static and dynamic characteristics of JJ. A theoretical description of thermal fluctuations in superconducting weak links has been developed via the Fokker-Planck equation for the probability density function (PDF) of the phase, by analogy with the Brownian motion of a particle in a tilted periodic potential, and has been applied to both d.c. and a.c. Josephson effects and to the driven Josephson oscillator (see, for example, Refs. [96, 97, 98, 99, 100, 101, 102]). The specific dynamics of tunneling was predicted by Josephson [96] in the junction built as two bulk superconductors separated by a thin dielectric layer, across which Cooper pairs of superconducting electrons may tunnel keeping their coherence, i.e., the thickness of the dielectric barrier is much smaller than the correlation length of the superconducting state [96, 98, 99]. A typical scheme of the long JJ is displayed in Fig. 4a. The phase difference $\phi_l - \phi_r$ between the wave functions for

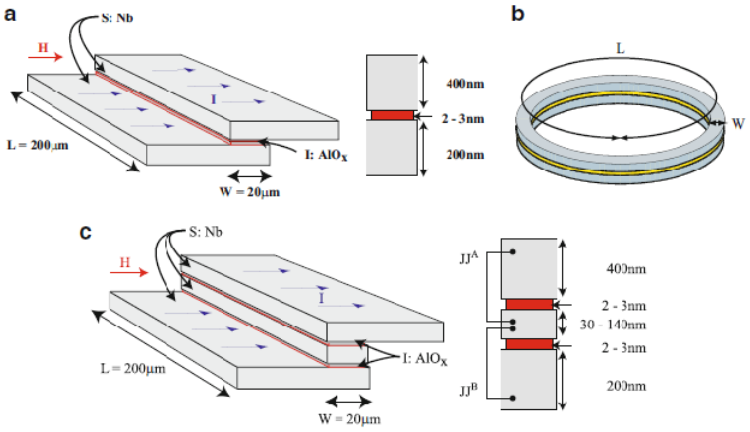

(a)

Figure 4: (a) Schematic drawings of a typical long Josephson junction and its cross section. In this case, the JJ is made of bulk niobium superconductors (S) and aluminum oxide used as the dielectric barrier. Typical values of the junctions length (L), width (W) and thickness are indicated in the figure. The bias current (I) driving the JJ, and the magnetic field (H) applied at its edges, are designated too. (b) A long circular JJ. (c) The same as in (a), but for a stack of two parallel magnetically coupled junctions. [97].

the left and right superconductors is given [98] by the Josephson equation

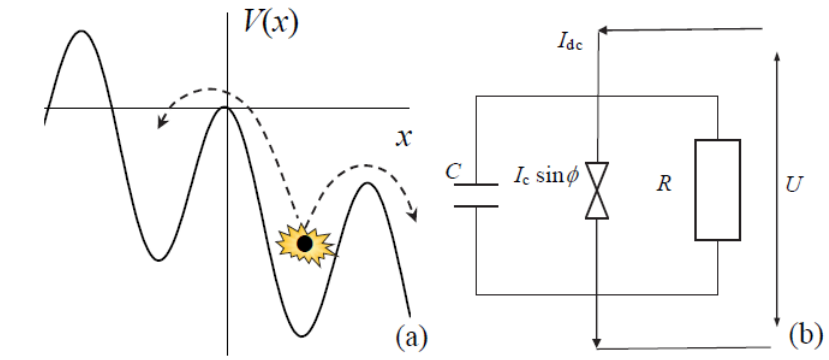

(a)

Figure 5: (a) Brownian particle in a tilted periodic potential. (b) Equivalent circuit of the JJ.

$$\frac{d\phi(t)}{dt} = \frac{2e}{\hbar}. \tag{1}$$

Here, $U(t)$ is the potential difference across the junction; e is the charge of the electron, and $\hbar = h/2\pi$, where h is Planck's constant. If the junction is small enough, it may be modeled (see Fig. 5) by a resistance R in parallel with a capacitance C, across which is connected a current generator I_{dc} (representing the bias current applied to the junction). At the other end of the junction (across the resistance R) is connected a phase-dependent current generator, $I_c \sin\phi$, representing the Josephson supercurrent resulting from the Cooper pairs tunneling through the junction. Since the junction operates at a temperature above absolute zero, there exists a white-noise current $j(t)$ superimposed on the bias current, which satisfies the conditions

$$\begin{aligned} \overline{j(t)} &= 0, \\ \overline{j(t_1)j(t_2)} &= \frac{2kT}{R}\delta(t_1 - t_2), \end{aligned} \tag{2}$$

where T is the temperature of the device, and k is the Boltzmann constant. The meaning of the noise is simply that the current through the normal shunt resistor equals $U/R - j(t)$, where the thermal fluctuations noise current $j(t)$ is assumed independent on V.

The current-balance equation for the junction is [98]

$$C\frac{dU(t)}{dt} + \frac{1}{R}U(t) + I_c \sin\phi(t) = I_{dc} + j(t). \tag{3}$$

Substitution of Eq. (1) in Eq. (3) yields the Langevin equation for the phase $\phi(t)$

$$\frac{\hbar C}{2e}\frac{d^2}{dt^2}\phi(t) + \frac{\hbar}{2eR}\frac{d}{dt}\phi(t) + I_c \sin\phi(t) = I_{dc} + j(t). \tag{4}$$

This is modeled in the Kirchhoff equation above (Fig. 5b) by making an equivalent assumption that the current through the resistor is V/R, but the bias current is $I_{dc} + j(t)$. In the next subsection, we show the mechanical model of Eq. (4) also called the Stewart-McCumber Model.

1.3.1-1 Mechanical Analogy for the Josephson Junction Model

In Josephson junction, the quantities of physical interest are the current-voltage characteristics, the linear and nonlinear junction impedance to an external high-frequency current, the Josephson radiation spectrum, and so on [96, 98, 99]. Here, the junction is treated as a purely classical system, where the phase difference ϕ across the junction and the charge CU on the junction are considered as classical variables, which can be determined with arbitrary accuracy. However, the classical accuracy is inherently limited by Heisenberg's uncertainty principle, which, in this case, is $\Delta\phi\Delta N \geq 1$, where N is the number of Cooper pairs transferred across the junction [98]. Hence, the results of classical theory require modification when quantum effects become important. These effects are usually negligible in the temperature range $T > 1K$; however, they can play a vital role at temperatures below $0.1K$ [98]. For typical Josephson junctions, such as those studied experimentally in Refs. [101] and [103], where their current-voltage characteristics have been measured, use of the classical resistively shunted junction (RSJ) model is entirely justified (see Fig. 5).

As shown in Fig 5a, Eq. (4) can be formulated in terms of Brownian classical particle of mass M moving in a spatially periodic potential $V(x) = V(x + L)$ of period L and

barrier height ΔV, subjected to an external, unbiased external force and a Gaussian white noise.

Indeed, The mechanical analogy is useful for the purpose of developing physical intuition about Josephson junction. The mechanical analogy, that is, a one-to-one correspondence with the so-called "phase particle" will help us to apply the laws of quantum mechanics to the description of Josephson junction. The analogy follows from the Stewart-McCumber dynamic equation (4), can be written as

$$\frac{\hbar^2 C}{(2e)^2}\ddot{\phi}(t) + \frac{\hbar^2}{(2e)^2 R}\dot{\phi}(t) + \frac{I_c \hbar}{2e}\sin\phi(t) - \frac{\hbar I_{dc}}{2e} = \frac{\hbar}{2e}j(t), \tag{5}$$

or

$$m_p\ddot{\phi}(t) = -\gamma\dot{\phi}(t) - \frac{I_c\hbar}{2e}\sin\phi(t) + \frac{\hbar I_{dc}}{2e} + \frac{\hbar}{2e}j(t), \tag{6}$$

where the effective "phase particle" mass is defined as $m_p = \dfrac{\hbar^2 C}{(2e)^2}$, so that the left term appears as mass times acceleration. Note that the effective mass is proportional to the parallel capacitance of the junction C. We also have introduced the damping coefficient

$$\gamma = \frac{\hbar^2}{(2e)^2}\frac{1}{R} = \frac{\hbar^2}{2\pi}\frac{R_q}{R}. \tag{7}$$

The definition shows that the damping is proportional to the normal conductance of the shunt, $G = \dfrac{1}{R}$ and inversely proportional to the normal resistance R. This means that plasma oscillations become more and more damped if more and more normal electrons couple to the oscillating condensate. The reason is that as the condensate flows, a charge builds up on the electrodes, causing some voltage and the electric field to occur. This voltage accelerates normal electrons, which then dissipate their kinetic energy into heat. Thus, the energy of the plasma oscillations converts into heat with a rate proportional to G.

Now, to stress the analogy with classical mechanics, we introduce three effective forces, namely, the damping (friction) force $F_d = -\gamma\dot{\phi}$, the phase difference force $F_\phi = \dfrac{I_c\hbar}{2e}\sin\phi$, and the bias current force $F_b = \dfrac{I_c\hbar}{2e}$. Also, let us look at ϕ as though it is the

position of the effective phase particle. We will denote this position as x, and define it simply as $x = \phi$. In that case, $F_d = -\gamma\dot{x}$, $F_\phi = \dfrac{I_c\hbar}{2e}\sin x$, and $\Gamma(t) = \dfrac{\hbar}{2e}j(t)$ equals to the Gaussian white noise coming from a fluctuating current representing the Johnson-Nyquist thermal current noise j in the shunt resistor R. Then, the dynamics equation of the Josephson Junction is the Langevin equation

$$m_p\ddot{x} = F_d + F_\phi + F_b + \Gamma(t) = -\gamma\dot{x} - \frac{I_c\hbar}{2e}\sin x + \frac{I_c\hbar}{2e} + \frac{\hbar}{2e}j(t). \tag{8}$$

The fact that a classical particle and the Josephson Junction are both described by the same differential equation implies that the known classical-particle solution and methods of solving the equation apply to Josephson Junction.

As is usual in classical physics, the conservative forces, that is, F_ϕ and F_b, can be represented by corresponding potentials. The potential corresponding to the force F_ϕ is $U_\phi = E_j(1 - \cos x)$, so that, as usual, $F_\phi = -\dfrac{dU_\phi}{dx}$. Here, $E_j = \dfrac{I_c\hbar}{2e}$ is called the Josephson energy. The bias potential energy is $U_b = \dfrac{I_c\hbar x}{2e}$, so that $F_b = -\dfrac{dU_b}{dx} = \dfrac{I_c\hbar}{2e}$. The total potential energy, which is, in fact, the Gibbs free energy of the current-biased junction, is

$$U_{wb} = U_\phi + U_b = E_j\left[(1 - \cos x) - ix\right], \tag{9}$$

where $i = I/I_c$ is the normalized bias current which defines the tilt. The potential energy U_{wb} is frequently called the "tilted washboard potential" (Figure 5a) because it resembles a hand-washing board.

Using these notations, the equation of motion of the Stewart-McCumber (MS) model becomes

$$m_p\ddot{x} = -\frac{dU_{wb}}{dx} - \gamma\dot{x} + \Gamma(t). \tag{10}$$

Equation (10) is the same as the Langevin equation for a single particle moving in a tilted washboard potential. The analogy between the MS model and the Brownian particle is contained in the fact that the same differential equation describes both systems. The equation tells us that the mass of the particle times its acceleration equals the force.

The damping force, which is proportional to the velocity, slows down the particle and dissipates its energy.

For the Josephson weak link we are most interested in the time-averaged voltage, $\langle V \rangle_t = \frac{\hbar}{2e} \left\langle \frac{d\phi}{dt} \right\rangle_t$ as a function of applied current. By analogy, for the mechanical model, we are most interested in the time-averaged rate of position, $\left\langle \frac{dx}{dt} \right\rangle_t$ as a function of applied load.

In addition, the mechanical model allows us to study the nonlinearities of the motion. It slows down the characteristic periods from the order of 10^{-10} to 1 sec. Furthermore, we are able to acquire a better physical intuition from the behavior of this mechanical system than from the electrical system [104]. In particular, the pair phase difference ϕ becomes directly observable as the position x of the Brownian particle. Thus, the model clearly illustrates the extremely complex nonlinear behavior of both ϕ and $\frac{d\phi}{dt}$ with time. By studying the motion of the mechanical model, we gain great insight into the behavior of a Josephson weak link.

The model Eq. (10) has been the subject of numerous theoretical and experimental investigations these recent years. Indeed, adding to Eq. (10), a time-periodic excitation, many phenomena have been found out. Among others, we have the absolute negative mobility [39, 105], illustrated in Fig .6, where the particle noisily moves backwards against a small constant bias. The negative differential mobility [106], where under the action of a constant external load, the velocity-load behavior becomes now considerably more complex (Fig. 7), exhibiting distinct non-monotonic characteristics. As we can see in Fig. 7, an increase of the bias F results in a corresponding decrease of the average velocity.

This observation was corroborated theoretically by Speer *et al*. [107] and Kostur *et al*. [108] and experimentally by Nagel *et al*. [109]. All these anomalous behaviour come from the fact that the inclusion of inertia adds significant complexity to the problem. This is so, because a periodically rocked, single degree of freedom with nonzero mass possesses a three dimensional phase-space that can exhibit a chaotic dynamics [110, 111,

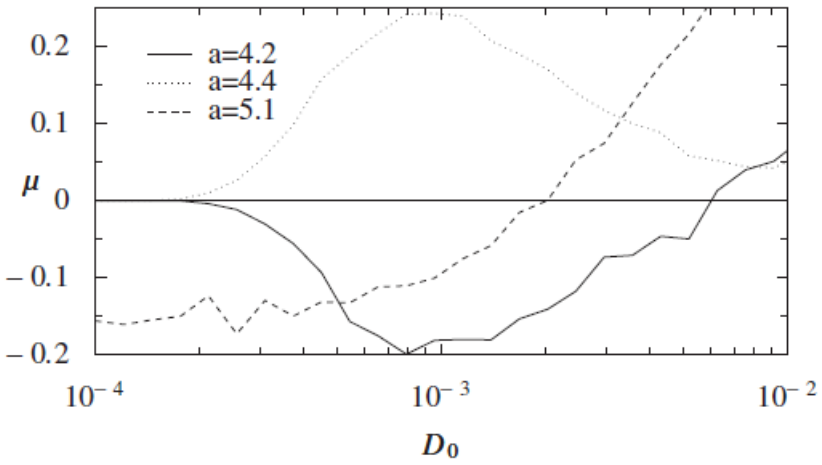

Figure 6: Illustration of the absolute negative mobility. The mobility coefficient $\mu = \partial \langle v \rangle / \partial f$ is depicted versus the dimensionless temperature strenght $D_0 \propto T$, for three values of the cosine-driving strength a [106].

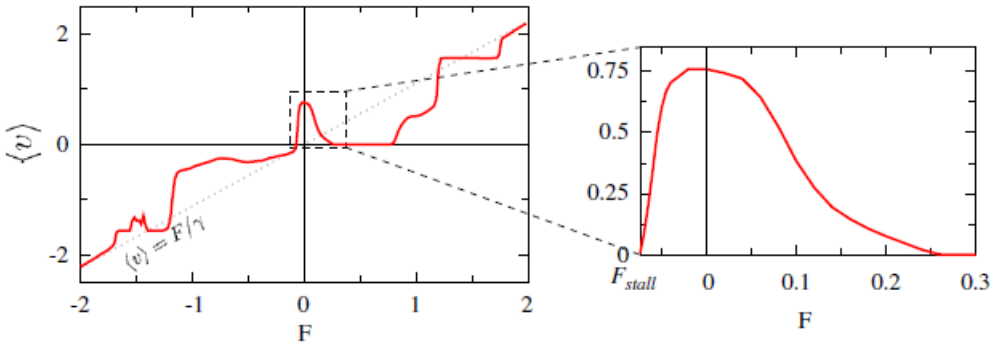

Figure 7: Illustration of the negative differential mobility. In fact, here the velocity of the inertial particle as a function of an external load, constant F exhibits a negative value. The Brownian particle performs against the load [39].

112], and consequently the ac cycle-averaged drift velocity $\langle \dot{x} \rangle$ may be oriented against the dc bias F, as the result of a delicate interplay of chaotic and stochastic dynamics.

I.3.2 Superionic conductors

Brownian particles have also been studied in detail in connection with superionic conductors. Superionic conductors, represent a class of solid materials that shows an unusually high ionic conductivity of an order of magnitude as usually found for molten salts [113, 114]. They consist of species of high mobile particles considered to be Brownian particles moving on a periodic structure with diffusion coefficients comparable to those found in liquids [33, 34, 115]. Their structure is characterized by a strong disorder in the sublattice of conductivity ions. All the ions of one sublattice are in this highly mobile state. There is another species of ions which cannot diffuse. They form a framework which is usually called the rigid sublattice. The activation energy required for the mobile ions to diffuse is far lower than that found in ordinary ionic solids. As an example, we consider silver iodide ($\alpha - AgI$) for illustration (see Fig. 8). Here, the lattice consists

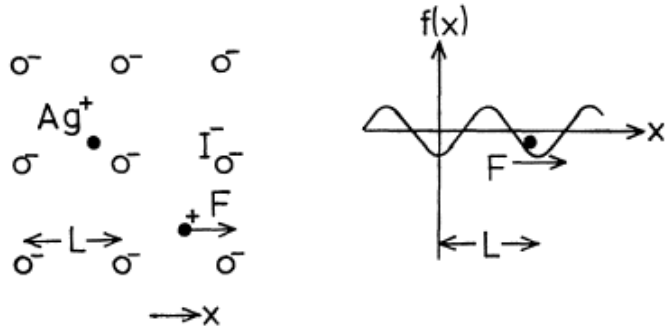

Figure 8: Highly movable Ag^+ ions in the nearly fixed iodide lattice and the corresponding potential in one dimension [9].

of iodide (I^-) ions, while the silver ions (Ag^+) are highly mobile (Fig. 8). In $\alpha - AgI$ at 300^0C, the diffusion coefficient for Ag^+ ions is close to $2 \times 10^{-5} cm^2/s$. The one of the I^- ions is negligible. In this context, the motion of ions considered as noninteracting Brownian particles is treated as a stochastic motion in a medium with periodic lattice

structure. These materials show high ionic conductivity and have led to very important advances in designing new devices based on the motion of ions through periodic structures. This may help to improve components in electrochemical energy storage and conversion devices such as batteries, fuel cells and electrochemical membranes [35, 36], which are critical in the societal shift to renewable energy. In a number of these materials, the conduction process is confined to lower dimensionality; examples include β-alumina ($d = 2$), potassium hollandite ($d = 1$), etc. If an external field F is applied to a one-dimensional model, neglecting interaction of different Ag^+ ions, then, the equation of motion divided by the mass m in the periodic potential $mf(x)$ is [37,115-117]

$$m\ddot{x} + \gamma\dot{x} + f'(x) = F + \Gamma(t). \tag{11}$$

In Eq. (11), we added a damping force $\gamma\dot{x}$ and a Gaussian white-noise force $\Gamma(t)$ (per mass)

$$\langle \Gamma(t)\Gamma(t') \rangle = 2\gamma \left(\frac{KT}{m} \right) \delta(t - t'). \tag{12}$$

By these two forces i.e., γ and $\Gamma(t)$, the effect of the small lattice vibrations on the motion of the Ag^+ ions is taken into account. It is relevant to mention that, the driving force or an external field F is defined as any influence which causes the jump frequency for a jump in one direction between two given sites to differ from that for a jump in the opposite direction between exactly analogous sites. Driving forces include gradients of stress, electrical potential, temperature or chemical potential. If the motion of the Ag^+ ions is slow compared to the lattice vibrations, the white-noise approximation in Eq. (12) is justified. In this application, we are mainly interested in the current. This current can be expressed by the drift velocity or by the mobility ($\langle \dot{x} \rangle, \mu$), or in the dynamical case, by the susceptibility. In the stochastic motion of Brownaian particles, the intuitive picture of particle migration is a thermal-activated series of jumps over a potential barrier from a potential well to another, with thermal noise playing a construction role by providing a mechanism by which particles can escape over the barriers. Thus, the jumps

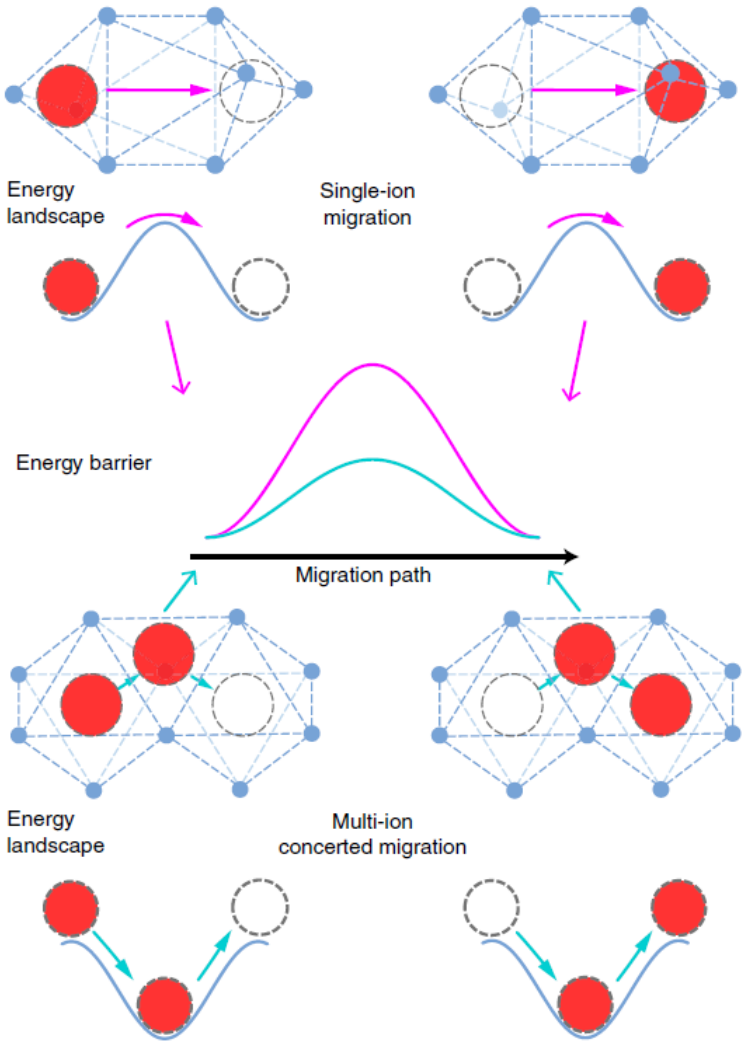

Figure 9: Schematic illustration of single-ion migration versus multi-ion concerted migration. For single-ion migration (upper insets), the migration energy barrier is the same as the barrier of the energy landscape. In contrast, the concerted migration of multiple ions (lower insets) has a lower energy barrier as a result of strong ion-ion interactions and unique mobile ion configuration in super-ionic conductors [35].

are performed by the diffusion of particles (diffusional spreading of Brownian particles around their mean motion) comparable to those found in the fluid (see Fig. 9). Notice that, the energy barriers significantly suppress the diffusion [9, 38]. During diffusion, a mobile particle migrates through the energy landscape, and the highest energy of the energy landscape along the diffusion path determines the energy barrier of the particle diffusion.

Indeed, in a superionic conductor, the Brownian motion of particles in a periodic potential is largely used for describing the conductivity of mobile ions in a superconductor. So, to understand the diffusion phenomenon, two main theoretical models have been developed [118-121]: the continuous diffusion and the jump models.

1.3.2-1 Continuous diffusion

The continuous model considers the mobile particles as the Brownian particles moving in a periodic potential. The dynamics of these particles are described either by the Langevin equation (11) or by the Fokker-Planck equation (FPE) [121, 122]. Due to the difficulty of solving these equations for a long time, a high dimensional space and for N particles, we use semi-analytic numerical methods such as the matrix continued fraction method (MCFM)(developed in the next chapter) [123, 124] or numerical simulations such as the finite element method or the Monte Carlo simulations [125, 126]. We take Eq. (11) as a plausible model which is traited as part in this thesis. The problem in the deformable lattice will be deeply discussed in the next chapter. Apart from the continuous variation of x, the main new effect is contained in the term $m\ddot{x}$, which contains the inertia of the particle and allows for oscillations. Normally, one converts the stochastic equation for x into an equation for the probability $p(x, v, t)$ to find the particle at time t at point x, with velocity v. This is the Fokker-Planck equation that will be derived in the next chapter, and it reads [127]

$$\frac{\partial p(x,v,t)}{\partial t} = \gamma\left(1 + \dot{x}\frac{\partial}{\partial \dot{x}} + \frac{kT}{\dot{x}}\frac{\partial^2}{\partial \dot{x}^2}\right)p(x,v,t) - \dot{x}\frac{\partial p(x,v,t)}{\partial x} - \frac{f'(x)}{m}\frac{\partial p(x,v,t)}{\partial \dot{x}}. \quad (13)$$

1.3.2-2 Hopping models

The hopping models (lattice gas) consider only the jump motion of particles. These models suppose that the particles are distributed at the minima of the substrate potential and perform sudden transitions. They are rather simple and a complete discussion of their dynamical properties is possible. One can also easily see their limitations. For these reasons, we present them in some detail.

The situation is the following: the lattice defines a periodic array of sites, where the mobile ions can sit. An ion placed at one site is kicked out of it after a certain time and hops away. Usually, only hopping to nearest-neighbour sites is considered and successive hops are taken to be independent: The time of flight is assumed to be short compared to the mean residence time τ_R and is neglected. This will be a good approximation if the temperature is small compared to the height of the potential barriers. In fact, the continuous diffusion can be reduced to a hopping model in such a limit. In the high friction limit, the particle jumps from a site to another vacant nearest neighbor and in the low friction limit, the particle can execute the long jumps [9, 38].

I.4 Diffusion of Brownian particles as the mechanism of transport

Diffusion can be observed almost everywhere: in the material world (diffusion of particles, atoms, molecules, proteins, cytoplasmic macromolecules) [128, 129] and in the non-material world of human civilization at various levels of society organizations (diffusion of ideas, opinions, innovations, price values) [130]. A physical archetype of diffusion is a Brownian motion resulting from interaction of a particle with its environment [8]. In the literature, one can find several quantifiers which characterize a diffusion process and spread of trajectories. An example is the mean-square displacement of the particle coordinate. In this thesis, we will consider the mean-square deviation (variance) of the

particle position $x(t)$ around its mean value, namely,

$$\sigma_x^2(t) = \left\langle [x(t) - \langle x(t) \rangle]^2 \right\rangle , \tag{14}$$

where the averaging is over all thermal realizations as well as over initial conditions. The diffusion process can be classified through the scaling function [131, 132]

$$\sigma_x^2(t) \sim t^{\alpha}. \tag{15}$$

The normal diffusion corresponds to the scaling index $\alpha = 1$. Any deviation from this linear time dependence is classified as anomalous diffusion. For the superdiffusive case, $\sigma_x^2(t)$ increases over time faster, while for the subdiffusion, it grows slower than for normal diffusion. An example of the former is ballistic diffusion with the scaling index $\alpha = 2$. The hallmark of the latter is famous Sinai subdiffusion which follows the logarithmic law $\sigma_x^2(t) \sim \ln^2 t$ [133]. This ultraslow process can be observed for a Brownian particle moving in a static random Gaussian force field imitating quenched disorder in heterogeneous media. "Quenched" means that random traps, barriers or comb-like structures do not evolve with time. This is usually the model considered to describe the dynamical properties of materials containing impurities, defects, or intrinsic randomness like it is the case for amorphous systems [134]. However, recent progress in single particle tracking techniques [135] has allowed to probe transport processes occurring in more complex setups. For instance, the diffusive motion of macromolecules and organelles inside living cells is typically subdiffusive [136, 137]. This behaviour is commonly attributed to macromolecular crowding of their interior, summarizing their densely packed, heterogeneous and fluctuating environment [138-141].

So, as part of this thesis, we are interested to the behaviour of the effective diffusion of Brownian particles in the presence of an external load. Actually, the diffusion of Brownian particles has been extensively investigated in periodic and double-well potential. Thus, the determination of the effective diffusion coefficient of the system for

arbitrary temperature, tilting force, and periodic force potential has been, and remains a challenging task both at the overdamped and underdamped limit in nonlinear stochastic systems [29, 116, 138]. Directed Brownian particle transport is typically controlled both by the fluctuation statistics of the jittering objects and the phase space available to their dynamics. Many phenomena have been observed on the behaviour of diffusion these recent years. In the presence of an external load, by using the two-state theory, the diffusion coefficient of underdamped Brownian particles moving on a tilted washboard potential is enhanced with decreasing noise in a finite range of forces (see Fig. 10). Moreover, it has been suggested and shown that in the presence of external perturbation, the maximal diffusion coefficient grows with the inverse temperature like a power and the force range of diffusion enhancement shrinks to zero when approaching zero temperature. This corresponds to regions of bistability of the deterministic velocity dynamics. This comes from the fact that, for example, as the particle in drifts with average speed $\langle \dot{x} \rangle$ in the direction of an external force F, the random switches between locked and running state cause a spatial dispersion of the particle around its average position [134, 135, 136, 137, 138, 139, 140]. Therefore, two simple approaches for giant enhancing diffusion were proposed, such as the periodic potential which is either tilted or rocked [26, 141].

I.5 Motivations

I.5.1 Deformable potential

The vast majority of works on Brownian motors is done in systems based on the standard sinusoidal periodic potential and, concentrates on the behaviour and the selective control of the emerging directed transport as a function of parameters of the system such as temperature, energy barrier, or some other control variable. However, these systems with periodic structure, although interesting, describe realistic systems only with certain approximations. To obtain a physically more realistic periodic substrate for several com-

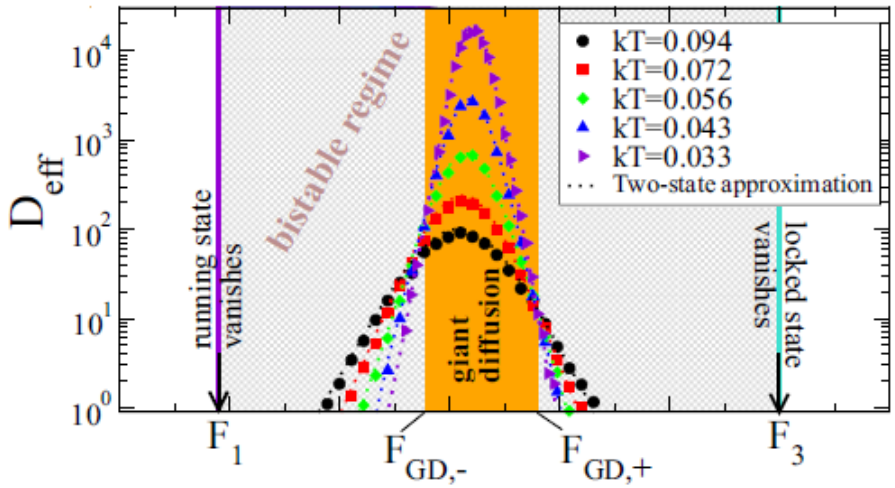

Figure 10: Finite force range for a giant enhancement of diffusion. The behavior of the diffusion coefficient for vanishing temperature defines the critical range of bias (orange), corresponding to enhanced diffusion [29].

plex systems (Atomic chains, ratchet models), the effects of physical parameters such as temperature and pressure should be considered. Under such constraints, some physical systems may undergo changes such as shape distortion, variation of crystalline structures, or conformational changes. Hence, it appears necessary to take into account the deformable character of the medium in Brownian particles. Indeed, deformable models have been considered both from mathematical and physical points of view. From a mathematical point of view, the foundations of deformable models represent a confluence of geometry, physics, and approximation theory. Geometry serves to represent object shape, physics imposes constraints on how the shape may vary over space and time, and optimal approximation theory provides the formal underpinnings of mechanisms for fitting the models to measured data. From a physical point of view, deformable models are viewed as elastic bodies that respond naturally to applied forces and constraints [142, 143]. In fact, the term deformable models stems primarily from the use of elasticity theory at the physical level, generally with a Lagrangian dynamics setting.

In fact, Fopossi et *al*. [144, 145] have shown that depending on the shape of the potential and a particular set of system parameters, dispersionless transport and anomalous diffusion can be generated in the system. Djuidje et *al*. [146] studied the phenomenon

of stochastic resonance as a function of the shape potential through the hysteresis loop area and showed that the shape parameter can induce the phenomenon of stochastic resonance. In the same vain, in the presence of the deformable potential, it was shown that the chaos can destroy the stochastic resonance phenomenon [147].

I.5.2 Deformable potential as realistic potential for Brownian particles and lattices

Indeed, in an overdamped Brownian particles modelling most often molecular motors, aiming at a more realistic description on the molecular level, some authors [15] have added an internal variable, which becomes necessary if the time required to achieve, for instance, a conformational change is not small compared with other time scales. In this thesis, the attention was focused on the influence of the system on the transport properties of Brownian particles. So, the deformable travelling-wave potential and the deformable potential are used. We model the deformation of the system by the modified Remoissenet-Peyrard on-site potential, which is distinguished by its sine-Gordon shape. This potential can be also model the conformational change in the realm of molecular motors.

I.5.3 Travelling potential

the travelling potential $V(x - \omega t)$ is given by aperiodic array of traps (local minima of the potential), travelling at a constant velocity ω along the x-axis. Hence, it models basically the working principle of a screw or screw like pumping device both invented by Archimedes [148] in the presence of random perturbation. Qualitatively, we expect that the Brownian particle $x(t)$ will be dragged in the direction of the travelling potential traps. In fact, the travelling-wave potential has been introduced by Borromeo *et al.* [149] to study Brownian surfers. They have shown that the travelling wave has the capability of dragging Brownian particles along. Indeed the travelling-wave potential represents a very common transport mechanism in condensed phase at thermal equilibrium. For

instance, laser plasma interactions are known to accelerate classical charged particles trapped by a perpendicularly propagating electrostatic wave, obtained by beating two laser beams, until they get out of phase with the beat wave [150]. A similar mechanism of travelling-wave potential has been proposed in quantum optics to upshift the frequency of the photons in a plasma (photon accelerators [151]). However, laser driven plasma waves are sensitive to the temperature as well. In fact, due to their velocity fluctuations, charged particles trapped by an electric wave propagating in a collisionless plasma may still get spatially dispersed, thus causing a reversible loss mechanism known as Landau damping [152]. Moreover, the travelling-wave potential has been used by Li *et al.* [46] to characterize the orientation of a molecular motor's internal electric dipole in order to describe the nature of the interaction between the motors and the filaments, as well as the interplay of the interaction and ATP hydrolysis, in order to understand the physical mechanism of molecular motors.

As part of the present study, underdamped Brownian particles in the deformable travelling potential could model driven laser plasma waves, known to accelerate classical charged particles trapped by perpendicular propagating electrostatic waves [150], and where the deformed on-site potential can represent a substrate that has abnormalities and defects. This deformable substrate potential could also model ionic solids, whose species, considered to be noninteracting Brownian particles, occupy vacant sites of the rigid framework diffusing through a lattice [149]. More examples of the mechanism under the travelling potential can be found in the transport of mesoscale particles along narrow channels, like ion channels in cellular membranes, percolating ducts in porous media, capillary vessels in the lymphatic system, etc.

The study presented in the present thesis is, to our knowledge, the first generalization of the known field theoretical treatment of the non-interacting Brownian particles when the substrate potential is controlled by a shape parameter, exhibiting thus its deformable character. We shall study in the next Chapters the feasibility of such a phenomenon on the basis of a simple model of itinerant particles on a deformable substrate potential.

I.6 Conclusion

In this Chapter, we have explained the concept of Brownian particles in numerous systems. Brownian particles are useful to model many systems from biology to nanotechnology. We have presented how Brownian particle manifest and their modus operandi in biology, JJ, superionic conductor also the diffusion which is the mode of transport of these particles in their noisy environment.

Under some particular constraints, some physical systems and nonlinear lattices may undergo changes. The investigations of these changes are our main motivations, developed in the next Chapters.

CHAPTER II

MODEL AND METHODOLOGY

II.1 Introduction

The previous chapter has globally presented the Brownian particles under its diverse forms, in many systems including biology, nanotechnology and engineering fields. So regarding the Brownian particles, from a theretical point of view, the problem is attractive because it is simple to formulate; it has many applications but also possesses a rich phenomenology as a nonlinear stochastic system. Indeed, rectification in nanodevices cannot ignore fluctuations and Brownian motion, in particular. New experiments on both biological and artificial devices showed how noise rectification can actually be utilized to effectively control particle transport on the small scale. The present chapter, presents the mathematical modeling, the theoretical and numerical methods, allowing to investigate, not only the transport properties of Brownian particles in the deformable potential, but also the formation of localized modes in deformable substrate lattices. The Chapter is divided as follows: in Section II and III, the General model of Brownian particles is presented in the travelling-wave deformable potential. Thus, we single out two limits in our study: the overdamped limit which most often models the dynamics of molecular motors in their environment, and the underdamped limit which models with success systems such as Josephson junction, the superionic conductors etc.... In the overdamped limit, we solve the Fokker-Planck equation, while in the underdamped limit, the spectral and the matrix continued fraction methods allow us to approximate the solution of the Fokker-Planck equation so as to deduce the effective diffusion of the system. Section IV gives some numerical methods to addresses stochastic systems.

II.2 Model of Brownian particles in the travelling-wave deformable potential

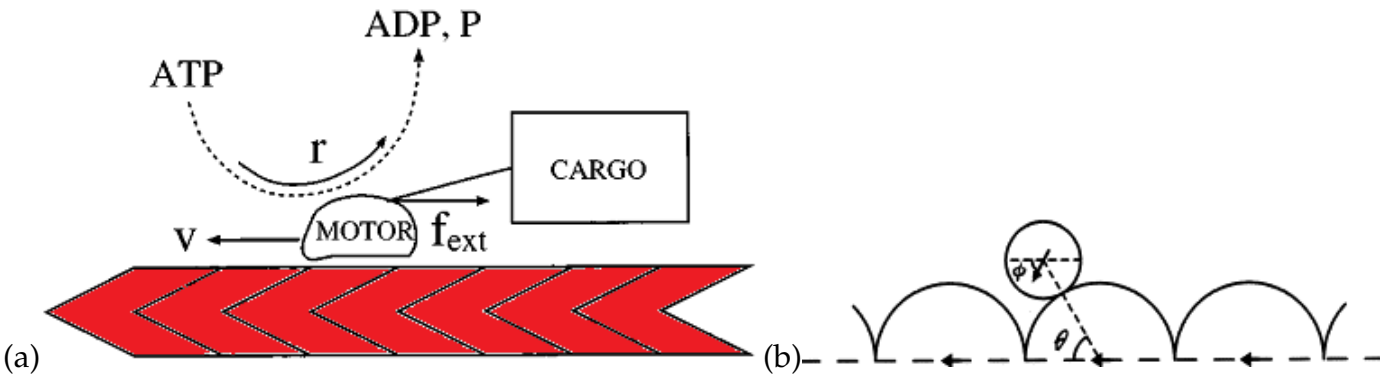

Figure 11: (a) Cartoon of a motor protein moving with velocity v along a periodic and polar track filament. As it carries some cargo along its way, it moves against an external force f_{ext} and consumes r *ATP* molecules per unit time, which are hydrolyzed to *ADP* and phosphate (P). As part of this thesis, the periodic filament is deformable and moving with a velocity ω [15]. (b) Representation of the Brownian particle and its track. The small circle and the inside arrow represent the Brownian particle and its internal dipole, respectively. The semicircles arranged in a row represent the track. The arrows fixed along a straight line denote track dipoles. The spatial and internal degrees of freedom of the Brownian particle are described by coordinates θ and ϕ, respectively.

We consider a one-dimensional Brownian particle with spatial position $x(t)$ Fig. 44, subjected to an external static force or load F. Indeed, a molecular motor moving through the fluid is acted on by frequent and uncorrelated momentum impulses arising from the thermal motions of the fluid. We model these fluctuations as a time-dependent random Brownian force, $\Gamma(t)$, whose statistical properties can be mimicked by a random number generator in a computer in a appropriate fashion. At the same time, the fluid continuum exerts on the moving protein a frictional drag force, f_d, proportional to the protein's velocity: $f_d = -\gamma v$, where γ is the frictional drag coefficient. The physics behind the friction is that the molecules of the fluid collide with the particle. The momentum of the particle is transferred to the molecules of the fluid and the velocity of the particle therefore decreases to zero [9]. Therefore, without loss of generality, we assume that the Brownian particle moves in a force field with deformable traveling-wave

Remoissenet-Peyrard (RP) potential energy function [153] modified according to [154]

$$V(x,t,r) = U\left[\frac{(1+r)^2(1-\cos(x-\omega t))}{(1-r)^2+2r(1-\cos(x-\omega t))} - 1\right], \tag{16}$$

where $|r| < 1$ represents the deformation parameter. $V(x,t,r)$: $V(x+L,t,r) = V(x,r)$, represents also the molecular interaction between the Brownian particle and its track and where L is 36 nm for actin for example. In figure 13 we represent the RP potential for the traveling potential speed $\omega = 0$. The RP potential reduces to a sinusoidal

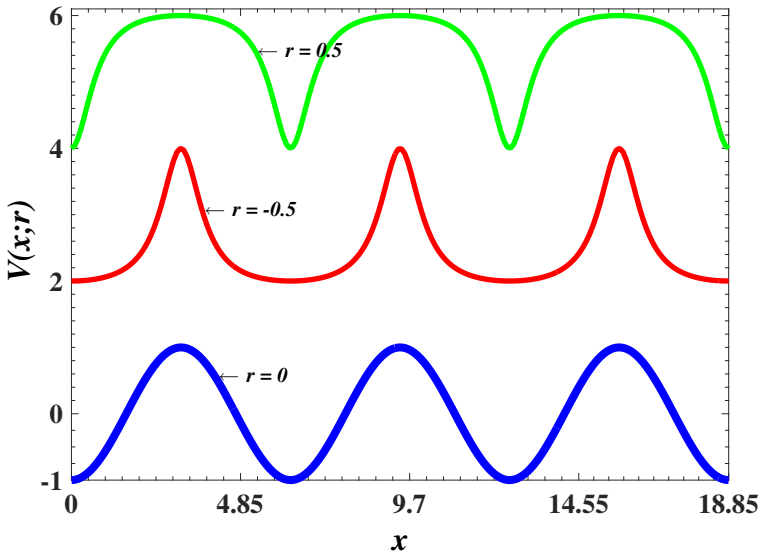

Figure 12: Schematic representation of $V(x,r)$ as a function of x for a few values of the shape parameter r, with $\omega = 0$.

shape for $r = 0$; it provides broad wells separated by narrow barriers and deep narrow wells separated by broad flat barriers, respectively, for $r < 0$ and $r > 0$, with U the potential height. It is relevant to mention that, the reflection symmetry of this potential must be broken, that is $V(x,t,r) \neq V(-x,t,r)$, because in the field of molecular motors for instance, the ab-heterodimers that build the microtubule, a highway for the biomachine are asymmetrical. This is a crucial fact because it determines the mechanism of the molecular motor movement-the *ratchet* effect [62, 155]. So, if we assume that the molecular motor is a particle of mass m moving in a periodic potential $V(x,t,r)$ of period L and

of the barrier height $U = Vmax - Vmin$. The equation of motion for the motor is the Newton equation with a complementary random force which corresponds to thermal fluctuations, i.e. the Langevin equation in the form:

$$m\ddot{x} + \gamma\dot{x} = \frac{dV(x,t,r)}{dx} + F + \sqrt{2\gamma k_B T}\Gamma(t), \tag{17}$$

which depicts the Markov process of Brownian particles. Inertial effects, related to the mass, are described by the first term on the left hand side where the overdot indicates differentiation with respect to time t. Since Eq. (17) is a stochastic differential equation, we consider a statistical ensemble of stochastic processes belonging to independent realizations of the random fluctuations $\Gamma(t)$. Because in the Langevin equation (17) the stochastic force $\Gamma(t)$ varies from system to system in the ensemble, the velocity of the particle will also vary from system to system, i.e., it will become a stochastic quantity too. Therefore, it is natural to ask for the probability to find the velocity in the interval $(v, v + dv)$, i.e., the number of systems of the ensemble. since v and x are continuous variable one introduces the probability density $P(x, v)$. Then, the probability density times the length of the interval dv and dx is the probability of finding the particle in the interval $(x, x + dx)$ and $(v, v + dv)$. This distribution function depends on time t and the initial distribution. The probability density $P(x, v, t)$ for x, v at time t follows as an ensemble average of the form

$$P(x, v, t) = \langle \delta(x - x(t))\delta(v - v(t)) \rangle \,, \tag{18}$$

where δ is the Dirac's δ-function whose the properties will be defined in below; by $\langle ... \rangle$ we indicate the ensemble average, which is the statistical average of the quantity inside the angular brackets at a given time over all systems of the ensemble. An immediate consequence of Eq. (18) is the normalization

$$\int_{-\infty}^{\infty}\int_{-\pi}^{\pi} P(x, v)dvdx = 1, \tag{19}$$

and that $P(x, v, t) \geq 0$ for all values of x, v, and t. The method of the Langevin equation gives a natural way for a stochastic generalization of the deterministic description. However, an adequate mathematical grounding for the approach of Langevin was not available until more than 40 years later, when Itô published his formulation of stochastic differential equations [156].

The dissipation is included via the Stokes force with the friction coefficient γ which is proportional to linear size R of the particle i.e.,

$$\gamma = 6\pi\eta R, \tag{20}$$

and is additionally determined by the viscosity η of the medium the particle moves in. The potential force

$$f(x, t, r) = -\frac{dV(x, t, r)}{dx}, \tag{21}$$

is zero over a period L,

$$\langle f(x, t, r)\rangle_L = \frac{1}{L}\int_0^L f(x, t, r)dx = \frac{1}{L}\left(V(L, t, r) - V(0, t, r)\right) = 0. \tag{22}$$

Equation (17) is called a stochastic differential equation because it contains the stochastic force $\Gamma(t)$.

To proceed further one has to know some properties of this Langevin force $\Gamma(t)$.

II.2.1 Gaussian white noise

Assuming the environment to be an equilibrium heat bath with independent collisions, $\Gamma(t)$ is the Gaussian white noise of zero mean

$$\langle\Gamma(t)\rangle = 0. \tag{23}$$

Usually, the duration time τ_0 of a collision is much smaller than the relaxation time $\tau = 1/\gamma$ of the velocity of the small particle. We may therefore take the limit $\tau_0 \to 0$ as a reasonable approximation. The white noise satisfies also the fluctuation-dissipation relation

$$\langle \Gamma(t)\Gamma(t')\rangle = 2D_0\delta(t-t'), \tag{24}$$

where t and t' are different times. Indeed, the fluctuation-dissipation theorem expresses the fact that the energy dissipation and random fluctuations are not independent of each other since both of them have the same origin, namely the interaction of the particle with a huge number of macroscopic degrees of freedom of the environment. $D_0 = k_B T/\gamma$ is the diffusion coefficient of the Brownian particle, k_B is the Boltzmann constant, and T is the temperature of the bath. The δ function denotes the Dirac delta function which appears because otherwise the average energy of the small particle cannot be finite as it should be according to the equipartition law

$$\frac{1}{2}m < v^2 >= \frac{1}{2}k_B T. \tag{25}$$

For smaller mass m, the thermal velocity $v_{th} = \sqrt{< v^2 >}$ =$\sqrt{kT/m}$ may be observable and therefore the velocity of a "small" particle cannot be described exactly by (17). The fact that the friction force only depends on the present state of the system and not on what happened in the past has its counterpart in the assumption that the random fluctuations are uncorrelated in time, i.e.

$$\langle \Gamma(t)\Gamma(t')\rangle = 0, \tag{26}$$

if $t \neq t'$. Furthermore, the fact that the friction involves no explicit time dependence has its correspondence in the time-translation invariance of all statistical properties of the fluctuations, i.e., the noise $\Gamma(t)$ is a stationary random process, which implies that $\langle \Gamma(t)\Gamma(t')\rangle = \langle \Gamma(t-t')\Gamma(0)\rangle$. Finally, the fact that the friction force acts permanently in time indicates that the same will be the case for the fluctuations [157]. In other words, a

noise $\Gamma(t)$ exhibiting rare but relatively strong "kicks", caused e.g. by impacts of single molecules in a diluted gas, is excluded. Technically speaking, one says that $\Gamma(t)$ cannot contain a shot noise component [158, 159, 160, 161, 162]. During a small time interval, the effect of the environment thus consists of a large number of small and, according to (26) practically independent, contributions. Due to the central limit theorem [163] the net effect of all these contributions on the particle coordinate $x(t)$is Gaussian-distributed.

Returning to Eq. (24), the Dirac δ function is a very convenient "function". More exactly it is the limiting case of a family of functions [164]. It has the property of singling out a particular value of a function $f(t)$ at a value $t = t_0$. The function is characterized by the following properties:

$$\delta(t - t_0) = \begin{cases} 0 & \text{if } t \neq t_0 \\ \infty & \text{if } t = t_0, \end{cases}$$

in such a way that for any $\epsilon > 0$,

$$\int_{t_0-\epsilon}^{t_0+\epsilon} \delta(t - t_0)dt = 1, \tag{27}$$

which means that the function $\delta(t - t_0)$ has a very sharp peak at $t = t_0$, but the area under the peak is unity.

A random force with the δ-correlation is called white noise, because the spectral density distribution [9], which is given by the Fourrier transform of (25), is independent of frequency. If the spectral density depends on frequency, one uses the color noise and Eq. (25) must be modified. Of course white noise does not exist as physically realizable process; it is, however fundamental in mathematical, and indeed in a physical sense, in that it is an idealization of many processes that do occur. Furthermore, situations in which white noise is not a good approximation can often be indirectly expressed in terms of white noise [156]. In this sense, white noise is the starting point from which a wide range of stochastic models can be derived.

II.2.2 Transport properties of Brownian particles and the Einstein relation

Averaging over many realizations of the stochastic process one finds the average particle position $\langle x(t)\rangle$ and the average velocity $\langle v(t)\rangle$. Usually one is interested in the asymptotic ($t \to \infty$) behavior of these quantities. In the absence of any external periodic perturbations, Eq. (17) yields that in the long time limit ($t \to \infty$), $\langle v\rangle = 0$ and $\langle x\rangle = \langle x(0)\rangle + \langle v(0)\rangle\, t$. The general definition of the particle current is,

$$\langle v\rangle = \lim_{t\to\infty} \frac{\langle x(t)\rangle - \langle x(0)\rangle}{t}. \tag{28}$$

Besides the average particle position and current, also interested is the behavior of the mean square displacement,

$$\left\langle \delta x^2(t)\right\rangle = \left\langle [x(t) - \langle x(t)\rangle]^2\right\rangle = \left\langle x^2(t)\right\rangle - \langle x(t)\rangle^2 . \tag{29}$$

Dealing with normal diffusion, in the long time limit the mean square displacement grows linearly in time, and the diffusion coefficient is defined in the the following way

$$D = \lim_{t\to\infty} \frac{\langle \delta x^2(t)\rangle - \langle \delta x^2(0)\rangle}{2t}, \tag{30}$$

while the effective diffusion coefficient is defined by

$$D_{eff} = \lim_{t\to\infty} \frac{\langle x^2(t)\rangle - \langle x(t)\rangle^2}{2t}. \tag{31}$$

The Monte Carlo error is defined by

$$\sigma = \frac{1}{\sqrt{L}} \sqrt{\langle v^2\rangle - \langle v\rangle^2}, \tag{32}$$

with L, the number of realizations of the fluctuating forces. Thus, Brownian particles move with a velocity in the range $\langle v\rangle \equiv [\langle v\rangle - \sigma, \langle v\rangle + \sigma]$. As previously mentioned by Machura *et al.* [105], if σ is greater than $\langle v\rangle$, the Brownian particles may move in the opposite direction, making the displacement of the particles less effective and complex. In the absence of an applied force, Eq. (30) defines the free diffusion coefficient D_0.

Let us find an expression for the coefficient D_0 characterizing the free diffusion. In the absence of any external force, Eq. (17) becomes

$$m\ddot{x} = -\gamma\dot{x} + \sqrt{2\gamma k_B T}\Gamma(t). \tag{33}$$

Multiplying the modified Langevin equation (33) by $x(t)$ and averaging over a large number of different realizations, one obtains

$$m\left\langle \frac{d^2x(t)}{dt^2}x(t)\right\rangle = -\gamma\left\langle \frac{dx(t)}{dt}x(t)\right\rangle + \langle\Gamma(t)x(t)\rangle\,. \tag{34}$$

The main characteristic of Eq. (34) is that it results from

$$m\frac{dv(t)}{dt} = -\gamma v(t) + \Gamma(t), \tag{35}$$

whose a crucial assumption is the independent of the friction force, and hence also of the fluctuation force $\Gamma(t)$, from the system coordinate $x(t)$ [156], i.e.

$$\langle\Gamma(t)x(t')\rangle = 0, \tag{36}$$

for $t \geq t'$. This relation reflects the assumption that the environment can be represented as a heat bath so that its properties are practically not influenced by the behavior of the particle [157]. The left hand side of Eq. (34) can be written as

$$m\left\langle \frac{d^2x(t)}{dt^2}x(t)\right\rangle = m\left\langle \frac{dx(t)}{dt}x(t)\right\rangle - m\left\langle \left(\frac{dx(t)}{dt}\right)^2\right\rangle. \tag{37}$$

From Eq. (30) with (29), we have for asymptotically large times that in the absence of an external force

$$2D_0 t = \left\langle x^2(t) \right\rangle, \tag{38}$$

as $\langle x(t) \rangle = const.$ for $t \to \infty$. By differentiating Eq. (38), we have $\left\langle \frac{dx(t)}{dt} x(t) \right\rangle = D_0$ and $\frac{d \langle \dot{x} x \rangle}{dt} = 0$. Observing Eqs. (25) and (36), we finally obtain from Eqs. (34) and (37) for the free diffusion coefficient, the following expression [2, 156, 165, 166]

$$D_0 = \frac{k_B T}{\gamma}, \tag{39}$$

known as Einstein relation. Equation (39) is a special form of the fluctuation-dissipation theorem. It implies that fluctuation and dissipation are intimately related, and that one cannot be present one without the other. However, dissipation would also occur if the collisions with the molecules were not randomly distributed, but occurred at regular intervals. In that case, the motion of the particle would damped, but would not fluctuate. The reason for the relation between dissipation and fluctuation is that the time between collisions is a random variable [160]. One can easily verify that the Einstein relation (39) is valid also in the presence of a space-independent force. In this case, the system is out of equilibrium and instead of Eq. (25), one has

$$\frac{1}{2} m \left\langle \delta v^2 \right\rangle = \frac{1}{2} k_B T, \tag{40}$$

where $\langle \delta v^2 \rangle = \langle v^2 \rangle - \langle v \rangle^2$.

II.2.3 Overdamped limit

The dynamics of fluctuations of microscopic system can often be described within a good approximation with the overdamped dynamics [161, 162]. This approximation perfectly described the dynamics of molecular motors in their environment. In this approximation, the inertia term $m\ddot{x}$ is neglected and the thermal fluctuations play any

notable role. We thus arrive at our minimal Smoluchowski-Feynman ratchet model

$$\gamma\dot{x} = \frac{dV(x,t,r)}{dx} + F + \sqrt{2\gamma k_B T}\Gamma(t). \tag{41}$$

The molecular motors (kinesin) are perfectly described in this approximation (see Figure 3). Indeed, one should note that the velocity $v(t) = \frac{dx(t)}{dt}$, in the corresponding Langevin equation, is the velocity of the kinesin head during the diffusion phase, which should be distinguished from the overall velocity of the kinesin moving along microtubules. The radius of the kinesin head (the ellipsoidal catalytic core head is often approximated as a sphere) is $R = 3nm$, and the mass of the head domain is of order $m = 100kDa = 1.66.10^{-22}kg$. The aqueous medium of the cell around the kinesin has a viscosity of approximately $\eta = 10^{-3}kg/ms$. Therefore, the friction coefficient $\gamma = 6.10^{-11}kg/s$ is calculated from the Stokes formula with the use of the viscosity of aqueous medium. The Langevin time relaxation is $\tau = 1.08.10^{-12}s$, which is so fast that the inertial term in the equation of motion can be neglected [167, 168, 169, 170]. In a typical Brownian domain, the activation energy is 5 time higher than the thermal energy $\Delta V = 5k_BT$, and the temperature inside cell is about $310K$ (37^oC).

Approximating the second order Langevin equation by the first order equation affects neither the fluctuation-dissipation relation (24), nor the transport properties deriving from the Einstein relation that we will see in the next section.

II.3 Fokker-Planck equation in the overdamped limit

Another widely used description of diffusion under an external force field is offered by the Fokker-Planck equation [9], which is just an equation of time evolution for the probability function. It follows as a generalization of the Einstein's approach, based on the discussion of the deterministic equations for the probability densities.

Thus, to derive the Fokker-Planck equation, let $x(t) : t \geq 0$ be a one-dimensional stochastic process with $t_1 > t_2 > t_3$. We use $P(x_1, t_1; x_2, t_2)$ to denote the joint proba-

bility distribution, i.e., the probability that $x(t_1) = x_1$ and $x(t_2) = x_2$, and $P(x_1, t_1|x_2, t_2)$ to denote the conditional (or transition) probability distribution, i.e., the probability that $x(t_1) = x_1$ given that $x(t_2) = x_2$, defined as $P(x_1, t_1; x_2, t_2) = P(x_1, t_1|x_2, t_2)P(x_2, t_2)$. We will assume $x(t)$ is a Markov process, namely

$$P(x_1, t_1|x_2, t_2; x_3, t_3) = P(x_1, t_1|x_2, t_2). \tag{42}$$

For any continuous state Markov process, the following Chapman-Kolmogorov equation is satisfied [9, 156]:

$$P(x_1, t_1|x_3, t_3) = \int P(x_1, t_1|x_2, t_2)P(x_2, t_2|x_3, t_3)dx_2. \tag{43}$$

In the following, we will also assume $x(t)$ is time homogeneous:

$$P(x_1, t_1 + s; x_2, t_2 + s) = P(x_1, t_1, x_2, t_2), \tag{44}$$

so that x is invariant with respect to a shift in time. For simplicity of notation, we use $P(x_1, t_1 - t_2|x_2) \equiv P(x_1, t_1|x_2, t_2)$.

We will now outline the derivation of the Fokker-Planck equation, a partial differential equation for the time evolution of the transition probability density function to finding a Brownian particle at any position and any time. Consider

$$\int_{-\infty}^{\infty} h(y)\frac{\partial P(y, t|x)}{\partial t}dy, \tag{45}$$

where $h(y)$ is any smooth function with compact support. Writing

$$\frac{\partial P(y, t|x)}{\partial t} = \lim_{\Delta t \to 0} \frac{P(y, t + \Delta t|x) - P(y, t|x)}{\Delta t}, \tag{46}$$

and interchanging the limit with the integral, it follows that

$$\int_{-\infty}^{\infty} h(y)\frac{\partial P(y,t|x)}{\partial t}dy = \lim_{\Delta t\to 0}\int_{-\infty}^{\infty} h(y)\left[\frac{P(y,t+\Delta t|x)-P(y,t|x)}{\Delta t}\right]dy. \tag{47}$$

Applying the Chapman-Kolmogorov identity Eq. (43), the right hand side of Eq. (47) can be written as

$$\lim_{\Delta t\to 0}\frac{1}{\Delta t}\left[\int_{-\infty}^{\infty} h(y)\int_{-\infty}^{\infty} P(y,t|Z)P(z,t)dzdy - \int_{-\infty}^{\infty} h(y)P(y,t|x)dx\right]. \tag{48}$$

Interchanging the limits of integration in the first term of Eq. (48), letting $y \to z$ in the second term, and using the identity $\int_{-\infty}^{\infty} P(y,\Delta t|z)dy = 1$, we have

$$\lim_{\Delta t\to 0}\frac{1}{\Delta t}\left[\int_{-\infty}^{\infty} P(z,t|x)\int_{-\infty}^{\infty} P(y,t|z)(h(y)-h(z))dzdy\right]. \tag{49}$$

Taylor expansion of $h(y)$ about z gives

$$\lim_{\Delta t\to 0}\frac{1}{\Delta t}\left[\int_{-\infty}^{\infty} P(z,t|X)\int_{-\infty}^{\infty} P(y,t|z)\sum_{n=1}^{\infty} h^n(z)\frac{(y-z)^n}{n!}dzdy\right]. \tag{50}$$

Defining the jump moments as

$$D^n(z) = \frac{1}{n!}\lim_{\Delta t\to 0}\frac{1}{\Delta t}\int_{-\infty}^{\infty}(y-z)^n P(y,\Delta t|z)dy, \tag{51}$$

it follows that

$$\int_{-\infty}^{\infty} h(y)\frac{\partial P(y,t|x)}{\partial t}dy = \int_{-\infty}^{\infty} P(z,t|x)\sum_{n=1}^{\infty} D^n(z)h^n(z)dz. \tag{52}$$

Integrating each term on the right side of Eq. (52) by parts n times and using the as-

sumptions on h, after moving terms to the left hand side, it follows that

$$\int_{-\infty}^{\infty} h(y) \left(\frac{\partial P(y,t|x)}{\partial t} - \sum_{n=1}^{\infty} \left(-\frac{\partial}{\partial z} \right)^n \left[D^n(z) P(z,t|x) \right] \right) dz = 0. \tag{53}$$

Now, because h is an arbitrary function, it is necessary that

$$\frac{\partial P(y,t|x)}{\partial t} = -\sum_{n=1}^{\infty} \left(-\frac{\partial}{\partial z} \right)^n \left[D^n(z) P(z,t|x) \right]. \tag{54}$$

We define the probability distribution function $P(x,t)$ of $x(t)$ as the solution of Eq. (54) with initial condition given by a δ-distribution at x_0 at $t = 0$. In this case, $P(x,t) = P(x,t|x_0,0)$ and we may write Eq. (54) as

$$\frac{\partial P(x,t)}{\partial t} = -\sum_{n=1}^{\infty} \left(-\frac{\partial}{\partial x} \right)^n \left[D^n(x) P(x,t) \right], \tag{55}$$

with

$$D^n(x_0) = \frac{1}{n!} \lim_{\Delta t \to 0} \frac{1}{\Delta t} \left\langle [x(t+\Delta t) - x(t)]^n \right\rangle |_{t=0}, \tag{56}$$

which is commonly called the Kramers-Moyal expansion. Now, if we assume $D^n(x) = 0$ for $n > 2$, then, we have the Fokker-Planck equation

$$\frac{\partial P(x,t)}{\partial t} = -\frac{\partial}{\partial x} \left[\alpha_2 P(x,t) \right] + \frac{\partial^2}{\partial x^2} \left[\alpha_1 P(x,t) \right], \tag{57}$$

where $\alpha_1 = D_0 = D^0(x_0)$ is the diffusion coefficient and keeps the same value also in the presence of an external force. Finding the first moment of Eq. (57), one sees that $D^1(x_0) = \partial \langle x \rangle / \partial t = \langle \alpha_2 \rangle$, which corresponds to the overdamped Langevin equation Eq. (41)

$$\frac{\partial P(x,t)}{\partial t} = -\frac{\partial}{\partial x} \left[\frac{f(x,t,r) + F}{\gamma} P(x,t) \right] + D_0 \frac{\partial^2}{\partial x^2} P(x,t). \tag{58}$$

The latter equation is the Fokker-Planck equation and is mathematically equivalent to the Langevin equation (41) [171]. It describes the overdamped Brownian motion under a force F field that can be space-and time-dependent. In fact, $P(x,t)$ is the probability

density function of the Brownian particle at position x for time t. The first term on the right-hand side is associated with the diffusion flux according to Fick's law. The second term is due to the convection associated with an overdamped Newtonian motion: $-\gamma\dot{x}+f(x,t,r)+F=0$. In the absence of an external force, the Fokker-Planck equation (58) reduces to the following diffusion equation

$$\frac{\partial P(x,t)}{\partial t}=D_0\frac{\partial^2}{\partial x^2}P(x,t), \tag{59}$$

which, by assuming, for the initial distribution, the δ-function, that is $P(x_0,t_0)=\delta(x_0-X_0)$, the solution is given by Gaussian distribution,

$$P(x,t)=\frac{1}{\sqrt{4\pi D_0(t-t_0)}}\exp\left[-\frac{(x-X_0)^2}{4D_0(t-t_0)}\right]. \tag{60}$$

The diffusion-like equation (58) was first proposed by A. D. Fokker in his dissertation in 1914 [172], and discussed by M. Planck in 1918 [173]. Fokker presented an equation for the distribution function of the velocity, $P(v,t)$. In 1915, Smoluchowski proposed the same equation for the distribution function of the position, $P(x,t)$, [57, 174] and therefore, Eq. (58) is also known as the Smoluchowski equation.

The Fokker-Planck equation (58) can be also written in the form of a continuity equation for the probability density $P(x,t)$:

$$\frac{\partial P(x,t)}{\partial t}=-\frac{\partial}{\partial x}J(x,t), \tag{61}$$

where $J(x,t)$ is the probability flux,

$$J(x,t)=\left(\frac{f(x,t,r)+F}{\gamma}P(x,t)\right)-D\frac{\partial P(x,t)}{\partial x}P(x,t). \tag{62}$$

A generalization of Eq. (58) to the N variables $x_1,...,x_N$ has the form

$$\frac{\partial P}{\partial t}=\left[-\sum_{i=1}^{N}\frac{\partial}{\partial x_i}D_i^{(1)}(x)+\sum_{i,j=1}^{N}\frac{\partial^2}{\partial x_i\partial x_j}D_{ij}^{(2)}(x)\right]P. \tag{63}$$

The drift vector $D_i^{(1)}$ and the diffusion for the distribution tensor $D_{ij}^{(2)}$ generally depend on the N variables $x_1, ..., x_N = x$. The Fokker-Planck equation (63) is an equation for the distribution function $P(x,t)$ of N macroscopic variables x. (Here, x_i may be variables of different kinds for instance position and velocity.)

II.3.1 Solution of the Fokker-Planck equation and transport properties of Brownian particles in the overdamped limit subjected to a travelling-wave deformable potential

Having presented above the general model of Brownian particles in the overdamped limit, in this subsection, we give a solution of the Fokker-Planck equation in the presence of the travelling-wave deformable potential. We set $\gamma = 1$ in this part. In fact, By solving the Fokker-Planck equation, one obtains distribution functions from which any averages of macroscopic variables are obtained by integration. Thus, the Fokker-Planck equation in the overdamped limit in presence of the travelling-wave deformable potential is given by

$$\frac{\partial P(x,t)}{\partial t} = -\frac{\partial}{\partial x}\left[-\frac{\partial V\left(x-\omega t, r\right)}{\partial x} - F - D_0\frac{\partial}{\partial x}\right] P(x,t)\,. \tag{64}$$

Assuming that the $x(t)$ motion is restricted to a periodically repeated segment length 2π, we apply the following periodic boundary condition and normalization condition,

$$P\left(x+2\pi,t\right) = P\left(x,t\right), \tag{65}$$

$$\int_0^{2\pi} dx p\left(x,t\right) = 1. \tag{66}$$

In the study of small micro- or even nano-machines, operating far from thermal equilibrium by extracting the energy from both thermal and non-equilibrium fluctuations, in

order to generate work against external loads, one usually refers to quantities such as the average directed velocity, the efficiency. In fact, the average velocity of Brownian particles is perfectly sufficient to describe its dynamics in a system as well as its transport properties. Here, our aim is to obtain the analytical link between the most important transport quantity, which is the average directed velocity $\langle v \rangle$ of the Brownian particle, where $v = v(t)$ denotes the stochastic process $\dfrac{dx}{dt}$ in Eq. (41), and other parameters of the system.

By setting $P\left(x,t\right) = P\left(x - \omega t\right)$, following the form of the travelling wave potential, the Fokker-Planck Eq. (64) becomes

$$-\frac{\partial}{\partial x}\left[-\frac{\partial V\left(x-\omega t,r\right)}{\partial x} - \left(F+\omega\right) - D_0\frac{\partial}{\partial x}\right] P(x-\omega t) = 0. \tag{67}$$

By integrating Eq. (67), we have

$$\left[-\frac{\partial V\left(x-\omega t,r\right)}{\partial x} - \left(F+\omega\right) - D_0\frac{\partial}{\partial x}\right] P(x-\omega t) = C, \tag{68}$$

with C, the constant of integration, depending on the parameters of the system, and which is given by Eq. (71). $P\left(x-\omega t\right)$ being function of space and time, one of the characteristics of the Markov processes is that their probability density $P(x,t)$ satisfies the famous master equation. With the boundary condition and the condition of normalization given above by Eqs. (65) and (66), we obtain, after some algebra, the following probability of Brownian particles

$$P(x-\omega t) = \frac{1}{Z}\int_0^{2\pi} \exp\left(\frac{V(x+\alpha-\omega t) - V(x-\omega t) + (F+\omega)\alpha}{D_0}\right) d\alpha, \tag{69}$$

with α, a small variation in space, while Z which is the normalization constant, is given by

$$Z = \int_0^{2\pi} d\alpha \int_0^{2\pi} dx \exp\left(\frac{V(x+\alpha) - V(x) + (F+\omega)\alpha}{D_0}\right). \tag{70}$$

Being different from the stationary situation, where distribution function is independent of time, the probability density given by Eq. (69) changes with time at any point x. Equivalent probability points propagate in the x direction with velocity ω. So, $P(x-\omega t)$ in Eq. (69) is a solitary wave with phase velocity ω. By replacing Eq. (69) into Eq. (68), we obtain after some algebra, the following expression of C

$$C = \frac{D_0\left(1-\exp\left((2\pi/D_0)(F+\omega)\right)\right)}{\int_0^{2\pi} d\alpha \int_0^{2\pi} \exp\left(\frac{1}{D_0}\right)\left(V(x+\alpha,r)-V(x,r)+(F+\omega)\alpha\right)dx}. \tag{71}$$

The expression of the average velocity is given by

$$\langle v\rangle = \int_0^{2\pi} vP(x-\omega t)dx. \tag{72}$$

By using the Langevin equation (41) and Eq. (69), the average velocity of Brownian particles is written as follows

$$\langle v\rangle \;\; = \;\; \omega + 2\pi C. \tag{73}$$

It is clearly seen that the average directed velocity of the Brownian particle is directly related to the travelling potential speed ω, but also depend on the shape of the system, the intensity of the noise and the external load through the constant C, respectively.

To optimize the effectiveness of the Brownian motor motion, we must introduce a measure for the efficiency η that account for velocity fluctuations. Assume that the Brownian motor works against an external force $\mathcal{F}$ not yet defined. Efficiency is usually defined as the ratio of useful work $E = \mathcal{F}\langle v\rangle\tau$ to energy input E_{in}, that is, $\eta = E/E_{in}$, where τ is the period of time of observation. Indeed, it is accepted that to measure the efficiency, a constant external opposing force is applied against, which the motor does useful work. For instance, for molecular motors, there are two aspects of biological functions. One is to generate forces such as the one which myosins uses in muscle contraction, another is to transport organelles as done kinesins in cells. In order to mea-

sure the ability of molecular motors to generate force and transport, respectively, it is better to express the efficiency in two forms η_F and η_T, for generating force and transportation. Because the ability to generate force can be measured by doing work against an external applied opposing constant force, η_F is defined as the ratio of the work to energy input. The ability of transportation is just how fast the average velocity is. In the absence of any external opposing force, energy input can be divided into two parts before dissipation into heat bath: one part is used to generate directed motion of the Brownian particle with average velocity, and the other part is for aggravating random motion of the Brownian particle. So, efficiency η_T for transportation can be defined as the ratio of work done against viscous friction moving with average velocity to energy input. The input energy is also the energy transfer between the system and the external agent [175]. For a Brownian motor working against a constant external load force F, the same definition of efficiency can be used to define the efficiency of generating force or energy conversion [46, 64, 157, 176], that is

$$\eta_F = \frac{F \langle v \rangle \tau}{E_{in}}. \tag{74}$$

This characterization leads to a vanishing measure of efficiency in the absence of the external force F.

In many cases, such as protein transport within a cell, the Brownian motor works at zero force regime ($F = 0$), in a viscous environment. In fact, in the presence of the dissipation γ, the force needed to displace a particle over a distance is proportional to its velocity. In this case, for a defined period of time τ, the transport is accomplished at an average motor velocity $\langle v \rangle$ and the necessary energy given is finite. Thus, by putting for $\mathcal{F}$ the average viscous force $\gamma \langle v \rangle$, we can then define the efficiency for transport as follows

$$\eta_T = \frac{\gamma \langle v \rangle^2 \tau}{E_{in}}. \tag{75}$$

In a period of time $T\left(T=\frac{2\pi}{\omega}\right)$, the energy input is calculated according to [177]

$$E_{in}=\int_0^T dt\int_0^{2\pi} dx\frac{\partial V(x-\omega t)}{\partial t}P(x-\omega t). \tag{76}$$

By using Eq. (68), it is easily shown that

$$E_{in}=2\pi\left(F+\langle v\rangle\right). \tag{77}$$

In the system, the energy from outside is input by changing the potential energy of the Brownian motor.

II.4 Approximated solution of the Fokker-Planck in the underdamped limit

II.4.1 Spectral methods

Unlike the previous case, we move to the two-dimensional Fokker-Planck equation in the deformable potential. In fact, this corresponds to the underdamped Brownian particle in the travelling-wave deformable potential (17). Therefore, the equivalent of the free Langevin equation ($F=0$) (17), in the underdamped limit, for the distribution function $P(x,v,t)$, in the phase space (x,v), is written as

$$\frac{\partial}{\partial t}P(x,v,t)=L_F P(x,v,t), \tag{78}$$

with the Fokker-Planck operator L_F

$$L_F=-v\frac{\partial}{\partial x}+\left(\frac{\partial}{\partial v}\right)\left(\frac{\partial V(x,t,r)}{\partial x}+\gamma v\right)+D_0\frac{\partial^2}{\partial v^2}. \tag{79}$$

As we said before, the relevance of such a model is well known in many areas of science, most notably motions of defects or interstitial in crystalline materials [178, 179], Josephson junctions [180], diffusion of ions, superionic conductors [30-38], relaxation and spectral properties of dipolar molecular liquids [181]. In these contexts, the model has repeatedly been used to explore the interplay between, on the one hand, the driving force and the shape of the potential and, on the other hand, the particle current and its fluctuations.

To solve the equation (78), a number of numerical methods have been developed. In Cartling [182], difference method has been applied, whereas in Moore and Flaherty [183], Galerkin's method with adaptive mesh refinement techniques has been applied to the above Fokker-Planck equation. Also recently, the matrix continued fraction method (MCFM) [9, 29, 184, 206] has been developed to approximate the analytical solution of the Fokker-Planck equation. This method appears as a powerful means of solving the Fokker-Planck equation, which we will develop in the next subsection. Nevertheless, we are going to use the spectral method, or again a "semi-analytical" method, to approximate the solution of the Fokker-Planck equation [186, 187].

Since the range of the velocity variable v is $(-\infty, +\infty)$, it is natural to represent the unknown function $P(x, v, t)$ by an expansion of Hermite polynomials in v, with coefficients depending on x and t, i.e.,

$$P(x, v, t) = \sum_{n=0}^{\infty} C_n(x, t)\psi_n(v), \tag{80}$$

where $C_n(x, t)$, n = 1, 2,... are the expansion coefficients. The $\psi_n(v)$ are the n^{th} order Hermite polynomial and its factorial factor are chosen so that the coefficient matrix of the induced partial differential equation system for C_n is symmetric, which implies that this partial differential equation is hyperbolic. It is relevant to note that Hermite functions, $\psi_n(v)$, were chosen because they form an orthonormal set and satisfy natural boundary conditions [9] in velocity space. The Hermite functions obey the following recurrence

relations

$$\frac{d\psi_n(v)}{dv} = -\alpha\sqrt{2(n+1)}\psi_{n+1}(v), \tag{81}$$

$$\frac{d^2\psi_n(v)}{dv^2} = -\alpha^2\sqrt{4(n+1)(n+2)}\psi_{n+2}(v), \tag{82}$$

$$v\frac{d\psi_n(v)}{dv} = \sqrt{(n+1)(n+2)}\psi_{n+2}(v) - (n+1)\psi_n(v), \tag{83}$$

$$v\psi_n(v) = \left(\frac{\alpha}{\sqrt{2}}\right)\left(\sqrt{n+1}\psi_{n+1}(v) + \sqrt{n}\psi_{n-1}(v)\right). \tag{84}$$

where α is a constant, equivalent to $\sqrt{2k_BT}$. By inserting Eq. (80) in the time-dependent Fokker-Planck equation, Eq. (78), and applying Eqs. (81)-(84), we obtain the following coupled system, which constitutes a partial differential equation system that obey the expansion coefficients

$$\begin{aligned}\frac{\partial C_n(x,t)}{\partial t} = &-\frac{\alpha\sqrt{n}}{\sqrt{2}}\frac{\partial C_{n-1}(x,t)}{\partial x} \\ &- \frac{\alpha\sqrt{n+1}}{\sqrt{2}}\frac{\partial C_{n+1}(x,t)}{\partial x} \\ &- \frac{\sqrt{2n}}{\alpha}\left(V'(x,t)\right)C_{n-1} - \gamma n C_n(x,t) \\ &+ \sqrt{n(n-1)}\left(\frac{2\gamma KT}{\alpha^2} - \gamma\right)C_{n-2}(x,t).\end{aligned} \tag{85}$$

To solve Eq. (85), we use the spectral method of order N. This method consists of solving the first $(N+1)$ equation of (85) for the $N+1$ expansion coefficients C_0, C_1, C_2,..., C_N. Thus, all the functions $C_n(x,t)$, $n \geq N+1$, are set to 0, i.e., take the approximate solution to $P(x,v,t)$ as the following truncated series $P_N(x,v,t)$.

C denotes a $(N+1)$ dimensional column vector defined by

C = **C(x,t)** = $[C_0(x,t), ..., C_N(x,t)]^T$. The coupled system (85) becomes

$$\frac{\partial \mathbf{C}}{\partial t} = -\alpha\mathbf{R}\frac{\partial \mathbf{C}}{\partial x} + \mathbf{SC}, \tag{86}$$

where R and S are $(N+1)\times(N+1)$ matrices given by

$$\mathbf{R}=\begin{pmatrix} 0 & \alpha_1 & & & \\ \alpha_1 & 0 & \alpha_2 & & \\ & \ddots & \ddots & \ddots & \\ & & \alpha_N & & \alpha_N \end{pmatrix} \tag{87}$$

and

$$\mathbf{S}=\begin{pmatrix} 0 & 0 & \cdots & 0 & \cdots \\ -\frac{\sqrt{2}}{\alpha}A & -\gamma & 0 & \cdots & \\ 0 & -\frac{2}{\alpha}A & -2\gamma & 0 & \cdots \\ 0 & 0 & -\frac{\sqrt{6}}{\alpha}A & -3\gamma & \cdots \\ \vdots & \ddots & \ddots & \ddots & \ddots \end{pmatrix} \tag{88}$$

with $A=\dfrac{\partial V(x,r,t)}{\partial x}$ and $\alpha_n=\sqrt{n/2}$.

Obviously, R is a symmetric matrix, and thus, $N+1$ real eigenvalues. Furthermore, we have

✠ **Theorem 1:** [see [187]] *The eigenvalues of R are the zeroes of the $(N+1)-th$ order Hermite polynomial $H_{N+1}(\lambda)$.*

✠ **Proof 1**: Let $P_{N+1}(\lambda)$ be the characteristic polynomial of R. Since R is tridiagonal, we have

$$P_{N+1}=\lambda P_N(\lambda)-\lambda_N^2 P_{N-1}(\lambda)=\lambda P_N(\lambda)-\frac{N}{2}P_{N-1}(\lambda),\quad \text{for}\quad N=2,3,4,....., \tag{89}$$

and

$$P_1=\lambda, \tag{90}$$

$$P_2=\lambda^2-\frac{1}{2}. \tag{91}$$

We shall prove that

$$P_N=2^{-N}H_N, \tag{92}$$

for $n \geq 1$.

Obviously, this is true for $N = 1, 2$. Assume Eq. (92) is true, for $N \leq n$. From Eq. (89) and the recurrence relations among Hermite polynomials, we have

$$P_{n+1} = \lambda P_n(\lambda) - \frac{n}{2} P_{n-1}(\lambda) = \lambda 2^{-n} H_n(\lambda) - n 2^{-n} H_{n-1}(\lambda) = 2^{-(n+1)} \left(2\lambda H_n(\lambda) - 2n H_{n-1}(\lambda)\right). \tag{93}$$

This complete the proof of the theorem. Let $\lambda_0 < \lambda_1 < ... < \lambda_n$, be the zeros of the Hermite polynomial H_{N+1} and C_k defined by

$$C_k = \left[\sum_{n=0}^{N} \frac{1}{2^n n!} \left[H_n(\lambda_k)\right]^2\right]^{-1/2}. \tag{94}$$

We have the following result regarding the eigenvectors of R.

✠ **Theorem 2:** [see [187]] *The eigenvector of R corresponding to the eigenvalue λ_k can be given by*

$$u_k = \left[u_{0k}, u_{1k}, ..., u_{Nk}\right]^T, \tag{95}$$

in which u_{nk} is defined by

$$u_{nk} = \frac{C_k}{\sqrt{2^n n!}} H_n(\lambda_k). \tag{96}$$

$$P_{N+1} = \lambda P_N(\lambda) - \alpha_N P_{N-1}(\lambda) = \lambda P_N(\lambda) - \frac{N}{2} P_{N-1}(\lambda), \tag{97}$$

✠ **Proof 2** Assume that an eigenvector of R corresponding to λ_k is $y = \left[y_0, y_1, ..., y_N\right]^T$. *Then*

$$Ry = \lambda_k y. \tag{98}$$

This is equivalent to the following difference equation

$$\sqrt{\frac{n}{2}} y_{n-1} + \sqrt{\frac{n+1}{2}} y_{n+1} = \lambda_k y_n, \text{if} \quad n = 0, 1, ..., N, \tag{99}$$

with boundary conditions $y_{-1} = y_{N+1} = 0$. This could be directly verified by setting $y_n = u_{nk}$, noticing the fact that $H_{N+1}(\lambda_k) = 0$. The theorem is therefore proved.

Obviously, the eigenvectors defined by Eq. (95) are normalized and they are mutually orthogonal, since R is a symmetric matrix.

R is a symmetric matrix. So, the set of its eigenvectors is also an orthogonal matrix. let us define the eigenvectors as $U = [u_0, u_1, ...u_N]$. It is easily verified that $U^T RU = \Delta = diag[\lambda_0, \lambda_1, \lambda_2, ..., \lambda_N]$. If we multiply Eq. (86) by U^T, we obtain,

$$\frac{\partial \tilde{C}}{\partial t} = -\alpha \Delta \frac{\partial \tilde{C}}{\partial x} + \tilde{S}\tilde{C}, \tag{100}$$

with $\tilde{C} = U^T C$ and $\tilde{S} = U^T SU$. Since Eq. (100) is a nonlinear and coupled system, it is difficult to obtain an analytical solution for all the different modes. Thus, the finite difference method should be used to approximate the solution $\tilde{C}(x,t)$. It is for this reason that we call it the "semi-analytic method". In order to ensure the stability of the finite difference method in our case, different schemes are used according to the sign of the eigenvalue of the matrix R. So, $\lambda_i < 0$, the forward space difference scheme should be used, and $\lambda_i > 0$, the backward space difference scheme should be used. Combining all this, we obtain the following different numerical schemes

$$\tilde{C}_i(x, t+dt) = \tilde{C}_i(x,t) - \frac{\alpha \lambda_i dt}{dx}(\tilde{C}_i(x,t) - \tilde{C}_i(x-dx,t)) + dt(\tilde{S}\tilde{C})_i(x,t) \quad \text{if} \quad \lambda_i > 0, \tag{101}$$

$$\tilde{C}_i(x, t+dt) = \tilde{C}_i(x,t) - \frac{\alpha \lambda_i dt}{dx}(\tilde{C}_i(x+dx,t) - \tilde{C}_i(x,t)) + dt(\tilde{S}\tilde{C})_i(x,t) \quad \text{if} \quad \lambda_i < 0, \tag{102}$$

and

$$\tilde{C}_i(x, t+dt) = \tilde{C}_i(x,t) + dt(\tilde{S}\tilde{C})_i(x,t) \quad \text{if} \quad \lambda_i = 0. \tag{103}$$

It is easy to see that the Eqs. (101)-(103) can produce stable solutions for the hyperbolic system (100).

Originally, system (86) is a Cauchy problem and we know that only those solutions

which go to zero as t goes to infinity make sense in physics. So, we may turn the Cauchy problem into an initial-boundary problem by setting the following artificial boundary conditions

$$\tilde{C}_j(M,t) = 0, \quad \forall \quad t \geq 0, \quad j = 0, 1, 2, ..., \frac{N-1}{2}, \tag{104}$$

and

$$\tilde{C}_j(-M,t) = 0, \quad \forall \quad t \geq 0, \quad j = \frac{N+1}{2}, \frac{N+1}{2} + 1, ..., N, \tag{105}$$

when N is odd, and

$$\tilde{C}_j(-M,t) = 0, \quad \forall \quad t \geq 0, \quad j = \frac{N}{2} + 1, \frac{N}{2} + 2, ..., N, \tag{106}$$

when N is even. So, the $C_i(x,t)$ are substituted into Eq. (80) to approximate the solution of the Fokker-Planck equation. Thus, in the next chapter, for some iterations, results will be displayed and commented as a function of the shape parameter.

II.4.2 Matrix continued fraction method in the presence of an external force

In the presence of an external force, the expression of the effective potential is given by $V_{eff}(x,r) = V(x,r) - xf$, with $V(x,r)$ given by Eq. (16) when the travelling speed of the potential is canceled. Thus, an illustration is given below for some values of the shape parameter. So, in this subsection, the Fokker-Planck equation in the deformable potential, in the presence of an external load, is solved applying the MCFM [29, 188, 189, 190]. The Fokker-Planck equation in the presence of an external load is written as

$$\frac{\partial}{\partial t} P(x,v,t) = L_F P(x,v,t), \tag{107}$$

with the Fokker-Planck operator L_F

$$L_F = -v\frac{\partial}{\partial x} + \left(\frac{\partial}{\partial v}\right)\left(\frac{\partial V(x,r)}{\partial x} + \gamma v - f\right) + D_0\frac{\partial^2}{\partial v^2}. \tag{108}$$

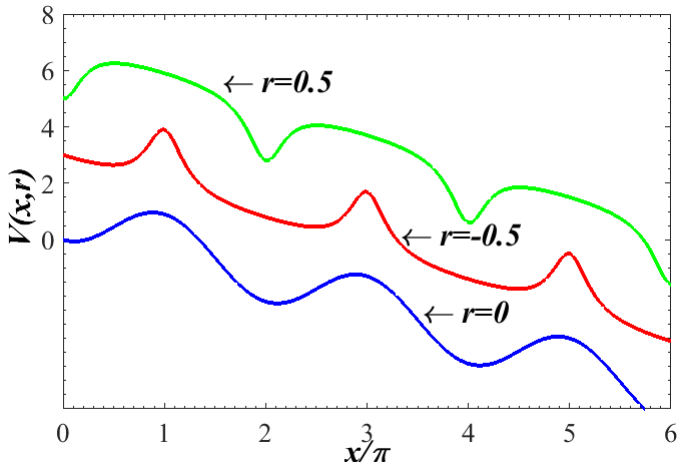

Figure 13: Schematic representation of the tilted deformable potential for the external load $f = 0.35$ as a function of the position x. The potential is represented for some values of the shape parameter $r = 0$, -0.5 and 0.5.

The Fokker-Planck operator (Eq. (108)) is not Hermitian and, on the contrary of what happens in the one-variable (position) case for the Fokker-Planck and the SWE (Smoluchowski-Wilemski equation) [191], it cannot be brought into an Hermitian form by some proper transformation. From Eq. (107), $P(x, v, t)dxdv$ represents the probability of finding the particle in the phase space element between (x, v) and $(x + dx, v + dv)$. Indeed, various methods to solve Eq. (107) have been used such as transformation of Fokker-Planck equation, Schrödinger equation, numerical integration methods and spectral methods. However, the MCFM developed by Risken (see Ref. [9], where a complete description of the method with many applications are given) is adopted in the present work in the presence of an external load. This method remains the most efficient semi-analytical method and has been largely adopted these last years to successfully analyze the problem of Brownian motion in periodic structures [29]. The MCFM can be applied to a wide class of Fokker-Planck operators because it does not require their transformation into a Hermitian form. So, it consists to the expansion of the solution into a basis set of plane waves for the position variable and of Hermite functions for the velocity variable. By analogy to what is done in quantum mechanics for the harmonic oscillator, let us

introduce, in the dimensionless v space, the operators b and $b^\dagger$

$$b = \frac{\partial}{\partial v} + \frac{1}{2}v, \quad b^\dagger = -\frac{\partial}{\partial v} + \frac{1}{2}v, \tag{109}$$

which have the well-known properties of annihilation and creation operators, when applied to the harmonic oscillator eigenfunctions $\psi_n(v)$

$$\begin{aligned} b^\dagger b = n\psi_n(v), \quad b\psi_n(v) = \sqrt{n}\psi_{n-1}(v), \\ b^\dagger\psi_n(v) = \sqrt{n+1}\psi_{n+1}(v), \\ \psi_0(v) = \frac{1}{(2\pi)^{\frac{1}{2}}}\exp\left(-\frac{1}{4}v^2\right), \quad \psi_n(v) = \frac{(b^\dagger)^n}{\sqrt{n!}}\psi_0(v). \end{aligned} \tag{110}$$

Furthermore, in the dimensionless x space, we define the operators

$$B(x) = \frac{\partial}{\partial x} - \frac{1}{2}\frac{\partial U(x,r)}{\partial x}, \quad \hat{B}(x) = \frac{\partial}{\partial x} + \frac{1}{2}\frac{\partial U(x,r)}{\partial x}, \tag{111}$$

where $U(x,r) = V(x,r) - xf$. Then, the Fokker-Planck operator (Eq. (108)) can be written as

$$L_{FP} = -\psi_0(v)\exp\left[-\frac{1}{2}U(x,r)\right]\left[\gamma b^\dagger b + bB + b^\dagger\hat{B}\right]\exp\left[\frac{1}{2}U(x,r)\right]\psi_0^{-1}(v). \tag{112}$$

In this form, L_{FP} is composed of algebraic and differential operators. The differential operator $\gamma b^\dagger b$ is irreversible and Hermitian, while the differential operator $bB + b^\dagger\hat{B}$ is reversible and anti-Hermitian. Thus, we define the dynamic structure factor $S(q,\omega)$, in the presence of the external force F. It plays an essential role in light and neutron scattering experiments [192, 193]. So, the Van Hove self-correlation function may be evaluated, if the distribution function of the stochastic process is known, as

$$H(q,t) = \int_{-\pi}^{\pi} dx_0 \int_{-\infty}^{\infty} dv_0 \int_{-\infty}^{\infty} dx \int_{-\infty}^{\infty} dv \exp(jq(x-x_0))P_{st}(x_0,v_0)P_c(x,v,t|x_0,v_0,t_0). \tag{113}$$

$P_{st}(x_0, v_0)$ is the stationary solution of Eq. (107) and is given by the Boltzmann distribution

$$P_{st}(x_0, v_0) = N\psi_0^2(v_0)\exp(-U(x_0, r)), \tag{114}$$

where $N^{-1} = \int_{-\infty}^{\infty} \exp(-U(x, r))dx$ is determined by imposing that P_{st} is normalized to 1, in the unit cell for x as well as in the whole space for v; $\psi_n(v)$ is the Hermite function. As already mentioned below, Hermite functions, $\psi_n(v)$, were chosen because they form an orthonormal set and satisfy natural boundary conditions in velocity space [9]. $P_c(x, v, t|x_0, v_0, t_0)$ is the transition probability of finding a particle at x and v, at time t, if there was a particle at the origin x_0 and v_0, at time $t = 0$. This transition probability is also the Green function of the Fokker-Planck equation, i.e., the solution of Eq. (107) with initial δ-condition in both variables x and v, given by

$$P_c(x, v, t|x_0, v_0) = \delta(x - x_0)\delta(v - v_0). \tag{115}$$

Since $H(q, t)$ is the correlation function of a stationary process, it is an even function of time and then, the dynamic factor structure $S(q, \omega)$ is defined as

$$S(q, \omega) = \frac{1}{2\pi}\int_{-\infty}^{\infty} dt \exp(-i\omega t)H(q, t). \tag{116}$$

In order to compute the transition probability $P_c(x, v, t|x_0, v_0)$, Bloch's theorem is applied and any nonstationary solution of $P(x, v, t)$ of the Fokker-Planck equation is developed into periodic functions $\tilde{P}(k, x, v, t)$,

$$P(x, v, t) = \int_{-1/2}^{1/2} dk \exp(ikx)\,\tilde{P}(k, x, v, t), \tag{117}$$

which are further expanded in Fourier series in x and into Hermite functions $\psi_n(v)$ in v as

$$\tilde{P}(k,x,v,t)\exp(ikx) = \psi_0(v)\exp\left[-\frac{1}{2}U(x,r)\right]\frac{1}{\sqrt{2\pi}}\sum_{p=-\infty}^{\infty}\sum_{n=0}^{\infty}c_n^p(k,t)\psi_n(v)\exp\left[i(p+k)x\right]. \tag{118}$$

To obtain a solution P of the Fokker-Planck equation (107) with initial δ-condition, it is sufficient to impose the same condition on $\tilde{P}$,

$$\tilde{P}(k,x,v,0)\exp(ikx) = \delta(x-x_0)\delta(v-v_0). \tag{119}$$

This gives

$$c_n^l(k,0) = \frac{1}{\sqrt{2\pi}}\frac{\psi_m(v_0)}{\psi_0(v_0)}\exp\left[-i(l+k)x_0\right]\exp\left[\frac{1}{2}U(x_0,r)\right]. \tag{120}$$

The coefficients at time t may be found in terms of Green functions as

$$c_n^p(k,t) = \sum_{l=-\infty}^{\infty}\sum_{m=0}^{\infty}G_{nm}^{pl}(k,t)c_n^l(k,0), \tag{121}$$

or, in matrix notation

$$c_n(k,t) = \sum_{m=0}^{\infty}\mathbf{G}_{nm}(k,t)c_m(k,0), \tag{122}$$

where G_{nm}^{pl} is the Green functions satisfying the initial condition

$$\mathbf{G}_{nm}(k,0) = \mathbf{I}\delta_{n,m}. \tag{123}$$

where $\mathbf{I}$ is the identity matrix and $\delta_{n,m}$ is the Kronecker delta

$$\delta_{n,m} = \begin{cases} 1 & \text{if } n = m \\ 0 & \text{if } n \neq m. \end{cases}$$

By Eqs. (117), (118), (120), (121), the conditional probability $P_c(x, v, t|x_0, v_0)$ may be written as (see Refs. [9, 188] for further details)

$$\begin{aligned} P_c(x, v, t|x_0, v_0) = \frac{1}{2\pi} \frac{\exp\left(-\frac{1}{2}U(x;r)\right)\psi_0(v)}{\exp\left(-\frac{1}{2}U(x_0;r)\right)\psi_0(v_0)} \sum_{n,m}^{\infty} \psi_n(v)\psi_m(v_0) \\ \times \int_{-1/2}^{1/2} dk \sum_{p,l=-\infty}^{\infty} \exp(ik(x-x_0)) \exp(ipx) \exp(-ilx_0) G_{nm}^{pl}(k,t). \end{aligned} \tag{124}$$

Inserting Eqs. (124) and (114) into Eq. (113), the self-correlation function becomes

$$H(q,t) = 2\pi N \sum_{p,l=-\infty}^{\infty} G_{0,0}^{p,l}(k,t) M_{p-r} M_{l-r}^*, \tag{125}$$

where $q = r + k$ must be multiple of the reciprocal lattice vector in the language of a Solid-State physicist, with $-1/2 < k \leq 1/2$ restricted to the first Brillouin zone, and where r is an integer. M_l is the modified Bessel function depending on the deformable potential and is written as

$$M_l = \frac{1}{2\pi} \int_0^{2\pi} \exp\left(-\frac{U(x,r)}{2}\right) \exp(ilx) dx. \tag{126}$$

Then, the Laplace transform of the dynamic structure factor will be written as

$$\tilde{S}(q,z) = 2\pi N \sum_{p,l=-\infty}^{\infty} \tilde{G}_{0,0}^{p,l}(k,z) M_{p-r} M_{l-r}^*, \tag{127}$$

and finally

$$S(q,\omega) = NRe\left(\sum_{p,l=-\infty}^{\infty} \tilde{G}_{0,0}^{p,l}(k,i\omega) M_{p-r} M_{l-r}^* \right), \tag{128}$$

with $Re(...)$ is the real part of the quantity in the bracket. $\tilde{G}_{0,0}^{p,l}(k,i\omega)$ is the Laplace transform of the matrix elements $G_{0,0}^{pl}(k,t)$. Notice that, if $U(x,r)$ is an even function of x, the coefficients M_l in Eq. (126) are real. Finally, the matrix $\tilde{G}_{0,0}$ is found by a matrix-continued fraction expansion. Inserting Eq. (118) into Eq. (107) and using Eq. (110), a

tridiagonal recurrence relation for c_n, (Brinkman's hierarchy [194]) is obtained

$$\frac{\partial c_n(k,t)}{\partial t} = -n\Gamma c_n(k,t) - i\sqrt{n+1}B_+ c_{n+1}(k,t) - i\sqrt{n}B_- c_{n-1}(k,t), \tag{129}$$

in which the matrices Γ, $\mathbf{B}_+$ and $\mathbf{B}_-$ are given by

$$\Gamma^{lp} = \frac{1}{2\pi}\int_{-\pi}^{\pi} dx \exp\left(-ilx\right)\gamma \exp\left(ipx\right) \tag{130}$$

$$iB_+^{lp}(k) = \frac{1}{2\pi}\int_{-\pi}^{\pi} dx \exp\left[-i(l+k)\right] B(x) \exp\left[i(p+k)\right], \tag{131}$$

$$iB_-^{lp}(k) = \frac{1}{2\pi}\int_{-\pi}^{\pi} dx \exp\left[-i(l+k)\right] \hat{B}(x) \exp\left[i(p+k)\right]. \tag{132}$$

Inserting Eq. (122) into Eq. (129), a tridiagonal recurrence relation for matrices $\mathbf{G}_{n,m}$ is obtained

$$\frac{\partial G_{n,m}(k,t)}{\partial t} = -n\Gamma G_{n,m}(k,t) - i\sqrt{n+1}B_+ G_{n+1,m}(k,t) - i\sqrt{n}B_- G_{n-1,m}(k,t)(k,t). \tag{133}$$

The last equation, for $m = 0$, is employed to get $\tilde{G}_{0,0}$. Performing the Laplace transform and recalling Eq. (123), the following relationship is obtained

$$z\tilde{\mathbf{G}}_{n,0}(k,z) - \mathbf{I}\delta_{n0} = -n\Gamma\tilde{\mathbf{G}}_{n,0}(k,z) - i\sqrt{n+1}\mathbf{B}_+\tilde{\mathbf{G}}_{n+1,0}(k,z) - i\sqrt{n}\mathbf{B}_-\tilde{\mathbf{G}}_{n-1,0}(k,z) \tag{134}$$

which is solved by standard methods [9], obtaining

$$\tilde{G}_{0,0}^{p,l}(k,i\omega) = \cfrac{\mathbf{I}}{i\omega\mathbf{I} + D^{p,l}\cfrac{\mathbf{I}}{(i\omega+\gamma)\mathbf{I}+2D^{p,l}\cfrac{\mathbf{I}}{(i\omega+2\gamma)\mathbf{I}+3D^{p,l}\cfrac{\mathbf{I}}{(i\omega+3\gamma)\mathbf{I}+\ldots}\tilde{D}^{p,l}}\tilde{D}^{p,l}}\tilde{D}^{p,l}}, \tag{135}$$

with $k = i\omega$. The matrix elements of the matrices $\mathbf{D}$ and $\tilde{\mathbf{D}}$ are given by the following equation

$$D^{p,l}(k) = (l+k)\delta_{p,l} + \frac{i}{4\pi}\int_0^{2\pi} \frac{\partial V(x,r)}{\partial x}\exp(i(l-p)x)dx - i\frac{f}{2}\delta_{p,l}, \tag{136}$$

and

$$\tilde{D}^{p,l}(k) = (l+k)\delta_{p,l} - \frac{i}{4\pi}\int_0^{2\pi} \frac{\partial V(x,r)}{\partial x}\exp(i(l-p)x)dx + i\frac{f}{2}\delta_{p,l}. \tag{137}$$

The diffusion coefficient is computed via the Green-Kubo relationship

$$D = \pi \lim_{\omega\to 0}\omega^2 \lim_{q\to 0}\frac{S(q,\omega)}{q^2}. \tag{138}$$

It is clearly seen that the Green function of the Fokker-Planck equation is related to the external force f, but also depends on the shape of the system and the friction, respectively.

II.5 Numerical methods to solve stochastic differential equations

In this section, we give some numerical techniques and methods to solve the differential equation. In the previous section, we have traited the Brownian motion in terms of the Fokker-Planck equation which is focused mainly on probalities as in Einstein's treatment. However, the Langevin equation (17) that describes the stochastic differential evolution of the Brownian particle focuses on its trajectories. In principle, both ways, i.e., the Fokker-Planck and the Langevin equations allow the characterization of the stochastic processes, such as calculating averages or correlations. However, in many instances, looking at the individual trajectories allows one to extract valuable information that is not so easy to obtain from the time evolution of the probability density function. In fact, the generation and visualization of some representative trajectories is usually quite helpful in providing physical understanding of what is going on.

Therefore, here, we focus on numerical methods to generate trajectories. To be more precise, consider that we have a given Langevin stochastic differential equation and we would like to obtain with a computer, several representative trajectories. As the noise will be different in each trajectory, even if we start always from the same initial condition, all the trajectories will be different and, in principle, there will be an infinite number of them. Therefore, we cannot aim at generating all possible trajectories, but just a finite number of them. Still, if properly done, this finite number of trajectories can be sufficient to obtain averages or correlations with a certain degree of accuracy.

Because for a given realization of the noise a stochastic equation becomes an ordinary differential equation, one may naively consider that it can be numerically integrated using any standard method, such as the Euler method, the popular fourth-order Runge-Kutta method, or a predictor-corrector method.

II.5.1 Euler-Muyurama method

To solve the differential Eq.(17), we set $\dot{x} = v$, and $\ddot{x}$ = $\dot{v}$, and we obtain the following equation:

$$\dot{x} = v, \quad \dot{v} = -\gamma v + f(x, r) + F + \sqrt{2\gamma k_B T}\Gamma(t). \tag{139}$$

The Euler method assumes that the function $f(x, r, t)$ is differentiable. Runge-Kutta methods or predictor-corrector methods assume that they are differentiable to a higher order. However, as described in subsection 2.2.1, the white noise $\Gamma(t)$ is not a differentiable function. Even for a single realization of the white noise term, $\Gamma(t)$ is highly irregular and not differentiable even at first order. As discussed in that subsection, it can be thought of as a series of Dirac delta functions spread all over the real axis. In fact, the numerical value that the noise takes at a given time is not properly defined since it is a Gaussian random number with infinite variance. As a consequence, we cannot directly use the standard methods for ordinary stochastic differential equations (139). If one were dealing with a stochastic differential equation with smooth functions as random processes, we could certainly use the standard methods [195, 196].

In what follows, we disregard that the equation can be solved and instead focus on a numerical solution in which we generate trajectories and velocities: that is, we want to obtain $x(t)$ and $v(t)$ at discrete time intervals. Thus, by integrating Eq. (139), we have

$$\int_t^{t+\Delta t} \dot{x}(s)dt = \int_t^{t+\Delta t} v(s)dt, \quad \int_t^{t+\Delta t} \dot{v}(s)dt = -\gamma \int_t^{t+\Delta t} v(s)dt + \int_t^{t+\Delta t} f(x(s),r)dt + \int_t^{t+\Delta t} Fdt + \sqrt{2\gamma k_B T} \int_t^{t+\Delta t} \Gamma(t)dt. \tag{140}$$

We discretize the time $t = t_i = t_0 + i\Delta t$, where t_0 is the time of the initial condition, $i = 0, 1, 2, ...$, and Δt is the integration time step. Our goal is to obtain a recurrence relation that provides the value of $v(t_{i+1})$, $x(t_{i+1})$ as a function of $v(t_i)$ and $x(t_i)$, respectively. We can write Eq. (140) as

$$x(t_{i+1}) = x(t_i) + \int_{ti}^{t_{i+1}} v(s)ds, \tag{141}$$

$$v(t_{i+1}) = v(t_i) - \gamma \int_{ti}^{t_{i+1}} v(s)ds + \int_{ti}^{t_{i+1}} f(x(s),r)ds + \int_{ti}^{t_{i+1}} Fds + \sqrt{2\gamma k_B T} \int_{ti}^{t_{i+1}} \Gamma(s)ds. \tag{142}$$

$f(x,r)$ being differentiable function, we expand it in a Taylor series around $x = x(t_i)$:

$$f(x(s),r) = f(x(t_i),r) + \frac{df(x,r)}{dx}|_{x(t_i)} (x(s) - x(t_i)) + 0\left((x(s) - x(t_i))^2\right). \tag{143}$$

Substitution of this expansion into Eq. (142) leads to

$$x(t_{i+1}) = x(t_i) + \Delta t v(t_i), \tag{144}$$

$$v(t_{i+1}) = v(t_i) + \Delta t v(t_i) - \gamma \Delta t v(t_i) + \Delta t f(x(t_i),r) + f'(x(t_i),r) \int_{t_i}^{t_{i+1}} (x(s) - x(t_i))ds + \Delta t \mathcal{O}\left[(x(s) - x(t_i))^2\right] + \Delta t F + \sqrt{2\gamma k_B T} w_h(t_i), \tag{145}$$

where we used the notation $f'(x(t_i), r) \equiv \frac{df((x), r)}{dx}|_{x(t_i)}$ and $w_h(t_i) = \int_{t_i}^{t_{i+1}} \Gamma(s)ds$, is the difference of the Wiener process at two different times. It is a Gaussian process and can be fully characterized by giving the mean and correlations:

$$\langle w_h(t) \rangle = \int_{t}^{t+\Delta t} \langle \Gamma(s) \rangle \, ds = 0, \tag{146}$$

$$\langle w_h(t) w_h(t') \rangle = \int_{t}^{t+\Delta t} \int_{t'}^{t'+\Delta t} \langle \Gamma(s)\Gamma(u) \rangle \, dsdu = \int_{t}^{t+\Delta t} \int_{t'}^{t'+\Delta t} \delta(s-u) dsdu. \tag{147}$$

To evaluate the integral, we make use of the properties of the Dirac δ function. We can assume, without loss of generality, that $t' > t$. If $t' > t + h$, the integral is 0, as there is no overlap in the integration intervals, and the delta function vanishes. If $t \leq t' < t + \Delta t$, the double integral equals the length of the overlap interval, that is

$$\langle w_h(t) w_h(t') \rangle = \int_{t'}^{t+\Delta t} ds = t - t' + \Delta t. \tag{148}$$

In particular, for $t' = t$, one has

$$\left\langle w_h(t)^2 \right\rangle = \Delta t. \tag{149}$$

In numerical calculations, time takes always discrete values as multiples of the integration time step. If we consider discrete times $t = t_i = ih$, $t' = t_j = jh$, the correlation becomes

$$\langle w_h(t_i) w_h(t_j) \rangle = \Delta t \delta_{ij}. \tag{150}$$

We introduce now a set of independent Gaussian random variables u_i of zero mean and variance 1:

$$\langle u_i \rangle = 0, \quad \langle u_i u_j \rangle = \delta_{ij}, \tag{151}$$

in terms of which we can write

$$\langle w_h(t_i) \rangle = \sqrt{h} u_i. \tag{152}$$

Bring all the terms together, the recurrence relation to generate numerically trajectories and velocity of the stochastic process are

$$x(t_{i+1}) = x(t_i) + \Delta t v(t_i), \tag{153}$$

and

$$v(t_{i+1}) = v(t_i) - \gamma \Delta t v(t_i) + \Delta t f(x(t_i), r) + \Delta t F + \sqrt{2\gamma k_B T h} u_i. \tag{154}$$

The recurrence equations (153) and (154) can be readily implemented in a program that allows the generation of a numerical trajectory. Averages and correlations can be obtained by integrating many trajectories with independent values for the noise. Besides, if the initial condition is given by a probability distribution, it is also necessary to sample this distribution of initial conditions.

II.5.2 Generating Gaussian random variables

To realize the simulation described above, we need to generate Gaussian random variables with zero mean. The following method generates two independent zero mean Gaussian variables with variance σ = 1 [195, 196, 197, 198]. We first take two random variables, x and y, that are uniformly distributed on the interval [0, 1] (All modern programming languages include in built functions to generate such variables). We then calculate

$$x' = 2x - 1, \tag{155}$$

$$y' = 2y - 1. \tag{156}$$

These new random variables are now uniformly distributed on the interval [-1,1]. We now calculate

$$r = x'^2 + y'^2. \tag{157}$$

If $r = 0$, or $r \geq 1$, then, we return to the first step and calculate new random variables x and y. If $r \in (0, 1)$, then, we calculate

$$g_1 = x' \sqrt{-2\ln(r)/r}, \tag{158}$$

$$g_2 = y' \sqrt{-2\ln(r)/r}. \tag{159}$$

The variables g_1 and g_2 are Gaussian with zero mean and unit variance, and mutually independent. If, instead, we want g_1 and g_2 to have variance a, then, we simply multiply them by $\sqrt{a}$.

II.5.3 Runge-Kutta method: Kasdin algorithm

In this part, we introduce an implementation of the fourth-order Runge-Kutta (RK) algorithm developed by Kasdin [199] for numerical integration of stochastic differential equation. This method is known for its performance and relatively easy implementation. To implement this method, we separate the one variable equation with second order derivatives (Eq. (17)) into two variable equations with first order derivatives, that is

$$\dot{\mathbf{X}} = \mathbf{F}(\mathbf{X}, t) + \mathbf{\Gamma}(t) \tag{160}$$

$$\begin{pmatrix} \dot{x} \\ \dot{v} \end{pmatrix} = \begin{pmatrix} v \\ -\gamma v - \dfrac{\partial V(x, r, t)}{\partial x} + F \end{pmatrix} + \begin{pmatrix} 0 \\ \Gamma(t) \end{pmatrix} \tag{161}$$

where $\dot{x} = v$ and $\dot{v} = \ddot{x}$ are used to reduce the derivative order of the equation. Now, we can use vectors $\mathbf{X}$, $\mathbf{F}(\mathbf{X}, t)$, and $\mathbf{\Gamma}(t)$ with two elements, each to describe the variables of the equation sets.

Assuming that we know the value for $\mathbf{X}_k = \binom{x}{v}$ at time step t_k, through fourth-step

calculation (see equations below), we obtain the value for $\mathbf{X}_{k+1}$ at time t_{k+1} as

$$\mathbf{k}_1 = \delta t \mathbf{F}(\mathbf{X}_k, t_k) + \delta t D^{1/2} \begin{pmatrix} 0 \\ r_1 \end{pmatrix}, \tag{162}$$

$$\mathbf{k}_j = \delta t \mathbf{F}\left(\mathbf{X}_k + \sum_{i=1}^{j-1} a_{ji}\mathbf{k}_i, t_k + c_j \delta t\right) + \delta t (D q_j)^{1/2} \begin{pmatrix} 0 \\ r_j \end{pmatrix}, \tag{163}$$

$$\mathbf{X}_{k+1} = \mathbf{X}_k + \alpha_1 \mathbf{k}_1 + ... + \alpha_n \mathbf{k}_n, \tag{164}$$

where δt is the time step, $D = \dfrac{2\gamma k_B T}{\delta t}$, $j = 2...n, n = 4$, for the fourth-order algorithm, and r is sampled by a standard Gaussian distribution with zero mean value and a variance of 1. The variables a_{ji}, a_i, and q_j are constant coefficients whose values are given in Table 1, and c is a constant that can be obtained by $c_j = \sum_{i=1}^{j-1} a_{ji}$. More details of the algorithm can be found in Kasdin's article [199, 200].

Table 1: Fourth-order, time-varying RK coefficients

Coefficient	Value
α_1	0.25001352164789
α_2	0.67428574806272
α_3	-0.00831795169360
α_4	0.08401868181222
a_{21}	0.66667754298442
a_{31}	0.63493935027993
a_{32}	0.00342761715422
a_{41}	- 2.32428921184321
a_{42}	2.69723745129487
a_{43}	0.29093673271592
q_1	3.99956364361748
q_2	1.64524970733585
q_3	1.59330355118722
q_4	0.26330006501868

II.6 Conclusion

In this chapter, we have presented the general model of Brownian particles in the deformable potential. In the overdamped limit (absence of mass of the Brownian particle), by solving the Fokker-Planck equation in the deformable traveling-wave potential, we

have found an expression of the density probability to find a Brownian particle, at position x, at time t. From the density probability, transport properties such as average velocity and efficiencies of Brownian particles have been derived. We have shown that all these quantities depend not only on the speed of the potential, the intensity of noise, but also on the shape of the system. Thanks to the spectral method, the solution of the Fokker-Planck equation in the absence of an external load in the travelling-wave deformable potential has been approximated in the underdamped limit. Using the matrix continued fraction methods and the dynamic structure factor, the solution of the Fokker-Planck equation is approximated in the presence of an external force. Some numerical methods to solve the stochastic differential equations used in this thesis such as the Euler-Muyurama method, the Kasdin's algorithm or the Fourth-order Runge-Kutta stochastic method have been used to solve numerically the Langevin equation (17). The different methods developed in this Chapter are used to obtain results presented in Chapter III.

CHAPTER III

RESULTS AND DISCUSSIONS

III.1 Introduction

In this chapter, we present and discuss the results of our thesis using both analytical and numerical methods presented in chapter II. This chapter is organized as follows: In the second Section, the transport properties of Brownian particles in the deformable travelling-wave potential in overdamped and underdamped limits are presented. In Section III, the transport properties of Brownian particles is discussed in the presence of an external load.

III.2 Transport properties of Brownian particles in the travelling-wave potential

Focusing on the transport properties of the deformable system, the long-time limit of statistical quantities of interest is determined in terms of the statistical average over different realizations of the process in Eq. (17). We perform our numerical studies with the Euler algorithm. The time step is $\Delta t = 10^{-2}$. For initial conditions, $x = 0$ at $t = 0$, the Brownian particle is at rest at the bottom of the deformable traveling-wave potential ($\dot{x} = 0$). All quantities are averaged over 500 to 1000 different realizations, each of which evolves over $t_{max} = 10^3$, for an overdamped case, and $t_{max} = 10^4$, for an underdamped case.

III.3 Overdamped limit

III.3.1 Average velocity in the overdamped Brownian motion

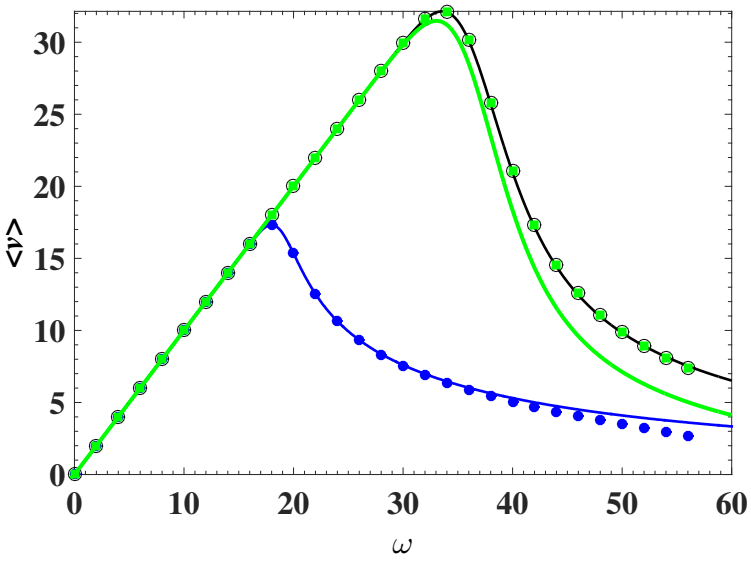

Figure 14: Numerical solution of the average velocity obtained from Eq.(41) as a function of the travelling speed ω, for $r = -0.5$ (black line), $r = 0$ (blue line), $r = 0.5$ (green line). Also represented is its analytical solution (Eq.(73)) for $r = -0.5$ (black open circle), $r = 0$ (blue closed circle), $r = 0.5$ (green square). Other parameters used are U = 20, γ = 1, $D = 0.5$.

In the previous chapter, we have derived, in the overdamped limit, an expression for the average velocity of Brownian particles in the deformable travelling-wave potential. In order to see the influence of the shape parameter of the deformable potential on the average velocity, we represent, first, the average velocity of the Brownian particles as a function of the travelling speed obtained through a numerical integration of Eq. (41), and, second, some analytical results [see Eq. (73)] for r = -0.5, 0.0, and 0.5 (see Fig.14). In this figure, it is noted that the general evolution of the average velocity is the same for different shapes of the travelling potential. In fact, the average velocity increases approximatively from 3% to 86% when r increases from 0 to ± 0.5 [201, 202]. We note that our numerical solution is in good agreement with the analytic solution. Indeed, in the absence of an external applied load ($F = 0$), the average velocity of the particle $\langle v \rangle$

increases in speed ω up to a critical value ω_{un} named the unlocking speed of the system, depending on the shape parameter r and then decreases monotonically to a nonzero value as the driving speed increases. In general, in the system, the potential advances with the travelling speed ω when the particle motion due to the force generated by the potential barrier lags behind. When ω is less than or equal to the unlocking speed of the system ω_{un}, the particle is pinned in one potential well and moves along at the full speed of the travelling wave potential. As the travelling potential speed increases ($\omega > \omega_{un}$), the driving force generated by the potential energy becomes large enough and the particle jumps in the next potential well. Continuously increasing, the travelling potential speed ω leads to a backward and forward movement of the Brownian particle, leading to a decrease of the average velocity to a nonzero value due to very few back-turns. It is important to mention that the maximum value of the average velocity of Brownian particle that can be generated by the potential barrier has an intrinsic link to the shape parameter of the travelling potential. In fact, when the absolute value of the shape parameter of the system increases, the unlocked value of the driving force due to the potential energy increases too. This increase matches with an increase of the unlocking speed ω_{un} and consequently to an increase of the corresponding average velocity of the particle as shown in Fig. 14. However, this behavior requires a comment. Indeed, referring to Fig. 14, which depicts the average velocity of the Brownian particle as a function of the travelling-wave potential speed ω, there exists a slight discrepancy with Fig. 2 of [201]. Moreover, as illustrated in these numerical simulations, the deformed system dissipated less thermal energy than the nondeformed system. In Ref. [201], the maximum average velocity of Brownian particles obtained from numerical simulation was greater for r = 0.5 than that of r = -0.5, given by 18.7910 and 19.9589, respectively, whereas in Fig. 14, by using Eq. (28), the average velocities are greater for the shape parameter r = -0.5 than r = 0.5, which are given by 32.1434 and 31.4817, respectively. Consequently, this last case exhibits a good enough agreement with the analytical result that we have derived [see Eq. (73)] [201]. In fact, in [201], the Kasdin algorithm was used to numerically simulate

the stochastic differential equation, and then, the formula

$$\langle v \rangle = \frac{1}{L} \sum_{i=1}^{L} \frac{1}{t_{max}} \int_{0}^{t_{max}} v(t) dt, \tag{165}$$

($t_{max} \longrightarrow \infty$) was used to compute the average velocity of Brownian particles. Thus, in this context, it turns out that the use of Eq. (28) seems to be more reliable to address the stochastic differential equation since it matches well effectively with the theory proposed in [201]. Nevertheless, from a phenomenological point of view, the average velocity of Brownian particles in both cases presents the same shape. However, by varying the shape parameter with both formulas, some discrepancies related to numerical methods take place. This suggests that Eq. (165) is more appropriate when the system is subjected to an external periodic excitation [39, 105, 203, 204], while Eq. (28) is more appropriate for systems that are not externally perturbed by a periodic excitation [29, 205].

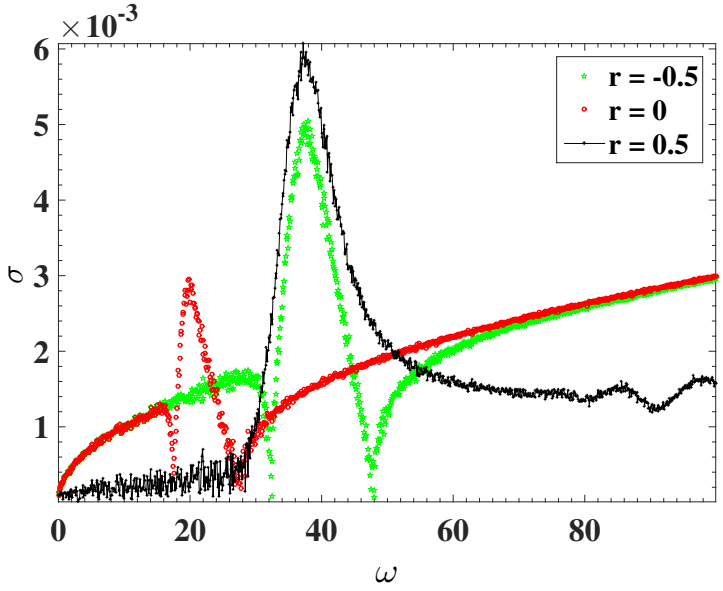

Figure 15: Monte Carlo error σ vs ω for different values of the shape parameter r, with $U = 20.0, D = 0.5, \gamma = 1$. Note that σ follows the same shape as the average velocity when $|r|$ increases.

To understand the displacement of the Brownian particles in the travelling deformable system, we compute Eq. (32) together with Eq. (41) using the numerical method outlined above. It turns out that the Monte Carlo error σ as a function of the driving speed

presents the same evolution as the average velocity for each value of the shape parameter. These fluctuations are always smaller than the corresponding average velocity (see Fig. 15). Also presented is the average velocity of Brownian particles given by Eq. (73)

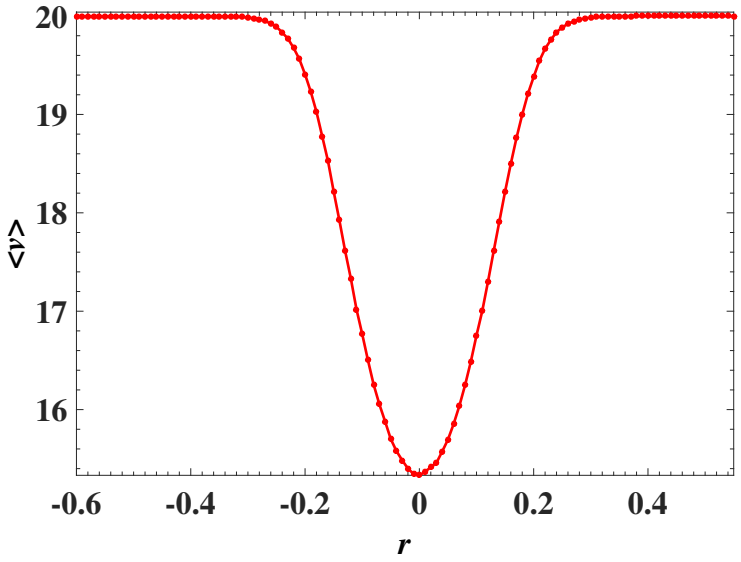

Figure 16: Schematic representation of the average velocity of the Brownian particle in the overdamped case as a function of r, for $U = 20.0, D = 0.5, \omega = 20.0$. This curve has nearly symmetric variations as the shape parameter evolves.

as a function of r (Fig. 16). The general behavior of $\langle v \rangle$ is almost the same when the absolute value of r increases, for a fixed value of the traveling speed. Although the effect of each collision between the particle and its surrounding is important in the overdamped regime, the Monte Carlo errors show that the transport properties of Brownian particles are performed with less turn-back. In the deformed system, and in the overdamped regime, the transport properties of Brownian particles are shown in the directed direction. Moreover, thermal energy is less dissipated in the deformable potential compared to the sinusoidal shape ($r = 0$).

III.3.2 Differences ω_{un}-$\langle v \rangle_{max}$ and $\langle v \rangle_{max}(-r)$ - $\langle v \rangle_{max}(r)$ versus the shape parameter

To fully characterize the role of the shape parameter of the system on the dynamics of Brownian particle in the presence of the travelling wave potential, our attention is fo-

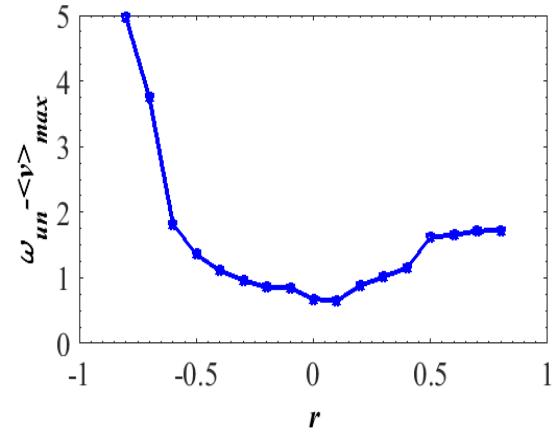

Figure 17: Differences between maximum values of the speed of the travelling wave potential and the corresponding maximum of the average velocity of the Brownian motor, and maximum values of the average velocity of the Brownian motor for symmetric values of the shape parameter r as a function of the shape parameter for $D = 0.5$, $F = 0$, $U = 10$ and $\gamma = 1$.

cused on the most important feature of Fig. 14, which is the dependence of the peak values of the average velocity $\langle v \rangle_{max}$, and the corresponding unlocking speed of the travelling wave potential ω_{un} on the shape parameter of the system. For this purpose, Fig. 17 represents two plots. In the upper panel of this figure, the difference between the unlocking speed of the travelling wave potential ω_{un} and the corresponding maximum value of the average velocity of the Brownian particle $\langle v \rangle_{max}$ as a function of the shape parameter r is plotted. In the lower panel, the difference between the maximum values of the average velocity of the Brownian particle $\langle v \rangle_{max}$ for each symmetrical couple ($-r$, r) as a function of the absolute value of r is presented. It can be seen in the upper panel of this figure that the difference between the unlocking speed of the travelling potential and the corresponding maximum of the average velocity ($\omega_{un} - \langle v \rangle_{max}$) is a decreasing function of the shape parameter r of the system. In fact, for each couple of symmetric values of the shape parameter r, the unlocking speed of the travelling wave potential and the corresponding values of the average velocity of the Brownian particle are different. For example, ω_{un} = 33.1, and 33.5 for $r = 0.5$ and $r = -0.5$, respectively and $\langle v \rangle_{max}$ is equal to 32.1434 and 31.4817 for r = -0.5 and r = 0.5, respectively. This means that the unlocking speed of the travelling wave potential is always greater than the corresponding maximum value of the average velocity of the Brownian particle. Consequently, differences ω_{un}-$\langle v \rangle_{max}$ decrease when r increases (according to data given here for $r = -0.5$, ω_{un}-$\langle v \rangle_{max}$ is equal to 1.6183 and $r = 0.5$, ω_{un}-$\langle v \rangle_{max}$ is equal to 1.3566). It is obviously seen that for each couple of symmetric values of the shape parameter r, the maximum value of the average velocity of the Brownian particle, that can be generated by the potential barrier, in the presence of the travelling speed, is higher for negative values of r (broad narrow wells and deep barriers). As shown in the lower panel of Fig. 17, the difference between $\langle v \rangle_{max}(r)$ - $\langle v \rangle_{max}(-r)$ is an increasing function of the absolute value of r. This behaviour of the Brownian particle in the presence of the travelling wave potential may be due to the fact that the energy gains through thermal fluctuations is less dissipated in deformable potentials with broad narrow wells and deep barriers. These observed changes of the dynamical quantities indicate that the shape parameter plays

an important role in systems with travelling wave potential. The behaviour of the average velocity of the Brownian particle $\langle v \rangle$ as a function of the intensity of noise D, for different values of the shape parameter r (see Fig. 18), is investigated. When the shape parameter r = 0, the unlocking speed and the corresponding maximum value of the average velocity of the Brownian particle are equal to the height of the potential barrier U (i.e $\langle v \rangle_{max} \simeq \omega \simeq U$, here U = 20) at zero temperature or intensity of the noise D as stated in [46, **?**] and shown in Fig. 18. This behaviour of the average velocity is also verified when the shape parameter of the system is different from zero ($r < 0$ and $r > 0$). Each curve in this figure (Fig. 18) is characterized by a particular shape of the system, but, in general, the average velocity is a decreasing function of the intensity of the noise.

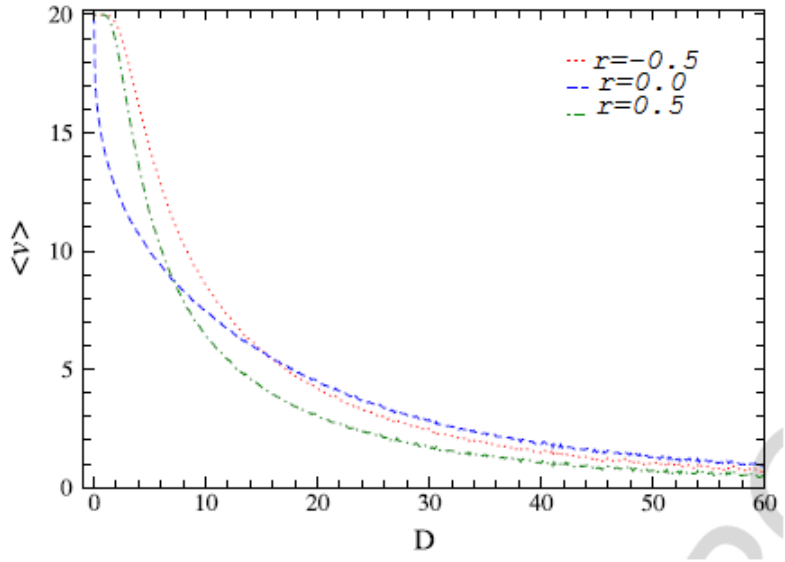

Figure 18: Mean velocity of the Brownian particle as a function of the intensity of noise D, for few values of the shape parameter of the travelling-wave potential, r = -0.5, 0.0, 0.5. Where F = 0, U = 20 and ω = 20.

III.3.3 Efficiency of generating force versus the external load

As stated before, the efficiency measures the capacity of a system to transform the input energy into useful work. The efficiency of generating force is obtained through numerical simulation of Eqs. (41), (74) and Eq. (77). Results of these simulations are plotted in Fig. 19, for some values of the shape parameter of the travelling-wave potential and

their corresponding analytical results. It can be seen in this figure that, for $r = 0$, there is a good agreement between numerical and analytical results. However, for $r = -0.5$ and $r = 0.5$, one observes also an enough good agreement between numerical and analytical solutions. It can be also seen, in this figure, that the efficiency of generating the force η_F is generally an increasing function of the external load F. Specifically, this increase of the efficiency in the travelling-wave potential is not only due to the external load and/or the low temperature regime, but is largely affected by the shape parameter of the system. For example, the maximum value of the efficiency η_F tends to 0.9435, 0.8979, 0.7438 for $r = -0.5, 0, 0.5$, respectively, as shown in Fig. 19. If the load increases continuously, the systems with positive shape parameter ($r < 0$) work efficiently even for large values of the load F, before dropping rapidly at a critical value F_{Max}. This value F_{Max} of the force represents, for each value of the shape parameter, the maximum value of the load that can be supported by the system and beyond or above, no useful work can be performed in the system any more. To gather insight on the influence of the shape parameter on the capacity of the Brownian motor to convert energy against an external load in the travelling-wave potential, Fig. 20a reports the maximum efficiency of generating force η_F(Max) as a function of the shape parameter r, for the same set of parameters used in Fig. 19. In Fig. 20b, the corresponding maximum values of the external load F_{Max} is depicted. It can be seen that $\eta_F(Max)$ is a decreasing function of the shape parameter r and tends to 0.94 as r tends to -0.8. The corresponding applied forces decrease also as a function of the shape parameter r. In general, for a fixed value of the speed of the travelling-wave potential and under the influence of the external load, the displacement of a Brownian particle in the system with broad wells and sharp barriers, namely $r < 0$, is done with a smaller loss of energy within the potential well. This implies a high efficiency of generating the force for an applied load less than or equal to the critical value F_{Max}, depending on the value of the shape parameter r. Thus, in the travelling-wave potential, broad well potentials favour the transport of Brownian particles in the presence of an external applied load.

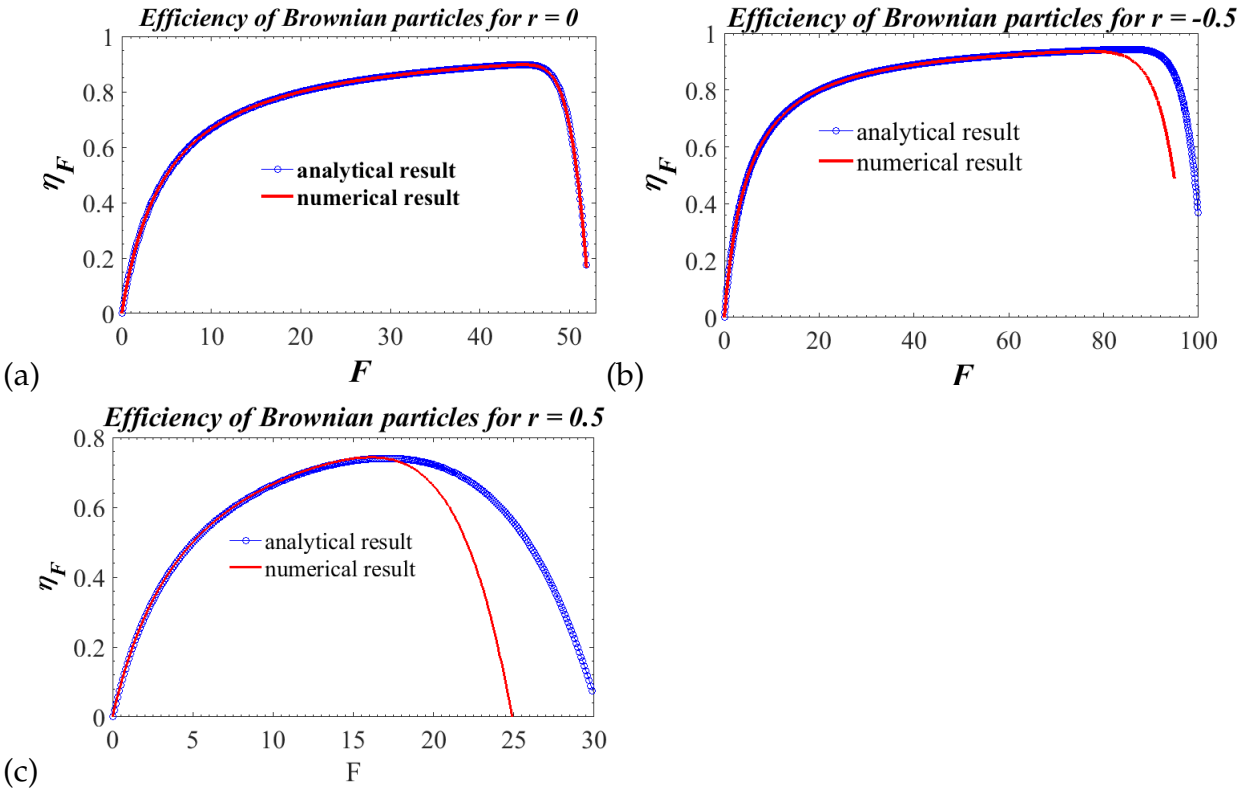

Figure 19: Efficiency of generating force as a function of F, for few values of the shape parameter r, with $D = 1$, $U = 60$ and $\omega = 5$.

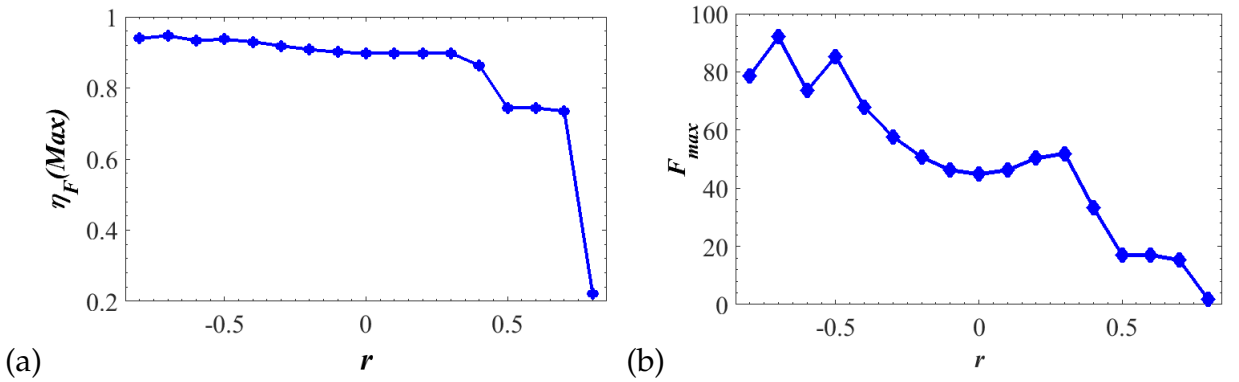

Figure 20: Maximum efficiency of generating force and maximum load F applied to the system to generate force as a function of r. The simulation parameters are the same as for Fig. 19.

III.3.4 Efficiency of transport versus driving speed

In the absence of the external load, Brownian motor works in a viscous environment. The efficiency of transport η_T of the Brownian motor is obtained from simulations of Eqs. (41), (75) and Eq. (77) and is represented in Fig. 21 as a function of the travelling potential speed ω, for few values of the shape parameter r of the system (r = -0.5, 0.0, 0.5), and for the following chosen set of parameters: U = 20, D = 0.5 and F = 0. This figure shows that η_T is widely influenced by the shape parameter r in the presence of

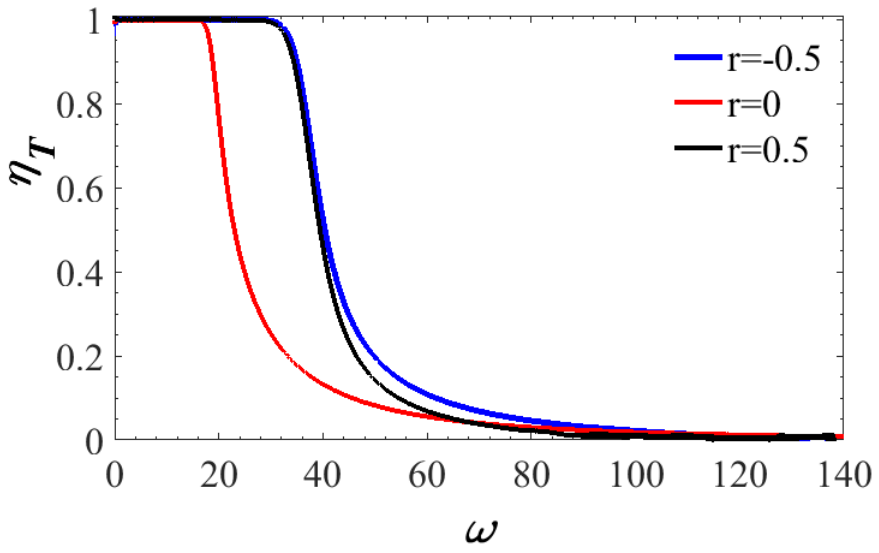

Figure 21: Efficiency of transport as a function of the travelling potential speed for three values of the shape parameter r, with U = 20, D = 0.5 and F = 0.

the travelling speed of the potential. Indeed, for $r \neq 0$, the unloaded transport efficiency of the Brownian particle remains equal to 1 up to a larger value of the travelling potential speed. Up to a critical value of this travelling potential speed, any increase of the speed leads to a monotonically decrease of the efficiency of transport to a nonzero constant value. This critical value of the travelling potential speed increases with the absolute value of the shape parameter r. In contrast to the case of the transport of Brownian motor in the presence of an external applied load, where the efficiency is an increasing function of the shape parameter r, the efficiency of transport evolves more or less the same for both positive and negative values of r. But, the relevant point here is that even

in the absence of any external load, the Brownian motor transport is more efficient in systems with a deformed potential for large speed of the travelling wave potential.

III.3.5 Effective diffusion in the overdamped Brownian motion

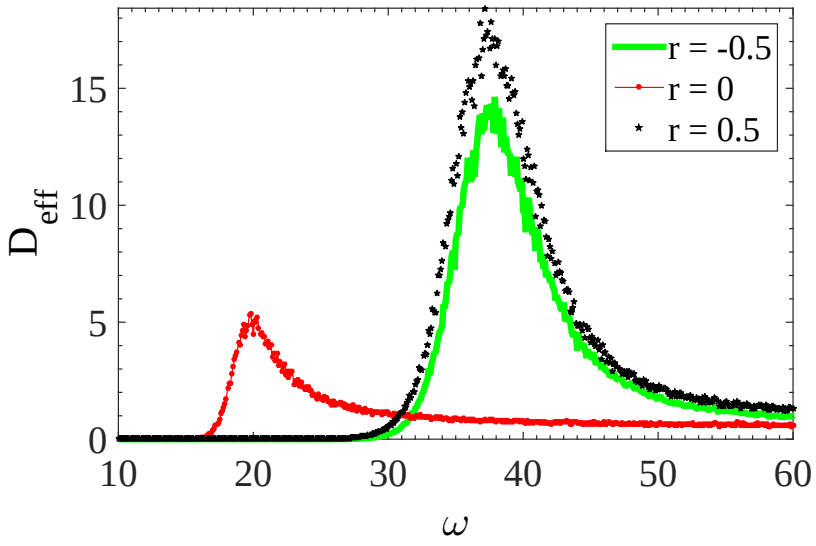

Figure 22: Schematic representation of the effective diffusion of the Brownian particle in the overdamped regime as a function of the travelling speed ω for few values of r. The other parameters are $U = 20$, $D = 0.5$, $\gamma = 1$.

The behavior of the effective diffusion coefficient of the Brownian particle D_{eff} as a function of the travelling speed of the deformable potential for different values of the shape parameter r is investigated in the overdamped case. It exhibits a pronounced "resonance" peak at $\omega = \omega_{opt}$, for different values of the shape parameter r (see Fig. 22). In fact, the presence of thermal fluctuations and/or the difference between the travelling speed of the potential and the velocity of the surrounding medium may induce the motion in the system, thus inducing the diffusion of a Brownian particle. The effective diffusion is closely linked to the geometry of the system since peaks change when the shape parameter varies from sinusoidal to nonsinusoidal case (see Fig. 22). For example, the peak of the effective diffusion coefficient is approximatively equal to 5, 14, and 18 times the Einstein diffusion ($D = k_B T/\gamma$) for $r = 0, -0.5$ and 0.5, respectively.

III.4 Underdamped limit

III.4.1 Average velocity in the underdamped Brownian motion

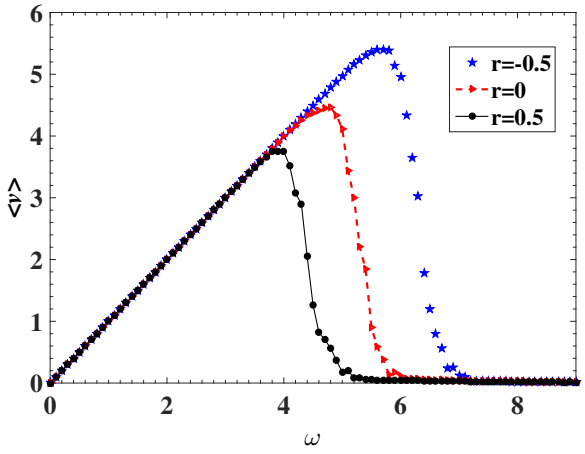

Figure 23: Representation of the average velocity as a function of ω, for different values of the shape parameter r, in the underdamped case. The transport properties are controlled by the shape parameter. The average velocity is higher for the negative value of the shape parameter, $r = -0.5$ than the positive values, $r = 0$ and $r = 0.5$. Note also that due to the presence of inertia, the potential energy is minimized. Other simulation parameters are $k_BT = 0.56$, $\gamma = 0.4$, and $m = 1$.

In this Section, we use the same numerical method as in the previous section to study the case in which the term $m\ddot{x}$ is not neglected. The results of numerical simulations of the average velocity of Brownian particles $\langle v \rangle$ as a function of the travelling speed ω of the deformable potential are plotted in Fig. 23, while the corresponding Monte Carlo error σ as a function of the traveling speed of the deformable potential ω is plotted in Fig. 24. It should be noted that in the underdamped case, the weight of the Brownian particle plays an important role in its displacement in the system. It helps to reduce the height of the potential barrier, as well as the time of displacement of the Brownian particle in the system. We can say that the dynamical behavior of the system, which is more regular, is controlled by the shape parameter r, as can be seen in Fig. 23. What is remarkable in this case is the behavior of Brownian particles whose average velocity decreases as the shape parameter r takes positive values. This behavior is contrary to what we

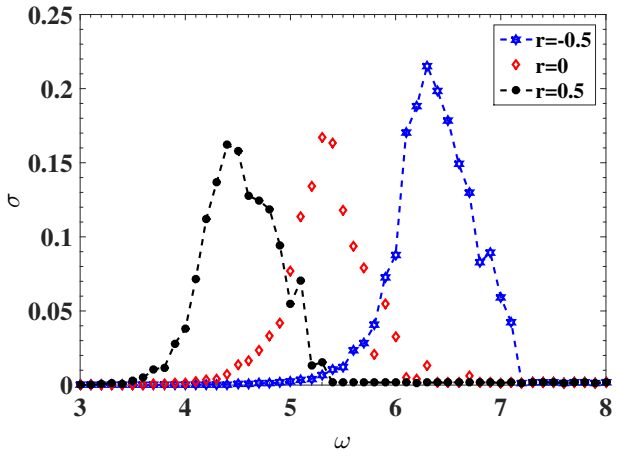

Figure 24: Monte Carlo error representation in the underdamped case. Other simulation parameters are $\gamma = 0.4$, $k_BT = 0.56$ and $m = 1$.

observed in Fig. 14 in the case of overdamped Brownian motion. In fact, we notice that in the overdamped case, more energy is needed for the Brownian particle to cross the potential barrier. Thus, in the overdamped and underdamped Brownian motions, this crossover energy depends strongly on the shape parameter r. Once the particle crosses the potential barrier, there is a smooth decreasing of the energy provided by the potential as ω increases and the Brownian particle slowly moves to a stable position where it oscillates. This behavior is illustrated by the smooth decrease seen in Fig. 14. Meanwhile, in the underdamped case, the influence of both inertia and damping contributes to lower the potential barrier, so that when the particle crosses the barrier, it jumps quickly to the equilibrium position (see Fig. 23). The Monte Carlo error plotted in Fig. 24 follows the same behavior as $\langle v \rangle$, but it always remains lower. Thus, in both cases (overdamped and underdamped), the Brownian particle moves in the directed direction. To gain good insight into the motion of the Brownian particle in the deformed travelling-wave potential in the underdamped case, we have plotted in Fig. 25 the maximum average velocity of the Brownian particle as a function of the shape parameter r, for several values of m, and the evolution of the average velocity obtained by direct simulation of Eq. (17) for m = 1 (Fig. 26). It is shown in Figs. 25 and 26 that the error bars are much pronounced in the underdamped case. However, in all cases, the maximum of $\langle v \rangle$ is a decreasing function of the shape parameter r. So, we observe that the maximum average velocity of

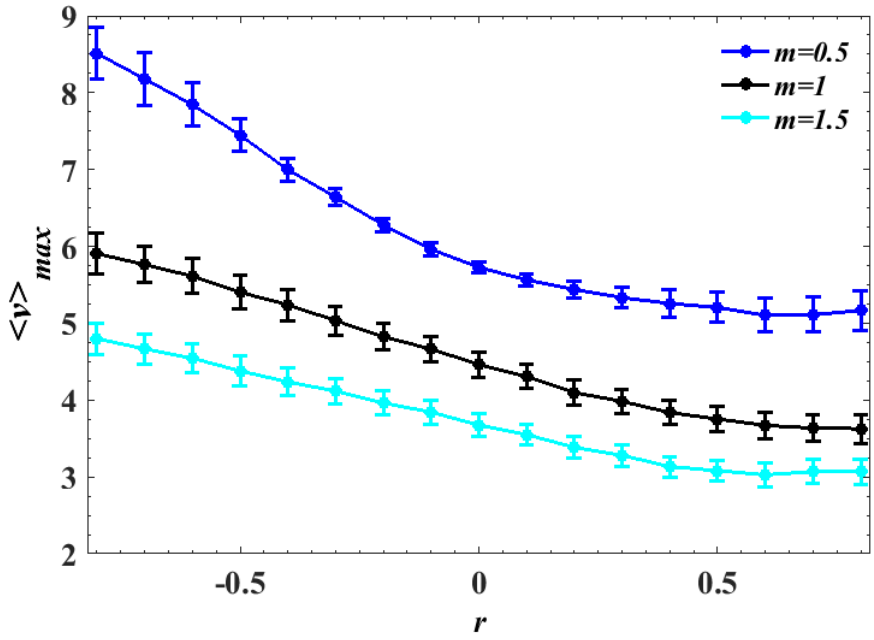

Figure 25: Schematic representation of the maximum average velocity of the Brownian particle as a function of the shape parameter r, in the underdamped case. Note here that, contrary to the overdamped case, the average velocity decreases as the shape parameter r evolves from negative values to positive ones.

Brownian particles increases when the mass of the system decreases, thus evolving into the overdamped case, where the error bars are weak (see Fig. 25). This behavior of the average velocity may be due to the complex displacement of the Brownian particle in the system in the presence of inertia and thermal noise. These results are in good agreement with the theory of the chaotic behavior in the system when inertia is taken into account [206]. Moreover, we observe an abrupt decrease of the average velocity of the Brownian particles as a function of the shape parameter r compared to the overdamped case. One can say that the inertia has a positive influence on the transport properties of the system since it reduces the effect of fluctuations in the system and controls the transport properties. This behavior of the Brownian particle in the underdamped case could be advantageous in the sense that even with lower energy, the unpinning of the system may be possible, but due to the inertia, the cargo may or may not reach the target.

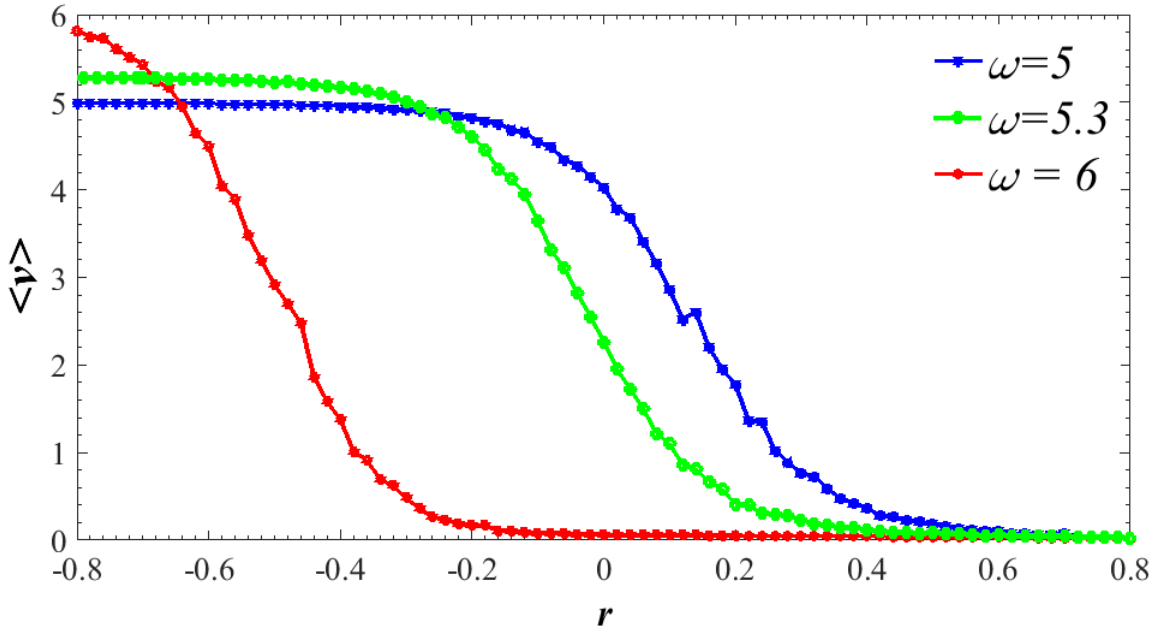

Figure 26: Numerical simulation of the average velocity as a function of the shape parameter r, for different values of ω. We can see the decrease of the average velocity as the shape parameter r evolves from negative values to positive values, for three values of the travelling potential speed. We also remark that the form of these curves follows the same shape as that of the Fig. 8. This decrease comes from the fact that the necessary thermal energy for the particle to make a transition to the adjacent potential well is less dissipated in the deformable potential with broad wells and narrow deep and the particle in this case holds a necessary momentum to cross the potential barrier. Other simulation parameters are $k_BT = 0.56$, $\gamma = 0.4$ and $m = 1$.

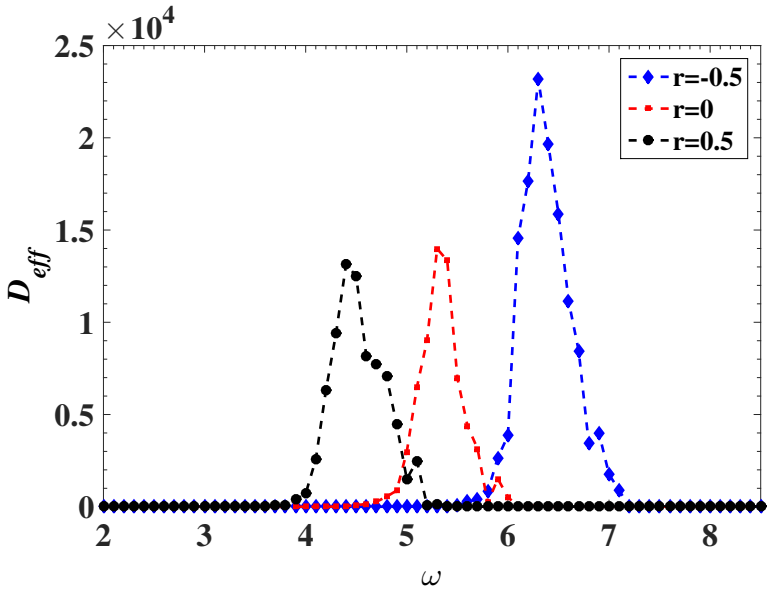

Figure 27: Plot of the effective diffusion D_{eff} as a function of the travelling potential speed ω for some values of shape parameter r ($r = -0.5$, $r = 0$, $r = -0.5$) as indicated in the figure. Other parameters of simulation are $U = 5$, k_BT = 0.56, $\gamma = 0.4$, and $m = 1$.

III.4.2 Diffusion in the underdamped Brownian motion

In Fig. 27, we depict the effective diffusion as a function of the travelling-wave potential speed ω, obtained numerically from Eqs. (17) and (31), for some values of the shape parameter r. Indeed, recent investigations have shown that under the effect of weak noise, and regardless of the value of the friction coefficient, there can appear a giant enhanced diffusion when the system undergoes an external constant load [7, 29, 207]. This is due to the presence of the locked-to-running transition that takes place when the Brownian particle diffuses on a one-dimensional periodic substrate and is subject to a weak tilt. However, it has also been demonstrated through a Fokker-Planck equation that, in the absence of external constant load, in the overdamped regime, a travelling-wave potential could induce a nonzero current $\langle \dot{x}(t) \rangle \neq 0$, if the total energy of the Brownian particle is higher than that of the potential barrier [46]. Thus, when the particle drifts under the force exerted by the potential, the random switches between locked and running states also take place and causes an average spreading $R(t) = \left\langle [x(t) - < x_{CM}(t) >]^2 \right\rangle$ of particles around its average position. In our case (see Fig. 27 for m = 1), this diffusion regime is very pronounced for negative values of the shape parameter r, and thus, the optimum values of the travelling-wave potential speed that can be generated by the shape parameter r are also higher for the negative values of r (deep barriers and broad wells) than the positive ones. Moreover, for each peak corresponding to each value of the shape parameter r, there exists a value of ω_{opt} for which the effective diffusion takes its maximum, which is slightly higher than that of the transition (ω_{opt}, for average velocity). Indeed, for $r = -0.5$, $\omega_{opt} = 6.3$, $D_{eff_{max}}$ = 2.3181 $\times$ 10^4; for $r = 0$, $\omega_{opt} = 5.3$, $D_{eff_{max}}$ = 1.398 $\times$ 10^4, and finally, for $r = 0.5$, $\omega_{opt} = 4.4$, $D_{eff_{max}}$ = 1.3158 $\times$ 10^4.

Next, we focus our attention on the effects of the shape parameter of the system on the peak values of the diffusion of Brownian particles in the underdamped case and the corresponding optimal deformable travelling-wave potential speed ω_{opt} for several values of m (m = 0.5, 1, 1.5).

To achieve this purpose, Fig. 28 represents two plots. In the upper panel of this fig-

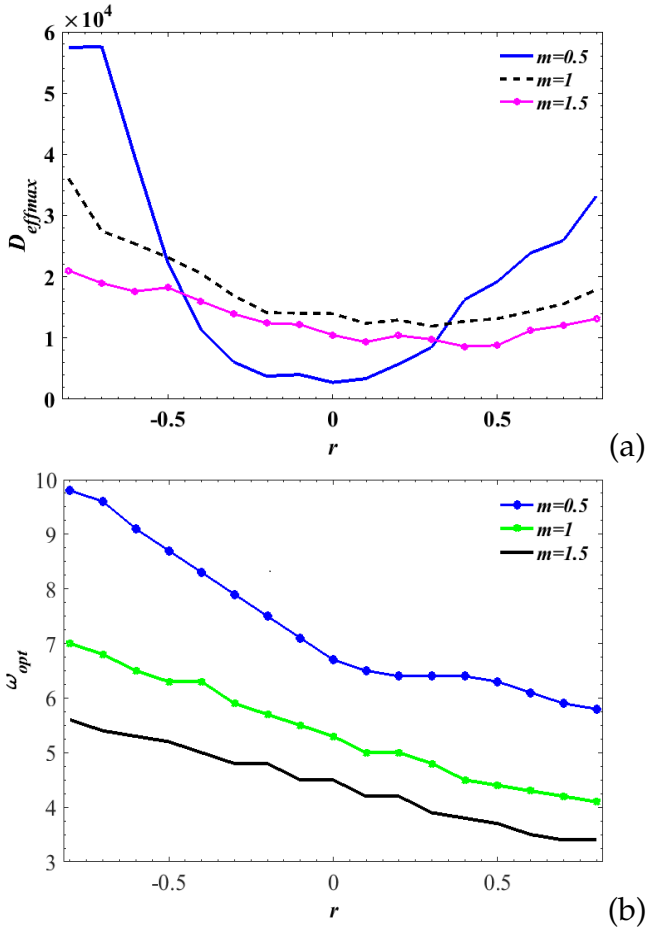

Figure 28: Maximum values of the effective diffusion for $m = 0.5, 1, 1.5$ of the Brownian particle and the corresponding travelling potential speed ω_{opt}, as a function of the shape parameter r.

ure, the maximum value of the effective diffusion of the Brownian particle as a function of the shape parameter r is plotted for m = 0.5, 1, 1.5. In the lower panel, the corresponding deformable travelling-wave potential speed ω_{opt} as a function of the shape parameter r is depicted for the same values of m. It can be seen in the upper panel of this figure that the maximum value of the effective diffusion is a decreasing function of the shape parameter r for m = 1 and 1.5. However, for m = 0.5, one notes an almost parabolic behavior of the maximum diffusion. One should note that this case obviously gets closer to the overdamped case. In the lower panel, the corresponding travelling potential speed ω_{opt} is also a decreasing function of the shape parameter r for all values of m. This behavior of the diffusion of the Brownian particle in the presence of the deformable travelling-wave potential may be due to the fact that, when the potential wells get narrow, the particle does not acquire the necessary space to cross the potential barrier, and then finds it difficult to disperse in the system, involving also the decrease of ω_{opt} as the shape parameter evolves from negative to positive values. To completely

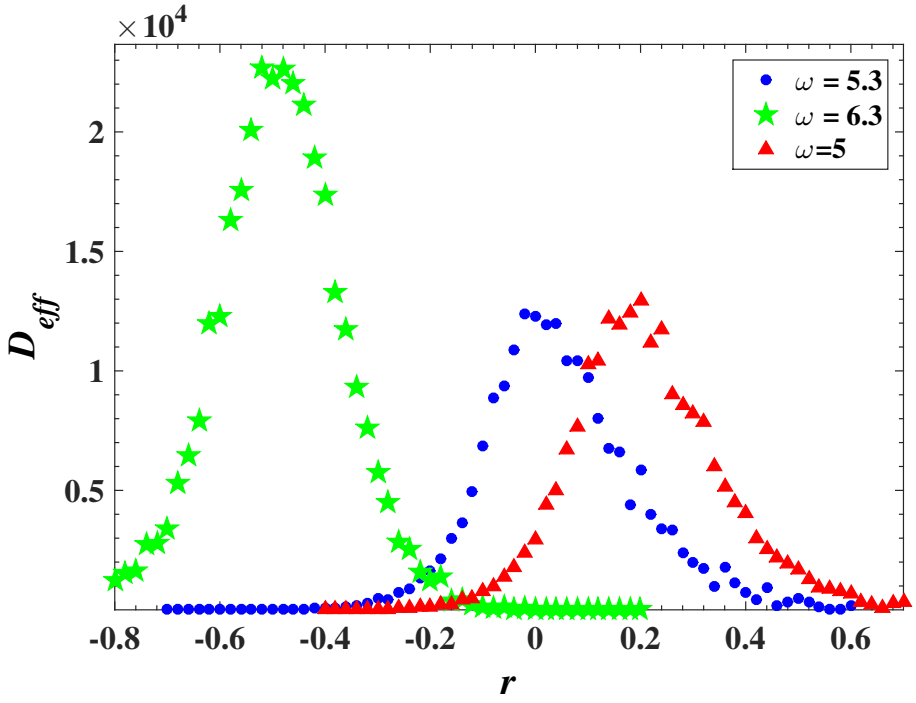

Figure 29: Effective diffusion as a function of the shape parameter r for a particle moving in the deformable travelling potential for some values of potential speed ω = 5, 5.3, 6, with the parameters previously used.

illustrate the behavior of the effective diffusion in the deformable medium, we plot, for m = 1 the effective diffusion as a function of the shape parameter r, for some values of the travelling-wave potential speed ω = 5, 5.3, and 6.3 (Fig. 29). When ω = 5 the red curve presents a maximum at r = 0.2. For ω = 5.3, the blue curve presents a maximum at r = 0. For ω = 6.3, the green curve shows a maximum at r = -0.5. As one might expect, the effective diffusion in this last case is very pronounced compare to the previous ones. This observation from numerical simulation corroborates effectively the previous observation, that is, in addition to the inertia term, the geometry of the potential, particularly the flat bottom, enhances the effective diffusion.

III.4.3 Fokker-Planck treatment in the underdamped Brownian motion

In this subsection, an analysis of the distribution for various shape parameters r is presented. These distributions are plotted for $r = -0.5$, $r = 0$ and $r = 0.5$ at $t = 1, 2$, in the phase space (x, v) and also, as the travelling potential speed is switched off ($\omega = 0$). Thus, by using the semi-analytic method (spectral method) developed in Chapter 2 as well as the numerical method (Finite element method), for $r = 0$, we observe in Figs. 30 and 31, the presence of two narrow peaks corresponding to the minimum of the potential. For $r = -0.5$, we observe a large peak which also corresponds to the minimum of the potential (see Figs. 32, 33). However, for $r = 0.5$, we observe a splitting of the number of peaks. Let us recall here that, the Fokker-Planck equation has been computed over two periods, characterized by the presence of two peaks. Indeed, for $r = -0.5$, the peaks are large compared to $r = 0$ and $r = 0.5$, respectively. This corresponds to a large dispersion of particles inside the potential well, indicating that the particles are spread out over a wider range of values due to the flat potential well and narrow barrier. However, for $r = 0.5$, which corresponds to a narrow well and flat barrier, we observe a splitting of the number of peaks which pass from two peaks to four peaks (see Figs. 34, 35). A similar behaviour is observed by adopting the semi-analytic method although

the two other peaks are not well visible. To explain all these behaviors, let us analyze the different periods of oscillation of particles in different forms of potential. The period of oscillation around the ground states in deformable potential is $T_r = 2\pi/\omega_r$, with ω_r = $V''(x_0)$, given by $\omega_r = \frac{U(1+r)^2}{1+r^2}$. Thus, the oscillation periods for $r = -0.5$, r = 0 and $r = 0.5$, are given by $T_1 = 10\pi U$, $T_2 = 2\pi U$ and $T_3 = 1.11\pi U$, respectively. In fact, the time that the particles take in shrink potential well to perform oscillations is smaller with respect to $r = 0$ and $r = -0.5$. For $r = 0.5$, as has been said before, the particles do not acquire the necessary momentum to cross potential barrier to the adjacent well and consequently, oscillate continuously around several equilibria position due to the thermal energy, so that the metastable positions can take place leading to the appearance of new extrema (multimodality) in the probability distribution.

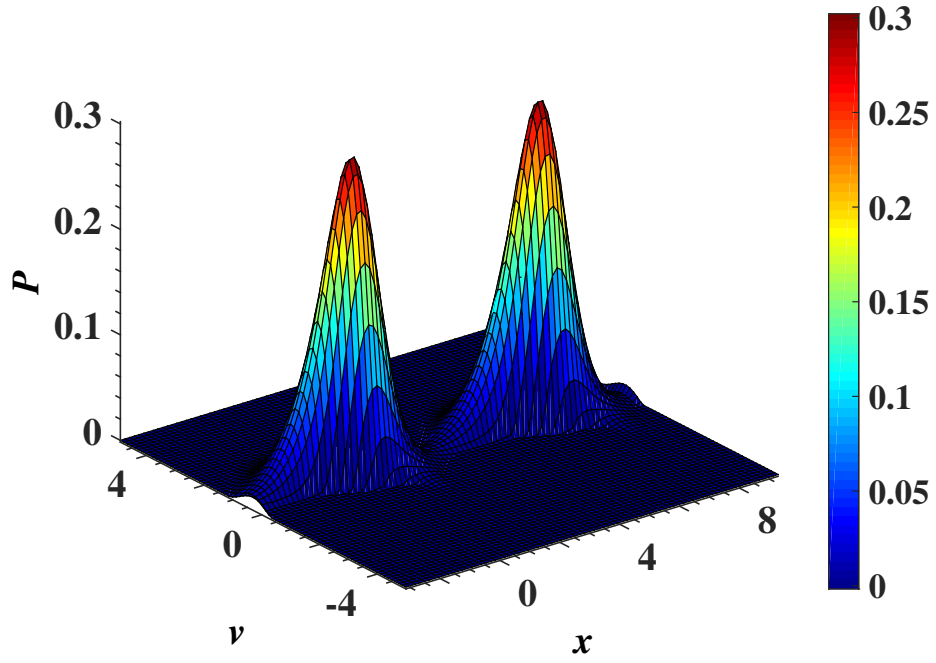

Figure 30: Approximate solution of the Fokker-Planck equation showing the distribution of the Brownian particle in deformable potential for $r = 0$ at $t = 1$. This case reduces to the sine-Gordon case. The distribution exhibits two peaks corresponding to two adjacent minima of the potential.

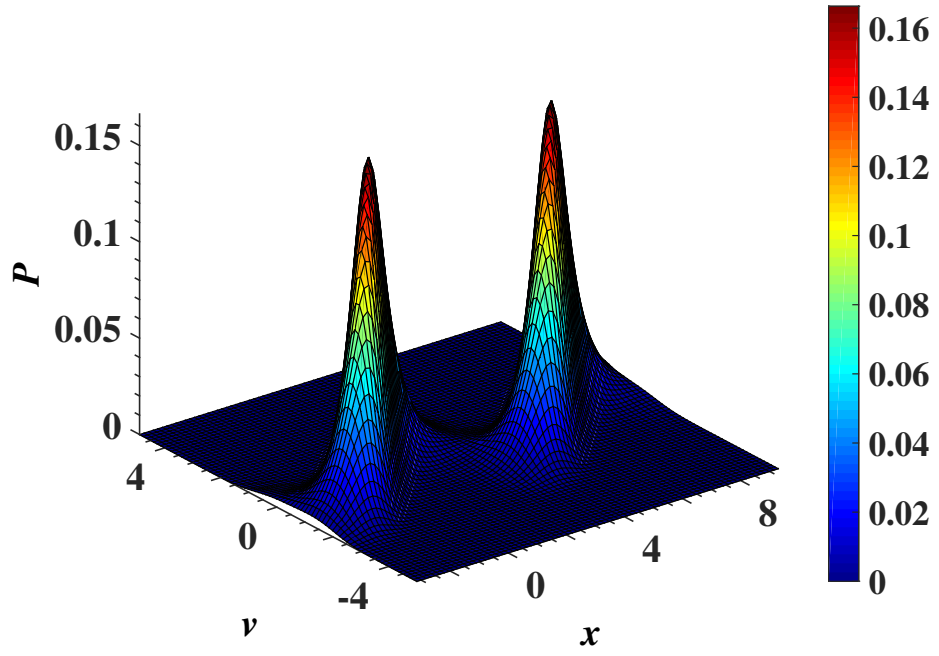

Figure 31: Numerical simulation of the Fokker-Planck equation in deformable potential for $r = 0$, obtained from the finite element method at $t = 1$.

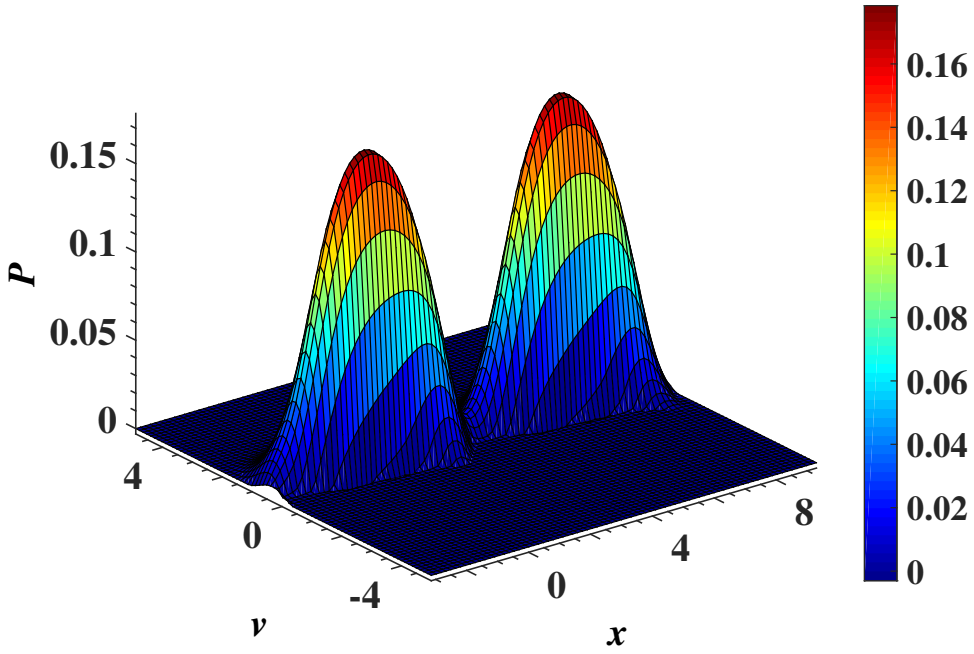

Figure 32: Approximate solution of the Fokker-Planck equation showing the distribution of the Brownian particle in deformable potential for $r = -0.5$ at $t = 2$. This case also exhibits two modes corresponding to two adjacent minima of the potential.

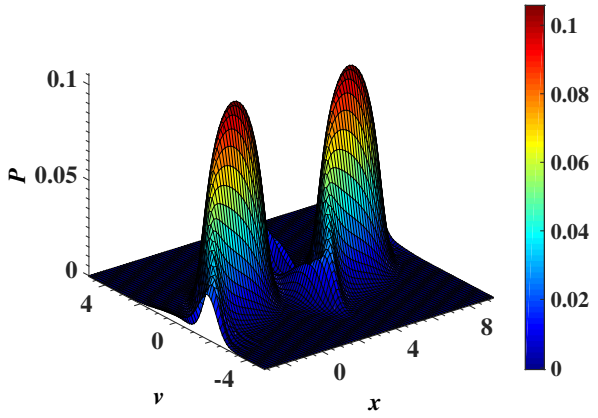

Figure 33: Numerical simulation of the Fokker-Planck equation in deformable potential for $r = -0.5$, obtained from the finite element method at $t = 2$.

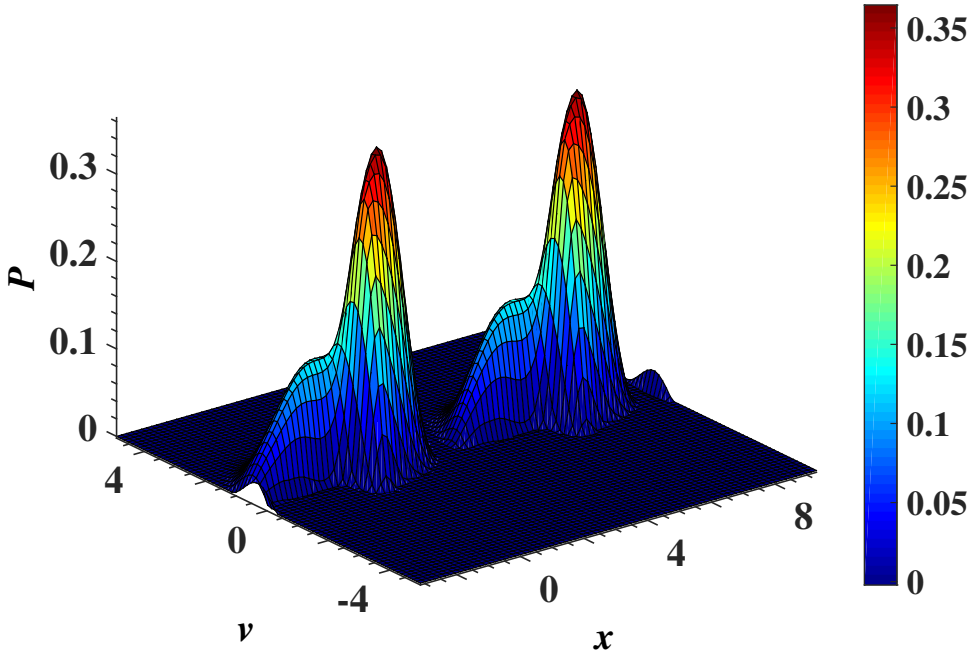

Figure 34: Approximate solution of the Fokker-Planck showing the distribution of the Brownian particle in deformable potential for $r = 0.5$ at $t = 2$. This case tends to split in several modes.

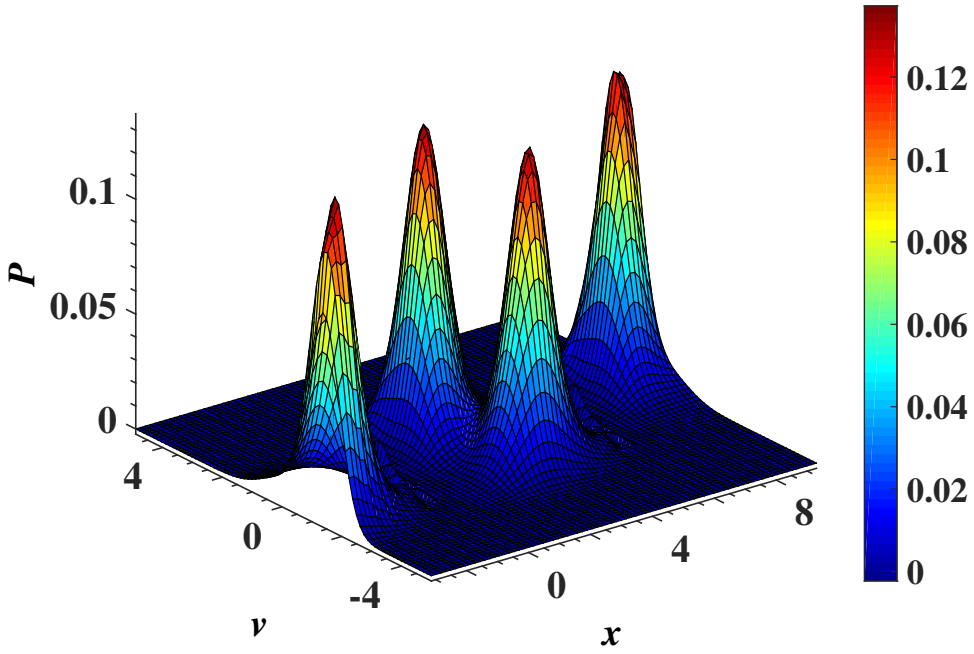

Figure 35: Numerical simulation of the Fokker-Planck equation in deformable potential for $r = 0.5$ at $t = 2$, obtained from the finite element method. We observe a complete splitting of modes which pass from two modes in previous cases to four modes. This may be due to the metastable states that take place in the system, which is due to deep wells potential and broad barriers.

III.5 Transport properties of Brownian particles in the deformable potential in the presence of an external load

In this subsection, results on the dynamics and diffusion of the underdamped Brownian particles are displayed and commented as a function of the shape parameter r, in presence of an external load.

III.5.1 Bistable behavior of velocity of Brownian particles and its corresponding distribution

In Figs. 36-39, we have plotted the asymptotic long-time velocity of Brownian particles as a function of time for some values of the shape parameter, $r = 0$, $r = -0.5$ and $r = 0.5$, for different mean thermal energy k_BT, and external forces. We have associated with these asymptotic long-time velocities $v(t)$ their corresponding probability distributions $P(v)$. So, in Figs. 36 and 39, the behaviour of velocities of particles and the probability distributions exhibit similar features. Indeed, in Fig. 36, we plot the velocity of Brownian particles and the probability distribution for r=-0.5, 0, and 0.5 for some values of the mean thermal energy in the case $k_BT = 0.03$ for $r = -0.5$, $k_BT = 0.02$ for $r = 0$, and $k_BT = 0.06$ for $r = 0.5$. In Fig. 39, we represent the behaviour of velocities and the probability distribution $P(v)$ of particles for r=-0.5, 0, and 0.5 for $f = 0.5$. We observe that for the given values of the mean thermal energy and external force, the distribution of particles $P(v)$ boils down to a single-peaked Maxwell distribution, around $v \approx 0$. This indicates that for the three values of the shape parameter r, the particles are mainly trapped in potential wells regardless the shape of the potential. The mean thermal energy and external force provided to the system are not sufficient to making the particles cross the potential barriers. In Fig. 37, for the three values of the shape parameter r and $k_BT < \omega_0^2$, the velocity exhibits a bistable behaviour as found in Ref. [29]. This behaviour is characterized by the presence of two discrete states, i.e, the locked state, where, due to small forces, Brownian particles remain at the minima during large

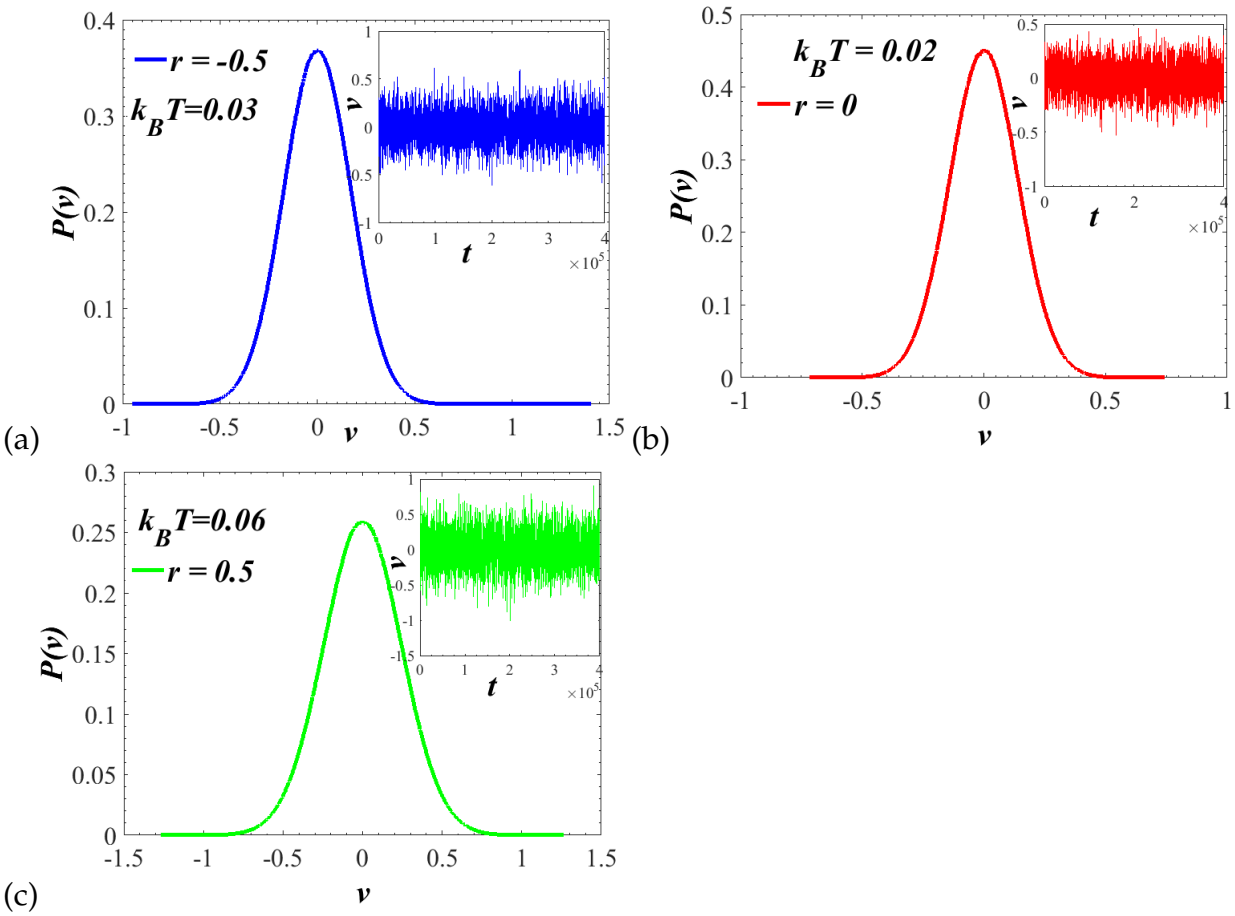

Figure 36: Plot of transitions of Brownian particles, associated with the different transition distribution in the deformable potential, for three values of the shape parameter r: r=-0.5, 0, and 0.5 for $k_BT = 0.06$. We can see that the distribution probability exhibits a single-peaked Maxwell distribution for all of the three values of the shape parameter r. In these cases there exist only locked solutions due to the weak value of the mean thermal energy. We used $f = 1$, for $r = -0.5$, $f = 0.72$, for $r = 0$, and $f = 0.72$, for $r = 0.5$. The dissipation coefficient used is $\gamma = 0.4$.

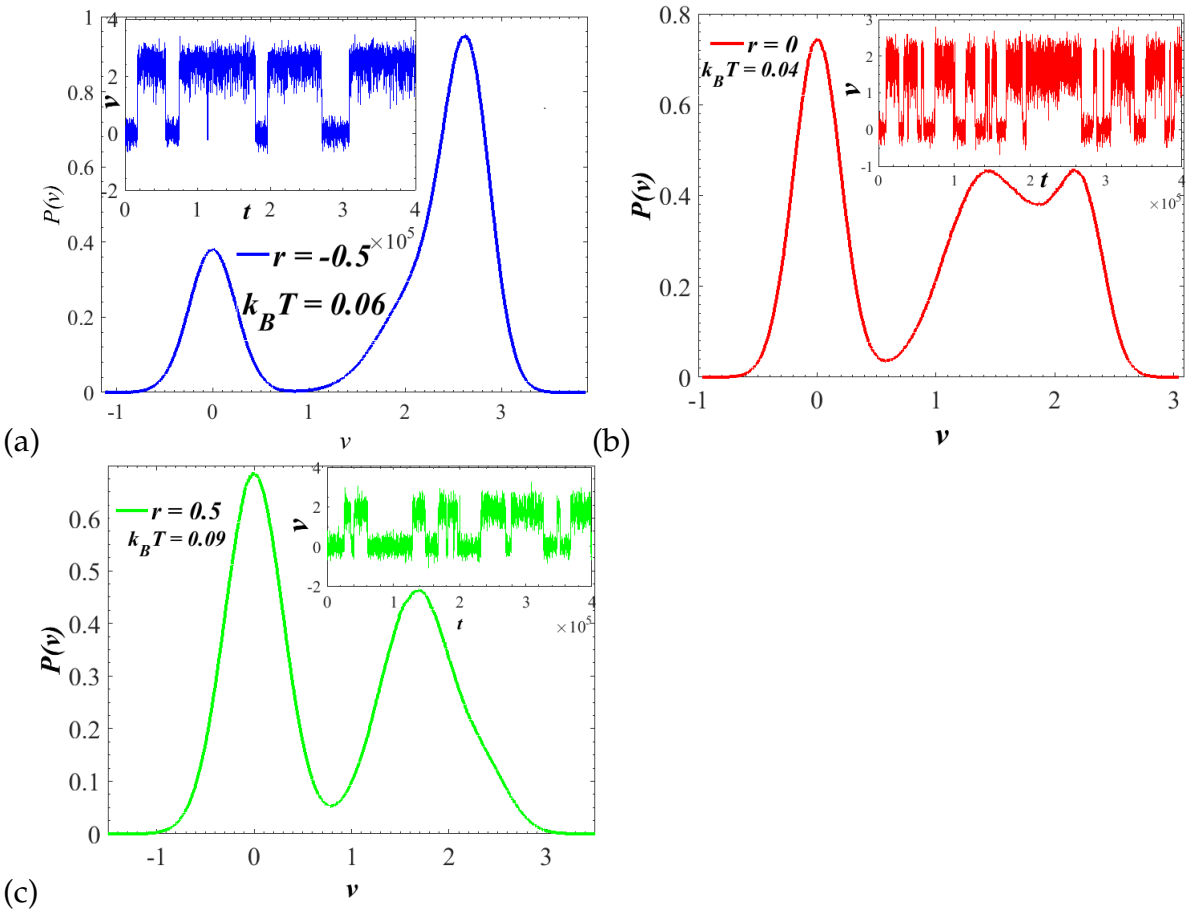

Figure 37: Plot of transitions of Brownian particles, associated with the different transition distribution in the deformable potential, for three values of the shape parameter r: $r = -0.5$, $k_BT = 0.06$, $f = 1$ is given by the blue curve; $r = 0$, $k_BT = 0.04$, $f = 0.72$ the red curve, while $r = 0.5$, $k_BT = 0.09$, $f = 0.72$ is given by the green curve. The dissipation coefficient is $\gamma = 0.4$

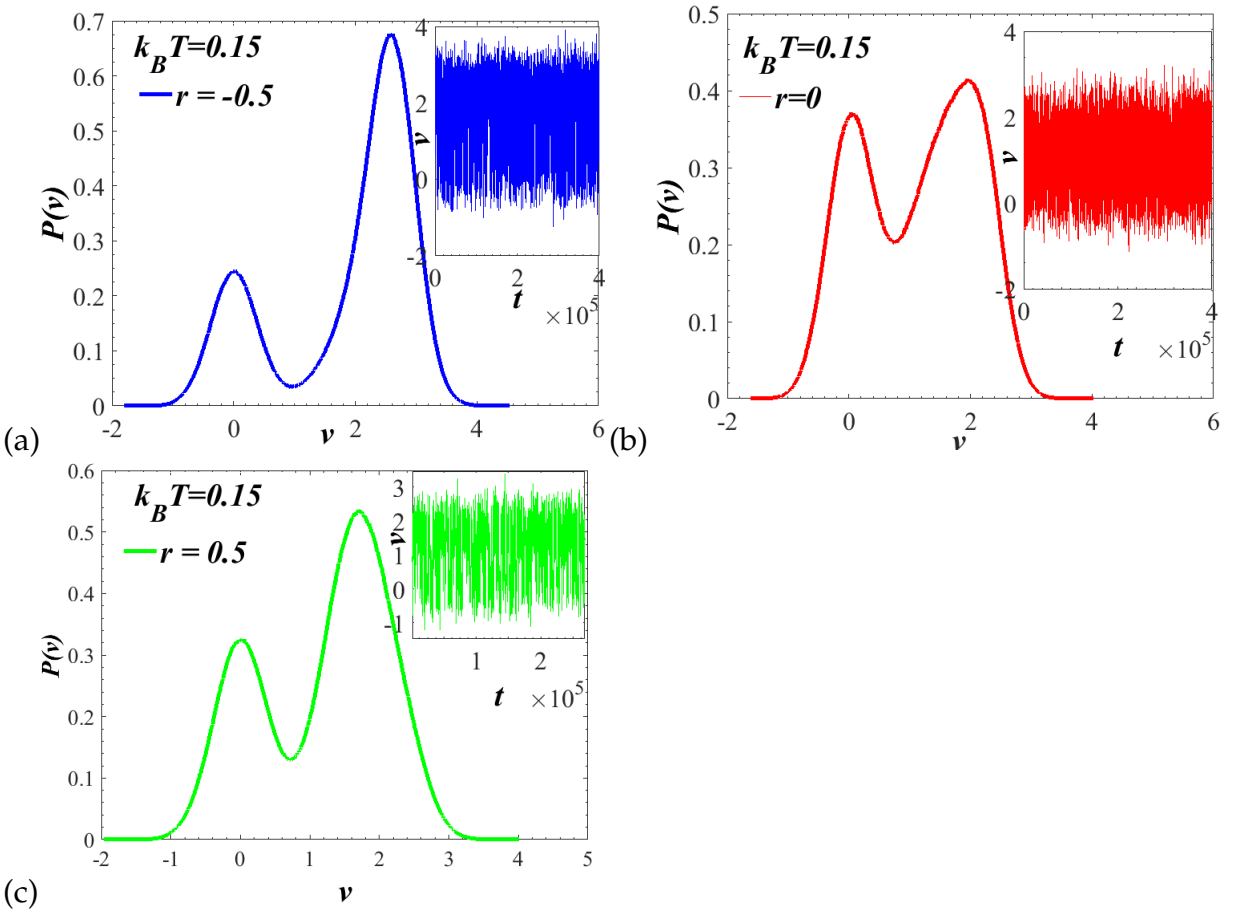

Figure 38: Plot of transitions of Brownian particles, associated with the different transition distribution in the deformable potential, for three values of the shape parameter r: r=-0.5, 0, and 0.5 for $k_BT = 0.15$. We can see that the distribution probability exhibits two peaks for all of the three values of the shape parameter r. We used $f = 1$, for $r = -0.5$, $f = 0.72$, for $r = 0$, and $f = 0.72$, for $r = 0.5$. The dissipation coefficient used is $\gamma = 0.4$.

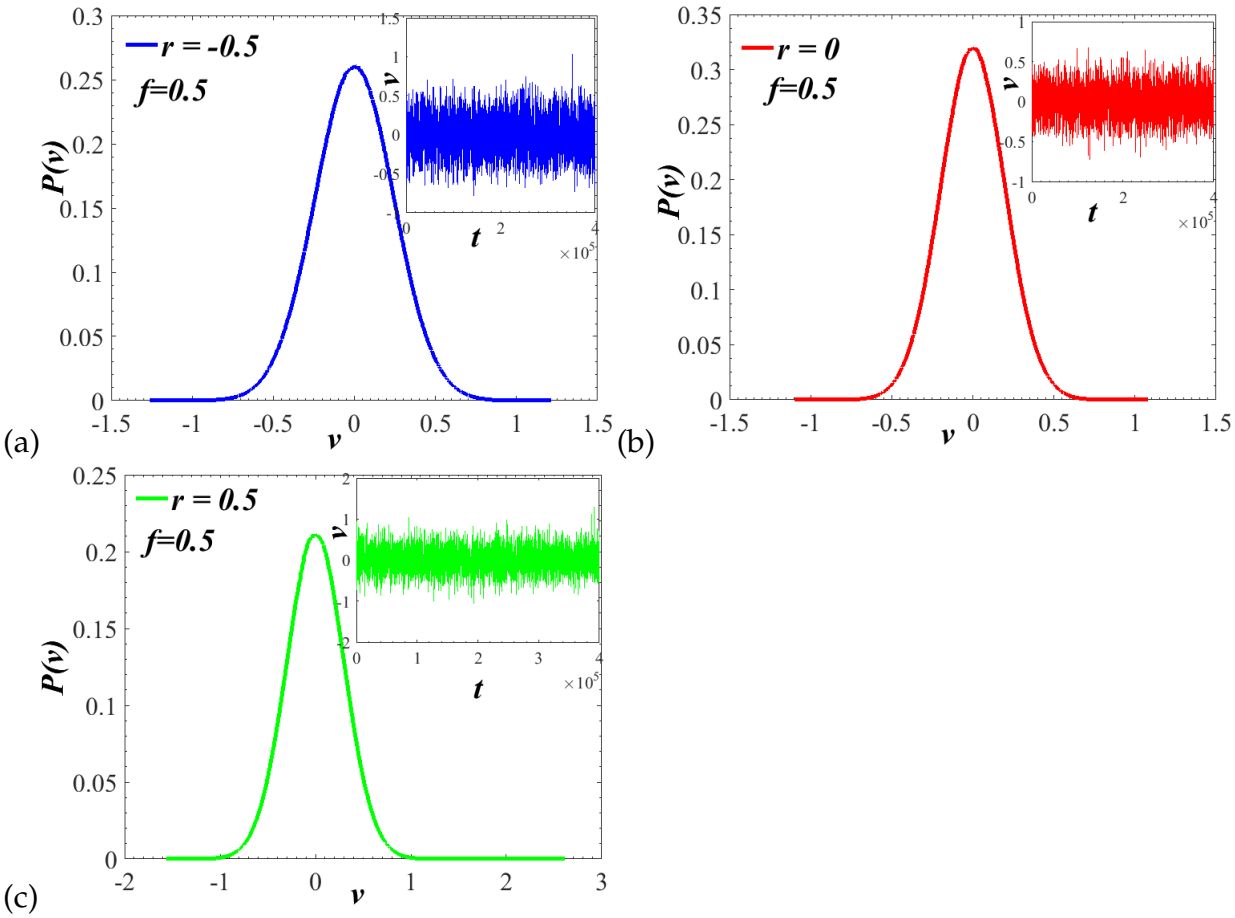

Figure 39: Plot of transitions of Brownian particles, associated with the different transition distribution in the deformable potential, for three values of the shape parameter r: r=-0.5, 0, and 0.5 for $f = 0.5$. We can see that the distribution probability exhibits a single-peaked Maxwell distribution, because this value of the external force does not allow particles to make transition from a well to another one, for the three values of the shape parameter r. We used $k_BT = 0.06$, for $r = -0.5$, $k_BT = 0.04$, for $r = 0$, and $k_BT = 0.09$, for $r = 0.5$. The dissipation coefficient used is $\gamma = 0.4$.

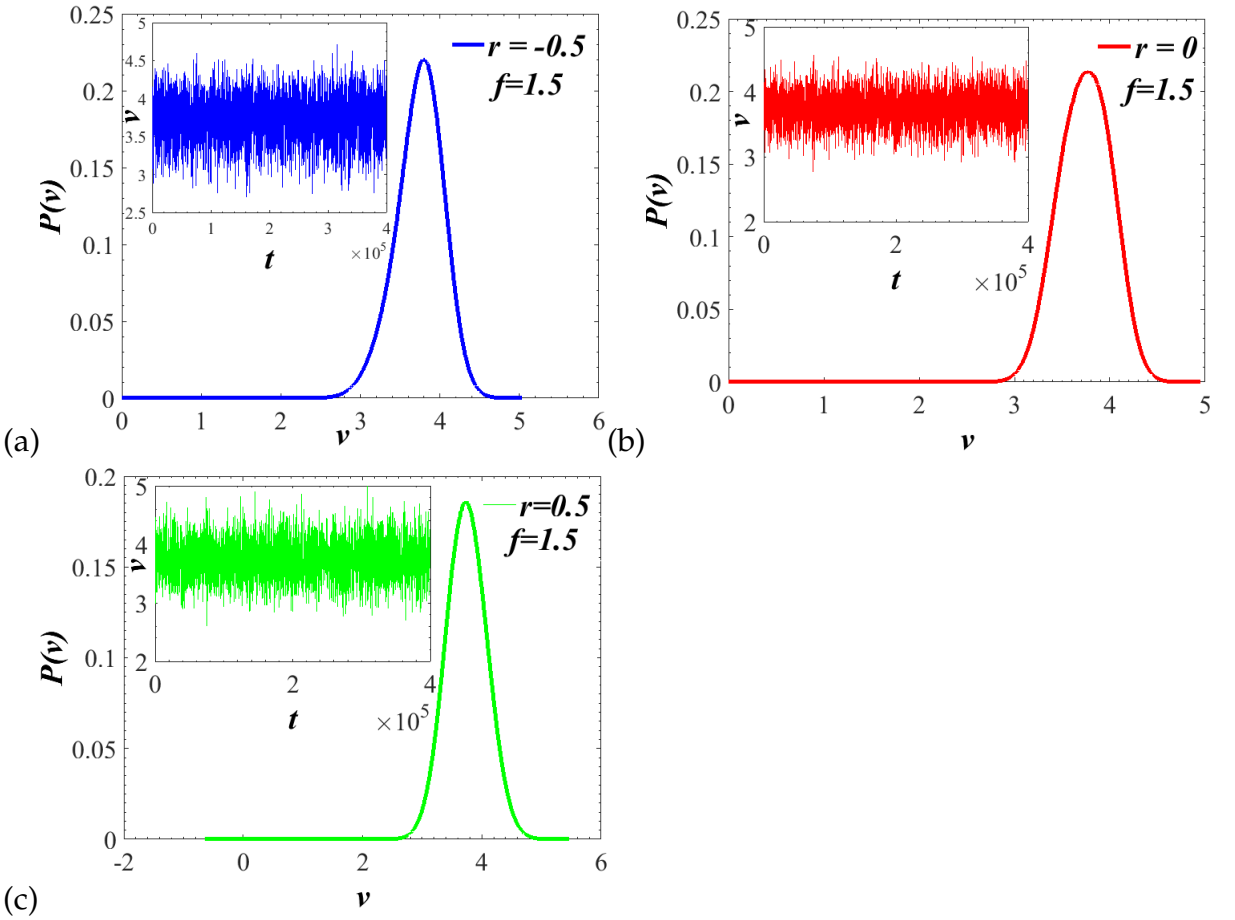

Figure 40: Plot of transitions of Brownian particles, associated with the different transition distribution in the deformable potential, for three values of the shape parameter r: r=-0.5, 0, and 0.5 for $f = 1.5$. We can see that upon increase of the external force, there are more running solution that locked solutions. We used $k_BT = 0.06$, for $r = -0.5$, $k_BT = 0.04$, for $r = 0$, and $k_BT = 0.09$, for $r = 0.5$. The dissipation coefficient used is $\gamma = 0.4$.

sojourn with zero velocity, and the running state, where Brownian particles jump away because of large forces. In general, under the action of an external load, the total periodic potential tilts. Thus, for large forces f, the potential has no minima, and in this case, the average velocity of particles saturates to the free particle value $v_0 = f/\gamma$. With regard to Fig. 37, different curves exhibit transitions from one bottom to another. These transitions depend on the shape parameter r of the deformable potential. It should be noted that although the three curves exhibit the phenomenon of bistability, this occurs with different mean thermal energies and external forces for the three values of the shape parameter r. For $r = 0.5$, $k_BT = 0.09$, and $f = 0.72$, for $r = -0.5$, $k_BT = 0.04$, and $f = 1$, one can remark that the mean thermal energy, whose the Brownian particle needs to cross the potential barrier, is high in the case of $r = 0.5$ than that of $r = -0.5$ and $r = 0$. Therefore, for $r = 0.5$, Brownian particles are easily pinned at the one-site of the lattice and require an extra thermal energy to perform transitions between the two discrete states, namely the locked and running states. This is because, under the action of the inertia effect, the potential with broad barriers and narrow wells exhibit large radiations coming from the phonon bath. Consequently, Brownian particles do not acquire necessary transfer momentum to overcome the potential barrier, hence require additional thermal energy.

Always in Fig. 37, by analyzing the probability distributions of the long-time velocity, we observe a fine asymmetry of the probability distribution for the three cases of the shape parameter. It is also relevant to note that for the three values of the shape parameter *r*, the distribution are nearly Maxwellian around $v \simeq 0$ [184, 208, 209]. For $r = 0.5$ and $r = -0.5$, for a vanishingly small damping value, the transition threshold is characterized by a bimodal distribution of the velocity with peak at $v \simeq 0$, describing the locked state which indicates that the particles are mainly trapped in potential wells for the deformed system, and $v = f/\gamma \simeq 1.698$ and $v = f/\gamma \simeq 2.629$, corresponding to the free running Brownian particles pulled by the external force, respectively. However, for $r = 0$, the distribution probability $P(v)$ exhibits three peaks. One should note that this multi-modal form of the distribution probability was not expected. Indeed, we connected, at the beginning, this result to the "running" solutions. We therefore thought

that by varying the parameters of interest of the system, the same behaviour could occur for $r = -0.5$ and $r = 0.5$. It turned out that this conjecture is incorrect since, as we can see in Figs. 38 and 40, by increasing the mean thermal energy of the system, we recover two peaks for the three values of the shape parameter r, see Fig. 38. In Fig. 40, by increasing the external force, there are more running solutions. We further checked the outcome for the velocity distribution when reflecting barriers were placed at the maxima of the potential. Under such constraint, we recovered as well the three-peaks structure. We can assimilate this characteristic behaviour of the three peaks in the case $r = 0$ to the nonlinear, anharmonic character of the corresponding well of the periodic asymmetric sinusoidal potential.

III.5.2 Average velocity of Brownian particles

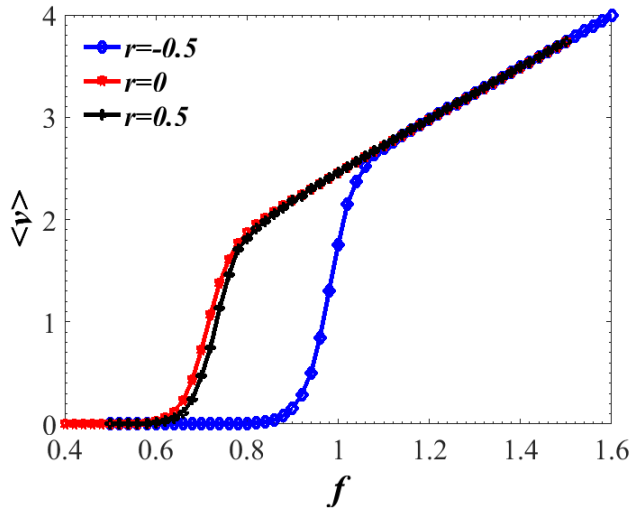

Figure 41: Average velocity of Brownian particles in deformable potential for some values of the shape parameter: $r = -0.5$, $r = 0$, $r = 0.5$. Other parameter values: $k_BT = 0.094$, $\omega_0 = 1.0$, $\gamma = 0.4$.

The asymptotic average velocity of the particles, as a function of f, is illustrated in Fig. 41, at fixed mean thermal energy k_BT, for some values of the shape parameter r, namely r=-0.5, 0, and 0.5. Qualitatively, the behaviour of particles does not change no matter what the shape parameter r. Thus, in the three cases representing the different

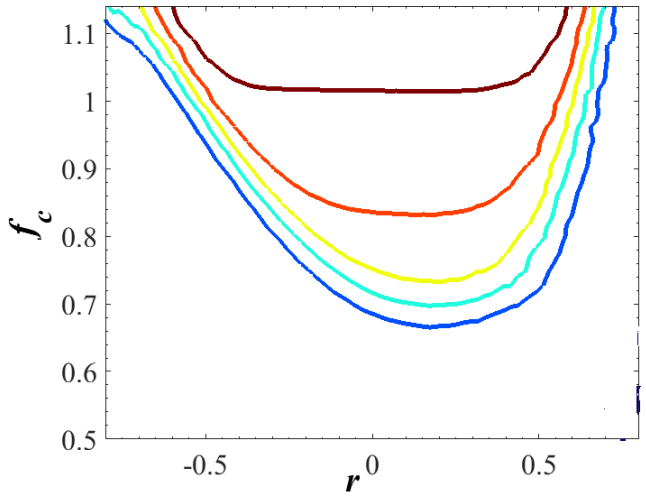

Figure 42: Contour plot of velocity showing how the force varies vs the shape parameter with the same parameters previously used.

values of the shape parameter, the average velocity rises quickly as particles emerge from wells, and settles to its steady state value in time. However, it should be noted that the critical forces inducing transitions depend on the shape parameter r namely, all velocities do not intersect at the same value of the external force. The critical force, which is the force from which the particles cross the potential barriers for the different shape parameters r, are given by $f_c \simeq 0.72, 0.74$ and 0.98, for $r = 0, 0.5$ and -0.5, respectively. So, the more the wells are flat, the critical force is high as it is illustrated in Fig. 42, showing the different critical forces as a function of the shape parameter. Indeed, the external force f determines the degree of tilt (asymmetry) of the effective deformable potential $U(x, r)$, and therefore, dominates the direction of movement of Brownian particles. The dynamics of the average velocity can be understood also by considering the magnitude of the slope of the potential. Thus, beneath the action of f, the slope of the potential with broad wells and narrow barriers is higher compared to the potential with narrow wells and broad barriers. Therefore, the Broad wells activate the inertia effects, which gives impetus for particles to cross the barrier. The higher average velocities indicate also that the energy of the system grows monotonically as the system deforms away from a specified shape and often includes terms that constrain the smoothness or symmetry of the model.

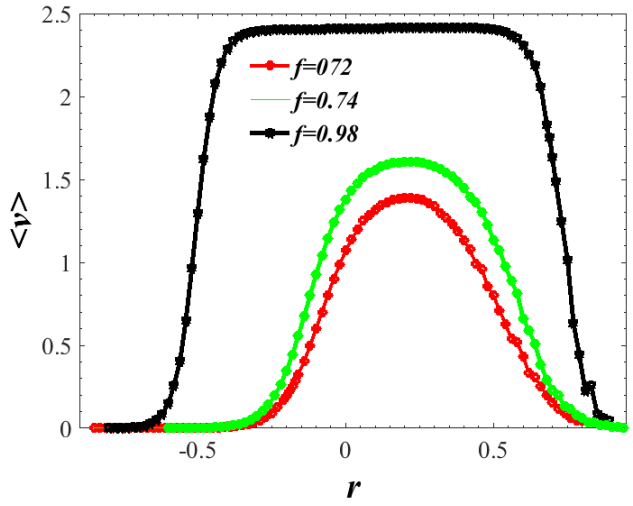

Figure 43: Average velocity of Brownian particles in the deformable potential as a function of the shape parameter for some values of the external load: $f = 0.72$, $f = 0.74$, $f = 0.98$. Other parameter values: $k_BT = 0.094$, $\omega_0 = 1.0$, $\gamma = 0.4$.

For a fixed value of the dissipative friction coefficient, we have plotted, in Fig. 43, the average velocity of Brownian particles as a function of the shape parameter r, for some values of the external force, namely $f = 0.72$, 0.74, and 0.98. Globally, the average velocity of Brownian particles is an increasing function of the negative values of the shape parameter corresponding to the potential with broad wells and narrow barriers, while it is the decreasing function of the positive values of the shape parameter corresponding to the potential with narrow wells and broad barriers for different external forces. In fact, for values 0.72 and 0.74 of the external force, the average velocity of Brownian particles behaves like an exponential law as a function of the shape parameter r. This shows that the average velocity of Brownian particles increases when increasing the shape parameter r, reaches a maximum corresponding to an optimal value of the shape parameter $r_{opt} \simeq 0.2$, and then, decreases back to zero at the large values of the shape parameter r corresponding to the shrinking of the potential wells. While for $f = 0.98$, the average velocity of Brownian particles increases until a value of the shape parameter $r \simeq -0.45$ and saturates until a value of the shape parameter $r \sim 0.6$. From this value of the shape parameter, the external force combined to the thermal energy no longer allows the particles to cross the potential barrier. $r_{opt} \simeq 0.2$ is the value of the shape parameter for which

the forces 0.72 and 0.74 easily induce a transition, allowing the particles to perform the directional motion towards the right.

When the particles cross the wide potential wells to the narrow potential wells, there is a decrease of the energy of the system due to the radiation at an on-site potential of the lattice associated with the dissipative force. This favors the slow down of the average velocity of Brownian particles, so that they oscillate at the bottom of the potential wells, which are quite narrow, being damped by the radiation and the friction coefficient. Under such effects, particles require additional thermal energy and/or an increase of the external force, which will allow them to jump the potential barrier such as after each jump. The system is allowed to relax before the next jump takes place. The potential with broad wells and narrow barriers facilitates sliding of the Brownian particles, because the particle acquires easily the necessary momentum to cross the potential barrier.

This potential, whose the shape changes, could appear useful for optimization of the directed transport, controlling the motion of Brownian particles in order to improve the conductivity in some artificial devices according to the shape parameter.

III.5.3 Effective diffusion coefficient of Brownian particles

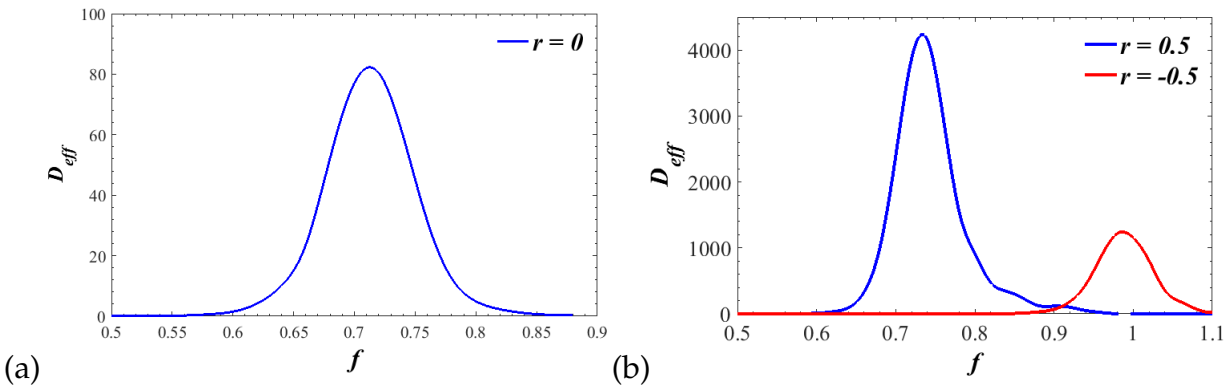

Figure 44: (a) The effective diffusion coefficient of Brownian particles as a function of the external force for $r = 0$. (b) The effective diffusion coefficient of Brownian particles as a function of the external force for $r = 0.5$ and $r = -0.5$. The effective diffusion coefficient for three values of the shape parameter grows many order of magnitude when the shape of the potential varies. Other parameter values: $k_BT = 0.094$, $\omega_0 = 1.0$, $\gamma = 0.4$.

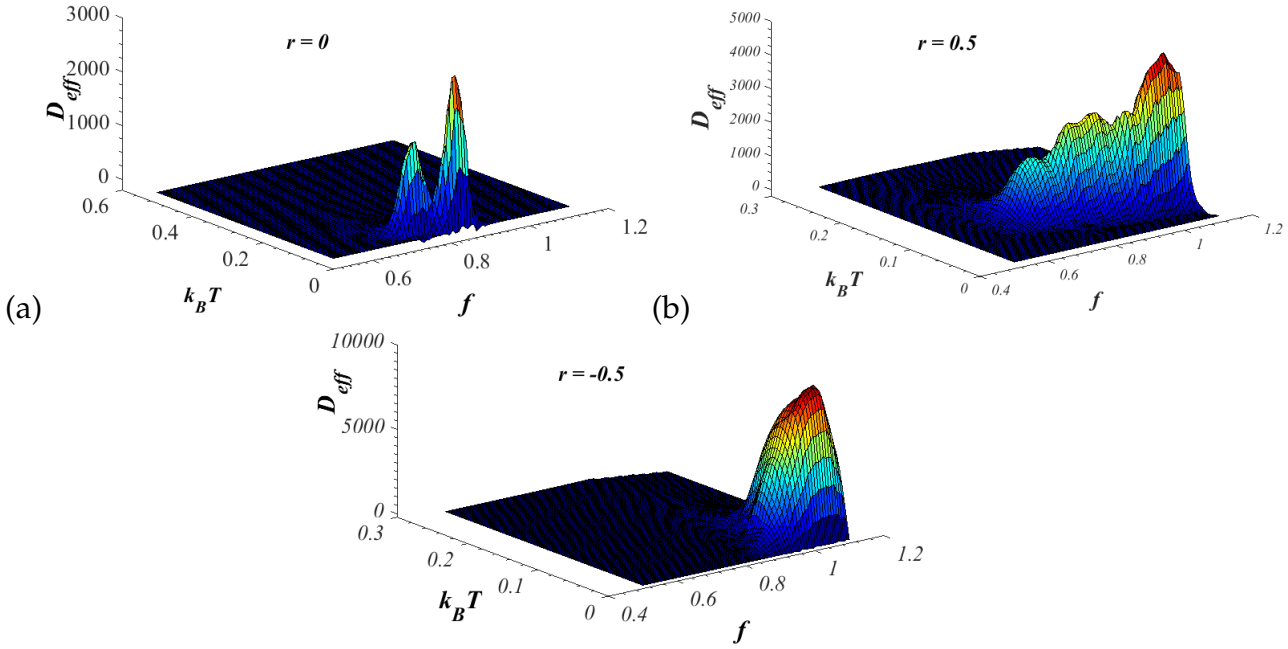

Figure 45: Three dimensional representation of the effective diffusion coefficient as a function of thermal energy and the external force, for $r = 0, 0.5$ and -0.5. The effective diffusion coefficient decreases with the temperature of the system. Other parameter values: $\omega_0 = 1.0$, $\gamma = 0.4$.

In Fig. 44, the effective diffusion coefficient of Brownian particles is plotted as a function of the external force for some values of the shape parameter r. In Fig. 44a, the effective diffusion coefficient is plotted for $r = 0$, while in Fig. 44b, the effective diffusion coefficient is plotted for $r = 0.5$ and $r = -0.5$, respectively. Indeed, in the periodic system [29, 205, 207, 210, 211], the effective diffusion coefficient in the underdamped limit grows several orders of magnitude in a particular domain of the external force f and meanwhile, becomes larger at smaller values of the temperature of the system. This is due to the locked-to-running transition that takes place in the system when the Brownian particle diffuses on a 1D periodic substrate potential and is subject to a macroscopic gradient of the potential and/or temperature. As is shown in Fig. 44, for the three cases of the shape parameter r, the geometry of the system induces an enhancement diffusion, albeit the value of the temperature of the system and the peaks in the effective diffusion coefficient D_{eff} versus the force f which is detectable in the vicinity of the transition force f_c, and which is a function of the shape parameter r. For $r = 0$, the critical force is

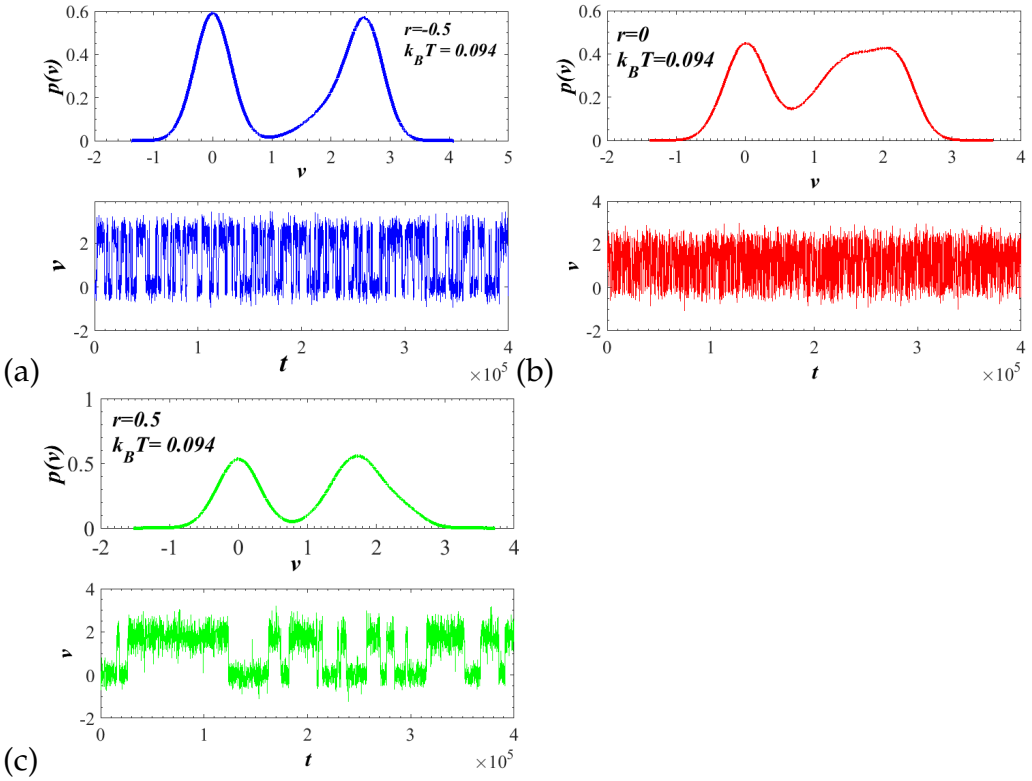

Figure 46: Plot of the transition of Brownian particles, associated with the different transition distribution in the deformable potential, for three values of the shape parameter r: r=-0.5, 0, and 0.5. For $r = -0.5$, $f = 0.98$, for $r = 0$, $f = 0.72$, and for $r = 0.5$, $f = 0.74$. As we can see, for their critical force, there are more transitions between locked and running states for $r = 0$ and $r = -0.5$ than $r = 0.5$. This moderate amount of occurrence of transitions in the case $r = 0.5$ promotes an excess diffusion peak.

given by $f_c = 0.72$, for $r = 0.5$, the critical force is given by $f_c = 0.74$ and for $r = -0.5$, the critical force is given by $f_c = 0.98$. We observe that the value of the external force is higher for the deformable potential with broad wells and narrow barriers compared to the sine-Gordon shape potential ($r = 0$), and the deformable potential with narrow wells and broad barriers. However, the effective diffusion coefficient is rather more pronounced for the deformable potential with narrow wells and broad barrier compared to the two other cases, i.e. $r = 0$ and $r = -0.5$. For $r = -0.5$, $r = 0$ and $r = 0.5$ the values of the threshold diffusion or the maximum diffusion are given by $D_{th} = 1.2181 \times 10^3$, $D_{th} = 80.4582$, and $D_{th} = 4.154 \times 10^3$, respectively. These threshold values do not occur at the same critical forces. In order to explain the origin of the excess peak diffusion of $r = 0.5$, we have plotted the Fig. 46. In fact, the presence of peak in the effective diffusion results from equiprobability between the locked and running states. In this case, the excess diffusion peak may stem from the number of transitions locked-to-running state. So, the diffusion will be higher if and only if the number of transition between the locked and running states is low, see Fig. 46.

In Fig. 45, the effective diffusion coefficient as a function of the mean thermal energy and the external force is plotted. It is clearly seen that the effective diffusion coefficient decreases and goes to 0 when the temperature of the system increases. Indeed, for $|f| < f_c$, for the three cases of the shape parameter, the effective diffusion coefficient enhances when the temperature $T \to 0$ [29, 207, 210, 211, 205]. So, the interplay between the shape of the potential and the temperature of the system contributes either to lower or enhance the effective diffusion coefficient according to the shape parameter. Coming back to Fig. 44, for f outside the range $|f| < f_c$, the effective diffusion coefficient decreases to 0 and we single out two cases: (i) the case of strong diffusion indicating the incoherent transport (strongly diffusive); (ii) the case of coherent transport (reliable directed) [7, 29, 210]. For r = -0.5, since the critical force is higher, compared to both other cases, this case exhibits a reliable transport for an enough long-range of the external force. The deformable potential with the narrow wells and broad barrier requires from Brownian particles a large quantity of thermal energy to cross the potential bar-

rier, indicating that the thermal energy of the system is quickly dissipated. However, the interaction between the external force, the inertia term and the damping, lead to an enhancement of the effective diffusion.

To fully characterize the role of the shape parameter of the system on the effective diffusion coefficient of Brownian particles, we focus our attention on the dependence of the peak values of the effective diffusion coefficient and the corresponding threshold f_c on the shape parameter. To achieve this, Fig. 47 has been plotted. In Fig. 47a, the maximum effective diffusion coefficient of Brownian particles D_{th}, as a function of the shape parameter *r*, is plotted, while the corresponding threshold f_c, as a function of the shape parameter *r*, is presented in Fig. 47b. By looking at the Fig. 47a, we remark that in the deformable potential, the threshold values of the effective diffusion as a function of the shape parameter have an almost parabolic behaviour. Thus, we can write

$$D_{th} \propto \mid r \mid^{\alpha}, \tag{166}$$

with $\alpha \simeq 2$. For $r > 0$, corresponding to the potential with broad barriers and narrow wells, the maximum effective diffusion coefficient increases. The more the deformable potential wells get shrink, the more the thermal energy of the system dissipates, which reduces the transition leading a giant enhancement diffusion. However, for $r < 0$, the maximum effective diffusion coefficient increases when the potential wells get large, showing that the trays effect also favors the diffusion of Brownian particles. In general, the critical force f_c is a decreasing function of the negative values of the shape parameter, as illustrated in Fig. 47b. For the positive values of the shape parameter r, the critical force is an increasing function of the shape parameter r. This indicates that the increase of the effective diffusion is accompanied of the increase of the critical force. Finally, in Fig. 48, we plot the effective diffusion coefficient as a function of the shape parameter *r*, for some values of the external force *f*. We observe that regardless the value of the external force, the effective diffusion coefficient grows for several orders of magnitude for $r > 0$. We also notice that for each value of the external force *f*, the effective diffusion

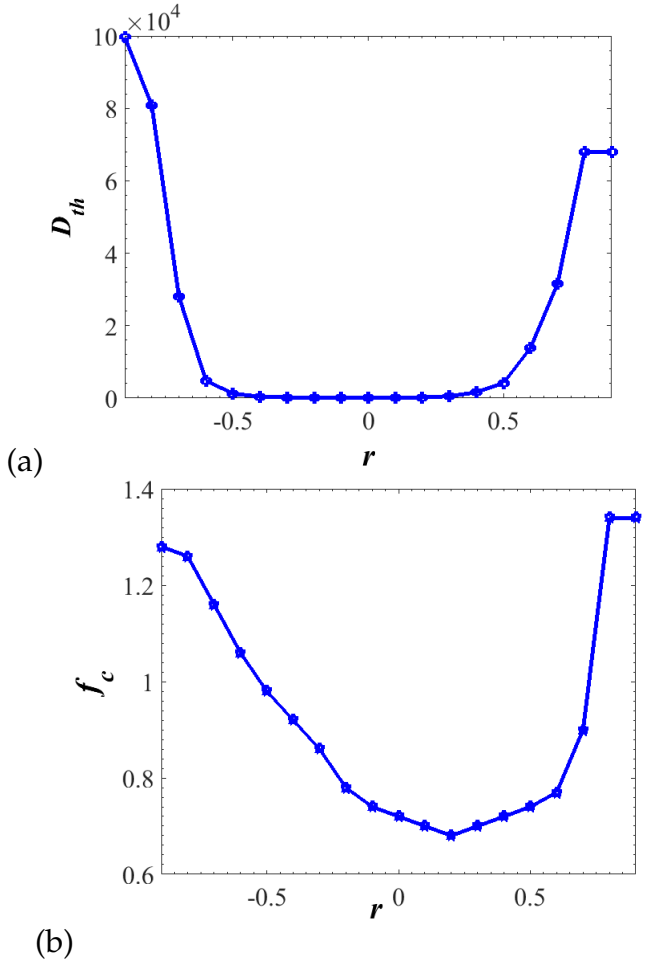

Figure 47: (a) Maximum values of the effective diffusion coefficient vs the shape parameter r. (b) Critical force of the system as a function of the shape parameter. Other parameter values: $k_BT = 0.094$ $\omega_0 = 1.0$, $\gamma = 0.4$.

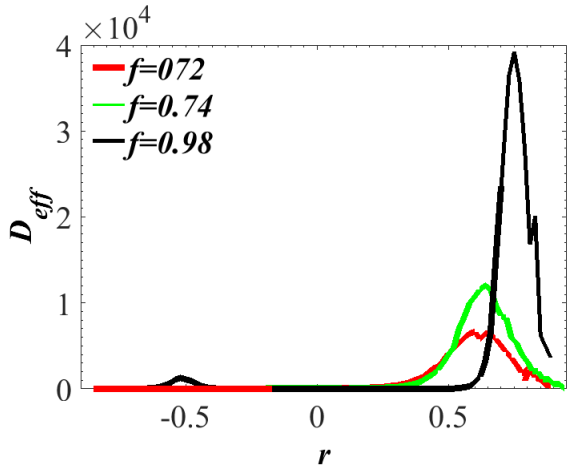

Figure 48: The effective diffusion coefficient as a function of the shape parameter r for some values of the external force: $f = 0.72$, 0.74 and 0.98. Other parameter values: $k_BT = 0.094$, $\omega_0 = 1.0$, $\gamma = 0.4$.

coefficient grows, and is centered at some specific values of the shape parameter, corresponding to the values for which the giant enhancement diffusion occurs. Hence, for f = 0.72, $D_{th} = 6.635 \times 10^3$, $r_c \simeq 0.6$, for f = 0.74, D_{th} = 1.3862 $\times 10^4$, $r_c \simeq 0.64$. However, for f = 0.98, there are two values of the shape parameter r for which the effective diffusion gets its maximums i.e., $r_{c1} = -0.5$ and $r_{c2} = 0.75$. The threshold diffusion for these two values of the shape parameter are given by D_{th} = 1.2181 $\times 10^3$ and D_{th} = 3.922 $\times 10^4$ for $r_{c1} = -0.5$ and $r_{c2} = 0.75$, respectively. $f = 0.98$ represents the critical force for $r = -0.5$ and 0.75. The result obtained in Fig. 48 further agrees with what has been said before, namely the geometry of the system induces a giant enhancement diffusion no matter the temperature of the system.

III.6 Conclusion

In this chapter, we have presented the numerical results obtained from the theoretical treatment of Brownian particles presented in chapter two. First of all, the dynamics of Brownian particles in the travelling-wave deformable potential has been discussed. We have found that the shape parameter of the system plays a significant role on the dynamics. So, the average velocity of Brownian particles in the overdamped limit is an increasing function of the shape parameter. We have shown analytically and numerically that the efficiency of a generating force and the transport are linked to the shape of the system.

In the underdamped limit, despite the complex behavior of Brownian particles due to the presence of mass associated with friction, the transport properties of particles are more controlled. Also, the underdamped Brownian motion of particles in a deformable potential in response to a constant external force has been commented. Thus, we have shown that, for the negative values of the shape parameter ($r < 0$), the average velocity versus the external tilting of Brownian particles is optimized, while for the positive values ($r > 0$), the average velocity of Brownian particles collapses. We have found as well the effective diffusion coefficient of Brownian particles evolves according to a power law

in terms of the shape parameter r.

General Conclusion and Perspectives

In this thesis, we have studied the dynamics of Brownian particles both in the travelling-wave deformable medium, taking into account a white-noise source. Two aspects of the dynamics have been examined: the case without inertia (the overdamped case), and the case with inertia (the underdamped case). We have also studied the underdamped Brownian motion in a tilted deformable potential, which is obviously more realistic and flexible for possible applications in condensed matter physics, in the presence of white thermal noise source.

The deformable model goes a modest step towards the real modelization of systems in the directed transport of the overdamped Brownian motor and provides useful trends and general understanding. In particular, it has been shown that in the absence of an external load, the critical value of the travelling potential speed ω for which the average velocity of the Brownian particle is maximal and where unpinning occurs does not only depend on the intensity of the noise as previously stated, but is also a function of the shape of the system. In fact, in the presence of the travelling-wave potential, the average velocity of the Brownian motor takes its maximum for each value of the shape parameter of the system in its range of variation. We have focused our attention on the statistical properties of Brownian particle motion (average velocity, Monte Carlo error bars, effective diffusion, and distribution) in the deformable travelling-wave medium. It was revealed that in the presence of the deformable travelling-wave potential, in the overdamped as well underdamped Brownian motions, each maximum value of the average velocity of Brownian particles is a function of the shape parameter r. In the overdamped limit, focusing mainly on the role of the geometry of the system on the ability of Brownian motor to transform the energy received into useful work for its function-

ing in the presence of the travelling wave speed, numerical results of the efficiency of generating force and the efficiency of transport of the directed Brownian motor were presented. It has been found out that these dynamical quantities are directly linked to the shape of the system. Especially, systems with broad wells and sharp barriers ($r < 0$) are more efficient than those with the shape parameter $r > 0$. Even though the efficiency in the presence of external load is lower in the case where $r > 0$ than in the case with $r = 0$, it is always advantageous to choose the deformed shape since in both $r > 0$ and $r < 0$ cases, the system can support an external load higher than in the situation where $r = 0$. Thus, the whole range of variations of the shape parameter must be taken into account in the modelization and the study of such stochastic systems in the presence of the travelling wave potential. In the absence of any external load force, systems with deformable shape are more efficient even at high travelling potential speeds compared to the case of the sinusoidal potential. The width of the velocity range where the efficiency remains equal to 1 becomes larger with increasing absolute value of the shape parameter r. We find that, in the underdamped limit, even in the presence of the deformable travelling-wave potential, the average velocity needed for the Brownian particle to cross the potential barrier, for each value of the shape parameter, is always smaller in the underdamped case. The Brownian particles are increasingly affected by inertia and also by damping. Comparing the behavior of the Brownian particle in both cases, the maximum average velocity values increase with the shape parameter r in the overdamped case, while in the underdamped case, the transport properties are controlled by the shape parameter r, i.e., the average velocity of Brownian particles increases when the potential wells broaden. When the deformable travelling potential speed increases, the Brownian particle experiences significant reverse motion, and it is almost at rest very quickly compared to the overdamped case. Moreover, we have observed that the interplay between the mass, the noise, and the force generated by the potential can lead to complex behavior of Brownian particles. Monte Carlo error bars have confirmed the directed motion of the Brownian particle in the overdamped and underdamped cases. It has also been shown that in the absence of any external load, the system in both the

overdamped and underdamped cases undergoes an enhancement diffusion. Indeed, in both cases, the effective diffusion is always greater than that of Einstein, regardless of the shape parameter r. Moreover, in the underdamped case, we have observed a "giant" enhancement diffusion induced by the geometry of the system. Then, the particle diffuses more freely in the deformable potential with $r < 0$ compared to $r > 0$, due to the presence of the mass of the Brownian particle. However, in the overdamped case, the effective diffusion exhibits a peak for different values of the shape parameter r, and these peaks are less pronounced compare to the underdamped case.

We have also shown numerically and by the semi-analytical method, through the Fokker-Planck equation in the free underdamped case (absence of any external load), that the distribution can present several modes for positive values of the shape parameter. This comes from the fact the metastable states can take place in the system, while for the negative value of the shape parameter and the sine-Gordon case ($r = 0$), the birth of each mode obviously corresponds to a minimum of the potential, although for $r < 0$, the distribution is very large. Generally, dynamical properties of the Brownian motor in the symmetric deformable potential, in the presence of the travelling-wave, are dictated by the deformed shape of the potential.

In the tilted deformable potential, i.e., in the presence of an external load, based on the dynamics of the system described by the Fokker-Planck equation, we have numerically computed the effective diffusion coefficient via the dynamic structure factor of the system using the matrix-continued-fraction method. It has been proven that due to the geometry of the system, many new effects occur in the transport process of the geometry of the system and is enhanced in a finite range of forces, that is also well within the region of bistability of the deterministic velocity dynamics, independently from the temperature. For $r > 0$, the diffusion coefficient intensifies and is more pronounced than when $r = 0$ and $r < 0$, which indicates a strong concentration of particles at a one site of the potential.

Many theoretical and practical studies of Brownian particles are modelled in the sinusoidal shape potential. As we said earlier, the deformable potential brings systems

close to realistic situations. So, the experimental work aiming at verification of different theories exhibited in this thesis are among our future objectives. These experimental studies on the deformable potential could help to improve the conduction in superionic conductors, giving that the average velocity of Brownian particles in this type of potential is higher than the sinusoidal one.

In this thesis, we have analyzed the dynamics of Brownian particles when they are exposed to white noise source. Despite significant results that we have found, it would be relevant to study the dynamics of these particles in the presence of many other external noises source such as the color noise, the non-Gaussian noise source. It is important to recall that the color noise is a generalization of the Gaussian noise, which is contrary to white noise, is correlated in time and tends to the white noise when its relaxation time goes to zero.

It would be relevant to study the fractional dynamics, as well on the time as on the noise in the presence of the deformable potential. Generally, it is assumed that the fractional order derivation is useful for a better description of real phenomena. Similarly, the fractional Brownian motion is a popular model for both short-range dependent and long-range dependent phenomena in various fields, including physics, biology, hydrology, network research.

Using large deviation theory, it would be relevant to explore current fluctuations of underdamped Brownian motion for the paradigmatic example of a single particle in a deformable periodic potential. On long time scales, the fluctuating particle current is directly connected to the entropy production and its fluctuations, which plays a central role in stochastic thermodynamics. The arguably best framework for studying fluctuations on large time scales is provided by the theory of large deviations, which defines the so-called large deviation function that characterizes the exponential decay in the probability of atypical fluctuations.

Bibliography

[1] G. Knight, "Chaotic Diffusion and Fractal Functions", (MSc thesis, Queen Mary, University of London, 2008).

[2] A. Einstein, "Über die von der molekularkinetischen Theorie der Wärme geforderte Bewegung von in ruhenden Flüssigkeiten suspendierten Teilchen", *Ann. Phys. (Leipzig)* **17**, 549 (1905).

[3] M. von Smoluchowski, "Zusammenfassende Bearbeitungen", *Ann. Phys. (Leipzig)* **21**, 756 (1906).

[4] T. N. Thiele, Sur la compensation de quelques erreurs qausi-systématiques par la méthode de moindres carrées (Reitzel, Copenhagen, 1880); see also: A. Hald, T. N. Thiele's contributions to statistics, *Int. Stat. Rev.* **49**, 1 (1981).

[5] L. Bachelier, *Ann. Sci. l'Ecole Normale Supérieure Sup. III*, **17**, 21 (1900).

[6] Lord Rayleigh, Philos. Mag. **32**, 424 (1891); in: Scientific Papers of Lord Rayleigh, Vol. III (Dover, New York, 1964), p. 471.

[7] P. Hänggi and F. Marchesoni, "Artificial Brownian motors: Controlling transport on the nanoscale", *Reviews of Modern Physics* **81**, 387, (2009).

[8] P. Hänggi, F. Marchesoni, and F. Nori, "Brownian motors", *Ann. Phys. (Leipzig)* **14**, 51 (2005).

[9] H. Risken, *The Fokker-Planck Equation: Methods of Solution and Applications*, Springer, Berlin, 1984.

[10] H. Touchette, T. Prelberg, W. Just, "Exact power spectra of Brownian motion with solid friction", *J. Phys. A: Math. Theor.* **45**, 395002 (2012).

[11] H. Touchette, E. Van der Straeten, W. Just, "Brownian motion with dry friction: Fokker-Planck approach", *J. Phys. A: Math. Theor.* **43**, 445002 (2010).

[12] A. Gnoli, A. Puglisi, H. Touchette, "Granular Brownian motion with dry friction", *EPL* **102**, 14002 (2013).

[13] A. Baule, H. Touchette, E. G. D. Cohen, "Stickslip motion of solids with dry friction subject to random vibrations and an external field", *Nonlinearity* **24**, 351 (2011).

[14] K. Svoboda, P. P. Mitra, S. M. Block, "Fluctuation analysis of motor protein movement and single enzyme kinetics", *Proc. Natl. Acad. Sci. USA* **91**, 11782 (1994).

[15] F. Jülicher, A. Adjari, J. Prost, "Modeling molecular motors", *Rev. Mod. Phys.* **69**, 4 (1997).

[16] B. Louis, Théorie de la Spéculation, *Thèse de Doctorat ès sciences mathématiques, Université de la Sorbonne, France*, 1900.

[17] D. Robert, T.-H. Nguyen, F. Gallet, C. Wilhelm, "In vivo determination of fluctuating forces during endosome trafficking using a combination of active and passive microrheology", *PLoS One* **5**, e10046 (2010).

[18] I. Goychuk, V. O. Kharchenko, R. Metzler, " Molecular motors pulling cargos in the viscoelastic cytosol: how power strokes beat subdiffusion", *Phys. Chem. Chem. Phys. 16*, 16524 (2014).

[19] I. Goychuk, V. O. Kharchenko, R. Metzler, "How molecular motors work in the crowded environment of living cells: coexistence and efficiency of normal and anomalous transport", *PLoS One* **9**, e91700 (2014).

[20] R. Metzler, J. Jeon, A. G. Cherstvy, E. Barkai, " Anomalous diffusion models and their properties: non-stationarity, non-ergodicity, and ageing at the centenary of single particle tracking", *Phys. Chem. Chem. Phys.* **16**, 24128 (2014).

[21] K. Chen, B. Wang, S. Granick, "Memoryless self-reinforcing directionality in endosomal active transport within living cells", *Nat. Mat.* **14**, 589 (2015).

[22] M. E. Fisher and A. B. Kolomeisky, "The force exerted by a molecular motor", *Proc. Natl. Acad. Sci. (U.S.A.)* **96**, 6597 (1999).

[23] S. Leibler, "Moving forward noisily", *Nature (London)* **370**, 412 (1994).

[24] M. O. Magnasco, "Forced thermal ratchets", *Phys. Rev. Lett.* **71**, 1477 (1993).

[25] B. Lindner and E. M. Nicola, "Diffusion in different models of active Brownian motion", *Eur. Phys. J. Spec. Top.* **157**, 43 (2008).

[26] P. Reimann, C. Van den Broeck, H. Linke, P. Hänggi, J. M. Rubi, and A. Pérez-Madrid, "Giant acceleration of free diffusion by use of tilted periodic potentials", *Phys. Rev. Lett.* **87**, 010602 (2001).

[27] I. G. Marchenko, I. I. Marchenko, and V. I. Tkachenko, "Temperature-Abnormal Diffusivity in underdamped spatially periodic systems", *JETP Lett.* **106**, 242 (2017).

[28] Z. -W. Bai and W. Zhang, "Diffusion of Brownian particles in a tilted periodic potential under the influence of an external OrnsteinUhlenbeck noise", *Chem. Phys.* **500**, 62 (2018).

[29] B. Lindner, I. M. Sokolov, Giant diffusion of underdamped particles in a biased periodic potential, *Phys. Rev. E* **93**, 042106 (2016).

[30] A. Asaklil, M. Mazroui, and Y. Boughaled, "Fokker-Planck dynamics in a bistable periodic potential", *Eur. Phys. J. B* **10**, 91 (1999).

[31] W. Dieterich, P. Fulde, and I. Peschel, "Theoretical models for superionic conductors", *Adv. Phys.* **29**, 527 (1980).

[32] W. Dieterich, "Theory of high ionic conductivity in solids", *Solid State Ion.* **5**, 21 (1981).

[33] W. Dieterich, P. Fulde, and I. Peschel, "Theoretical models for superionic conductors", *Adv. Phys.* **29**, 527 (1980).

[34] W. Dieterich, "Theory Of High Ionic Conductivity in Solids", *Solid State Ionics* **5**, 21 (1981).

[35] Xingfeng He, Yizhou Zhu, and Yifei Mo, "Origin of fast ion diffusion in super-ionic conductors", *Nature Communications*, **8** (2017).

[36] W. D. Richards et *al.*, "Design and synthesis of the superionic conductor $Na_{10}SnP_2S_{12}$", *Nature Communications* **7**, 11009 (2016).

[37] W. Dieterich, I. Peschel, W. R. Schneider, "Diffusion in periodic potentials", *Z. Physik* **B27**, 177 (1977).

[38] P. Maass, M. Meyer, A. Bunde, and W. Dieterich, "Microscopic explanation of the non-Arrhenius conductivity in glassy fast ionic conductors", *Phys. Rev. Lett.* **77**, 8 (1996).

[39] M. Kostur, L. Machura, P. Hänggi, J. Luczka, and P. Talkner, " Forcing inertial Brownian motors: Efficiency and negative differential mobility", *Physica A* **371**, 20 (2006).

[40] A. Kenfack, J. Gong, and A. K. Pattanayak, "Controlling the ratchet effect for cold atoms", *Phys. Rev. Lett.* **100**, 044104 (2008).

[41] M. Borromeo and F. Marchesoni, "Noise-assisted transport on symmetric periodic substrates", *Chaos* **15**, 026110 (2005).

[42] Y. Meroz and I. M. Sokolov, "A toolbox for determining subdiffusive mechanisms", *Phys. Rep.* **573**, 1 (2015).

[43] E. Barkai, Y. Garini, and R. Metzler, "of single molecules in living cells", *Phys. Today* **65**, 29 (2012).

[44] A. S. Bodrova, A. V. Chechkin, A. G. Cherstvy, H. Safdari, I. M. Sokolov, and R. Metzler, "Underdamped scaled Brownian motion: (non-)existence of the overdamped limit in anomalous diffusion", *Sci. Rep.* **6**, 30520 (2016).

[45] D. L. Ermak and H. Buckholz, "Numerical integration of the Langevin equation: Monte Carlo simulation", *J. Comput. Phys.* **35**, 169 (1980).

[46] Y. -X. Li, X.-Z. Wu, and Y.-Z. Zhuo, "Brownian motors: solitary wave and efficiency", *Physica A* **286**, 147 (2000).

[47] M. Motchongom Tingue, G. D. Kenmoe, T. C. Kofane, "Smart dampers control in a RemoissenetPeyrard substrate potential" *Nonlinear Dyn.* **69**, 37989 (2012).

[48] M. Motchongom Tingue, G. D. Kenmoe, T. C. Kofane, "Stickslip motion and static friction in a nonlinear deformable substrate potential" *Tribol. Lett.* **43**, 6572 (2011).

[49] A. Kenfack Jiotsa, M. Motchongom Tingue, D. C. Tsobgni Fozap, T. C. Kofane, "Dry friction: motionsmap, characterization and control" *Eur. Phys. J. B* **85**, 101 (2012).

[50] G. D. Kenmoe, A. Kenfack Jiotsa, T. C. Kofane, "Nonlinear spring model for frictional stick-slip motion", *Eur. Phys. J. B.* **70**, 353361 (2009).

[51] G. D. Kenmoe, A. Kenfack Jiotsa, T. C. Kofane, "Frictional stick-slip dynamics in a nonsinusoidal Remoissenet-Peyrard potential", *Eur. Phys. J. B.* **55** 347354 (2007).

[52] G. D. Kenmoe, A. Kenfack Jiotsa, T. C. Kofane, "Stick-slip motion in a driven two-nonsinusoidal RemoissenetPeyrard potential", *Physica D* **191** 3148 (2004).

[53] G. D. Kenmoe, E. D. Tchaptchet, T. C. Kofane, "Thermal effect on atomic friction with deformable substrate", *Tribol. Lett.* **55**, 533542 (2014).

[54] P. Woafo, T. C. Kofane and A. S. Bokosah, "Soliton Mechanismof Surface Diffusion with a Deformable Substrate Potential", *Physica Scripta* **56**, 655 (1997).

[55] P. R. Bevington and D. K. Robinson, Data Reduction and Error Analysis for the Physical Sciences (McGraw-Hill, New York, 2003).

[56] N. Metropolis, A. W. Rosenbluth, M. N. Rosenbluth, A. H. Teller, and E. Teller, "Equation of state calculations by fast computing machines", *J. Chem. Phys.* **21**, 1087 (1953).

[57] M. V. Smoluchowski, Experimentell nachweisbare, der üblichen Thermodynamik widersprechende Molekularphänomene, *Phys. Z.* **13**, 1069 (1912).

[58] R. P. Feynman, R. B. Leighton, and M. Sands, *The Feynman Lectures on Physics, Vol. I, Ch. 46. Addison Wesley, Reading, MA (1963).*

[59] S. Sassine, "Transport lectronique contrôlé par micro-ondes dans des microstructures asymétriques : Effet ratchet mésoscopique", (Ph.D thesis, Universite de Toulouse, 2007)).

[60] M. T. Downton et *al.*, "Single-polymer Brownian motor: A simulation study", *Phys. Rev. E* **73**, 011909 (2006).

[61] H. Linke, M. T. Downton, M. J. Zuckermann, "Performance characteristics of Brownian motors", *Chaos* **15**, 026111 (2005).

[62] R. Dean Astumian, P. Hänggi, "Brownian motors", *Phys. Today* **55**, 33 (2002).

[63] R. D. Astumian, "Thermodynamics and kinetics of a Brownian motor", *Science* **276**, 917 (1997).

[64] P. Reimann, P. Hänggi, "Introduction to the physics of Brownian motors", *Appl. Phys. A* **75**, 169 (2002).

[65] R. D. Astumian, "Making molecules into motors", *Scientific American* **285**, 57 (2001).

[66] P. Reimann *et al.*, "Quantum ratchets", *Phys. Rev. Lett.* **79**, 10 (1997).

[67] A. M. Kenneth, B. L. Jonathan, and R. S. Susan, *Biology*, 9th ed. (McGraw-Hill, New York, 2011).

[68] A. Bruce, B. Dennis, H. Karen, J. Alexander, L. Julian, R. Martin, R. Keith, and W. Peter, *Essential Cell Biology*, 3rd ed. (Garland Science, Taylor & Francis Group, 2010).

[69] S. M. Block, "Nanometres and piconewtons: the macromolecular mechanics of kinesin", *Trends Cell Biol.* **5**, 169 (1995).

[70] K. Svoboda, C. F. Schmidt, B. J. Schnapp, and S. M. Block, "Direct observation of kinesin stepping by optical trapping interferometry", *Nature (London)* **365**, 721 (1993).

[71] M. J. Schnitzer and S. M. Block, "Kinesin hydrolyses one ATP per $8 - nm$ step", *Nature (London)* **388**, 386 (1997).

[72] W. Hua, E. C. Young, M. L. Fleming, and J. Gelles, "Coupling of kinesin steps to ATP hydrolysis", *Nature (London)* **388**, 390 (1997).

[73] J. Howard, "Molecular motors: structural adaptations to cellular functions", *Nature* **389**, 561 (1997).

[74] R. D. Milligan, "The way things move: looking under the hood of molecular motor proteins", *Science* **288**, 88 (2000).

[75] R. D. Vale, "The molecular motor toolbox for intracellular transport", *Cell.* **112**, 467 (2003).

[76] N. Hirokawa, Y. Noda, Y. Tanaka, and S. Niwa, "Kinesin superfamily motor proteins and intracellular transport", *Nat. Rev. Mol. Cell Biol.* **10**, 682 (2009).

[77] T. Ariga, M. Tomishige, and D. Mizuno, "Nonequilibrium energetics of molecular motor kinesin", *Phys. Rev. Lett.* **121**, 218101 (2018).

[78] K. Svoboda and S. M. Block, "Force and velocity measured for single kinesin molecules", *Cell.* **77**, 773 (1994).

[79] T. Mori, R. D. Vale, and M. Tomishige, "How kinesin waits between steps", *Nature (London)* **450**, 750 (2007).

[80] K. Kaseda, H. Higuchi, and K. Hirose, "Alternate fast and slow stepping of a heterodimeric kinesin molecule", *Nat. Cell Biol.* **5**, 1079 (2003).

[81] C. L. Asbury, A. N. Fehr, and S. M. Block, "Kinesin moves by an asymmetric hand-over-hand mechanism", *Science* **302**, 2130 (2003).

[82] A. Yildiz, M. Tomishige, R. D. Vale, and P. R. Selvin, "Kinesin walks hand-over-hand", *Science* **303**, 676 (2004).

[83] M. Nishiyama, H. Higuchi, and T. Yanagida, "Chemomechanical coupling of the forward and backward steps of single kinesin molecules", *Nat. Cell Biol.* **4**, 790 (2002).

[84] Y. Taniguchi, M. Nishiyama, Y. Ishii, and T. Yanagida, "Entropy rectifies the Brownian steps of kinesin", *Nat. Chem. Biol.* **1**, 342 (2005).

[85] Anatoly B. Kolomeisky, "Motor Proteins and Molecular Motors: How to Operate Machines at Nanoscale", *J Phys. Condens. Matter* **25**, 46 (2013).

[86] M. Schliwa, G. Woehlke, "Molecular motors", *Nature* **422**, 759 (2003).

[87] M. Štrajbl, A. Shurki, A. Warshel, "Converting conformational changes to electrostatic energy in molecular motors: The energetics of ATP synthase", *PNAS* **100**, 14834 (2003).

[88] N. J. Carter and R. A. Cross, "Mechanics of the kinesin step", *Nature (London)* **435**, 308 (2005).

[89] Fiona E. Müllner, Sheyum Syed, Paul R. Selvin, and Fred J. Sigworth, "Improved Hidden Markov Models for Molecular Motors, Part 1: Basic Theory", *Biophys. J* **99**, 3684 (2010).

[90] Fiona E. Müllner, Sheyum Syed, Paul R. Selvin, and Fred J. Sigworth, "Improved Hidden Markov Models for Molecular Motors, Part 2: Extensions and Application to Experimental Data", *Biophys. J* **99**, 3696 (2010).

[91] H. Kojima, E. Muto, H. Higuchi, and T. Yanagida, "Mechanics of single kinesin molecules measured by optical trapping nanometry", *Biophys. J.* **73**, 2012 (1997).

[92] K. Visscher, M. J. Schnitzer, and S. M. Block, "Single kinesin molecules studied with a molecular force clamp", *Nature (London)* **400**, 184 (1999).

[93] R. P. Feynman, There's Plenty of Room at the Bottom (*Caltechs Engineering & Science Magazine, Pasadena* 1960) .

[94] K. E. Drexler, "Nanosystems: Molecular Machinery, Manufacturing and Computation" (*Wiley, New York*, 1992).

[95] M. Gross, Travels to the Nanoworld (*Perseus, New York*, 1999).

[96] B. D. Josephson, "Possible new effects in superconductive tunnelling", *Phys. Lett.* **1**, 251 (1962).

[97] Jesús Cuevas-Maraver, Panayotis G. Kevrekidis, Floyd Williams, "The sine-Gordon Model and its Applications: From Pendula and Josephson Junctions to Gravity and High-Energy Physics", *Springer* (2014).

[98] G. Barone and A. Paterno, Physics and Applications of the Josephson Effect, *Wiley, New York* (1982).

[99] K. K. Likharev, "Dynamics of Josephson Junctions and Circuits", *Gordon and Breach, New York* (1986).

[100] Yu. M. Ivanchenko and L. A. Zil'berman, "Josephson effect in small tunnel contacts", *Zh. Eksp. Teor. Phys.* **55**, 2395; (1968) *Sov. Phys. JETP*, **28**, 1272 (1968).

[101] V. Ambegaokar and B.I. Halperin, "Voltage due to thermal noise in the dc Josephson effect", *Phys. Rev. Lett.* **22**, 1364 (1969).

[102] M. P. Stephen, "Theory of a Josephson oscillator" *Phys. Rev. Lett.* **21**, 1629 (1968); M. P. Stephen, "Noise in a driven Josephson oscillator", *Phys. Rev.* **186**, 393 (1969).

[103] M. Simmonds and W. H. Parker, "Thermal fluctuations in superconducting weak links", *Phys. Rev. Lett.* **24**, 876 (1970).

[104] P. K. Hansma and G. I. Rochlin, "Josephson weak links: shunted junction and mechanical model results", *J. Appl. Phys.* **43**, 4721 (1972).

[105] L. Machura, M. Kostur, P. Talkner, J. Luczka, F. Marchesoni, and P. Hänggi, Brownian motors: Current fluctuations and rectification efficiency, *Phys. Rev. E* **70**, 061105 (2004).

[106] L. Machura, M. Kostur, P. Talkner, J. Luczka, and P. Hänggi, "Absolute Negative Mobility Induced by Thermal Equilibrium Fluctuations", *Phys. Rev. Lett.* **98**, 040601 (2007).

[107] D. Speer, R. Eichhorn, and P. Reimann, "Transient chaos induces anomalous transport properties of an underdamped Brownian particle", *Phys. Rev. E* **76**, 051110 (2007).

[108] M. Kostur, L. Machura, P. Talkner, P. Hänggi, and J. Luczka, "Anomalous transport in biased ac-driven Josephsonn junctions: Negative conductances", *Phys. Rev. B* **77**, 104509 (2008).

[109] J. Nagel, D. Speer, A. Sterck, R. Eichhorn, P. Reimann, K. Illin, M. Siegel, D. Koelle, and R. Kleiner, "Observation of negative absolute resistance in a Josephson junction", *Phys. Rev. Lett.* **100**, 217001 (2008).

[110] J. L. Mateos, "Chaotic transport and current reversal in deterministic ratchets", *Phys. Rev. Lett.* **84**, 258 (2000); J. L. Mateos, "Current reversals in chaotic ratchets: the battle of the attractors", *Physica A* **325**, 92 (2003).

[111] S. Flach, O. Yevtushenko, and Y. Zolotaryuk, "Directed current due to broken time-space symmetry", *Phys. Rev. Lett.* **84**, 2358 (2000); S. Denisov and S. Flach, "Dynamical mechanisms of dc current generation in driven Hamiltonian systems", *Phys. Rev. E* **64**, 056236 (2001); H. Schanz, M. F. Otto, R. Ketzmerick, and T. Dittrich, "Classical and quantum Hamiltonian ratchets", *Phys. Rev. Lett.* **87**, 070601 (2001); T. Dittrich, R. Ketzmerick, M. F. Otto, and H. Schanz, "Classical and quantum transport in deterministic Hamiltonian ratchets", *Ann. Phys. (Leipzig)* **9**, 755 (2000).

[112] P. Jung *et al.*,"Regular and chaotic transport in asymmetric periodic potentials: Inertia ratchets", *Phys. Rev. Lett.* **76**, 3436 (1996).

[113] M. B. Salamon, ed., "Physics of Superionic Conductors" (*Springer, Berlin,* 1979), and references therein.

[114] K. Funke, in Advances in Solid State Physics, **20**, *J. Treusch, ed.* (Vieweg, Braunschweig, 1980), p. 1.

[115] A. Asaklil, Y. Boughaleb, M. Mazroui, M. Chhib, L. El Arroum, "Diffusion of Brownian particles: dependence on the structure of the periodic potentials", *Solid State Ionics* **159**, 331343 (2003).

[116] P. Fulde, L. Pietronero, W. R. Schneider, S. Strässler, "Problem of Brownian motion in a periodic potential", *Phys. Rev. Lett.* **35**, 1776 (1975).

[117] H. Risken, H. D. Vollmer, "Correlation functions for the diffusive motion of particles in a periodic potential", *Z. Physik* **B31**, 209 (1978).

[118] T. Geisel, In Physics of Superionic Conductors, ed. by M. B. Salamon, *Topic Current Phys.*, **15** (Springer, Berlin, Heidelberg, New York 1979); Ouahmane, L. Arfa, L. El Arroum, M. Mazroui, "Brownian diffusion in a triple-well potential", *Mol. Cryst. Liq. Cryst.* **628**, 94 (2016).

[119] G. K. Batchelor, "Brownian diffusion of particles with hydrodynamic interaction", *J. Fluid Mech.* **74**, 1 (1976); G. K. Batchelor, J. Fluid Mech. **74**, 1 (1976).

[120] H. A. Kramers, "Brownian motion in a field of force and the diffusion model of chemical reactions", *Physica* **7**, 284 (1940).

[121] H. D. Vollmer, H. Risken, "Bistability effects of the Brownian motion in periodic potentials", *Z. Phys. B. Condens. Matter* **37**, 343 (1980).

[122] Y. Boughaleb, R. O. Rosenberg, M. A. Ratner, A. Nitzan, "Correlation effects on ionic motion in framework solid electrolytes", *Solid State Ionics* **18** 160 (1986).

[123] P. Giannozzi, G. Grosso, S. Moroni, G. Pastori Parravicini, "The ordinary and matrix continued fractions in the theoretical analysis of Hermitian and relaxation operators", *Appl. Numer. Math.* **4**, 273 (1988).

[124] W. T. Coffey, Y. P. Kalmykov, S. V. Titov, "Fractional Fokker-Planck equation for anomalous diffusion in a potential: Exact matrix continued fraction solutions",*Eur. Phys. J. Spec. Top.* **222**, 1847 (2013).

[125] G. M. D'Ariano, C. Macchiavello, "On the Monte Carlo simulation approach to Fokker-Planck equations in quantum optics", *Mod. Phys. Lett.* **B8**, 239 (1994).

[126] M. Suzuki, "Quantum Monte Carlo methods-recent developments", *Physica A* **194**, 432 (1993).

[127] S. Chandrasekhar, "Stochastic problems in physics and astronomy", *Rev. mod. Phys.* **15**, 1 (1943).

[128] H. Mehrer, *Diffusion in Solids: Fundamentals, Methods, Materials, Diffusion-Controlled Processes* (Springer, Berlin, 2007).

[129] J. Kärger, D. M. Ruthven, D. N. Theodorou, *Diffusion in Nanoporous Materials (Wiley-VCH, Weinheim, 2012)*.

[130] E. M. Rogers, Diffusion of Innovations (*Free Press Simon and Schuster*, *New York*, 2003).

[131] V. Zaburdaev *et al.*, "Levy walks", *Rev. Mod. Phys.* **87**, 483 (2015).

[132] J. Spiechowicz, J. Luczka, "Subdiffusion via dynamical localization induced by thermal equilibrium fluctuations", *Scientific Reports* **7**, 16451 (2017).

[133] Ya. G. Sinai, "The limiting behavior of a one-dimensional random walk in a random medium", *Theory Prob. Appl.* **27**, 256 (1983).

[134] J. P. Bouchaud, A. Georges, "Anomalous diffusion in disordered media: statistical mechanisms, models and physical applications", *Phys. Rep.* **195**, 127 (1990).

[135] Metzler, R. *et al.*, "Anomalous difusion models and their properties: non-stationarity, non-ergodicity, and ageing at the centenary of single particle tracking", *Phys. Chem. Chem. Phys.* **16**, 24128 (2014).

[136] D. S. Banks, C. Fradin, "Anomalous Diffusion of Proteins Due to Molecular Crowding", *Biophys. J.* **89**, 2960 (2005).

[137] B. M. Regner, *et al.*, "Anomalous Difusion of Single Particles in Cytoplasm", *Biophys. J.* **104**, 1652 (2013).

[138] E. Heinsalu, T. Örd, and R. Tammelo, "Diffusion and coherence in tilted piecewise linear double-periodic potentials", *Phys. Rev. E* **70**, 041104 (2004).

[139] E. Barkai, *et al*, "Strange kinetics of single molecules in living cells", *Physics Today* **65**, 29 (2012).

[140] F. Häfing, T. Franosch, "Anomalous transport in the crowded world of biological cells", *Rep. Prog. Phys.* **76**, 046602 (2013).

[141] Jind-Dong Bao, Yan Zhan, and Kun Lü, "Anomalous diffusion in periodic potentials under self-similar colored noise", *Phys. Rev. E* **74** , 041125 (2006).

[142] R. Hegadi, A. Kop, and M. Hangarge, "A Survey on Deformable Model and its Applications to Medical Imaging", *Special Issue on RTIPPR (Recent Trends in Image Processing and Pattern Recognition (IJCA, 2010)*, p. 64.

[143] D. Terzopoulos and K. Fleischer, "Deformable models", *Visual Comput.* **4**, 306 (1988).

[144] A . M. Fopossi Mbemmo, G. Djuidjé Kenmoé, and T. C. Kofane, "Shape Potential Effects on Transport and Diffusion Phenomena", *Fluctuation and Noise Letters* **16**, 1750011 (2017).

[145] A. M. Fopossi Mbemmo, G. Djuidje Kenmoe, and T. C. Kofane, "Anomalous transport and diffusion phenomena induced by biharmonic forces in deformable potential systems", *Eur. Phys. J. B* **89**, 211 (2016).

[146] G. Djuidje Kenmoe Y. J. Wadop Ngouongo, T. C. Kofane, "Effect of the Potential Shape on the Stochastic Resonance Processes", *J. Stat. Phys.* **161** 475485 (2015).

[147] Y. J. Wadop Ngouongo, G. Djuidje Kenmoe, T. C. Kofane, "Y. J. Wadop Ngouongo", *Physica A* **527**, 121321 (2019).

[148] Archimedes of Syracuse, Ca. 250 b. c., unpublished.

[149] M. Borromeo and F. Marchesoni, "Brownian surfers", *Phys. Lett. A* **249**, 199 (1998).

[150] T. Katsouleas, J. Dawson, "Unlimited electron acceleration in laser-driven plasma waves", *Phys. Rev. Lett.* **51**, 392 (1983).

[151] S. C. Wilks, J. M. Dawson, W. B. Mori, T. Katsouleas, M. E. Jones, "Photon accelerator", *Phys. Rev. Lett.* **62**, 2600 (1989).

[152] E. M. Lifshitz, L. P. Pitaevskii, *Physical kinetics*, Ch. 3 (*Pergamon, Oxford*, 1981).

[153] M. Peyrard and M. Remoissenet, "Solitonlike excitations in a one-dimensional atomic chain with a nonlinear deformable substrate potential", *Phys. Rev. B* **26**, 2886 (1982).

[154] G. Costantini, F. Marchesoni, and M. Borromeo, "String ratchets: ac driven asymmetric kinks", *Phys. Rev. E* **65**, 051103 (2002).

[155] J. Luczka, R. Bartussek, P. Hänggi, "White-noise-induced transport in periodic structures", *Europhys. Lett.* **31**, 431 (1995).

[156] C. W. Gardiner, Handbook of stochastic Methods, Springer-Verlag, Berlin, 2002.

[157] P. Reimann, "Brownian motors: noisy transport far from equilibrium", *Physics Report* **361**, 57 (2002).

[158] P. Hänggi, "Langevin description of Markovian integro-differential master equations", *Z. Phys. B* **36**, 271 (1980).

[159] C. Van den Broeck, "On the relation between white shot noise, Gaussian white noise, and the dichotomic Markov process", *J. Stat. Phys.* **31**, 467 (1983).

[160] B. G. deGrooth, A simple model for Brownian motion leading to the Langevin equation, *Am. J. Phys.* **67** 1248 (1998).

[161] J. Kula, M. Kostur, J. Luczka, "Brownian transport controlled by dichotomic and thermal fluctuations", *Chem. Phys.* **235**, 27 (1998).

[162] R. Graham, A. Schenzle, "Stabilization by multiplicative noise", *Phys. Rev. A* **26**, 1676 (1982).

[163] N. G. Van Kampen, Stochastic processes in physics and chemistry, North-Holland, Amsterdam, 1992.

[164] F. Reif, *Fundamentals of Statistical and Thermal Physics*, (McGraw Hill, Singapore, 1985).

[165] A. Einstein, Zur Theorie der Brownschen Bewegung, *Ann. Phys.* **19**, 371 (1906).

[166] A. Einstein, Investigations on the Theory of the Brownian Movement, Dover, New York, 1956.

[167] R. P. Erickson, Zhiyuan Jia, S. P. Gross, C. C. Yu, " How molecular motors are arranged on a cargo is important for vesicular transport", *PLoS Comput Biol* **7**, 5, (2011).

[168] R. Lipowsky, Y. Chai, S. Klumpp, S. Liepelt, M. J. I. Müller, "Molecular motor traffic: From biological nanomachines to macroscopic transport", *Physica A* **372**, 34 (2006).

[169] A. B. Kolomeisky, "Motor proteins and molecular motors: how to operate machines at the nanoscale", *J Phys. Condens. Matter* **25**, 46 (2013).

[170] R. F. Fox, M. H. Choi, "Rectified motion and kinesin motion along microtubule", *Phys. Rev. E* **63**, 051901 (2001).

[171] N. Wax, *Selected Papers on Noise and Stochastic Processes* (Dover, New York, 1954).

[172] A. D. Fokker, "Die mittlere Energie rotierender elektrischer Dipole im Strahlungsfeld", *Ann. Physik* **43**, 810 (1914).

[173] M. Planck, "Uber einen satz der statistischen Dynamik and seine Erweiterung in der Quantetheorie", *Sitzber. Preuss. Akad. Wiss* **50**, 324 (1917).

[174] M. V. Smoluchowski,"Über Brownsche Molekularbewegung unter Einwirkung äuerer Kräfte und deren Zusammenhang mit der verallgemeinerten Diffusionsgleichung", *Ann. Physik* **48**, 1103 (1915).

[175] J. M. R. Parrondo, J. M. Blanco, F. J. Cao, R. Brito,"Efficiency of Brownian motors", *Europhys. Lett.* **43**, 248 (1998).

[176] H. Linke, "Ratches and Brownian motors: Basics, experiments and applications", *Appl. Phys. A* **75**, 167 (2002).

[177] K. Sekimoto, "Kinetic characterization of heat bath and the energetics of thermal ratchet models", *J. Phys. Soc. Jap.* **66**, 1234 (1997).

[178] C. J. Reid, "Numerical solutions for Brownian motion of particles in a periodic potential: Application to dielectric relaxation", *Mol. Phys.* **49**, 331 (1983).

[179] G. T. Evans, "An analysis of the density dependence of the butane isomerization rate", *J. Chem. Phys.* **78**, 4963 (1983).

[180] M. Büttiker, E. P. Harris, and R. Landauer, "Thermal activation in extremely underdamped Josephson-junction circuits", *Phys. Rev. B* **28**, 1268 (1983).

[181] J. H. Weiner and R. E. Forman, "Rate theory for solids. IV. Classical Brownian-motion model", *Phys. Rev. B* **10**, 315 (1977).

[182] B. Cartling, "Kinetics of activated processes from nonstationary solution of the Fokker-Planck equation for bistable potential", *J. Chem. Phys.* **87**, 2638 (1987).

[183] P. Moore, J. Flaherty, Adaptive local overlapping in two space dimensions, *J. Comp. Phys.* **98**, 54 (1992).

[184] H. D. Vollmer, H. Risken, "Distribution Functions for the Brownian Motion of Particles in a Periodic Potential Driven by an External Force", *Z. Physik B* **34**, 313 (1979).

[185] P. Jung, "Periodically driven stochastic systems", *Phys. Rep.* **234**, 175 (1993).

[186] T. Chen, Ms. Sci., "A theoretical and numerical study for the Fokker-Planck equation, Simon Fraser University", 1992.

[187] T. Tang, S. Mckee, M. W. Reeks, "A spectral method for the numerical solution of a kinetic equation describing the dispersion of small particles in a turbulent flow", *J. Comput. Phys.* **103**, 2 (1992).

[188] R. Ferrando , R. Spadacini, G. E. Tommei, G. Caratti, "Time scales and diffusion mechanisms in the Kramers equation with periodic potentials", *Physica A* **195**, 506 (1993).

[189] R. Ferrando, R. Spadacini, G. E. Tommei and A. C. Levi, "Diffusion in classical periodic systems: The Smoluchowski equation approach", *Physica A* **173**, 141 (1991).

[190] R. Ferrando, R. Spadacini and G. E. Tommei, "Theory of classical diffusion in two dimensional periodic systems", *Surf. Sci.* **251** 773 (1991).

[191] J. Wilemski, "On the derivation of Smoluchowski equations with corrections in the classical theory of Brownian motion", *J. Stat. Phys.* **14**, 153 (1976).

[192] L*é*on Van Hove, "Correlations in Space and Time and Born Approximation Scattering in Systems of Interacting Particles", *Phys. Rev* **95**, 1 (1954).

[193] C. T. Chudley, R. J. Elliot, "Neutron Scattering from a Liquid on a Jump Diffusion Model", *Proc. Phys. Soc.* **77**, 55 (1960).

[194] H. C. Brinkman,"Brownian motion in a field of force and the diffusion theory of chemical reactions. II", *Physica* **22**, 149 (1956).

[195] Kurt Jacobs, *Stochastic processes for Physicists*, Cambridge University press, 2010.

[196] Raúl Toral and Pere Colet, *Stochastic Numerical Methods*, Wiley-VCH Verlag GmbH & Co. KGaA, 2014.

[197] D. E. Knuth, *The Art of Computer Programming* (Addison-Wesley, Reading, MA, 1969), Vol.2.

[198] W. H. Press, S. A. Teukolsky, W. T. Vetterling, and B. P. Flannery, *Numerical Recipes in C: The Art of Scientific Computing* (Cambridge University Press, Cambridge, 1992).

[199] N. Kasdin, "Runge-Kutta algorithm for the numerical integration of stochastic differential equations", *J. Guid. Control Dyn.* **18**, 114 (1995).

[200] Y. Dong, A. Vadakkepatt, and A. Martini, "Analytical Models for Atomic Friction", *Tribol. Lett.* **44**, 367 (2011).

[201] R. L. Woulache, F. M. Kepnang Pebeu, T. C. Kofane, "Dynamics of Brownian motors in deformable medium", *Physica A* **460**, 326 (2016).

[202] M. F. Kepnang Pebeu, R. L. Woulache, and T. C. Kofane, "Brownian motors in variable-shape medium: Overdamped versus underdamped cases", *Phys. Rev. E* **98**, 052107 (2018).

[203] J. Spiechowicz, J. Luczka, and P. Hanggi, "Absolute negative mobility induced by white Poissonian noise", *J. Stat. Mech.* P02044 (2013).

[204] A. M. Fopossi Mbemmo, G. D. Kenmoe, T. C. Kofane, "Anomalous transport and diffusion phenomena induced by biharmonic forces in deformable potential systems", *Eur. Phys. J. B* **89**, 211 (2016).

[205] K. Lindenberg, J. M. Sancho, A. M. Lacasta, and I. M. Sokolov, "Dispersionless Transport in a Washboard Potential", *Phys. Rev. Lett.* **98**, 020602 (2007).

[206] P. Jung, J. G. Kissner, and P. Hänggi, "Regular and chaotic transport in asymmetric periodic potentials: Inertia ratchets", *Phys. Rev. Lett.* **76**, 3436 (1996).

[207] G. Costantini and F. Marchesoni, "Threshold diffusion in a tilted washboard potential", *Europhys. Lett.* **48**, 491 (1999).

[208] M. S. Suñé, J. M. Sancho, and K. Lindenberg, "Transport and diffusion of underdamped Brownian particles in random potentials", *Eur. Phys. J. B*, 87:201 (2014).

[209] M.F. Kepnang Pebeu, R.L. Woulache, C.B. Tabi et al., "Transport and diffusion of Brownian particles in a tilted deformable potential", *Physica A* **541**, 123284 (2020).

[210] B. Lindner and E. M. Nicola, "Critical Asymmetry for Giant Diffusion of Active Brownian Particles", *Phys. Rev. Lett.* **101**, 190603 (2008).

[211] C. Van den Broeck, P. Hänggi, "Activation rates for nonlinear stochastic flows driven by non-Gaussian noise", *Phys. Rev. A* **30** 2730 (1984).

List of Publications

1- R. L. Woulache, M. **F**. **Kepnang Pebeu**, and T. C. Kofane. *Dynamics of Brownian motors in deformable medium*. *Physica A: Statistical Mechanics and Applications* **460**, 326 (2016).

2- M. **F**. **Kepnang Pebeu**, R. L. Woulache, and T. C. Kofane. *Brownian motors in variable-shape medium: Overdamped versus underdamped cases*. *PHYSICAL REVIEW E* **98**, 052107 (2018).

3- M. **F**. **Kepnang Pebeu**, R. L. Woulache, C.B. Tabi, T. C. Kofane. *Transport and diffusion of Brownian particles in a tilted deformable potential*, *Physica A* **541**, 123284 (2020).

Physica A 460 (2016) 326–334

Contents lists available at ScienceDirect

Physica A

journal homepage: www.elsevier.com/locate/physa

Dynamics of Brownian motors in deformable medium

Rosalie Laure Woulaché [a,b,c,*], Fabrice Maxime Kepnang Pebeu [a], Timoléon C. Kofané [a,b,c]

[a] Laboratoire de Mécanique, Département de Physique, Faculté des Sciences, Université de Yaoundé I, B.P. 812, Yaoundé, Cameroon

[b] The Abdus Salam International Centre for Theoretical Physics, Strada Costiera, 11-34014 Trieste, Italy

[c] Centre d'Excellence Africain en Technologies de l'Information et de la Communication (CETIC), Yaoundé, Cameroon

HIGHLIGHTS

- Directed transport of Brownian motors in deformable potential.
- Influence of the travelling wave speed on the dynamics of the system.
- The efficiency of generating the force is affected by the geometry.
- The travelling wave speed favours the transport in deformed systems.
- It is always advantageous to consider the whole range of the shape.

ARTICLE INFO

Article history:
Received 5 February 2016
Received in revised form 27 April 2016
Available online 14 May 2016

Keywords:
Brownian motor
Deformable medium
Efficiency

ABSTRACT

The directed transport in a one-dimensional overdamped, Brownian motor subjected to a travelling wave potential with variable shape and exposed to an external bias is studied numerically. We focus our attention on the class of Remoissenet–Peyrard parametrized on-site potentials with slight modification, whose shape can be varied as a function of a parameter *s*, recovering the sine–Gordon shape as the special case. We demonstrate that in the presence of the travelling wave potential the observed dynamical properties of the Brownian motor which crucially depends on the travelling wave speed, the intensity of the noise and the external load is significantly influenced also by the geometry of the system. In particular, we notice that systems with sharp wells and broad barriers favour the transport under the influence of an applied load. The efficiency of transport of Brownian motors in deformable systems remains equal to 1 (in the absence of an applied load) up to a critical value of the travelling wave speed greater than that of the pure sine–Gordon shape.

1. Introduction

In the studies on Brownian motion, the perpetual irregular motions exhibited by small grains or colloidal particles of micrometric size maintained by the collisions with the molecules of the surrounding fluid can be probed. Examples of such Brownian particles are molecular motors such as kinesins whose importance is known in living biological cells and which have led to a great number of theoretical and experimental works in recent years [1–5]. Particularly, many experimental studies have been performed recently in the domain of living cells and showed the emergence of the anomalous diffusion;

* Corresponding author at: Laboratoire de Mécanique, Département de Physique, Faculté des Sciences, Université de Yaoundé I, B.P. 812, Yaoundé, Cameroon.
E-mail address: rwoulach@yahoo.com (R.L. Woulaché).

http://dx.doi.org/10.1016/j.physa.2016.05.040
0378-4371/

the relevant behaviour in these works is that although the mean displacement of the tracking particle is not linear, but random, its resulting motion is directed [4, and Refs therein]. The transport of Brownian particles along periodic structures in the apparent absence of any external driving forces, generally termed Brownian motor has been extensively studied [6–9]. Specifically, noise induced transport by Brownian motors or "rachets" has attracted the attention of an increasing number of researchers due to possible applications in many different contexts of physics, chemistry and biology [10–12].

The vast majority of works on Brownian motors is done in systems based on the standard sinusoidal potential and, concentrates on the behaviour and the selective control of the emerging directed transport as a function of parameters of the system such as temperature, energy barrier, or some other control variable. It is well known that under variation of some physical parameters such as temperature and pressure, certain physical systems may undergo changes which are either shape distortions, variation of crystalline structure or conformation changes. Thus, the standard sinusoidal potential used for modelling soft systems is interesting, but appears as a severe approximation because of the rigidity of its shape. In solid state physics deformable shape potential, which retrieves sine–Gordon shape as a special case has been employed widely and successfully to model the dynamics of systems in several realistic situations [13–17]. For example, recently, it has been revealed through the study of synchronization and information transmission in spatio-temporal networks that the final state of Frenkel–Kontorova oscillators was highly dependent on the initial conditions due to the shape of the system [18]. Similarly, it has been shown that the variations of the shape parameter affect significantly and not trivially the existence and the robustness of the velocity "quantization" phenomena [17]. Although the role of the shape parameter of the on-site potential is known in solid state physics, there exist only few information on its behaviour in soft condensed matter and biological systems [19–21]. Particularly in Refs. [20,21], the authors studied, the directed transport in asymmetric deformable systems and showed that there exists a value of the shape parameter at which the current takes its maximum. In those works, the only interest was the dependence of the current on the shape parameter of the system. In addition to the average drift velocity and/or current, each motor is characterized by the efficiency of converting the energy introduced by perturbations into useful work [2,22–24]. Moreover, the notion "travelling wave" introduced by Borromeo et al. [25] in their study of Brownian surfers where they showed its influence on the dynamics of an underdamped Brownian particle and used later by Li et al. [22] may also be considered.

In the present paper, the directed transport of Brownian particles in a travelling wave symmetric potential subjected to static bias is studied numerically. The generalization of the results [22] where the study of the influence of the travelling wave potential on the dynamical properties of Brownian particles for the shape parameter $s = 0$ is done by modelling the system, rather than with a standard sinusoid potential, but with the Remoissenet-Peyrard (RP) potential (with slight modification), whose shape can be varied continuously as a function of a shape parameter, and which acquires the sinusoidal shape as a special case [26,27]. Particular emphasis is laid on finding how the shape parameter of the system influences the directed transport in the case of symmetric travelling wave potential.

2. The model

Consider a one-dimensional Brownian particle with spatial position $x(t)$, γ the viscous friction constant which takes into account various sources of dissipation in the substrate (electronic excitations, phonons, etc.) and fluid (viscosity), subjected to an external static force or load F, plus a random thermal noise $\xi(t)$. In extremely small systems, particles dynamics and fluctuations occurring in biological and liquid environment are well described by the overdamped Langevin equation

$$\gamma \frac{\mathrm{d}x}{\mathrm{d}t} = -\frac{\mathrm{d}V(x - \mathrm{v}t, s)}{\mathrm{d}x} - F + \xi(t), \tag{1}$$

where the coupling between Brownian particles and the thermal bath is represented by $\xi(t)$, a standard Gaussian white noise of zero average and correlation $\langle \xi(t)\xi(t') \rangle = 2D\delta(t - t')$, with $D = k_B T/\gamma$ the noise intensity. Throughout this work, γ is set equal to one. The travelling wave potential $V(x - \mathrm{v}t, s)$ is assumed to be the RP potential with slight modification [26,27] written as

$$V(x - \mathrm{v}t, s) = U\left[\frac{(1+s)^2\,[1 - \cos(x - \mathrm{v}t)]}{1 + s^2 - 2s\cos(x - \mathrm{v}t)} - 1\right], \quad |s| < 1. \tag{2}$$

The quantity U and v are respectively the amplitude and the driving speed of the deformed travelling wave potential. In the absence of the driving speed ($\mathrm{v} = 0$), Fig. 1 represents the deformable substrate potential $V(x, s)$ for a few values of the shape parameter s. For $s = 0$, the potential $V(x, s)$ yields a sinusoidal shape, for $s < 0$, a shape of broad wells separated by narrow barriers, and for $s > 0$, a shape of deep narrow wells separated by broad gently sloping barriers (see Fig. 1).

It is well known that this stochastic process can be recast in terms of the probability density $p(x, t)$ which satisfies the Fokker–Planck equation [10]

$$\frac{\partial p(x,t)}{\partial t} = -\frac{\partial}{\partial x}\left[-\frac{\partial V(x - \mathrm{v}t, s)}{\partial x} - F - D\frac{\partial}{\partial x}\right] p(x,t). \tag{3}$$

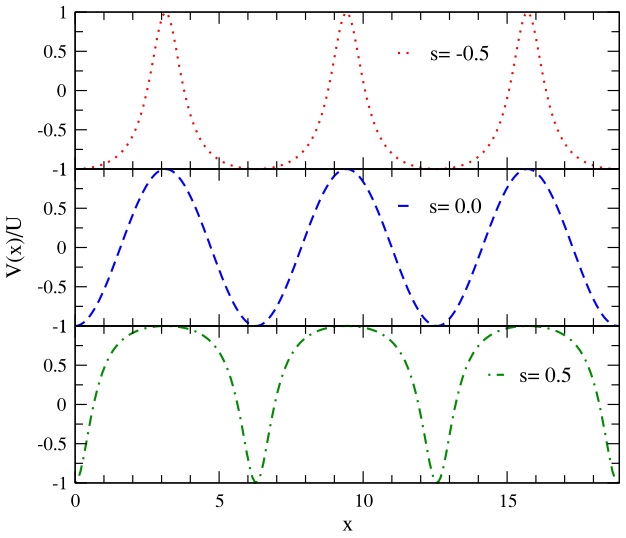

Fig. 1. The schema of the travelling wave potential, illustrated below for v = 0 and for three values of the shape parameter $s = -0.5, 0, s = 0.5$.

Assuming that the x motion is restricted to a periodically repeated segment length 2π, we apply the following periodic boundary condition and normalization condition,

$$p\,(x + 2\pi\,, t) = p\,(x, t)\,, \tag{4}$$

$$\int_0^{2\pi} \mathrm{d}x p\,(x, t) = 1. \tag{5}$$

In the study of small micro- or even nano-machines operating far from thermal equilibrium by extracting the energy from both thermal and non-equilibrium fluctuations in order to generate work against external loads, one usually refers to quantities such as the average directed velocity, the efficiency. Here, our aim is to obtain the analytical link between the most important transport quantity, which is the average directed velocity $\langle v\rangle$ of the Brownian particle, where $v = v(t)$ denotes the stochastic process $\frac{\mathrm{d}x}{\mathrm{d}t}$ in Eq. (1), and other parameters of the system. By setting $p\,(x, t) = p\,(x - \mathrm{v}t)$ following the form of the travelling wave potential, the Fokker–Planck equation (3) can be solved using the periodic boundary condition equation (4) and normalization condition equation (5). Using the same procedure as in Ref. [22], the probability density of Brownian particles reads

$$p\,(x - \mathrm{v}t) = \frac{1}{Z}\int_0^{2\pi} \mathrm{d}\alpha \exp\left(\frac{1}{D}\right)\left[V(\alpha + x - \mathrm{v}t, s) - V(x - \mathrm{v}t, s) + (F + \mathrm{v})\alpha\right], \tag{6}$$

with the normalization constant Z given by

$$Z = \int_0^{2\pi} \mathrm{d}\alpha \int_0^{2\pi} \mathrm{d}x \exp\left(\frac{1}{D}\right)\left[V(x + \alpha, s) - V(x, s) + (F + \mathrm{v})\alpha\right]. \tag{7}$$

This probability density (Eq. (5)) allows to obtain the average directed velocity of the Brownian particle written as follows [11,22]

$$\langle v\rangle = \mathrm{v} + 2\pi C, \tag{8}$$

where C is a constant depending on the parameters of the system and is given by

$$C = \frac{D\,(1 - \exp\left((2\pi/D)(F + \mathrm{v})\right))}{\int_0^{2\pi} \mathrm{d}\alpha \int_0^{2\pi} \exp\left(\frac{1}{D}\right)(V(x + \alpha, s) - V(x, s) + (F + \mathrm{v})\alpha)\,\mathrm{d}x}. \tag{9}$$

It is clearly seen that the average directed velocity of the Brownian motor is directly related to the travelling potential speed v but also depends on the shape of the system, the intensity of the noise and the external load through the constant C.

To optimize the effectiveness of the Brownian motor motion, we must introduce a measure for the efficiency η that account for velocity fluctuations. Assume that the Brownian motor works against an external force $\mathcal{F}$ not yet defined. The efficiency of a machine η is defined as the ratio of work $E = \mathcal{F}\,\langle v\rangle\,\tau$ against this external force and the input energy E_{in}, that is, $\eta = E/E_{in}$, where τ is the period of time of observation. For a Brownian motor working against a constant external

load force F, the same definition of efficiency can be used to define the efficiency of generating force or energy conversion [11,22,28,29]; that is

$$\eta_F = \frac{F\,\langle v\rangle\,\tau}{E_{in}}. \tag{10}$$

This characterization leads to a vanishing measure of efficiency in the absence of the external force F. In many cases, such as protein transport within a cell, the Brownian motor works at zero force regime ($F = 0$) in a viscous environment. In fact, in the presence of the dissipation γ, the force needed to displace a particle over a distance is proportional to its velocity. In this case, for a defined period of time τ, the transport is accomplished at an average motor velocity $\langle v\rangle$ and the necessary energy given is finite. Thus, by putting for $\mathcal{F}$ the average viscous force $\gamma\,\langle v\rangle$, we can then define the efficiency for transport as follows

$$\eta_T = \frac{\gamma\,\langle v\rangle^2\,\tau}{E_{in}}. \tag{11}$$

The average input energy for a Brownian motor in a period of time $\tau(\tau = 2\pi/\mathrm{v})$ can be evaluated as in Ref. [22] and is given by

$$E_{in} = 2\pi\,(F + \langle v\rangle)\,. \tag{12}$$

Using Eq. (12), the efficiencies for generating force η_F and for transport η_T can be deduced accordingly.

For convenience, to take into account the effects of the full noisy environment of the Brownian motors on its dynamical properties, we perform a direct numerical simulation of Eq. (1). For numerical simulations, the stochastic Runge–Kutta algorithm of order 4 [30,31]. The initial position $x(t = 0) = 0$ is used. At time $t = 0$, the Brownian particle is considered at rest at the bottom of the potential well. To improve accuracy and minimize statistical errors 10^5 to 10^6 realizations are considered. In order to provide the requested accuracy of the system dynamics time step is chosen to be between 10^{-3} and 10^{-5}. The average particle velocity is done over time.

3. Results

3.1. Velocity-driving speed behaviour

Fig. 2 depicts the driving speed–velocity characteristics of the non-equilibrium Brownian motor defined by Eq. (1). This average velocity of the Brownian motor is obtained by direct numerical integration of Eq. (1). In this figure, it is noted that the general evolution of the average velocity is the same for different shapes of the travelling potential. Indeed, in the absence of an external applied load ($F = 0$), the average velocity of the particle $\langle v\rangle$ increases in speed v up to a critical value v_{un} named the unlocking speed of the system, depending on the shape parameter s and then decreases monotonically to a nonzero value as the driving speed increases. In general, in the system, the potential advances with the travelling speed v when the particle motion due to the force generated by the potential barrier lags behind. When v is less than or equal to the unlocking speed of the system v_{un}, the particle is pinned in one potential well and moves along at the full speed of the travelling wave potential. As the travelling potential speed increases ($\mathrm{v} > \mathrm{v}_{un}$), the driving force generated by the potential energy becomes large enough and the particle jumps in the next potential well. Continuously increasing the travelling potential speed v leads to a backward and forward movement of the Brownian particle, leading to a decrease of the average velocity to a nonzero value due to very few back-turns. It is important to mention that the maximum value of the average velocity of the Brownian particle that can be generated by the potential barrier has an intrinsic link to the shape parameter of the travelling potential. In fact, when the absolute value of the shape parameter of the system increases, the unlocked value of the driving force due to the potential energy increases too. This increase matches with an increase of the unlocking speed v_{un} and consequently to an increase of the corresponding average velocity of the particle as shown in Fig. 2.

3.2. Differences $\mathrm{v}_{un} - \langle v\rangle_{max}$ and $\langle v\rangle_{max}(s) - \langle v\rangle_{max}(-s)$ versus shape parameter

To fully characterize the role of the shape parameter of the system on the dynamics of Brownian motor in the presence of the travelling wave potential, our attention is focused on the most important feature of Fig. 2 which is the dependence of the peak values of the average velocity $\langle v\rangle_{max}$ and the corresponding unlocking speed of the travelling wave potential v_{un} on the shape parameter of the system. For this purpose, Fig. 3 represents two plots. In the upper panel of this figure, the difference between the unlocking speed of the travelling wave potential v_{un} and the corresponding maximum value of the average velocity of the Brownian motor $\langle v\rangle_{max}$ as a function of the shape parameter s is plotted. In the lower panel, the difference between the maximum values of the average velocity of the Brownian motor $\langle v\rangle_{max}$ for each symmetrical couple $(s, -s)$ as a function of the absolute value of s is presented. It can be seen in the upper panel of this figure that the difference between the unlocking speed of the travelling potential and the corresponding maximum of the average velocity ($\mathrm{v}_{un} - \langle v\rangle_{max}$) is a decreasing function of the shape s of the system. In fact, for each couple of symmetric values of the shape parameter s, the unlocking speed of the travelling wave potential is the same, while the corresponding values of the average velocity

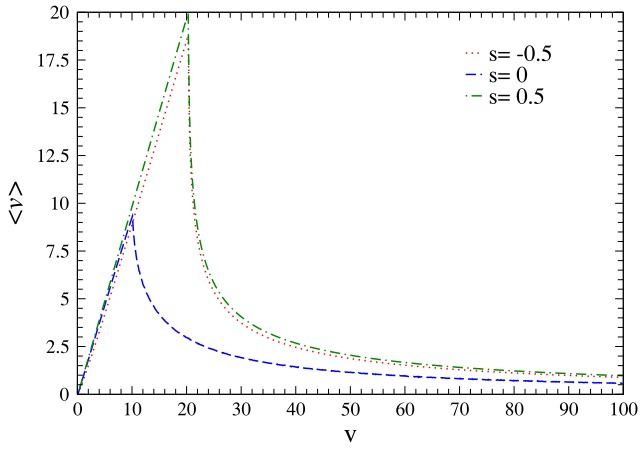

Fig. 2. Average velocity $\langle v \rangle$ of the Brownian motor as a function of the driving speed v of the travelling potential, for three values of s, $s = -0.5, 0.0, 0.5$. Other system parameters are: $D = 0.5$, $F = 0$, and $U = 10$.

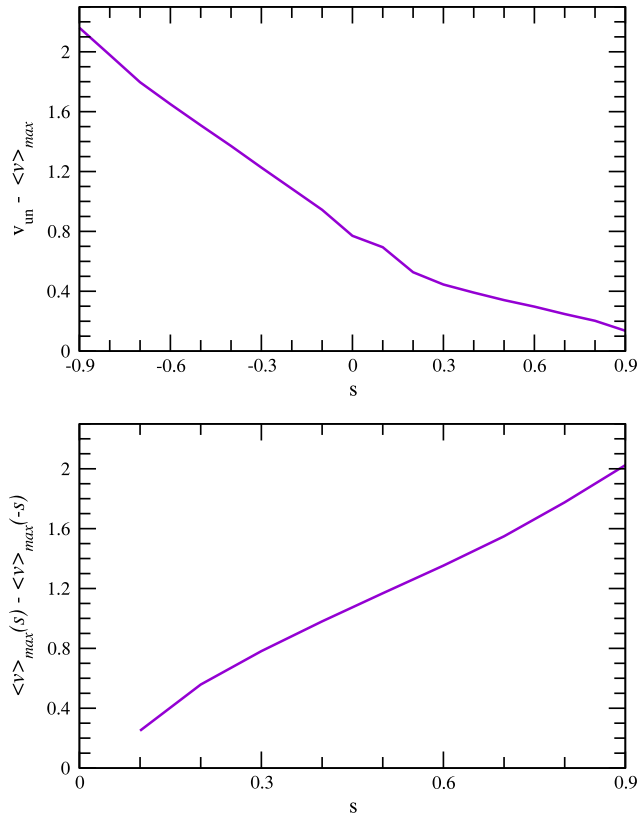

Fig. 3. Differences between maximum values of the speed of the travelling wave potential and the corresponding maximum of the average velocity of Brownian motor, and maximum values of the average velocity of the Brownian motor for symmetric values of the shape parameter s as a function of the shape parameter for $D = 0.5$, $F = 0$, $U = 10$ and $\gamma = 1$.

of the Brownian motor are different. For example, $v_{un} \simeq 20.3$ for $s = \pm 0.5$ and $\langle v \rangle_{max}$ is equal to 18.7910 and 19.9589 for $s = -0.5$ and $s = 0.5$ respectively. This means that the unlocking speed of the travelling wave potential is always greater than the corresponding maximum value of the average velocity of the Brownian motor. Consequently, differences $v_{un} - \langle v \rangle_{max}$ decrease when s increases (according to data given here for $s = \pm 0.5$, $v_{un} - \langle v \rangle_{max}$ is equal to 1.50900, for $s = -0.5$ and 0.34110 for $s = 0.5$). It is obviously seen that for each couple of symmetric values of the shape parameter s, the maximum value of the average velocity of the Brownian particle that can be generated by the potential barrier in the presence of the travelling speed is higher for positive values of s (deep narrow wells and broad barriers). As shown in the lower panel of Fig. 3, the difference between $\langle v \rangle_{max}(s) - \langle v \rangle_{max}(-s)$ is an increasing function of the absolute value of s.

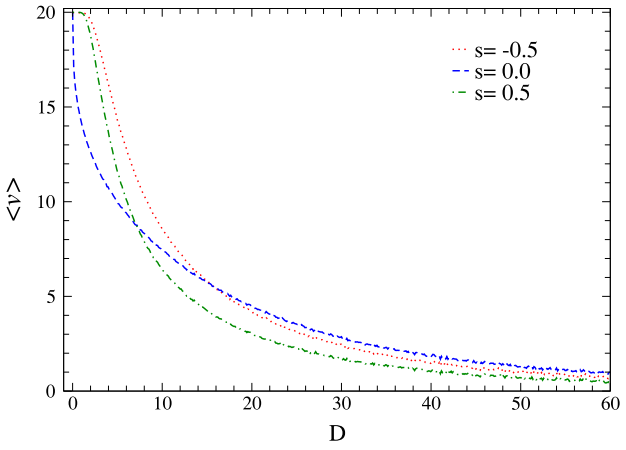

Fig. 4. Mean velocity of the Brownian motor as a function of the intensity of noise D for few values of shape parameter of the travelling wave potential, $s = -0.5, 0.0, 0.5$. Where $F = 0$, $U = 20$ and v $= 20$.

This behaviour of the Brownian motor in the presence of the travelling wave potential may be due to the fact that the energy gains through thermal fluctuations is less dissipated in potentials with deep narrow wells and broad barriers. These observed changes of the dynamical quantities indicate that the shape parameter plays an important role in systems with travelling wave potential.

The behaviour of the average velocity of the Brownian motor $\langle v \rangle$ as a function of the intensity of noise D for different values of the shape parameter s (see Fig. 4) is investigated. When the shape parameter $s = 0$, the unlocking speed and the corresponding maximum value of the average velocity of the Brownian particle are equal to the height of the potential barrier U (i.e $\langle v \rangle_{max} \simeq$ v $\simeq U$, here $U = 20$) at zero temperature or intensity of the noise D as stated by Li et al. [22] and shown in Fig. 4. This behaviour of the average velocity is also verified when the shape parameter of the system is different from zero ($s < 0$ and $s > 0$). Each curve in this figure (Fig. 4) is characterized by a particular shape of the system, but in general the average velocity is a decreasing function of the intensity of the noise.

3.3. Efficiency of generating force versus the external load

As stated before, the efficiency measures the capacity of a system to transform the input energy into useful work. The efficiency of generating force is obtained through numerical simulation of Eqs. (1), (10) and (12). The result of these simulations is plotted in Fig. 5 for some values of the shape parameter of the travelling wave potential. It can be seen in this figure that the efficiency of generating the force η_F is generally an increasing function of the external load F. Specifically, this increase of the efficiency in the travelling wave potential is not only due to the external load and/or the low temperature regime, but is largely affected by the shape parameter of the system. For example, the maximum value of the efficiency η_F tends to 0.85, 0.87, 0.94 for $s = -0.5, 0, 0.5$, respectively, as shown in Fig. 5. If the load increases continuously, the systems with positive shape parameter ($s > 0$) work efficiently even for large values of the load F before dropping rapidly at a critical value F_{Max}. This value F_{Max} of the force represents, for each value of the shape parameter, the maximum value of the load that can be supported by the system and beyond or above, no useful work can be performed in the system any more.

To gather insight on the influence of the shape parameter on the capacity of the Brownian motor to convert energy against an external load in the travelling wave potential, the upper panel of Fig. 6 reports the maximum efficiency of generating force $\eta_F(Max)$ as a function of s, for the same set of parameters used in Fig. 5. In the lower panel of Fig. 6, the corresponding maximum values of the external load F_{Max} are depicted. It can be seen that $\eta_F(Max)$ is an increasing function of the shape parameter s and tends to 0.98 as s tends to 0.9. The corresponding applied forces are nearly symmetric values of the shape parameter s. In general, for a fixed value of the speed of the travelling wave potential and under the influence of the external load, the displacement of a Brownian particle in the system with sharp wells and broad barriers namely $s > 0$ is done with a smaller loss of energy within the potential well. This implies a high efficiency of generating the force for an applied load less than or equal to the critical value F_{Max}, depending on the value of the shape parameter s. Thus, in the travelling wave potential, sharp wells potentials favour the transport of Brownian particles in the presence of an external applied load.

3.4. Efficiency of transport versus driving speed

In the absence of the external load, Brownian motor works in a viscous environment. The efficiency of transport η_T of the Brownian motor is obtained from simulations of Eqs. (1), (11) and (12) and is represented in Fig. 7 as a function of the travelling potential speed v for a few values of the shape parameter of the system ($s = -0.5, 0.0, 0.5$), and for the following chosen set of parameters: $U = 20$, $D = 0.5$ and $F = 0$. This figure shows that η_T is widely influenced by the shape parameter

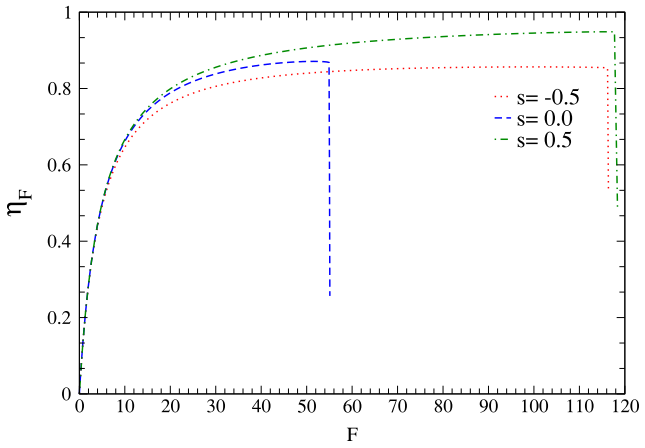

Fig. 5. Efficiency of generating force as a function of F for a few values of the shape parameter s, with $D = 1$, $U = 60$ and $v = 5$.

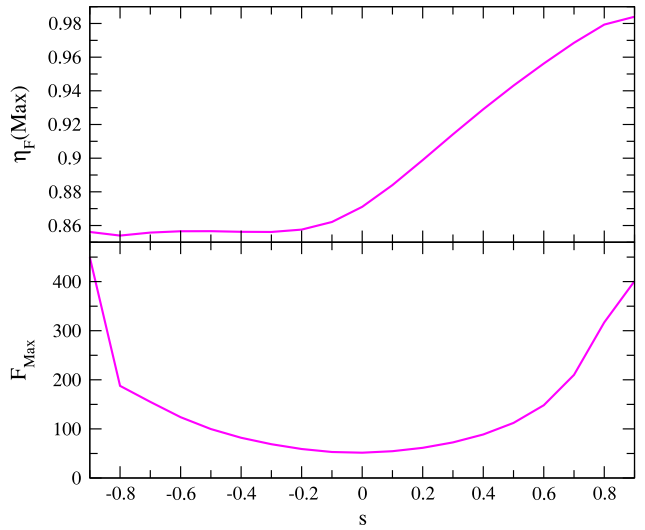

Fig. 6. Maximum efficiency of generating force and Maximum load F to apply to the system to generate force as a function of s. The simulation parameters are the same as for Fig. 5.

s in the presence of the travelling speed of the potential. Indeed, for $s \neq 0$, the unloaded transport efficiency of the Brownian motor remains equal to 1 up to a larger value of the travelling potential speed. Up to a critical value of this travelling potential speed, any increase of the speed leads to a monotonically decrease of the efficiency of transport to a nonzero constant value. This critical value of the travelling potential speed increases with the absolute value of the shape parameter s. In contrast to the case of the transport of Brownian motor in the presence of an external applied load, where the efficiency is an increasing function of the shape parameter s, the efficiency of transport evolves more or less the same for both positive and negative values of s. But, the relevant point here is that even in the absence of any external load the Brownian motor transport is more efficient in systems with a deformed potential for large speed of the travelling wave potential.

4. Discussion and conclusion

This paper reports a simulation study of the effect of a travelling wave potential with variable shape on the dynamical behaviour of an overdamped Brownian motor. This deformable model goes a modest step towards the real modelization of systems in the directed transport of the overdamped Brownian motor and provides useful trends and general understanding. In particular, it has been shown that in the absence of an external load, the critical value of the travelling potential speed v for which the average velocity of the Brownian motor is maximal and where unpinning occurs does not only depend on the intensity of the noise as previously stated [22] but is also a function of the shape of the system. In fact, in the presence of the travelling wave potential the average velocity of the Brownian motor takes its maximum for each value of the shape parameter of the system in its range of variation.

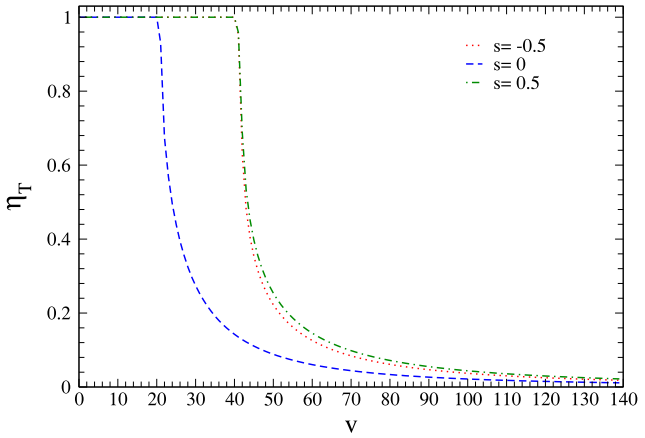

Fig. 7. The efficiency of transport as a function of the travelling potential speed for three values of the shape parameter s, with $U = 20, D = 0.5$ and $F = 0$.

Focusing mainly on the role of the geometry of the system on the ability of Brownian motor to transform the energy received into useful work for its functioning in the presence of the travelling wave speed, numerical results of the efficiency of generating force and the efficiency of transport of the directed Brownian motor were presented. It has been found out that these dynamical quantities are directly linked to the shape of the system. Especially, systems with sharp wells and broad barriers ($s > 0$) are more efficient than those with the shape parameter $s \leq 0$. Even though the efficiency in the presence of external load is lower in the case where $s < 0$ than in the case with $s = 0$, it is always advantageous to choose the deformed shape since in both $s > 0$ and $s < 0$ cases the system can support an external load higher than in the situation where $s = 0$. Thus, the whole range of variations of the shape parameter must be taken into account in the modelization and the study of such stochastic systems in the presence of the travelling wave potential. In the absence of any external load force, systems with deformable shape are more efficient even at high travelling potential speeds compared to the case of the sinusoidal potential. The width of the velocity range where the efficiency remains equal to 1 becomes larger with increasing absolute value of the shape parameter s. Generally, dynamical properties of the Brownian motor in the symmetric deformable potential in the presence of the travelling wave are dictated by the deformed shape of the potential. This influence of the travelling potential shape in the dynamics of the system might also be due to the presence of noise. In fact, in the presence of noise in the system, Brownian particle instead of diffusing freely undergoes a constrained motion, thus feels the shape of the well and revealing the effect of the potential shape.

Globally biological systems are soft matters and their shape may change due to some external effects. So, when modelling such systems it should be necessary to take into account their geometry. A systematic study of the effect of inertia on these dynamical properties of the Brownian motor in the presence of the travelling wave potential with variable shape may lead to qualitatively different results.

Acknowledgements

R.L.W. is grateful to the Abdus Salam International Centre for Theoretical Physics (AS-ICTP) where a part of this work was carried out during her visit under the Associateship federation scheme. R.L.W. thanks Prof. Nicola Manini for fruitful comments and discussions.

References

[1] D. Robert, T.-H. Nguyen, F. Gallet, C. Wilhelm, PLoS One 5 (2010) e10046.
[2] I. Goychuk, V.O. Kharchenko, R. Metzler, Phys. Chem. Chem. Phys. 16 (2014) 16524.
[3] I. Goychuk, V.O. Kharchenko, R. Metzler, PLoS One 9 (2014) e91700.
[4] R. Metzler, J. Jeon, A.G. Cherstvy, E. Barkai, Phys. Chem. Chem. Phys. 16 (2014) 24128.
[5] k. Chen, B. Wang, S. Granick, Nat. Mat. 14 (2015) 589.
[6] M.O. Magnasco, Phys. Rev. Lett. 71 (1993) 1477.
[7] R.D. Astumian, M. Bier, Phys. Rev. Lett. 72 (1994) 1766.
[8] M.O. Magnasco, Phys. Rev. Lett. 72 (1994) 2656.
[9] F. Marchesoni, Phys. Rev. Lett. 77 (1996) 1477.
[10] H. Risken, The Fokker–Planck Equation. Methods, Solutions and Applications, second ed., Springer, Berlin, 1989.
[11] P. Reimann, Phys. Rep. 361 (2002) 57.
[12] P. Hänggi, F. Marchesoni, Rev. Modern Phys. 81 (2009) 387.
[13] D. Yémélé, T.C. Kofané, Phys. Rev. E 56 (1997) 1037.
[14] B. Hu, J. Tekié, Phys. Rev. E 72 (2005) 056602.
[15] R.L. Woulaché, D. Yémélé, T.C. Kofané, Phys. Rev. E 72 (2005) 031604.
[16] R.L. Woulaché, D. Yémélé, T.C. Kofané, Eur. Phys. J. B 65 (2008) 99.
[17] R.L. Woulaché, A. Vanossi, N. Manini, Phys. Rev. E 88 (2013) 012810.

[18] F.M. Moukam Kakmeni, M.S. Baptista, Pranama - J. Phys. 70 (2008) 1063.
[19] G. Costantini, F. Marchesoni, Phys. Rev. Lett. 87 (2001) 114102.
[20] X.Q. Huang, P. Deng, J.W. Xiong, B.Q. Ai, Eur. Phys. J. B 162 (2012) 85.
[21] X.Q. Huang, P. Deng, B.Q. Ai, Physica A 392 (2013) 411.
[22] Y.X. Li, X.Z. Wu, Y.Z. Zhuo, Physica A 286 (2000) 147.
[23] L. Machura, M. Kostur, P. Talker, J. Luczka, F. Marchesoni, P. Hänggi, Phys. Rev. E 70 (2004) 061105.
[24] M. Kostur, L. Machura, P. Hänggi, J. Luczka, P. Talker, Physica A 371 (2006) 20.
[25] M. Borromeo, F. Marchesoni, Phy. lett. A 249 (1998) 199.
[26] M. Remoissenet, M. Peyrard, J. Phys. C 14 (1981) L481.
[27] G. Costantini, F. Marchesoni, M. Borromeo, Phys. Rev. E 65 (2002) 051103.
[28] P. Reimann, P. Hänggi, Appl. Phys. A 75 (2002) 169.
[29] H. Linke, Appl. Phys. A 75 (2002) 167.
[30] N.J. Kasdin, J. Guid. Control Dyn. 18 (1995) 116.
[31] G.N. Milstein, M.V. Tret'yakov, SIAM J. Numer. Anal. 34 (1997) 2141.

Brownian motors in variable-shape medium: Overdamped versus underdamped cases

M. F. Kepnang Pebeu,[1,*] R. L. Woulaché,[1,2] and T. C. Kofane[1,2]
[1]*Laboratory of Mechanics, Department of Physics, Faculty of Science, University of Yaounde I, P. O. Box 812, Yaounde, Cameroon*
[2]*Centre d'Excellence Africain en Technologies de l'Information et de la Communication, University of Yaounde I, Cameroon*

(Received 24 April 2018; revised manuscript received 12 September 2018; published 7 November 2018)

In this paper, we investigate the statistical behavior of Brownian particles in a deformable traveling-wave potential in the absence of external load. We model the deformation of the system by the modified Remoissenet-Peyrard on-site potential, which is distinguished by its sine-Gordon shape. We examine numerically the effect of the deformed on-site potential with traveling speeds on the transport properties in overdamped as well as underdamped Brownian particles. Using the Langevin Monte Carlo method, we show that the average velocity of Brownian particles is an increasing function of the shape parameter in the overdamped case, and a decreasing function of the shape parameter in the underdamped case. It is found that, in the overdamped case, the numerical behavior of the average velocity of Brownian particles validates its analytical results. In the presence of the deformable traveling-wave potential, for negative as well as positive values of the shape parameter, the underdamped case favors the transport properties in the medium. The average velocity needed to cross the potential barriers is lowest in the underdamped case. Moreover, the effective diffusion coefficient in both cases exhibits peaks, and the diffusion process enhancement is discussed for some values of the shape parameter. Finally, in the underdamped case, by using the Smoluchowski equation and the finite-element methods, we analyze the distribution of Brownian particles in the deformed system.

DOI: 10.1103/PhysRevE.98.052107

I. INTRODUCTION

Brownian particles in periodic structures have attracted the attention of many researchers due to their multidisciplinary applications [1–10]. For instance, in biology, overdamped Brownian particles are molecular motors moving along a periodic structure performing basic tasks in living organisms, and they do not necessarily need an external applied load to accomplish their task, that is, carrying a load across a viscous environment [11,12]. Importantly, with modern microscopic techniques, superresolution has led to the discovery of a multitude of anomalous diffusion processes in living cells and complex fluids [13–16].

Likewise, Brownian particles have also been studied in detail in connection with superionic conductors, Josephson junctions, the dynamics of phase-locked loops [3,17–21], to mention but a few. The common feature of these latter cases is that they consist of species of high mobile particles considered to be Brownian particles moving on a periodic structure with diffusion coefficients comparable to those found in liquids [22–24]. In either case, Brownian particles are nanomachines that operate far from thermal equilibrium, using the thermal energy imbalance to perform mechanical work so as to generate the directed transport, with noise playing an important role in the process [25,26]. Thus, the drift of particles is generated when conditions such as the presence of thermal noise, the anisotropy of the medium, and the time dependence are supplied by external variations of the constraints on the system [27]. Moreover, the interactions of the Brownian particles with the surrounding bath may be considered statistically rather than treating each Brownian particle individually due to the fluctuating forces described only by their statistical properties [28].

Indeed, most of the studies in the field of Brownian particles are modeled by physical systems having a rigid-shape on-site substrate potential. However, these systems with periodic structure, although interesting, describe realistic systems only with certain approximations. To obtain a physically more realistic periodic substrate for Brownian particles, the effects of physical parameters such as temperature and pressure should be considered. Under such constraints, some physical systems may undergo changes such as shape distortion, variation of crystalline structures, or conformational changes. Hence, it appears necessary to take into account the deformable character of the medium in Brownian particles. Indeed, deformable models have been considered both from mathematical and physical points of view. From a mathematical point of view, the foundations of deformable models represent a confluence of geometry, physics, and approximation theory. Geometry serves to represent object shape, physics imposes constraints on how the shape may vary over space and time, and optimal approximation theory provides the formal underpinnings of mechanisms for fitting the models to measured data. From a physical point of view, deformable models are viewed as elastic bodies that respond naturally to applied forces and constraints [29,30]. In fact, the term "deformable models" stems primarily from the use of elasticity theory at the physical level, generally with a Lagrangian dynamics setting. Furthermore,

*Author to whom all correspondence should be addressed: kepemafa@gmail.com

in an overdamped case, aiming at a more realistic description on the molecular level, some authors [9] have added an internal variable, which becomes necessary if the time required to achieve, for instance, a conformational change is not small compared with other time scales.

In the present work, we study the transport properties of Brownian particles in a deformable traveling-wave potential both in overdamped and underdamped limits. Note, however, that the traveling-wave potential has been introduced by Borromeo *et al.* [31] to study Brownian surfers. They have shown that the traveling wave has the capability of dragging Brownian particles along. Moreover, the traveling-wave potential has been used by Li *et al.* [32] to characterize the orientation of a molecular motor's internal electric dipole in order to describe the nature of the interaction between the motors and the filaments, as well as the interplay of the interaction and ATP hydrolysis, in order to understand the physical mechanism of molecular motors. However, some works have been done on the dynamics of Brownian particles using the variable shape potential [33,34]. For example, in the overdamped case an optimal transport may be obtained by changing the shape of the system [33]. Moreover, in the presence of the deformable traveling-wave potential, systems with sharp wells and broad barriers may favor the transport under the influence of an applied load [34].

Most of the above-mentioned works deal with overdamped deformable Brownian systems in which the inertial term due to the finite mass of the particles is neglected. To the best of our knowledge, underdamped Brownian particles in the presence of a traveling variable shape potential have yet to be investigated.

Therefore, underdamped Brownian particles in the deformable traveling potential could model driven laser plasma waves, known to accelerate classical charged particles trapped by perpendicular propagating electrostatic waves [35], and where the deformed on-site potential can represent a substrate that has abnormalities and defects. This deformable substrate potential could also model ionic solids, whose species, considered to be noninteracting Brownian particles, occupy vacant sites of the rigid framework diffusing through a lattice [2].

This paper examines the dynamic properties of free Brownian particles under the influence of the deformable traveling-wave potential in the overdamped and underdamped cases, using the Langevin Monte Carlo method [36,37]. Since the traveling-wave potential speed can induce a nonzero current in the absence of any external force, we subsequently analyze, in both cases, the effective diffusion coefficient of particles moving in a periodic deformable traveling-wave potential.

The paper is organized as follows. In Sec. II we introduce the global model of free Brownian particles moving in a deformable traveling-wave potential, and the quantities of interest, such as the average velocity, the effective diffusion coefficient, and the Monte Carlo error. Analytical results of the transport properties of the overdamped Brownian particles are presented in Sec. III A along with a validation of the method using direct numerical simulations. The transport properties of the underdamped Brownian particles based on the Fokker-Planck equation are addressed in Sec. III B. Finally, our results are summarized in Sec. IV.

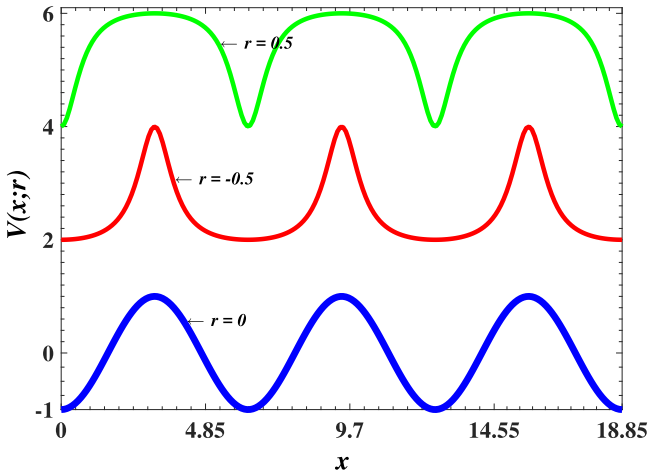

FIG. 1. Schematic representation of $V(x;r)$ as a function of x for a few values of the shape parameter r, with $\omega = 0$.

II. MODEL

We consider a Brownian particle of mass m free from any external load moving in a periodic traveling-wave potential with shape deformation. In this work, we choose the Remoissenet-Peyrard (RP) potential [38], modified according to [39]

$$V(x,t;r) = U\left[\frac{(1+r)^2[1-\cos(x-\omega t)]}{(1-r)^2+2r[1-\cos(x-\omega t)]} - 1\right], \quad (1)$$

where $|r| < 1$ represents the deformation parameter. We represent the RP potential for the traveling potential speed $\omega = 0$ (see Fig. 1). The RP potential reduces to a sinusoidal shape for $r = 0$; it provides broad wells separated by narrow barriers and deep narrow wells separated by broad flat barriers, respectively, for $r < 0$ and $r > 0$, with U the potential height.

The dynamical behavior of the Brownian particles can be modeled by a stochastic differential equation of Langevin type written as [3]

$$m\ddot{x} + \gamma\dot{x} = -\frac{dV(x,t;r)}{dx} + \sqrt{2\gamma K_B T}\varepsilon(t), \quad (2)$$

which depicts the Markov process of Brownian particles. In Eq. (2), the overdot indicates differentiation with respect to time t. γ represents the friction coefficient of the medium, $D = K_B T/\gamma$ is the diffusion coefficient of the Brownian particle, K_B is the Boltzmann constant, and T is the temperature of the bath. Assuming the environment to be an equilibrium heat bath with independent collisions, $\varepsilon(t)$ is the Gaussian white noise of zero mean $[\langle\varepsilon(t)\rangle = 0]$, and it satisfies the fluctuation-dissipation relation $\langle\varepsilon(t)\varepsilon(t')\rangle = 2D\delta(t-t')$, where $\delta(t)$ denotes the Dirac delta function, and t and t' are different times. The Dirac δ function is a very convenient "function." More exactly, it is the limiting case of a family of functions [40]. It has the property of singling out a particular value of a function $f(t)$ at a value $t = t_0$. The function is characterized by the following properties:

$$\delta(t-t_0) = \begin{cases} 0 & \text{if } t \neq t_0, \\ \infty & \text{if } t = t_0, \end{cases}$$

in such a way that for any $\epsilon > 0$,

$$\int_{t_0-\epsilon}^{t_0+\epsilon} \delta(t-t_0)dt = 1, \tag{3}$$

which means that the function $\delta(t-t_0)$ has a very sharp peak at $t = t_0$, but the area under the peak is unity.

Since Eq. (2) is a stochastic differential equation, we consider a statistical ensemble of stochastic processes belonging to independent realizations of the random fluctuations $\varepsilon(t)$. The equivalent of the Langevin equation (2) is the Fokker-Planck or Smoluchowski equation for the distribution function $P(x, v, t)$ in phase space (x, v), written as

$$\frac{\partial}{\partial t}P(x, v, t) = L_F P(x, v, t), \tag{4}$$

with the Fokker-Planck operator L_F,

$$L_F = -v\frac{\partial}{\partial x} + \left(\frac{\partial}{\partial v}\right)\left(\frac{\partial V(x,t;r)}{\partial x} + \gamma v\right) + D\frac{\partial^2}{\partial v^2}. \tag{5}$$

To understand the behavior of the Brownian particles in our system, we focus on the average velocity of Brownian particles. In fact, the average velocity of Brownian particles is perfectly sufficient to describe its dynamics in a system as well as its transport properties. In the overdamped case, an analytical expression of the average velocity for a Fokker-Planck equation was obtained earlier in previous works [34]. Here, we recall its expression (for more details of computation, see Ref. [34]),

$$\langle v\rangle = \omega + 2\pi C, \tag{6}$$

with

$$C = \frac{D\left[1-\exp\left(\frac{2\pi\omega}{D}\right)\right]}{\int_0^{2\pi} d\alpha \int_0^{2\pi} dx \exp\left(\frac{V(x+\alpha;r)-V(x;r)+\omega\alpha}{D}\right)}. \tag{7}$$

Due to the nonlinearity of the RP potential, no analytical solution of Eq. (2) is available in the underdamped case. Thus, only its numerical solution is presented in this work. For the numerical treatment in both cases, we define the average velocity of Brownian particles in the long-time limit as

$$\langle v\rangle = \lim_{t\to\infty}\frac{\langle x(t)\rangle}{t}, \tag{8}$$

where $\langle\cdots\rangle$ means the ensemble average, which is the statistical average of the quantity inside the angular brackets at a given time over all systems of the ensemble. Other important quantities taken into account are the fluctuations around the average velocity of Brownian particles, $V_{\rm av} = \langle v^2\rangle - \langle v\rangle^2$, and the effective diffusion coefficient given by

$$D_{\rm eff} = \lim_{t\to\infty}\frac{\langle x(t)^2\rangle - \langle x(t)\rangle^2}{2t}, \tag{9}$$

while the Monte Carlo error is

$$\sigma = \frac{1}{\sqrt{L}}\sqrt{\langle v^2\rangle - \langle v\rangle^2}, \tag{10}$$

with L the number of realizations of the fluctuating forces. The Brownian particles thus move with a velocity in the range $\langle v\rangle \equiv [\langle v\rangle - \sigma, \langle v\rangle + \sigma]$. As previously mentioned by Machura *et al.* [41], if σ is greater than $\langle v\rangle$, the Brownian particles may move in the opposite direction, making the displacement of the particles less effective and complex.

III. NUMERICAL RESULTS AND DISCUSSION

Focusing on the transport properties of the deformable system, the long-time limit of statistical quantities of interest is determined in terms of the statistical average over different realizations of the process in Eq. (2). We perform our numerical studies with the Euler algorithm. The time step is $h = 10^{-2}$. For initial conditions, $x = 0$ at $t = 0$, the Brownian particle is at rest at the bottom of the deformable traveling-wave potential ($\dot{x} = 0$). All quantities are averaged over 500–1000 different realizations, each of which evolves over $t_{\rm max} = 10^3$ for an overdamped case and $t_{\rm max} = 10^4$ for an underdamped case.

A. Overdamped Brownian motion

1. The average velocity in the overdamped Brownian motion

We represent first the average velocity of the Brownian particles as a function of the traveling speed obtained through a numerical integration of Eq. (2), and second some analytical results [see Eq. (6)] for $r = -0.5$, 0.0, and 0.5 (see Fig. 2). In fact, the average velocity increases approximatively from 3% to 86% when r increases from 0 to ± 0.5 [34]. We note that our numerical solution is in good agreement with the analytic solution. However, this behavior requires a comment. Indeed, referring to Fig. 2, which depicts the average velocity of the Brownian particle as a function of the traveling-wave potential speed ω, there exists a slight discrepancy with Fig. 2 of [34]. Moreover, as illustrated in these numerical simulations, the deformed system dissipated less thermal energy than the nondeformed system. In Ref. [34], the maximum average

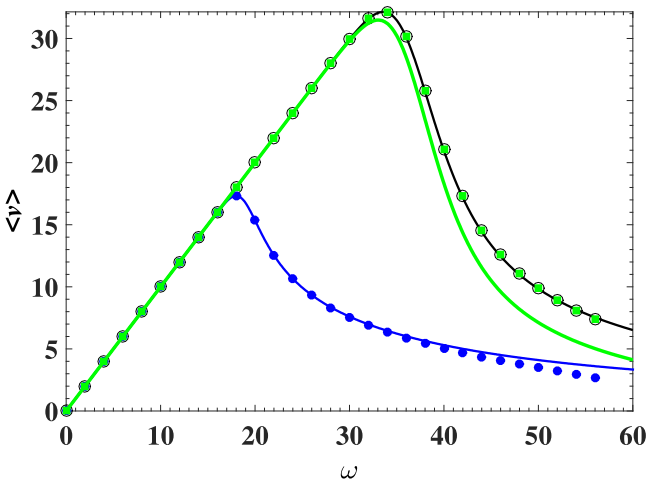

FIG. 2. Numerical solution of the average velocity obtained from Eq. (2) as a function of the traveling speed ω for $r = -0.5$ (black line), $r = 0$ (blue line), and $r = 0.5$ (green line). Also represented is its analytical solution [Eq. (5)] for $r = -0.5$ (black open circle), $r = 0$ (blue closed circle), and $r = 0.5$ (green square). Other parameters used are $U = 20$, $\gamma = 1$, and $D = 0.5$.

velocity of Brownian particles obtained from numerical simulation was greater for $r = 0.5$ than that of $r = -0.5$, given by 18.7910 and 19.9589, respectively, whereas in Fig. 2, by using Eq. (8), the average velocities are greater for the shape parameter $r = -0.5$ than $r = 0.5$, which are given by 32.1434 and 31.4817, respectively. Consequently, this last case exhibits a good enough agreement with the analytical result that we have derived [see Eq. (6)] [34]. In fact, in [34] the Kasdin algorithm was used to numerically simulate the stochastic differential equation, and then the formula

$$\langle v \rangle = \frac{1}{L} \sum_{i=1}^{L} \frac{1}{t_{\max}} \int_0^{t_{\max}} v(t) dt \tag{11}$$

was used to computed the average velocity of Brownian particles. Thus, in this context, it turns out that the use of Eq. (8) seems to be more reliable to address the stochastic differential equation since it matches well effectively with the theory proposed in [34]. Nevertheless, from a phenomenological point of view, the average velocity of Brownian particles in both cases presents the same shape. However, by varying the shape parameter with both formulas, some discrepancies related to numerical methods take place. This suggests that Eq. (11) is more appropriate when the system is subjected to an external periodic excitation [41–43], while Eq. (8) is more appropriate for systems that are not externally perturbed by a periodic excitation [21,44].

To understand the displacement of the Brownian particles in the traveling deformable system, we compute Eq. (10) together with Eq. (2) using the numerical method outlined above. It turns out that the Monte Carlo error σ as a function of the driving speed presents the same evolution as the average velocity for each value of the shape parameter. These fluctuations are always smaller than the corresponding average velocity (see Fig. 3). Also presented is the average velocity of Brownian particles given by Eq. (8) as a function of r (Fig. 4). The general behavior of $\langle v \rangle$ is almost the same when the absolute value of r increases for a fixed value of

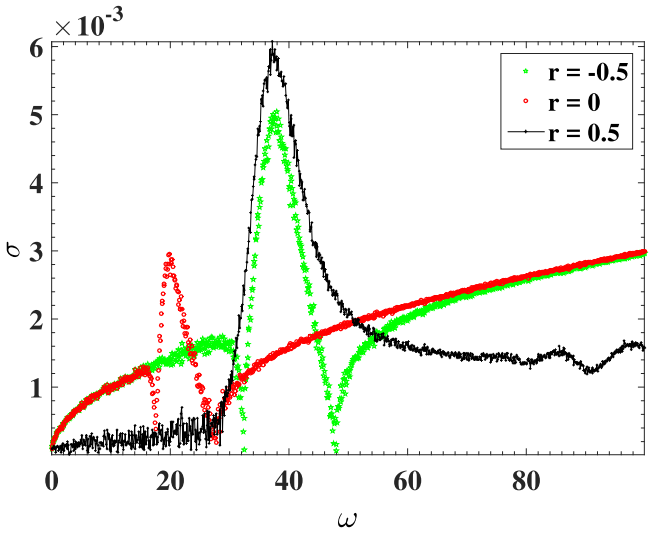

FIG. 3. Monte Carlo error σ vs ω for different values of the shape parameter r, with $U = 20.0$, $D = 0.5$, and $\gamma = 1$. Note that σ follows the same shape as the average velocity when $|r|$ increases.

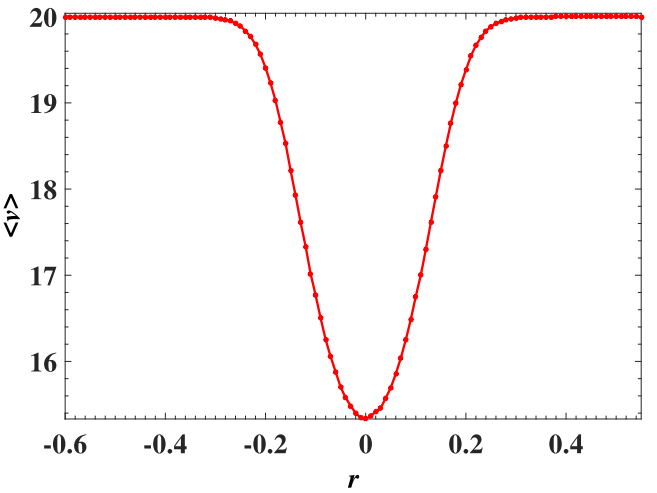

FIG. 4. Schematic representation of the average velocity of the Brownian particle in the overdamped case as a function of r for $U = 20.0$, $D = 0.5$, and $\omega = 20.0$. This curve has nearly symmetric variations as the shape parameter evolves.

the traveling speed. Although the effect of each collision between the particle and its surrounding is important in the overdamped regime, the Monte Carlo errors prove that the transport properties of Brownian particles are performed with less turn-back. In the deformed system, and in the overdamped regime, the transport properties of Brownian particles are shown in the directed direction. Moreover, thermal energy is less dissipated in the deformable potential compared to the sinusoidal shape ($r = 0$).

2. *Diffusion in the overdamped Brownian motion*

The behavior of the effective diffusion coefficient of the Brownian particle D_{eff} as a function of the traveling speed of the deformable potential for different values of the shape parameter r is investigated in the overdamped case. It exhibits a pronounced "resonance" peak at $\omega = \omega_{\text{opt}}$ for different values of the shape parameter r (see Fig. 5). In fact, the presence of thermal fluctuations and/or the difference between the traveling speed of the potential and the velocity of the

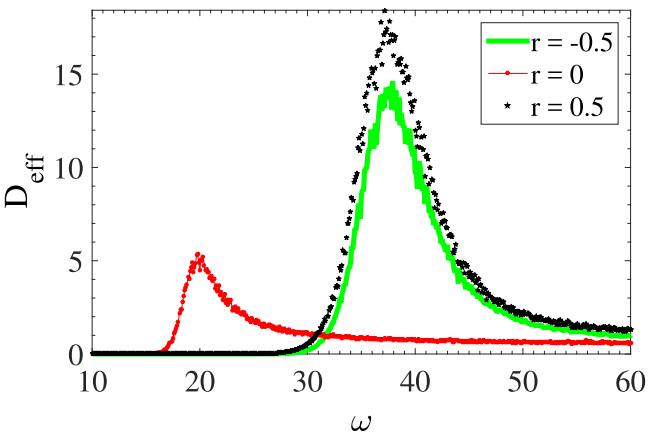

FIG. 5. Schematic representation of the effective diffusion of the Brownian particle in the overdamped regime as a function of the traveling speed ω for a few values of r. The other parameters are $U = 20$, $D = 0.5$, and $\gamma = 1$.

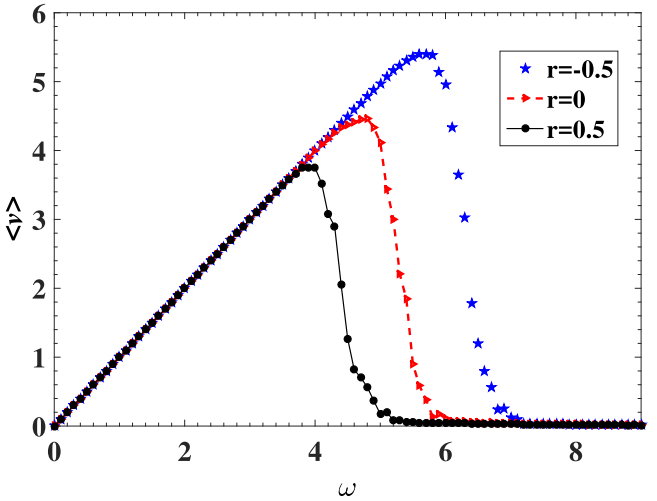

FIG. 6. Representation of the average velocity as a function of ω for different values of the shape parameter r in the underdamped case. The transport properties are controlled by the shape parameter. The average velocity is higher for the negative value of the shape parameter, $r = -0.5$, than the positive values, $r = 0$ and 0.5. Note also that due to the presence of inertia, the potential energy is minimized. Other simulation parameters are $K_BT = 0.56$, $\gamma = 0.4$, and $m = 1$.

surrounding medium may induce the motion in the system, thus inducing the diffusion of a Brownian particle. The effective diffusion is closely linked to the geometry of the system since peaks change when the shape parameter varies from sinusoidal to nonsinusoidal (see Fig. 5). For example, the peak of the effective diffusion coefficient is approximatively equal to 5, 14, and 18 times the Einstein diffusion ($D = K_BT/\gamma$) for $r = 0$, -0.5, and 0.5, respectively.

B. Underdamped Brownian motion

1. The average velocity in the underdamped Brownian motion

In this subsection, we use the same numerical method as in the previous section to study the case in which the term $m\ddot{x}$ is not neglected. The results of numerical simulations of the average velocity of Brownian particles $\langle v\rangle$ as a function of the traveling speed ω of the deformable potential are plotted in Fig. 6, while the corresponding Monte Carlo error σ as a function of the traveling speed of the deformable potential ω is plotted in Fig. 7.

It should be noted that in the underdamped case, the weight of the Brownian particle plays an important role in its displacement in the system. It contributes to reducing the height of the potential barrier, as well as the time of displacement of the Brownian particle in the system. We can say that the dynamical behavior of the system, which is more regular, is controlled by the shape parameter r, as can be seen in Fig. 6. What is remarkable in this case is the behavior of Brownian particles whose average velocity decreases as the shape parameter r takes positive values. This behavior is contrary to what we observed in Fig. 2 in the case of overdamped Brownian motion. In fact, we notice that in the overdamped case, more energy is needed for the Brownian particle to cross the potential barrier. Thus, in the overdamped

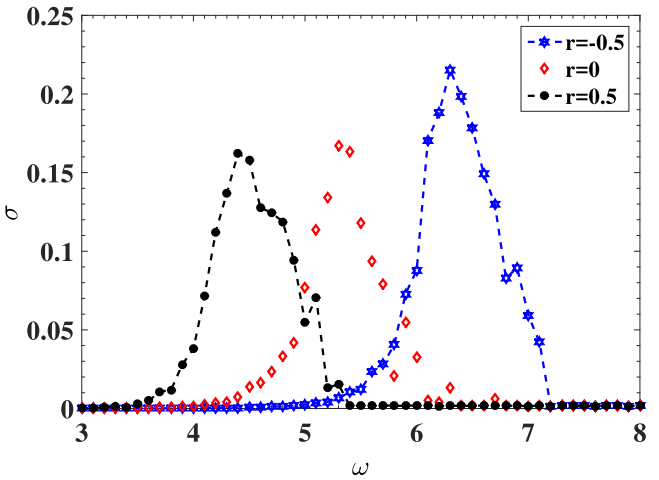

FIG. 7. Monte Carlo error representation in the underdamped case. Others simulation parameters are $\gamma = 0.4$, $K_BT = 0.56$, and $m = 1$.

and underdamped Brownian motions, this crossover energy depends strongly on the shape parameter r. Once the particle crosses the potential barrier, there is a smooth decreasing of the energy provided by the potential as ω increases and the Brownian particle slowly moves to a stable position where it oscillates. This behavior is illustrated by the smooth decrease seen in Fig. 2. Meanwhile, in the underdamped case the influence of both inertia and damping contributes to lower the potential barrier, so that when the particle crosses the barrier, it jumps quickly to the equilibrium position (see Fig. 6). The Monte Carlo error plotted in Fig. 7 follows the same behavior as $\langle v\rangle$, but it always remains lower. Thus, in both cases (overdamped and underdamped), the Brownian particle moves in the directed direction.

To gain good insight into the motion of the Brownian particle in the deformed traveling-wave potential in the underdamped case, we have plotted in Fig. 8 the maximum average

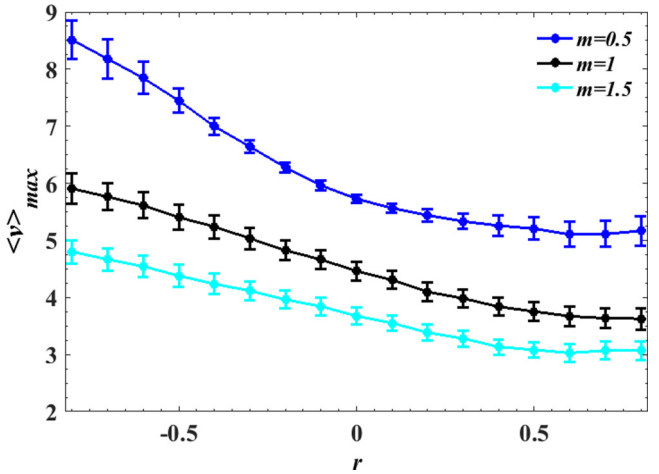

FIG. 8. Schematic representation of the maximum average velocity of the Brownian particle as a function of the shape parameter r in the underdamped case. Note here that, contrary to the overdamped case, the average velocity decreases as the shape parameter r evolves from negative values to positive ones.

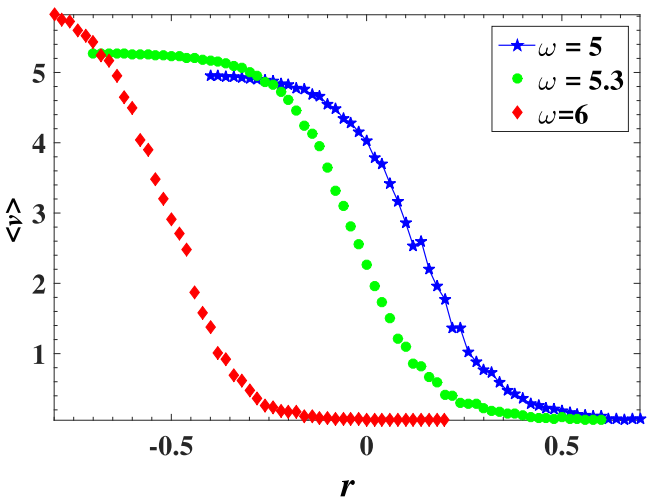

FIG. 9. Numerical simulation of the average velocity as a function of the shape parameter r for different values of ω. We can see the decrease of the average velocity as the shape parameter r evolves from negative values to positive values for three values of the traveling potential speed. We also remark that the form of these curves follows the same shape as that of Fig. 8. This decrease comes from the fact that the necessary thermal energy for the particle to make a transition to the adjacent potential well is less dissipated in the deformable potential with broad wells and narrow deep wells, and the particle in this case has the necessary momentum to cross the potential barrier. Other simulation parameters are $K_BT = 0.56$, $\gamma = 0.4$, and $m = 1$.

velocity of the Brownian particle as a function of the shape parameter r for several values of m, and the evolution of the average velocity obtained by direct simulation of Eq. (2) for $m = 1$ (Fig. 9). It is shown in Figs. 8 and 9 that the error bars are much pronounced in the underdamped case. However, in all cases the maximum of $\langle v \rangle$ is a decreasing function of the shape parameter r. So, we observe that the

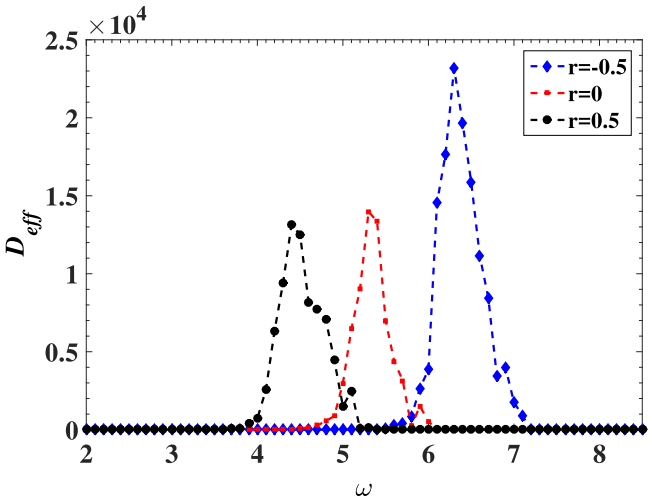

FIG. 10. Plot of the effective diffusion D_{eff} as a function of the traveling potential speed ω for some values of the shape parameter r ($r = -0.5$, 0, and -0.5) as indicated in the figure. Other parameters of simulation are $U = 5$, $KT = 0.56$, $\gamma = 0.4$, and $m = 1$.

maximum average velocity of Brownian particles increases when the mass of the system decreases, thus evolving into the overdamped case, where the error bars are weak (see Fig. 8). This behavior of the average velocity may be due to the complex displacement of the Brownian particle in the system in the presence of inertia and thermal noise. These results are in good agreement with the theory of the chaotic behavior in the system when inertia is taken into account [45]. Moreover, we observe an abrupt decrease of the average velocity of the Brownian particles as a function of r compared to the overdamped case. One can say that the inertia has a positive influence on the transport properties of the system since it reduces the effect of fluctuations in the system and controls the transport properties.

This behavior of the Brownian particle in the underdamped case could be advantageous in the sense that even with lower energy, the unpinning of the system may be possible, but due to the inertia, the cargo may or may not reach the target.

2. *Diffusion in the underdamped Brownian motion*

In Fig. 10, we depict the effective diffusion as a function of the traveling-wave potential speed ω, obtained numerically from Eqs. (2) and (9) for some values of the shape parameter r. Indeed, recent investigations have shown that under the effect of weak noise, and regardless of the value of the friction coefficient, there can appear a giant enhanced diffusion when the system undergoes an external constant load [1,21,46]. This is due to the presence of the locked-to-running transition that takes place when the Brownian particle diffuses on a one-dimensional periodic substrate and is subjected to a weak tilt. However, it has also been demonstrated through a Fokker-Planck equation that, in the absence of external constant load in the overdamped regime, a traveling-wave potential could induce a nonzero current $\langle \dot{x}(t) \rangle \neq 0$ if the total energy of the Brownian particle is higher than that of the potential barrier [34]. Thus, when the particle drifts under the force exerted by the potential, the random switches between locked and running states also take place and cause an average spreading $R(t) = \langle [x(t) - \langle x_{\text{CM}}(t) \rangle]^2 \rangle$ of particles around its average position. In our case (see Fig. 10 for $m = 1$), this diffusion regime is very pronounced for negative values of the shape parameter r, and thus the optimum values of the traveling-wave potential speed that can be generated by the shape parameter r are also higher for the negative values of r (deep barriers and broad wells) than the positive ones. Moreover, for each peak corresponding to each value of the shape parameter r, there exists a value of ω_{opt} for which the effective diffusion takes its maximum, which is slightly higher than that of the transition (ω_{opt}, for average velocity). Indeed, for $r = -0.5$, $\omega_{\text{opt}} = 6.3$, $D_{\text{eff}_{\text{max}}} = 2.3181 \times 10^4$; for $r = 0$, $\omega_{\text{opt}} = 5.3$, $D_{\text{eff}_{\text{max}}} = 1.398 \times 10^4$; and finally for $r = 0.5$, $\omega_{\text{opt}} = 4.4$, $D_{\text{eff}_{\text{max}}} = 1.3158 \times 10^4$.

Next, we focus our attention on the effects of the shape parameter of the system on the peak values of the diffusion of Brownian particles in the underdamped case and the corresponding optimal deformable traveling-wave potential speed ω_{opt} for several values of m ($m = 0.5$, 1, 1.5). To achieve this purpose, Fig. 11 represents two plots. In the upper panel of this figure, the maximum value of the effective diffusion of

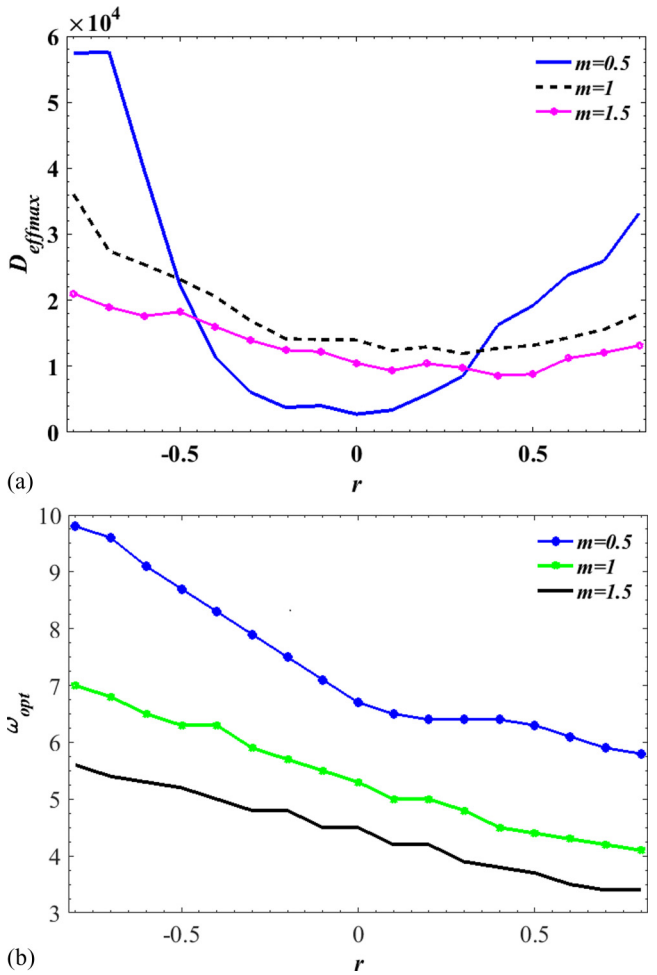

FIG. 11. Maximum values of the effective diffusion for $m = 1$ of the Brownian particle and the corresponding traveling potential speed ω_{opt} as a function of the shape parameter r.

the Brownian particle as a function of the shape parameter r is plotted for $m = 0.5, 1, 1.5$. In the lower panel, the corresponding deformable traveling-wave potential speed ω_{opt} as a function of the shape parameter r is depicted for the same values of m. It can be seen in the upper panel of this figure that the maximum value of the effective diffusion is a decreasing function of the shape parameter r for $m = 1$ and 1.5. However, for $m = 0.5$ one notes an almost parabolic behavior of the maximum diffusion. One should note that this case obviously gets closer to the overdamped case. In the lower panel, the corresponding traveling potential speed ω_{opt} is also a decreasing function of the shape parameter r for all values of m. This behavior of the diffusion of the Brownian particle in the presence of the deformable traveling-wave potential may be due to the fact that, when the potential wells get narrow, the particle does not acquire the necessary space to cross the potential barrier, and then finds it difficult to disperse in the system, involving also the decrease of ω_{opt} as the shape parameter evolves from negative to positive values. To completely illustrate the behavior of the effective diffusion in the deformable medium, we plot for $m = 1$ the effective diffusion as a function of the shape parameter r for some values of the traveling-wave potential speed $\omega = 5$,

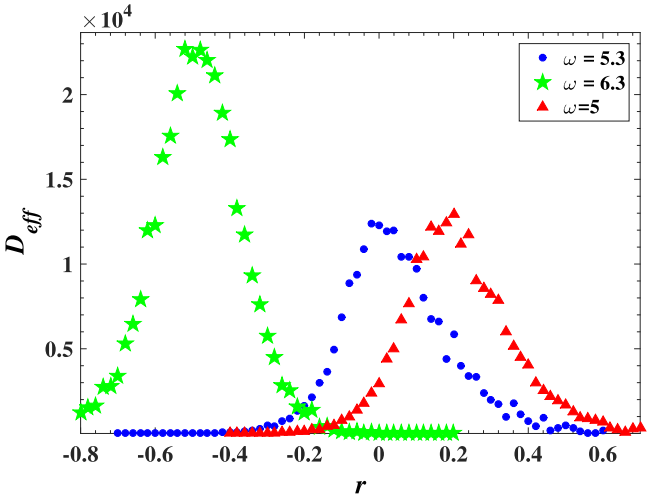

FIG. 12. Effective diffusion as a function of the shape parameter r for a particle moving in the deformable traveling potential for some values of potential speed $\omega = 5$, 5.3, and 6, with the parameters previously used.

5.3, and 6.3 (Fig. 12). When $\omega = 5$ the red curve presents a maximum at $r = 0.2$, for $\omega = 5.3$ the blue curve presents a maximum at $r = 0$, while for $\omega = 6.3$ the green curve shows a maximum at $r = -0.5$. As one might expect, the effective diffusion in this last case is very pronounced compare to the previous ones. This observation from numerical simulation corroborates effectively the previous observation, that is, in addition to the inertia term, the geometry of the potential, particularly the flat bottom, enhances the effective diffusion.

3. The Fokker-Planck treatment

In this subsection, an analysis of the distribution for various shape parameters r is presented. These distributions are

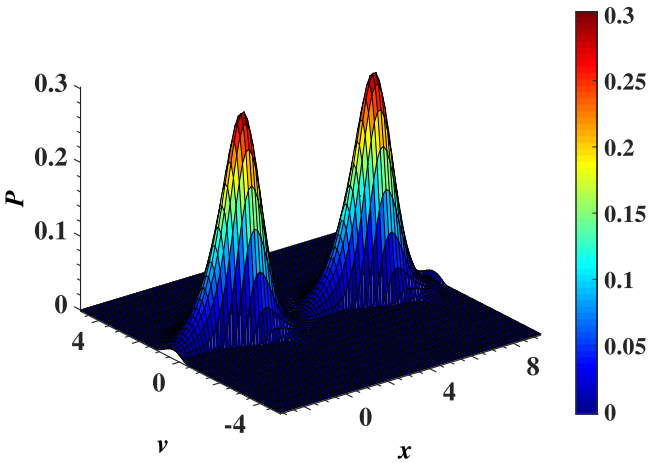

FIG. 13. Approximate solution of the Fokker-Planck equation showing the distribution of the Brownian particle in a deformable potential for $r = 0$ at $t = 1$. This case reduces to the sine-Gordon case. The distribution exhibits two peaks corresponding to two adjacent minima of the potential.

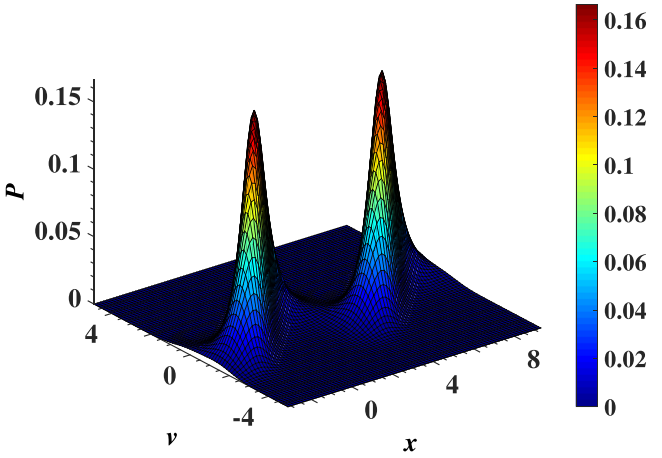

FIG. 14. Numerical simulation of the Fokker-Planck equation in a deformable potential for $r = 0$, obtained from the finite-element method at $t = 1$.

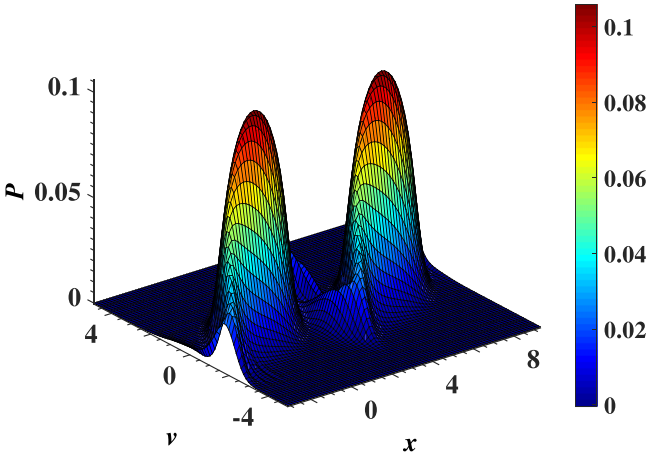

FIG. 16. Numerical simulation of the Fokker-Planck equation in a deformable potential for $r = -0.5$, obtained from the finite-element method at $t = 2$.

plotted for $r = -0.5$, 0, and 0.5 at $t = 1, 2$ in the phase space (x, v) and also as the traveling potential speed is switched off ($\omega = 0$). Thus, by using the semianalytic method developed in the Appendix as well as the numerical method (the finite-element method) for $r = 0$, we observe in Figs. 13 and 14 the presence of two narrow peaks corresponding to the minimum of the potential. For $r = -0.5$, we observe a large peak that also corresponds to the minimum of the potential (see Figs. 15 and 16). However, for $r = 0.5$ we observe a splitting of the number of peaks. Let us recall here that the Fokker-Planck equation has been computed over two periods, characterized by the presence of two peaks. Indeed, for $r = -0.5$ the peaks are large compared to $r = 0$ and 0.5, respectively; this corresponds to a large dispersion of particles inside the potential well, indicating that the particles are spread out over a wider range of values due to the flat potential well and narrow barrier. However, for $r = 0.5$, which corresponds to a narrow well and a flat barrier, we observe a splitting of the number of peaks that pass from two peaks to four peaks (see Figs. 17 and 18). A similar behavior is observed by adopting the semianalytic method, although the two other peaks are not well visible. To explain all these behaviors, let us analyze the different periods of oscillation of particles in different forms of potential. The period of oscillation around the ground states in the deformable potential is $T_r = 2\pi/\omega_r$, with $\omega_r = V''(x_0)$ given by $\omega_r = \frac{U(1+r)^2}{1+r^2}$. Thus, the oscillation periods for $r = -0.5$, 0, and 0.5 are given by $T_1 = 10\pi U$, $T_2 = 2\pi U$, and $T_3 = 1.11\pi U$, respectively. In fact, the time that the particles take in shrinking the potential well to perform oscillations is smaller with respect to $r = 0$ and -0.5. For $r = 0.5$, as has been said before, the particles do not acquire the necessary momentum to cross the potential barrier to the adjacent well and consequently oscillate continuously around several equilibria positions due to the thermal energy, so that the metastable positions can take place leading to the appearance of new extrema (multimodality) in the probability distribution.

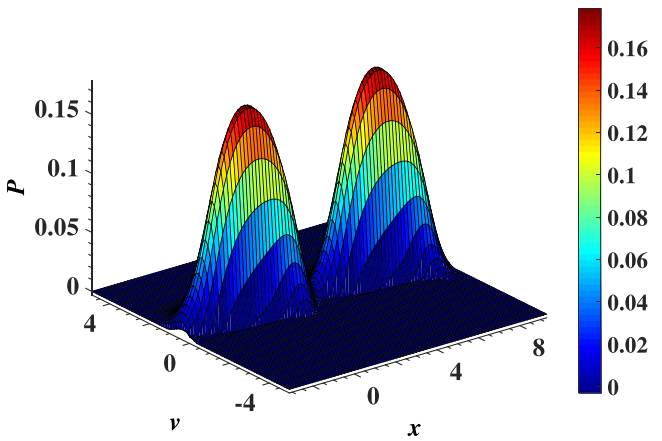

FIG. 15. Approximate solution of the Fokker-Planck equation giving the distribution of the Brownian particle in a deformable potential for $r = -0.5$ at $t = 2$. This case also exhibits two modes corresponding to two adjacent minima of the potential.

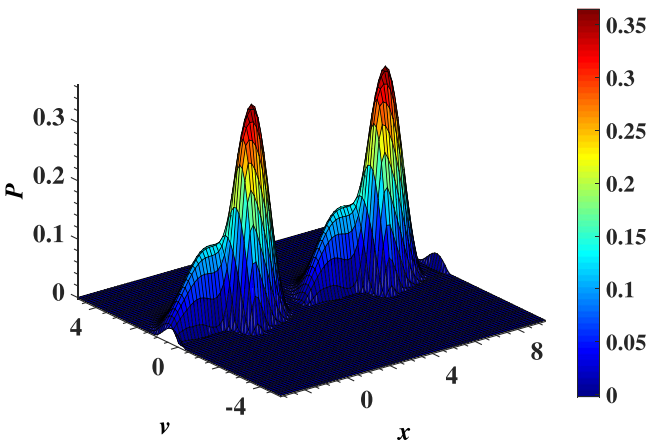

FIG. 17. Approximate solution of the Fokker-Planck equation showing the distribution of the Brownian particle in a deformable potential for $r = 0.5$ at $t = 2$. This case tends to split in several modes.

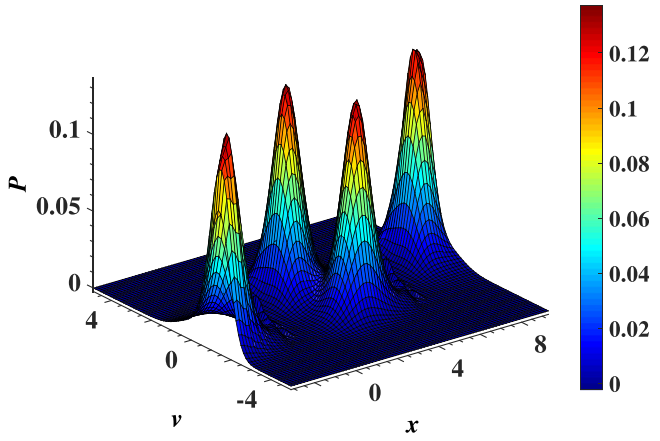

FIG. 18. Numerical simulation of the Fokker-Planck equation in a deformable potential for $r = 0.5$ at $t = 2$, obtained from the finite-element method. We observe a complete splitting of modes that pass from two modes in the previous cases to four modes. This may be due to the metastable states that take place in the system, which is due to a deep-well potential and broad barriers.

IV. CONCLUSION

In this work, we have studied the behavior of Brownian particles in a deformable traveling medium, taking into account a white-noise source. Two aspects of the dynamics have been examined: the case without inertia (the overdamped case), and the case with inertia (the underdamped case). We have focused our attention on the statistical properties of Brownian particle motion (average velocity, Monte Carlo error bars, effective diffusion, and distribution) in the deformable traveling-wave medium. It was revealed that in the presence of the deformable traveling-wave potential, in the overdamped as well as underdamped Brownian motions, each maximum value of the average velocity of Brownian particles is a function of the shape parameter r. However, the effective diffusion in both cases (overdamped and underdamped cases) and the distribution of Brownian particles depend strongly on the shape parameter r. It is also shown that even in the presence of the deformable traveling-wave potential, the average velocity needed for the Brownian particle to cross the potential barrier, for each value of the shape parameter, is always smaller in the underdamped case. The Brownian particles are increasingly affected by inertia and also by damping. Comparing the behavior of the Brownian particle in both cases, the maximum average velocity values increase with the shape parameter r in the overdamped case, while in the underdamped case the transport properties are controlled by the shape parameter r, i.e., the average velocity of Brownian particles increases when the potential wells broaden. When the deformable traveling potential speed increases, the Brownian particle experiences significant reverse motion, and it is almost at rest very quickly compared with the overdamped case. A comparative analysis between the values of the maxima of the average velocity of Brownian particles and the direct numerical simulation of the nonlinear stochastic differential equation has shown that in the underdamped case, the average velocity of the particle depends on the deformable traveling potential speed ω. Moreover, we have observed that the interplay between the mass, the noise, and the force generated by the potential can lead to complex behavior of Brownian particles. Monte Carlo error bars have confirmed the directed motion of the Brownian particle in the overdamped and underdamped cases. It has also been shown that in the absence of any external load, the system in both the overdamped and underdamped cases undergoes an enhancement diffusion. Indeed, in both cases the effective diffusion is always greater than that of Einstein, regardless of the shape parameter r. Moreover, in the underdamped case we have observed a "giant" enhancement diffusion induced by the geometry of the system. Then, the particle diffuses more freely in the potential with $r < 0$ compared with $r > 0$, due to the presence of the mass of the Brownian particle. However, in the overdamped case the effective diffusion exhibits a peak for different values of the shape parameter r, and these peaks are less pronounced compare with the underdamped case.

We have also shown numerically and by the semianalytical method, through the Fokker-Planck equation in the underdamped case, that the distribution can present several modes for positive values of the shape parameter. This comes from the fact that the metastable states can take place in the system, while for the negative value of the shape parameter and the sine-Gordon case ($r = 0$), the birth of each mode obviously corresponds to a minimum of the potential, although for $r < 0$ the distribution is very large.

ACKNOWLEDGMENTS

M.F.K. thanks the Stellenbosch University where a part of this work was carried out during his visit under the Fellowship "Pafroid" project funded by the European Commission, which is gratefully acknowledged. We are indebted to Hugo Touchette from Stellenbosch University for useful discussions and orientations. T.C.K. thanks the African University of Science and Technology–Abuja Nigeria (AUST) and the Nelson Mandela Institution (NMI) where a part of this work was carried out during his visit. Thanks to the Electronic Journal Delivery Service of the International Centre of Theoretical Physics (ICTP) for providing valuable references used in this study.

APPENDIX: SEMIANALYTICAL TREATMENT OF THE FOKKER-PLANCK EQUATION

In the case of $r = 0$, we have the particular case of the sine-Gordon potential, which leads to the sinusoidal case. Therefore, the analytical solution of the Fokker-Planck equation can be easily approximated by the matrix continued fraction (MCF) shown in Refs. [3,47,48] and more recently in [21]. Nevertheless, we are going to use the spectral method, or again a "semianalytical" method, to approximate the solution [49]. In fact, according to Refs. [3,21,48] we set

$$P(x,t,v) = \sum_{n=0}^{\infty} C_n(x,t)\psi_n(v), \tag{A1}$$

where $C_n(x,t)$ are the expansion coefficients. As was mentioned before, the coupled system of $C_n(x,t)$ may be solved using matrix continued fraction methods, notably for the cosine potential, parabolic, and so on. The $\psi_n(v)$ is the

nth-order Hermite polynomial, and its factorial factor is chosen so that the coefficient matrix of the induced partial differential equation system for C_n is symmetric, which implies that this partial differential equation is hyperbolic. The Hermite functions obey the following recurrence relations:

$$\frac{d\psi_n(v)}{dv} = -\alpha\sqrt{2(n+1)}\psi_{n+1}(v), \tag{A2}$$

$$\frac{d^2\psi_n(v)}{dv^2} = -\alpha^2\sqrt{4(n+1)(n+2)}\psi_{n+2}(v), \tag{A3}$$

$$v\frac{d\psi_n(v)}{dv} = \sqrt{(n+1)(n+2)}\psi_{n+2}(v) - (n+1)\psi_n(v) \tag{A4}$$

$$v\psi_n(v) = \left(\frac{\alpha}{\sqrt{2}}\right)(\sqrt{n+1}\psi_{n+1}(v) + \sqrt{n}\psi_{n-1}(v)). \tag{A5}$$

By inserting Eq. (A1) in the time-dependent Fokker-Planck equation, Eq. (4), and applying Eqs. (A2)–(A5), we obtain the following coupled system, which constitutes a partial differential equation system that obeys the expansion coefficients:

$$\begin{aligned}\frac{\partial C_n(x,t)}{\partial t} = &-\frac{\alpha\sqrt{n}}{\sqrt{2}}\frac{\partial C_{n-1}(x,t)}{\partial x} - \frac{\alpha\sqrt{n+1}}{\sqrt{2}}\frac{\partial C_{n+1}(x,t)}{\partial x}\\ &-\frac{\sqrt{2n}}{\alpha}[V'(x,t)]C_{n-1} - \gamma n C_n(x,t)\\ &+\sqrt{n(n-1)}\left(\frac{2\gamma KT}{\alpha^2} - \gamma\right)C_{n-2}(x,t).\end{aligned} \tag{A6}$$

To solve Eq. (A6), we use the spectral method of order N. This method consists of solving the first $(N+1)$ equation of (A6) for the $N+1$ expansion coefficients $C_0, C_1, C_2, \ldots, C_N$. Thus, all the functions $C_n(x,t)$, $n \geqslant N+1$, are set to 0, i.e., take the approximate solution to $P(x,v,t)$ as the following truncated series $P_N(x,v,t)$.

$\mathbf{C}$ denotes an $(N+1)$-dimensional column vector defined by $\mathbf{C} = \mathbf{C}(\mathbf{x},\mathbf{t}) = [C_0(x,t), C_1(x,t), \ldots, C_N(x,t)]^T$. The coupled system (A6) becomes

$$\frac{\partial \mathbf{C}}{\partial t} = -\alpha\mathbf{R}\frac{\partial \mathbf{C}}{\partial x} + \mathbf{S}\mathbf{C}, \tag{A7}$$

where $\mathbf{R}$ and $\mathbf{S}$ are $(N+1)\times(N+1)$ matrices given by

$$\mathbf{R} = \begin{pmatrix} 0 & \alpha_1 & & & \\ \alpha_1 & 0 & \alpha_2 & & \\ & \ddots & \ddots & \ddots & \\ & & \alpha_N & & \alpha_N \end{pmatrix} \tag{A8}$$

and

$$\mathbf{S} = \begin{pmatrix} 0 & 0 & \cdots & 0 & \cdots \\ -\frac{\sqrt{2}}{\alpha}A & -\gamma & 0 & \cdots & \\ 0 & -\frac{2}{\alpha}A & -2\gamma & 0 & \cdots \\ 0 & 0 & -\frac{\sqrt{6}}{\alpha}A & -3\gamma & \cdots \\ \vdots & \ddots & \ddots & \ddots & \ddots \end{pmatrix} \tag{A9}$$

with $A = \frac{\partial V(x,t)}{\partial x}$ and $\alpha_n = \sqrt{n/2}$. $\mathbf{R}$ is a symmetric matrix, so the set of its eigenvectors is also an orthogonal matrix; let us define the eigenvectors as $U = [u_0, u_1, \ldots, u_N]$. It is easily verified that $U^T R U = \Delta = \mathrm{diag}[\lambda_0, \lambda_1, \lambda_2, \ldots, \lambda_N]$. If we multiply Eq. (A7) by U^T, we obtain

$$\frac{\partial \tilde{C}}{\partial t} = -\alpha\Delta\frac{\partial \tilde{C}}{\partial x} + \tilde{S}\tilde{C}, \tag{A10}$$

with $\tilde{C} = U^T C$ and $\tilde{S} = U^T S U$. Since Eq. (A10) is a nonlinear and coupled system, it is difficult to obtain an analytical solution for all the different modes; thus, the finite-difference method should be used to approximate the solution $\tilde{C}(x,t)$. It is for this reason that we call it the "semianalytic method." To ensure the stability of the finite-difference method in our case, the different schemes are used according to the sign of the eigenvalue of the matrix R. So, for $\lambda_i < 0$, the forward space difference scheme should be used, and for $\lambda_i > 0$, the backward space difference scheme should be used. Combining all this, we obtain the following different numerical schemes:

$$\begin{aligned}\tilde{C}_i(x,t+dt) = \tilde{C}_i(x,t) - \frac{\alpha\lambda_i dt}{dx}[\tilde{C}_i(x,t) - \tilde{C}_i(x-dx,t)]\\ + dt(\tilde{S}\tilde{C})_i(x,t)\end{aligned} \tag{A11}$$

for $\lambda_i > 0$,

$$\begin{aligned}\tilde{C}_i(x,t+dt) = \tilde{C}_i(x,t) - \frac{\alpha\lambda_i dt}{dx}[\tilde{C}_i(x+dx,t) - \tilde{C}_i(x,t)]\\ + dt(\tilde{S}\tilde{C})_i(x,t)\end{aligned} \tag{A12}$$

for $\lambda_i < 0$, and

$$\tilde{C}_i(x,t+dt) = \tilde{C}_i(x,t) + dt(\tilde{S}\tilde{C})_i(x,t) \tag{A13}$$

for $\lambda_i = 0$. So, the $C_i(x,t)$ are substituted into Eq. (A1) to approximate the solution of the Fokker-Planck equation. To illustrate this, we chose $N = 9$, and some results displayed in the text show the different approximation forms.

[1] P. Hänggi and F. Marchesoni, Rev. Mod. Phys. **81**, 387 (2009).

[2] P. Hänggi, F. Marchesoni, and F. Nori, Ann. Phys. (Leipzig) **14**, 51 (2005).

[3] H. Risken, *The Fokker-Planck Equation: Methods of Solution and Applications* (Springer, Berlin, 1984).

[4] H. Touchette, T. Prelberg, and W. Just, J. Phys. A **45**, 395002 (2012).

[5] H. Touchette, E. Van der Straeten, and W. Just, J. Phys. A **43**, 445002 (2010).

[6] A. Gnoli, A. Puglisi, and H. Touchette, Europhys. Lett. **102**, 14002 (2013).

[7] A. Baule, H. Touchette, and E. G. D. Cohen, Nonlinearity **24**, 351 (2011).

[8] K. Svoboda, P. P. Mitra, and S. M. Block, Proc. Natl. Acad. Sci. (U.S.A.) **91**, 11782 (1994).

[9] F. Jülicher, A. Ajdari, and J. Prost, Rev. Mod. Phys. **69**, 1269 (1997).
[10] B. Louis, doctoral thesis, Université de la Sorbonne, France, 1900.
[11] M. E. Fisher and A. B. Kolomeisky, Proc. Natl. Acad. Sci. (U.S.A.) **96**, 6597 (1999).
[12] S. Leibler, Nature (London) **370**, 412 (1994).
[13] R. Metzler, J.-H. Jeon, A. G. Cherstvy, and E. Barkai, Phys. Chem. Chem. Phys. **16**, 24128 (2014).
[14] Y. Meroz and I. M. Sokolov, Phys. Rep. **573**, 1 (2015).
[15] E. Barkai, Y. Garini, and R. Metzler, Phys. Today **65**(8), 29 (2012).
[16] A. S. Bodrova, A. V. Chechkin, A. G. Cherstvy, H. Safdari, I. M. Sokolov, and R. Metzler, Sci. Rep. **6**, 30520 (2016).
[17] B. Lindner and E. M. Nicola, Eur. Phys. J. Spec. Top. **157**, 43 (2008).
[18] P. Reimann, C. Van den Broeck, H. Linke, P. Hänggi, J. M. Rubi, and A. Pérez-Madrid, Phys. Rev. Lett. **87**, 010602 (2001).
[19] I. G. Marchenko, I. I. Marchenko, and V. I. Tkachenko, JETP Lett. **106**, 242 (2017).
[20] Z.-W. Bai and W. Zhang, Chem. Phys. **500**, 62 (2018).
[21] B. Lindner and I. M. Sokolov, Phys. Rev. E **93**, 042106 (2016).
[22] A. Asaklil, M. Mazroui, and Y. Boughaled, Eur. Phys. J. B **10**, 91 (1999).
[23] W. Dieterich, P. Fulde, and I. Peschel, Adv. Phys. **29**, 527 (1980).
[24] W. Dieterich, Solid State Ion. **5**, 21 (1981).
[25] M. Kostur, L. Machura, P. Hänggi, J. Luczka, and P. Talkner, Physica A **371**, 20 (2006).
[26] A. Kenfack, J. Gong, and A. K. Pattanayak, Phys. Rev. Lett. **100**, 044104 (2008).
[27] M. Borromeo and F. Marchesoni, Chaos **15**, 026110 (2005).
[28] D. L. Ermak and H. Buckholz, J. Comput. Phys. **35**, 169 (1980).
[29] R. Hegadi, A. Kop, and M. Hangarge, A Survey on Deformable Model and its Applications to Medical Imaging, Special Issue on RTIPPR (Recent Trends in Image Processing and Pattern Recognition (IJCA, 2010), pp. 64–75.
[30] D. Terzopoulos and K. Fleischer, Visual Comput. **4**, 306 (1988).
[31] M. Borromeo and F. Marchesoni, Phys. Lett. A **249**, 199 (1998).
[32] Y.-X. Li, X.-Z. Wu, and Y.-Z. Zhuo, Physica A **286**, 147 (2000).
[33] X. Q. Huang, P. Deng, J. W. Xiong, and B. Q. Ai, Eur. Phys. J. B **85**, 162 (2012).
[34] R. L. Woulache, F. M. Kepnang Pebeu, and T. C. Kofane, Physica A **460**, 326 (2016).
[35] T. Katsouleas and J. M. Dawson, Phys. Rev. Lett. **51**, 392 (1983).
[36] P. R. Bevington and D. K. Robinson, *Data Reduction and Error Analysis for the Physical Sciences* (McGraw-Hill, New York, 2003).
[37] N. Metropolis, A. W. Rosenbluth, M. N. Rosenbluth, A. H. Teller, and E. Teller, J. Chem. Phys. **21**, 1087 (1953).
[38] M. Peyrard and M. Remoissenet, Phys. Rev. B **26**, 2886 (1982).
[39] G. Costantini, F. Marchesoni, and M. Borromeo, Phys. Rev. E **65**, 051103 (2002).
[40] F. Reif, *Fundamentals of Statistical and Thermal Physics* (McGraw-Hill, Singapore, 1985).
[41] L. Machura, M. Kostur, P. Talkner, J. Luczka, F. Marchesoni, and P. Hänggi, Phys. Rev. E **70**, 061105 (2004).
[42] J. Spiechowicz, J. Łuczka, and P. Hänggi, J. Stat. Mech. (2013) P02044.
[43] A. M. Fopossi Mbemmo, G. D. Kenmoe, and T. C. Kofane, Eur. Phys. J. B **89**, 211 (2016).
[44] K. Lindenberg, J. M. Sancho, A. M. Lacasta, and I. M. Sokolov, Phys. Rev. Lett. **98**, 020602 (2007).
[45] P. Jung, J. G. Kissner, and P. Hänggi, Phys. Rev. Lett. **76**, 3436 (1996).
[46] G. Costantini and F. Marchesoni, Europhys. Lett. **48**, 491 (1999).
[47] H. D. Vollmer and H. Risken, Z. Phys. B **34**, 313 (1979).
[48] P. Jung, Phys. Rep. **234**, 175 (1993).
[49] T. Chen, Ms. Sci., A theoretical and numerical study for the Fokker-Planck equation, Simon Fraser University, 1992.

Physica A 541 (2020) 123284

Contents lists available at ScienceDirect

Physica A

journal homepage: www.elsevier.com/locate/physa

Transport and diffusion of Brownian particles in a tilted deformable potential

M.F. Kepnang Pebeu [a,*], R.L. Woulaché [a,b], C.B. Tabi [c], T.C. Kofane [a,b,c]

[a] Laboratory of Mechanics, Department of Physics, Faculty of Science, University of Yaounde I, P.O. Box 812, Yaounde, Cameroon
[b] African Center of Excellence in Information and Communication Technologies, University of Yaounde I, Cameroon
[c] Botswana International University of Science and Technology, P/B 16 Palapye, Botswana

ARTICLE INFO

Article history:
Received 25 February 2019
Received in revised form 3 July 2019
Available online 23 October 2019

Keywords:
Brownian particles
Deformable potential
Effective diffusion coefficient
Average velocity
Distribution

ABSTRACT

The underdamped Brownian motion of particles in a deformable potential in response to a constant external force is investigated. Using the matrix continued fraction method, we compute the diffusion coefficient of Brownian particles via the dynamics factor structure at low temperature and intermediate values of friction coefficient. It is numerically found that the transport properties of Brownian particles such as the effective diffusion coefficient, the average velocity and the distribution probability are sensitive to the shape parameter r of the modified nonsinusoidal Remoissenet–Peyrard deformable potential. The bistable behaviour and the distribution of velocity which also shed light on the diffusion anomalies are discussed for some values of the shape parameter. We show that for the negative values of the shape parameter ($r < 0$), the average velocity versus the external tilting of Brownian particles is optimized, while for the positive values ($r > 0$), the average velocity of Brownian particles collapses due to the geometry of the system combined with the friction. Finally, the mechanism of enhancement of the effective diffusion coefficient for a range of the external force is discussed as a function of the shape parameter. We find a power law for the effective diffusion coefficient in terms of the shape parameter r, and show that, it evolves as $D_{th} \sim \mid r \mid^2$.

1. Introduction

Brownian particles in periodic structures play a prominent role in a range of applications because of their intrinsic interest and technological importance [1–4]. For instance, they describe very well numerous systems, ranging from superionic conductors [5,6], damped pendula with torque [7], Josephson junctions [8], intercalation compounds to submonolayer films adsorbed on surfaces of crystalline substrates [9]. In the above mentioned systems, the intuitive picture of particle migration is a thermal-activated series of jumps over a potential barrier from a potential well to another, with thermal noise playing a construction role by providing a mechanism by which particles can escape over the barriers. Thus, the jumps are performed by the diffusion of particles (diffusional spreading of Brownian particles around their mean motion). Notice that, the energy barriers significantly suppress the diffusion [1,6].

Actually, the determination of the effective diffusion coefficient of the system for arbitrary temperature, tilting force, and periodic force potential has been, and remains a challenging task both at the overdamped and underdamped limit in

* Corresponding author.
E-mail addresses: kepemafa@gmail.com (M.F. Kepnang Pebeu), rwoulach@yahoo.com (R.L. Woulaché), tabic@biust.ac.bw (C.B. Tabi), tckofane@yahoo.com (T.C. Kofane).

https://doi.org/10.1016/j.physa.2019.123284
0378-4371/

nonlinear stochastic systems [5,10]. Therefore, two simple approaches for giant enhancing diffusion were proposed, such as the periodic potential which is either tilted or rocked [2,11]. Recently, it has been found [4] that, by using the two-state theory, the diffusion coefficient of underdamped Brownian particles moving on a tilted washboard potential is enhanced with decreasing noise in a finite range of forces. This corresponds to regions of bistability of the deterministic velocity dynamics. Moreover, the threshold value of the driving force at which the dynamical unlocking occurs is determined by the combined action of damping and fluctuations [12].

These observations lead to very important advances in designing new devices based on the motion of ions through periodic structures. This may help to improve components in electrochemical energy storage and conversion devices such as batteries, fuel cells and electrochemical membranes [13,14]. Those devices are critical in the societal shift to renewable energy. Most of these systems, considered as superionic conductors, represent a class of solid materials that shows an unusually high ionic conductivity. Their structure is characterized by a strong disorder in the sublattice of conductivity ions. In this context, the motion of ions considered as noninteracting Brownian particles is treated as a stochastic motion in a medium with periodic lattice structure.

However, periodic structure models, although interesting, describe realistic systems only within some approximations. Indeed, particular situations in physics such as variations of temperature and pressure could modify the on-site potential, leading to shape distortions, variation of crystalline structures and conformation changes. Deformable models have been considered both from mathematical and physical point of views. Mathematically, the foundations of deformable models represent the confluence of geometry, physics, and approximation theory. Geometry serves to represent object shapes, physics imposes constraints on how the shapes may vary over space and time, and optimal approximation theory provides the formal underpinnings of mechanisms for fitting the models to measured data. From the physical point of view, the interpretation views deformable models as elastic bodies which respond naturally to applied forces and constraints.

The aim of this paper is to study the influence of the shape parameter of a nonlinear deformable tilted potential on the transport properties of Brownian particles, based on a symmetric periodic Remoissenet-Peyrard (RP) potential [15,16]. Notice, however, that some relevant results on the dynamics of Brownian particles in the deformable potential have been obtained [17,18]. In doing so, it has been shown that the directed transport of Brownian particles, subject to a deformable travelling wave potential, can be optimized when the shape of the system changes [17,18]. Similarly, the diffusion process mechanism of noninteracting Brownian particles through a deformed potential at low temperature has been investigated [19]. It was shown that the diffusion is characterized by a simple jump diffusion process with jump length close to the lattice constant or a combination of a jump diffusion model with jump length close to the lattice constant and a liquid-like motion inside the unit cell. Nevertheless, the dynamics of Brownian particles in the nonsinusoidal deformable potential and subject to an external load has yet to be investigated. The deformable potential can also represents a substrate potential which has no defects (sinusoidal shape) and which has defects and abnormalities (nonsinusoidal shape) controlled by the shape parameter. Using the matrix continued fraction, the effective diffusion coefficient is computed in the presence of the external force via the dynamic structure factor. The dynamic structure factor contains the complete statistical information about the diffusing particles and gives also the probability distribution of energies at which the lattice can absorb energy at a wave vector k [20].

The layout of this paper is organised as follows. In Section 2, we introduce the model of Brownian particles in deformable tilted potential and the basic quantities of interest, namely the average particle velocity, the effective diffusion coefficient. Later on, using the matrix continued fraction method (MCFM), we compute the effective diffusion coefficient via the dynamic structure factor and show that it depends on the external force and the shape parameter of the system. Since the instantaneous velocity of Brownian particles is a stochastic variable, the bistable behaviour of this latter, associated with its distribution, are discussed as a function of the shape parameter in Section 3.1. In Section 3.2, we analyse how the shape parameter of the potential influences the long-time limit of the average velocity of Brownian particles. The effective diffusion coefficient of Brownian particles is analysed in Section 3.3. Section 4 concludes the paper and summarizes the main findings.

2. Model

We consider the underdamped motion of identical noninteracting Brownian particles of mass m each, subjected to an external constant force moving in a one-dimensional (1D) periodic potential landscape with variable shape. In this work, the modified nonsinusoidal deformable RP potential [21], is given by

$$V(x,r)=\omega_0^2\left(\frac{(1+r)^2(1-\cos x)}{(1-r)^2+2r(1-\cos x)}-1\right), \tag{1}$$

where $|r|<1$, represents the parameter of deformation of the potential, with ω_0 standing for the characteristic frequency of vibrations of the Brownian particle at a minimum of the potential, while ω_0^2 is the strength of the potential barrier. In Fig. 1, we represent the nonsinusoidal deformable RP potential for some values of the shape parameter r for a fixed value of the external load. It can be seen in this figure that for $r=0$, the RP potential reduces to a sinusoidal shape. For $r<0$, it provides broad wells separated by narrow barriers. For $r>0$, it provides deep narrow wells separated by broad flat barriers. The dynamical behaviour of the Brownian particle can be modelled using a stochastic differential equation of the Langevin type written as [7]

$$m\ddot{x}+\gamma\dot{x}=-V'(x,r)+f+\sqrt{2\gamma k_BT}\varepsilon(t), \tag{2}$$

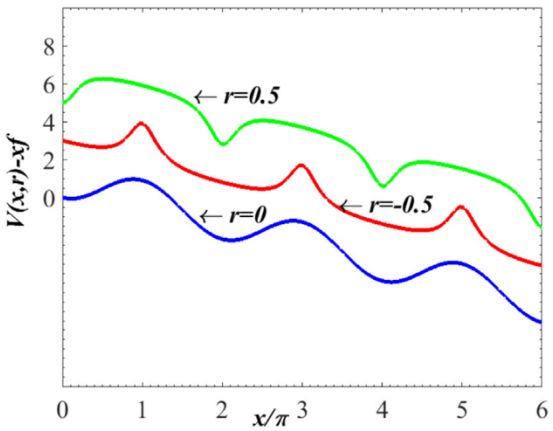

Fig. 1. Schematic representation of the titled deformable potential for the external load $f = 0.35$ as a function of the position x. The potential is represented for some values of the shape parameter $r = 0$, -0.5 and 0.5, with $\omega_0 = 1$.

which describes the Markov process of Brownian particles. In the potential $V(x, r)$ the prime indicates differentiation with respect to x, and the overdot, differentiation with respect to time. γ represents the drag coefficient describing a frictional force experienced by the Brownian particle, where it is moving relative to its environment. The coefficient $D = k_B T/\gamma$ is the diffusion of the Brownian particle, with k_B denoting the Bolztmann constant and T, the temperature of the bath. $\varepsilon(t)$ is a zero-mean delta-correlated Gaussian white noise that describes the fluctuations imposed onto the particle by the interaction with a 'heat bath' at equilibrium temperature T. It satisfies the fluctuation–dissipation relation with $\langle \varepsilon(t)\varepsilon(s)\rangle = \delta(t-s)$, as well as the properties of the Dirac function defined in Ref. [17]. We set particle mass $m = 1$, throughout the paper.

Eq. (2) being a stochastic differential equation, a natural step is to consider a statistical set of stochastic processes belonging to independent realizations of the random fluctuations $\varepsilon(t)$. Equivalent to the Langevin equation (2) is the Fokker–Planck or Smoluchowski equation for the distribution function $P(x, v, t)$ in the phase space (x, v), that is,

$$\frac{\partial}{\partial t}P(x, v, t) = L_F P(x, v, t), \tag{3}$$

with the Fokker–Planck operator L_F being

$$L_F = -v\frac{\partial}{\partial x} + \left(\frac{\partial}{\partial v}\right)(V'(x, r) + \gamma v - f) + D\frac{\partial^2}{\partial v^2}. \tag{4}$$

The relevance of such a model is well known in many areas of science, most notably, motions of defects or interstitial in crystalline materials [22,23], diffusion of ions, superionic conductors [6,24], relaxation and spectral properties of dipolar molecular liquids [25]. In fact, in a periodic potential, no net current occurs except if an external load is applied to induce symmetry breaking [1]. In these conditions, the long-term properties of Brownian particles are characterized by their mean velocity which is given by

$$\langle v\rangle = \lim_{t\to\infty}\frac{\langle x(t)\rangle}{t}, \tag{5}$$

where $\langle\cdots\rangle$ denotes the statistical average over the realizations of the noise $\varepsilon(t)$. Another important quantity that is taken into consideration is the effective diffusion, which is calculated as the mean square displacement of particles over time:

$$D_{eff} = \lim_{t\to\infty}\frac{\langle x(t)^2\rangle - \langle x(t)\rangle^2}{2t}. \tag{6}$$

However, the diffusion coefficient can also be calculated using the MCFM.

Returning to Eq. (3), $P(x, v, t)dxdv$ represents the probability of finding the particle in the phase-space element between (x, v) and $(x + dx, v + dv)$. The MCFM developed by Risken (see Ref. [7] where a complete description of the method with many applications are given) is adopted in the present work in the presence of an external load. This method remains the most efficient semi-analytical one and has been largely adopted these last years to successfully analyse the problem of Brownian motion in periodic structures [4]. This consists of the expansion of the solution into a basis set of plane waves for the position variable and of Hermite functions for the velocity variable. By analogy to what is done in quantum mechanics for the harmonic oscillator, let us introduce, in the dimensionless v space, the operators b and $b^\dagger$:

$$b = \frac{\partial}{\partial v} + \frac{1}{2}v, \quad b^\dagger = -\frac{\partial}{\partial v} + \frac{1}{2}v, \tag{7}$$

which have the well-known properties of annihilation and creation operators when applied to the harmonic oscillator eigenfunctions $\psi_n(v)$ (see [7] for more details). In the dimensionless x-space, and n an integer, we define the operators

$$B(x) = \frac{\partial}{\partial x} - \frac{1}{2}\frac{\partial U(x,r)}{\partial x}, \quad \hat{B}(x) = \frac{\partial}{\partial x} + \frac{1}{2}\frac{\partial U(x,r)}{\partial x}, \tag{8}$$

where

$$U(x,r) = V(x,r) - xf, \tag{9}$$

is a nonlinear effective deformable tilted RP potential. As pointed out in the introduction, the diffusion of particles is computed through the dynamic structure factor $S(q,\omega)$. It also plays an essential role in light and neutron scattering experiments [26,27]. The Van Hove self-correlation function may be evaluated, if the distribution function of the stochastic process is known. It is given by

$$F(q,t) = \int_{-\pi}^{\pi} dx_0 \int_{-\infty}^{\infty} dv_0 \int_{-\infty}^{\infty} dx \int_{-\infty}^{\infty} dv \exp(jq(x-x_0))P_{st}(x_0,v_0)P_c(x,v,t|x_0,v_0,t_0). \tag{10}$$

$P_{st}(x_0,v_0)$ is the stationary solution of Eq. (3) and is given by the Boltzmann distribution

$$P_{st}(x_0,v_0) = N\psi_0^2(v_0)\exp(-U(x_0,r)), \tag{11}$$

where $N^{-1} = \int_{-\infty}^{\infty}\exp(-U(x,r))dx$ is determined by imposing that P_{st} is normalized to 1 in the unit cell for x as well as in the whole space for v; $\psi_n(v)$ is the Hermite function. $P_c(x,v,t|x_0,v_0,t_0)$ is the transition probability of finding a particle at x and v at time t, if there was a particle at the origin x_0 and v_0 at time $t=0$. This transition probability is also the Green function of the Fokker–Planck equation, i.e., the solution of Eq. (3) with initial δ-condition in both the variable x and v given by

$$P_c(x,v,t|x_0,v_0) = \delta(x-x_0)\delta(v-v_0). \tag{12}$$

Since $F(q,t)$ is the correlation function of a stationary process, it is an even function of time and then the dynamic factor structure $S(q,\omega)$ is defined as

$$S(q,\omega) = \frac{1}{2\pi}\int_{-\infty}^{\infty} dt\exp(-i\omega t)F(q,t). \tag{13}$$

In order to compute the transition probability $P_c(x,v,t|x_0,v_0)$, Bloch's theorem is applied and any nonstationary solution of $P(x,v,t)$ of the Fokker–Planck equation is developed into periodic functions. In these conditions, $P_c(x,v,t|x_0,v_0)$ may be written as (see Refs. [7,28] for further details)

$$\begin{aligned} P_c(x,v,t|x_0,v_0) &= \frac{1}{2\pi}\frac{\exp\left(-\frac{1}{2}U(x,r)\right)\psi_0(v)}{\exp\left(-\frac{1}{2}U(x_0,r)\right)\psi_0(v_0)}\sum_{n,m}^{\infty}\psi_n(v)\psi_m(v_0) \\ &\times\int_{-1/2}^{1/2} dk\sum_{p,l=-\infty}^{\infty}\exp(ik(x-x_0))\exp(ipx)\exp(-ilx_0)G_{nm}^{pl}(k,t), \end{aligned} \tag{14}$$

where G_{nm}^{pl} is the Green functions satisfying the initial condition

$$\mathbf{G}_{nm}(k,0) = \mathbf{I}\delta_{n,m}, \tag{15}$$

with $\mathbf{I}$ being the identity matrix and $\delta_{n,m}$, the Kronecker delta:

$$\delta_{n,m} = \begin{cases} 1 & \text{if } n = m \\ 0 & \text{if } n \neq m. \end{cases}$$

Inserting Eqs. (14), (11) and (10) into Eq. (3), the final expression for $S(q,\omega)$ can be written as

$$S(q,\omega) = N\,\mathrm{Re}\left(\sum_{p,l=-\infty}^{\infty}\tilde{G}_{0,0}^{p,l}(k,i\omega)M_{p-a}M_{l-a}^{*}\right), \tag{16}$$

where Re (...) is the real part of the quantity in the bracket. $q = a + k$ must be multiple of the reciprocal lattice vector in the language of a solid-state physicist, with $-1/2 < k \leq 1/2$ restricted to the first Brillouin zone, and where a is an integer. M_l is the modified Bessel function depending on the shape of the system r and is written as:

$$M_l = \frac{1}{2\pi}\int_0^{2\pi}\exp\left(-\frac{U(x,r)}{2}\right)\exp(ilx)dx. \tag{17}$$

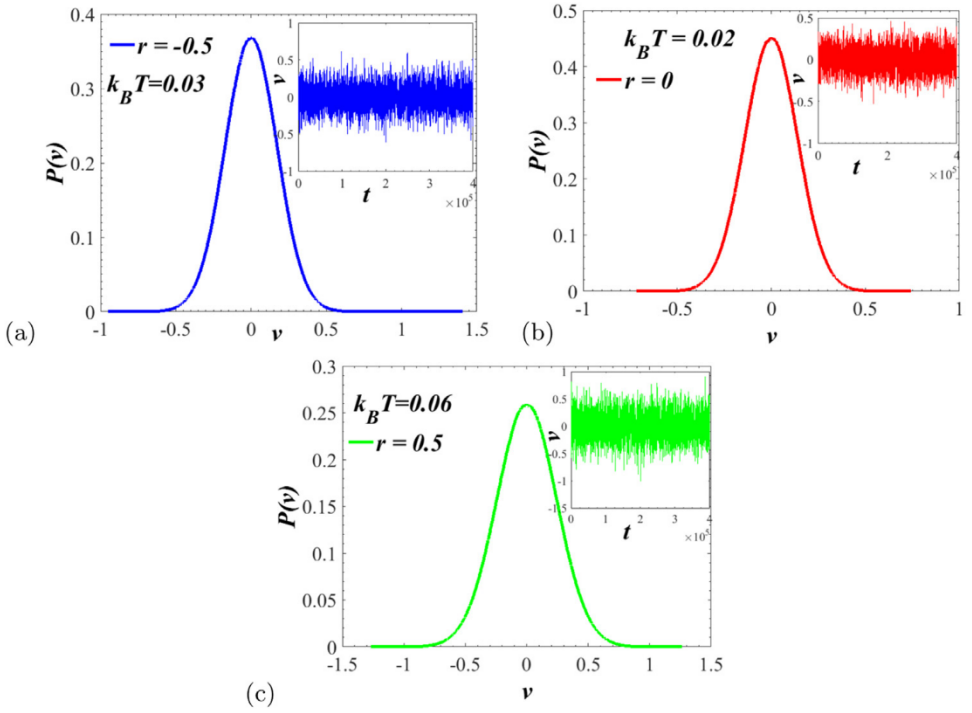

Fig. 2. Plot of transitions of Brownian particles, associated with the different transition distribution in the deformable potential, for three values of the shape parameter r: r = −0.5, 0, and 0.5 for $k_BT = 0.06$. We can see that the distribution probability exhibits a single-peaked Maxwell distribution for all of the three values of the shape parameter r. In these cases there exist only locked solutions due to the weak value of the mean thermal energy. We used $f = 1$, for $r = -0.5$, $f = 0.72$, for $r = 0$, and $f = 0.72$, for $r = 0.5$. The dissipation coefficient used is $\gamma = 0.4$.

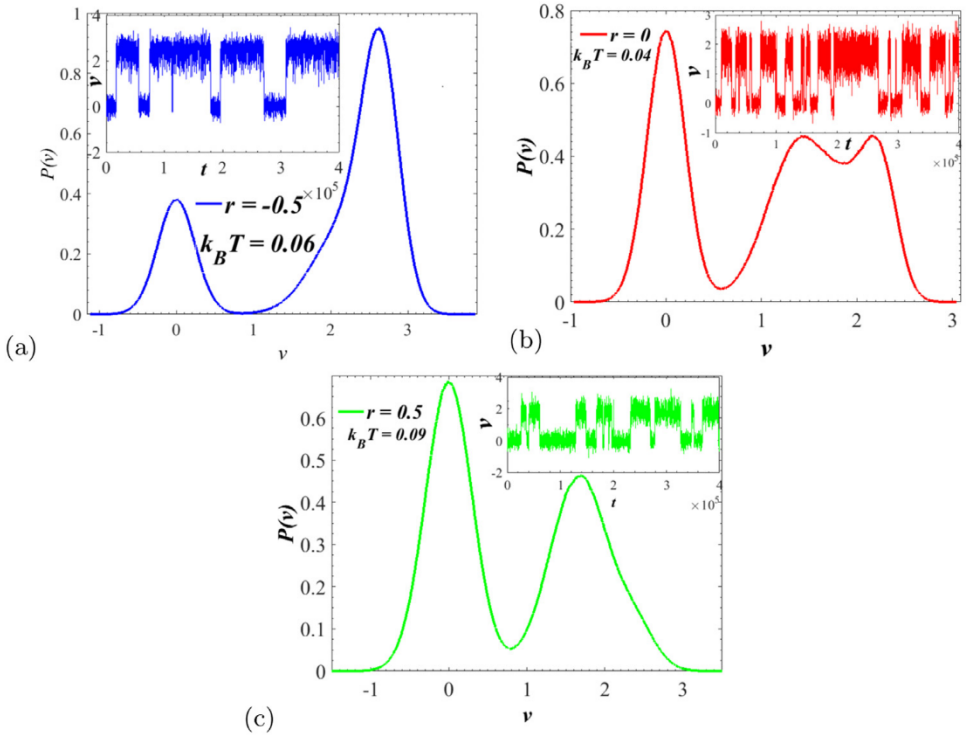

Fig. 3. Plot of transitions of Brownian particles, associated with the different transition distribution in the deformable potential, for three values of the shape parameter r: $r = -0.5$, $k_BT = 0.06$, $f = 1$ is given by the blue curve; $r = 0$, $k_BT = 0.04$, $f = 0.72$ the red curve, while $r = 0.5$, $k_BT = 0.09$, $f = 0.72$ is given by the green curve. The dissipation coefficient is $\gamma = 0.4$.

$\tilde{G}^{p,l}_{0,0}(k, i\omega)$ is the Laplace transform of the matrix elements $G^{pl}_{0,0}(k, t)$ given by the following matrix continued fraction expansion

$$\tilde{G}^{p,l}_{0,0}(k, i\omega) = \cfrac{\mathbf{I}}{i\omega\mathbf{I} + D^{p,l}\cfrac{\mathbf{I}}{(i\omega+\gamma)\mathbf{I}+2D^{p,l}\cfrac{\mathbf{I}}{(i\omega+2\gamma)\mathbf{I}+3D^{p,l}\cfrac{\mathbf{I}}{(i\omega+3\gamma)\mathbf{I}+\cdots}\tilde{D}^{p,l}}\tilde{D}^{p,l}}\tilde{D}^{p,l}}. \tag{18}$$

Replacing Eq. (9) into Eq. (8), the matrix elements of the matrices $\mathbf{D}$ and $\tilde{\mathbf{D}}$ are given by

$$D^{p,l}(k) = (l+k)\delta_{p,l} + \frac{i}{4\pi}\int_0^{2\pi}\frac{\partial V(x,r)}{\partial x}\exp(i(l-p)x)dx - i\frac{f}{2}\delta_{p,l}, \tag{19}$$

and

$$\tilde{D}^{p,l}(k) = (l+k)\delta_{p,l} - \frac{i}{4\pi}\int_0^{2\pi}\frac{\partial V(x,r)}{\partial x}\exp(i(l-p)x)dx + i\frac{f}{2}\delta_{p,l}. \tag{20}$$

The diffusion coefficient is computed via the Green-Kubo relationship

$$D = \pi\lim_{\omega\to 0}\omega^2\lim_{q\to 0}\frac{S(q,\omega)}{q^2}. \tag{21}$$

It is obvious that the Green function of the Fokker–Planck equation is not only related to the external force f, but also depends on the shape parameter of the system and the friction, respectively.

3. Numerical results and discussion

To study the transport properties in more general cases, we have to invoke numerical simulations of Eq. (2). Indeed, although the matrix continued fraction method is an efficient numerical method to compute the effective diffusion solution, over a wide range of values of temperature, the method is limited to the low temperature case. Note that the integration is realized by a single step Euler method with time step Δt, so that we have to multiply the white noise by $\Delta t^{1/2}$, where $\Delta t = 0.01$. In order to integrate Eq. (2) numerically, we produce white noise $\varepsilon(t)$ with the Box–Muller formula [29]. Each data point is obtained by averaging over 10^3–10^4 realizations, where each of them evolves over $t_{max} = 10^5$. Initially, all the particles are placed at the minimum of one potential well, being $x = 0$, and at rest at the bottom of the deformable potential ($\dot{x} = 0$).

3.1. Bistable behaviour of the velocity and distribution of Brownian particles in the deformable potential

In Figs. 2–5, we have plotted the asymptotic long-time velocity of Brownian particles as a function of time for some values of the shape parameter, $r = 0$, $r = -0.5$ and $r = 0.5$, for different mean thermal energy k_BT, and external forces. We have associated with these asymptotic long-time velocities $v(t)$ their corresponding probability distributions $P(v)$. So, in Figs. 2 and 5, the behaviour of velocities of particles and the probability distributions exhibit similar features. Indeed, in Fig. 2, we plot the velocity of Brownian particles and the probability distribution for $r = -0.5$, 0, and 0.5 for some values of the mean thermal energy in the case $k_BT = 0.03$ for $r = -0.5$, $k_BT = 0.02$ for $r = 0$, and $k_BT = 0.06$ for $r = 0.5$. In Fig. 5, we represent the behaviour of velocities and the probability distribution $P(v)$ of particles for $r = -0.5$, 0, and 0.5 for $f = 0.5$. We observe that for the given values of the mean thermal energy and external force, the distribution of particles $P(v)$ boils down to a single-peaked Maxwell distribution, around $v \approx 0$. This indicates that for the three values of the shape parameter r, the particles are mainly trapped in potential wells regardless the shape of the potential. The mean thermal energy and external force provided to the system are not sufficient to making the particles cross the potential barriers. In Fig. 3, for the three values of the shape parameter r and $k_BT < \omega_0^2$, the velocity exhibits a bistable behaviour as found in Ref. [4]. This behaviour is characterized by the presence of two discrete states, i.e, the locked state, where, due to small forces, Brownian particles remain at the minima during large sojourn with zero velocity, and the running state, where Brownian particles jump away because of large forces. In general, under the action of an external load, the total periodic potential tilts. Thus, for large forces f, the potential has no minima, and in this case, the average velocity of particles saturates to the free particle value $v_0 = f/\gamma$. With regard to Fig. 3, different curves exhibit transitions from one bottom to another. These transitions depend on the shape parameter r of the deformable potential. It should be noted that although the three curves exhibit the phenomenon of bistability, this occurs with different mean thermal energies and external forces for the three values of the shape parameter r. For $r = 0.5$, $k_BT = 0.09$, and $f = 0.72$, for $r = -0.5$, $k_BT = 0.04$, and $f = 1$, one can remark that the mean thermal energy, whose the Brownian particle needs to cross the potential barrier, is high in the case of $r = 0.5$ than that of $r = -0.5$ and $r = 0$. Therefore, for $r = 0.5$, Brownian particles are easily pinned at the one-site of the lattice and require an extra thermal energy to perform transitions between the two discrete states, namely the locked and running states. This is because, under the action of the inertia effect, the potential with broad barriers and narrow wells exhibit large radiations coming from the phonon

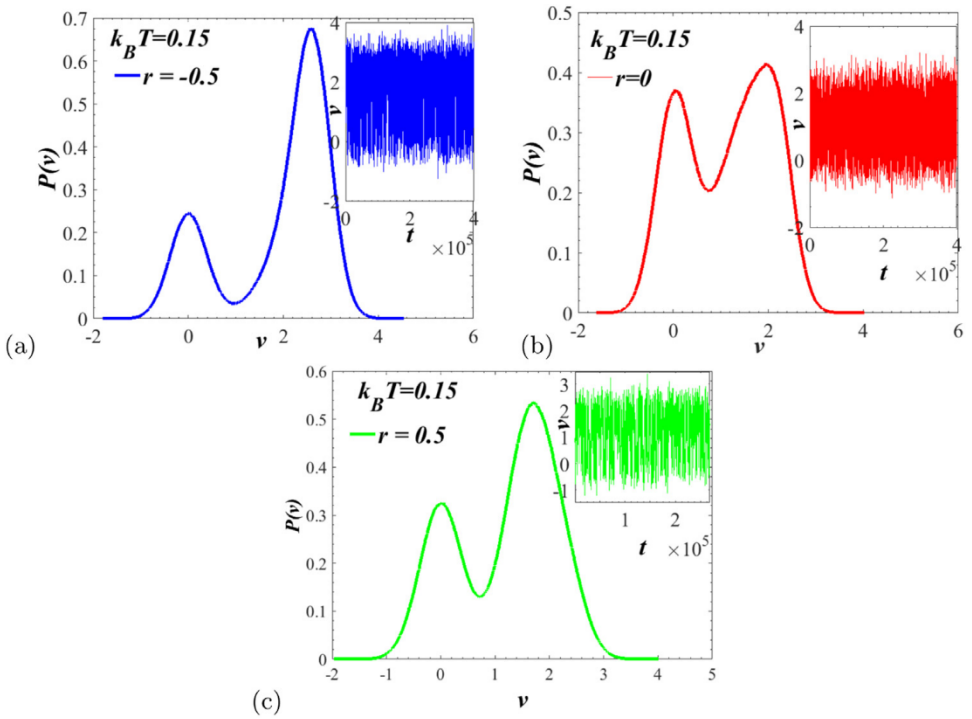

Fig. 4. Plot of transitions of Brownian particles, associated with the different transition distribution in the deformable potential, for three values of the shape parameter r: r = −0.5, 0, and 0.5 for $k_BT = 0.15$. We can see that the distribution probability exhibits two peaks for all of the three values of the shape parameter r. We used $f = 1$, for $r = -0.5$, $f = 0.72$, for $r = 0$, and $f = 0.72$, for $r = 0.5$. The dissipation coefficient used is $\gamma = 0.4$.

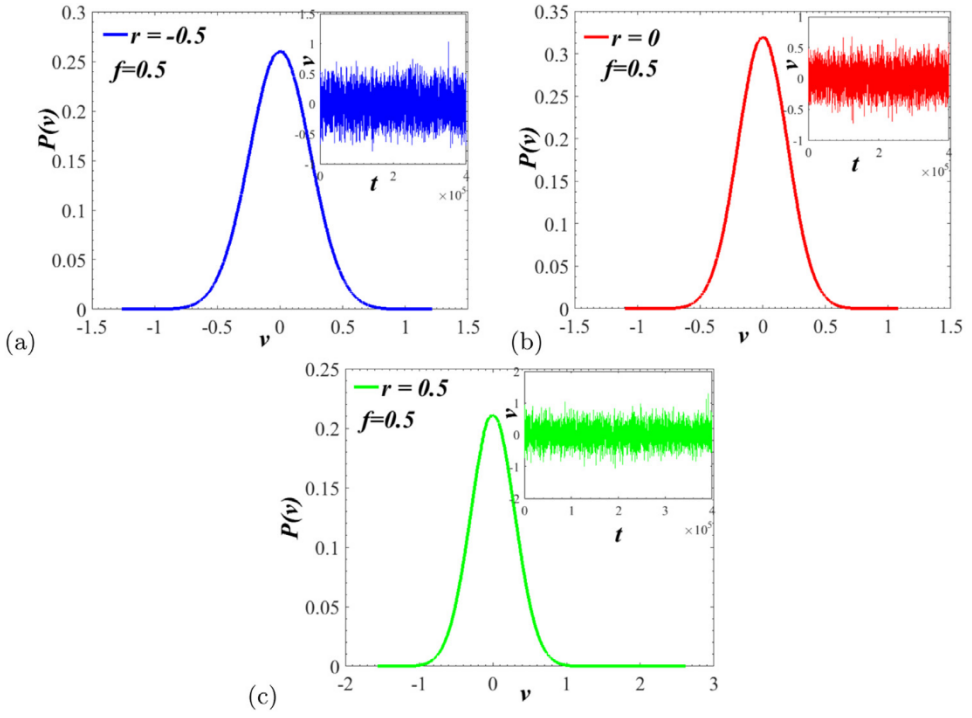

Fig. 5. Plot of transitions of Brownian particles, associated with the different transition distribution in the deformable potential, for three values of the shape parameter r: r = −0.5, 0, and 0.5 for $f = 0.5$. We can see that the distribution probability exhibits a single-peaked Maxwell distribution, because this value of the external force does not allow particles to make transition from a well to another one, for the three values of the shape parameter r. We used $k_BT = 0.06$, for $r = -0.5$, $k_BT = 0.04$, for $r = 0$, and $k_BT = 0.09$, for $r = 0.5$. The dissipation coefficient used is $\gamma = 0.4$.

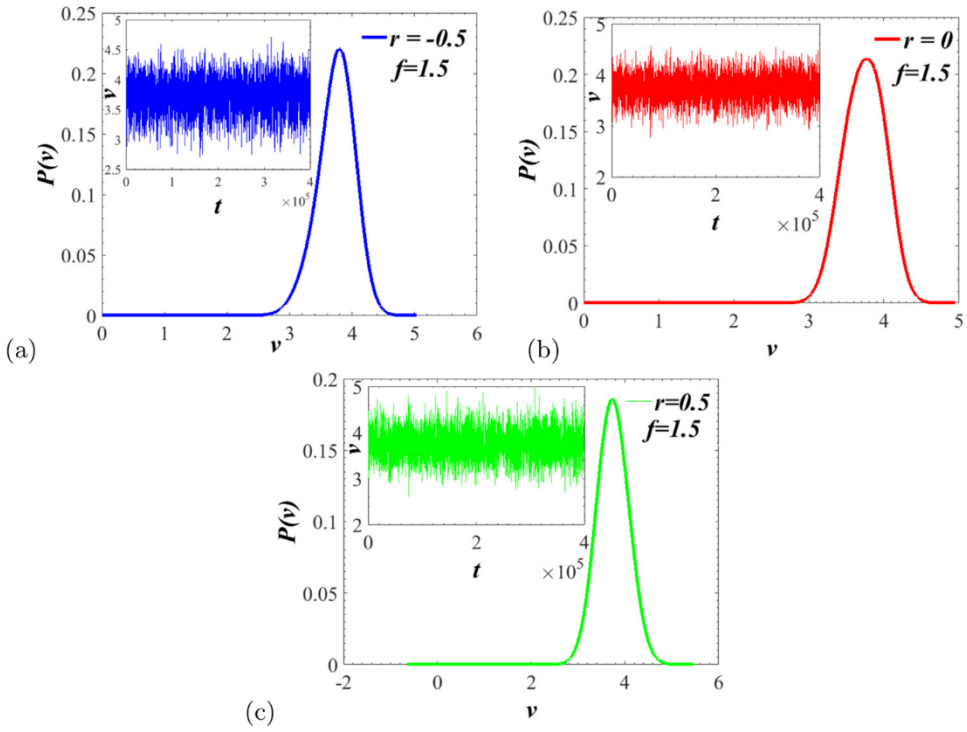

Fig. 6. Plot of transitions of Brownian particles, associated with the different transition distribution in the deformable potential, for three values of the shape parameter r: $r = -0.5$, 0, and 0.5 for $f = 1.5$. We can see that upon increase of the external force, there are more running solution that locked solutions. We used $k_BT = 0.06$, for $r = -0.5$, $k_BT = 0.04$, for $r = 0$, and $k_BT = 0.09$, for $r = 0.5$. The dissipation coefficient used is $\gamma = 0.4$.

bath. Consequently, Brownian particles do not acquire necessary transfer momentum to overcome the potential barrier, hence require additional thermal energy.

Always in Fig. 3, by analysing the probability distributions of the long-time velocity, we observe a fine asymmetry of the probability distribution for the three cases of the shape parameter. It is also relevant to note that for the three values of the shape parameter r, the distribution are nearly Maxwellian around $v \simeq 0$ [30,31]. For $r = 0.5$ and $r = -0.5$, for a vanishingly small damping value, the transition threshold is characterized by a bimodal distribution of the velocity with peak at $v \simeq 0$, describing the locked state which indicates that the particles are mainly trapped in potential wells for the deformed system, and $v = f/\gamma \simeq 1.698$ and $v = f/\gamma \simeq 2.629$, corresponding to the free running Brownian particles pulled by the external force, respectively. However, for $r = 0$, the distribution probability $P(v)$ exhibits three peaks. One should note that this multi-modal form of the distribution probability was not expected. Indeed, we connected, at the beginning, this result to the "running" solutions. We therefore thought that by varying the parameters of interest of the system, the same behaviour could occur for $r = -0.5$ and $r = 0.5$. It turned out that this conjecture is incorrect since, as we can see in Figs. 4 and 6, by increasing the mean thermal energy of the system, we recover two peaks for the three values of the shape parameter r, see Fig. 4. In Fig. 6, by increasing the external force, there are more running solutions. We further checked the outcome for the velocity distribution when reflecting barriers were placed at the maxima of the potential. Under such constraint, we recovered as well the three-peaks structure. We can assimilate this characteristic behaviour of the three peaks in the case $r = 0$ to the nonlinear, anharmonic character of the corresponding well of the periodic asymmetric sinusoidal potential.

3.2. Average velocity of Brownian particles

The asymptotic average velocity of the particles, as a function of f, is illustrated in Fig. 7, at fixed mean thermal energy k_BT, for some values of the shape parameter r, namely $r = -0.5$, 0, and 0.5. Qualitatively, the behaviour of particles does not change no matter what the shape parameter r. Thus, in the three cases representing the different values of the shape parameter, the average velocity rises quickly as particles emerge from wells, and settles to its steady state value in time. However, it should be noted that the critical forces inducing transitions depend on the shape parameter r namely, all velocities do not intersect at the same value of the external force. The critical force, which is the force from which the particles cross the potential barriers for the different shape parameter r, are given by $f_c \simeq 0.72$, 0.74 and 0.98, for $r = 0$, 0.5 and -0.5, respectively. So, the more the wells are flat, the critical force is high as it is illustrated in Fig. 8, showing the

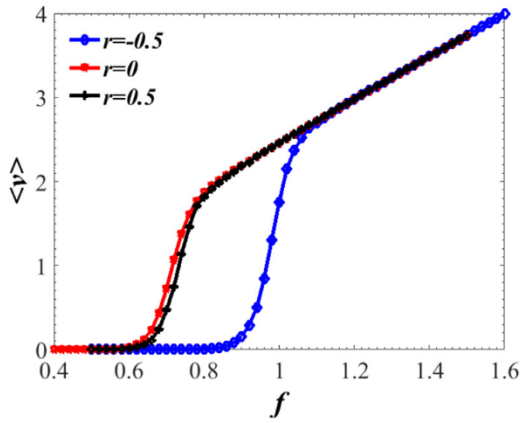

Fig. 7. Average velocity of Brownian particles in deformable potential for some values of the shape parameter: $r = -0.5$, $r = 0$, $r = 0.5$. Other parameter values: $K_BT = 0.094$, $\omega_0 = 1.0$, $\gamma = 0.4$.

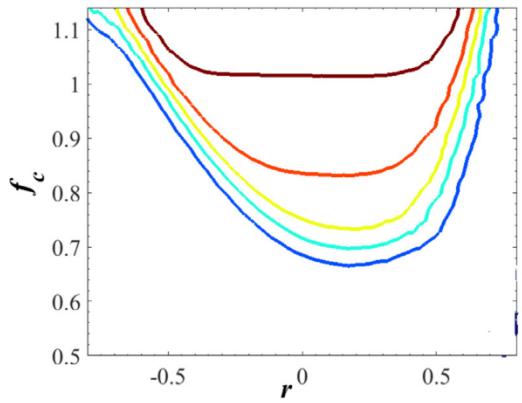

Fig. 8. Contour plot of velocity showing how the force varies vs the shape parameter with the same parameters previously used.

different critical forces as a function of the shape parameter. Indeed, the external force f determines the degree of tilt (asymmetry) of the effective deformable potential $U(x, r)$, and therefore dominates the direction of movement of Brownian particles. The dynamics of the average velocity can be understood also by considering the magnitude of the slope of the potential. Thus, beneath the action of f, the slope of the potential with broad wells and narrow barriers is higher compared to the potential with narrow wells and broad barriers. Therefore, the Broad wells activate the inertia effects, which gives impetus for particles to cross the barrier. The higher average velocities indicate also that the energy of the system grows monotonically as the system deforms away from a specified shape and often includes terms that constrain the smoothness or symmetry of the model.

For a fixed value of the dissipative friction coefficient, we have plotted in Fig. 9 the average velocity of Brownian particles as a function of the shape parameter r for some values of the external force, namely $f = 0.72$, 0.74, and 0.98. Globally, the average velocity of Brownian particles is an increasing function of the negative values of the shape parameter corresponding to the potential with broad wells and narrow barriers, while it is the decreasing function of the positive values of the shape parameter corresponding to the potential with narrow wells and broad barriers for different external forces. In fact, for values 0.72 and 0.74 of the external force, the average velocity of Brownian particles behaves like an exponential law as a function of the shape parameter r. This shows that the average velocity of Brownian particles increases when increasing the shape parameter r, reaches a maximum corresponding to an optimal value of the shape parameter $r_{opt} \simeq 0.2$, and then decreases back to zero at the large values of r corresponding to the shrinking of the potential wells. While for $f = 0.98$, the average velocity of Brownian particles increases until a value of the shape parameter $r \simeq -0.45$ and saturates until a value of the shape parameter $r \sim 0.6$. From this value of the shape parameter, the external force combined to the thermal energy no longer allows the particles to cross the potential barrier. $r_{opt} \simeq 0.2$ is the value of the shape parameter for which the forces 0.72 and 0.74 easily induce a transition, allowing the particles to perform the directional motion towards the right.

When the particles cross the wide potential wells to the narrow potential wells, there is a decrease of the energy of the system due to the radiation at an on-site potential of the lattice associated with the dissipative force. This favours the slow

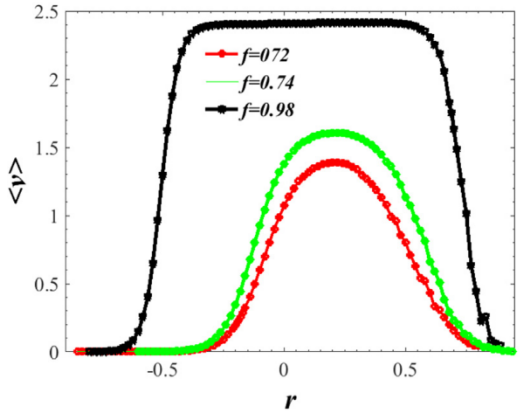

Fig. 9. Average velocity of Brownian particles in the deformable potential as a function of the shape parameter for some values of the external load: $f = 0.72$, $f = 0.74$, $f = 0.98$. Other parameter values: $K_BT = 0.094$, $\omega_0 = 1.0$, $\gamma = 0.4$.

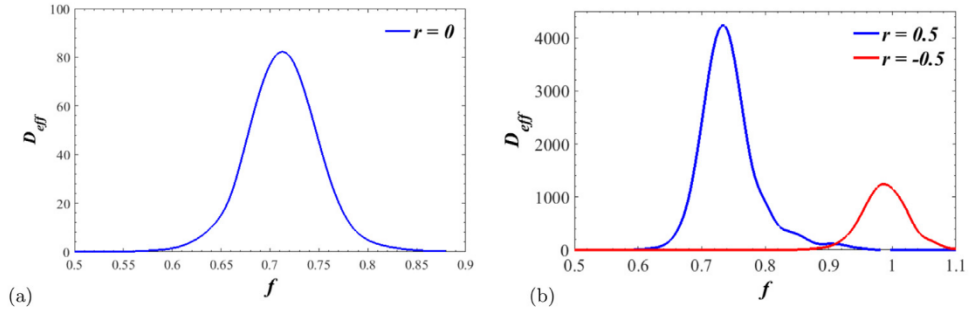

Fig. 10. (a) The effective diffusion coefficient of Brownian particles as a function of the external force for $r = 0$. (b) The effective diffusion coefficient of Brownian particles as a function of the external force for $r = 0.5$ and $r = -0.5$. The effective diffusion coefficient for three values of the shape parameter grows many order of magnitude when the shape of the potential varies. Other parameter values: $K_BT = 0.094$, $\omega_0 = 1.0$, $\gamma = 0.4$.

down of the average velocity of Brownian particles, so that they oscillate at the bottom of the potential wells, which are quite narrow, being damped by the radiation and the friction coefficient. Under such effects, particles require additional thermal energy and/or an increase of the external force which will allow them to jump the potential barrier such as after each jump, the system is allowed to relax before the next jump takes place. The potential with broad wells and narrow barriers facilitates sliding of the Brownian particles, because the particle acquires easily the necessary momentum to cross the potential barrier.

This potential, whose the shape changes, could appear useful for optimization of the directed transport, controlling the motion of Brownian particles in order to improve the conductivity in some artificial devices according to the shape parameter.

3.3. The effective diffusion coefficient of Brownian particles

In Fig. 10, the effective diffusion coefficient of Brownian particles is plotted as a function of the external force for some values of the shape parameter r. In Fig. 10a, the effective diffusion coefficient is plotted for $r = 0$, while in Fig. 10b, the effective diffusion coefficient is plotted for $r = 0.5$ and $r = -0.5$, respectively. Indeed, in the periodic system [4,32–35], the effective diffusion coefficient in the underdamped limit grows several orders of magnitude in a particular domain of the external force f and meanwhile, becomes larger at smaller values of the temperature of the system. This is due to the locked-to-running transition that takes place in the system when the Brownian particle diffuses on a 1D periodic substrate potential and is subject to a macroscopic gradient of the potential and/or temperature. As is shown in Fig. 10 for the three cases of the shape parameter r, the geometry of the system induces an enhancement diffusion, albeit the value of the temperature of the system and the peaks in the effective diffusion coefficient D_{eff} versus the force f which is detectable in the vicinity of the transition force f_c, as a function of the shape parameter r. For $r = 0$, the critical force is given by $f_c = 0.72$, for $r = 0.5$, the critical force is given by $f_c = 0.74$ and for $r = -0.5$, the critical force is given by $f_c = 0.98$. We observe that the value of the external force is higher for the deformable potential with broad wells and narrow barriers compared to the sine-Gordon shape potential ($r = 0$), and the deformable potential with narrow wells and broad barriers. However, the effective diffusion coefficient is rather more pronounced for the deformable potential

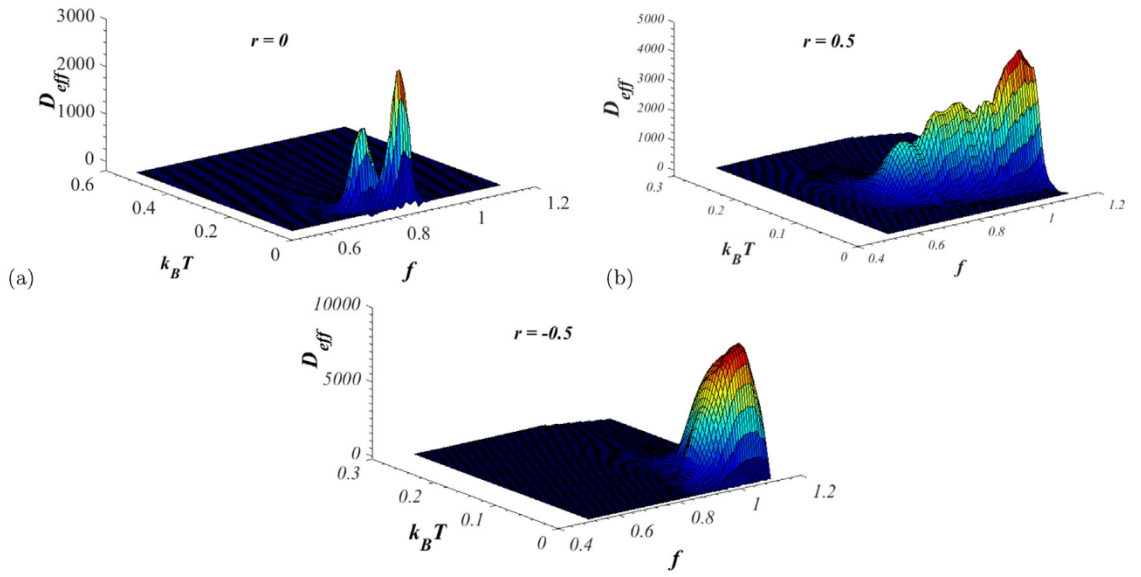

Fig. 11. Three dimensional representation of the effective diffusion coefficient as a function of thermal energy and the external force, for $r = 0, 0.5$ and -0.5. The effective diffusion coefficient decreases with the temperature of the system. Other parameter values: $\omega_0 = 1.0$, $\gamma = 0.4$.

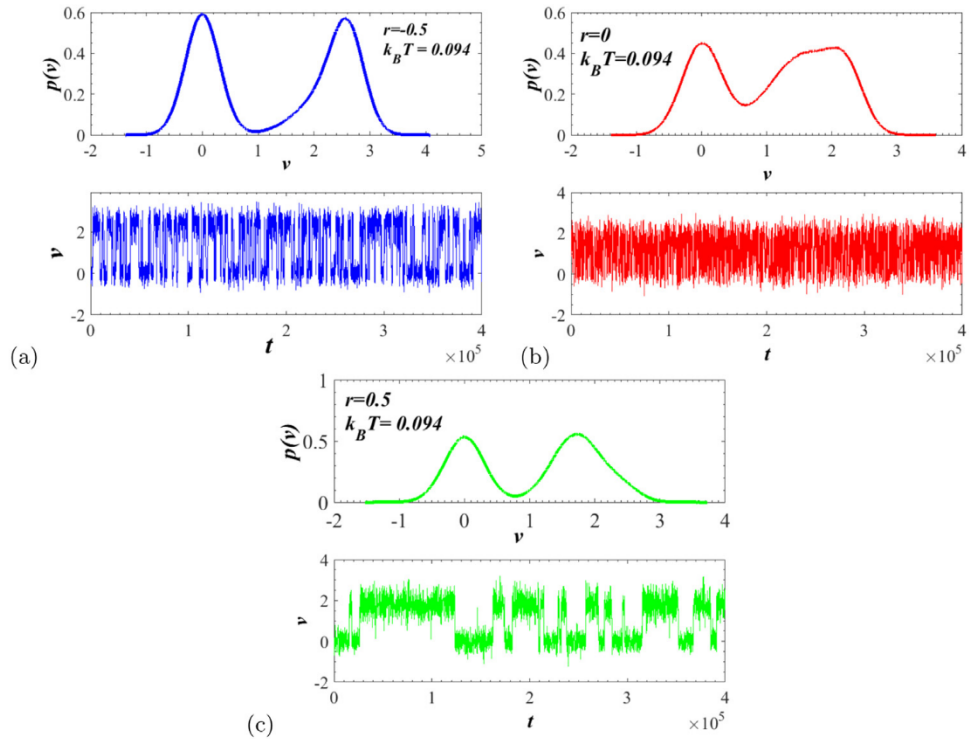

Fig. 12. Plot of the transition of Brownian particles, associated with the different transition distribution in the deformable potential, for three values of the shape parameter r: $r = -0.5$, 0, and 0.5. For $r = -0.5$, $f = 0.98$, for $r = 0$, $f = 0.72$, and for $r = 0.5$, $f = 0.74$. As we can see, for their critical force, there are more transitions between locked and running states for $r = 0$ and $r = -0.5$ than $r = 0.5$. This moderate amount of occurrence of transitions in the case $r = 0.5$ promotes an excess diffusion peak.

with narrow wells and broad barrier compared to the two other cases, i.e. $r = 0$ and $r = -0.5$. For $r = -0.5$, $r = 0$ and $r = 0.5$ the values of the threshold diffusion or the maximum diffusion are given by $D_{th} = 1.2181 \times 10^3$, $D_{th} = 80.4582$, and $D_{th} = 4.154 \times 10^3$, respectively. These threshold values do not occur at the same critical forces. In order to explain

the origin of the excess peak diffusion of $r = 0.5$, we have plotted Fig. 12. In fact, the presence of peak in the effective diffusion results from equiprobability between the locked and running states. In this case, the excess diffusion peak may stem from the number of transitions locked-to-running state. So, the diffusion will be higher if and only if the number of transition between the locked and running states is low, see Fig. 12.

In Fig. 11, the effective diffusion coefficient as a function of the mean thermal energy and the external force is plotted. It is clearly seen that the effective diffusion coefficient decreases and goes to 0 when the temperature of the system increases. Indeed, for $|f| < f_c$, for the three cases of the shape parameter, the effective diffusion coefficient enhances when the temperature $T \to 0$ [4,32–35]. So, the interplay between the shape of the potential and the temperature of the system contributes either to lower or enhance the effective diffusion coefficient according to the shape parameter. Coming back to Fig. 10, for f outside the range $|f| < f_c$, the effective diffusion coefficient decreases to 0 and we single out two cases: (i) the case of strong diffusion indicating the incoherent transport (strongly diffusive); (ii) the case of coherent transport (reliable directed) [1,4,36]. For $r = -0.5$, since the critical force is higher, compared to both other cases, this case exhibits a reliable transport for an enough long-range of the external force. The deformable potential with the narrow wells and broad barrier requires from Brownian particles a large quantity of thermal energy to cross the potential barrier indicating that the thermal energy of the system is quickly dissipated. However, the interaction between the external force, the inertia term and the damping, lead to an enhancement of the effective diffusion.

To fully characterize the role of the shape parameter of the system on the effective diffusion coefficient of Brownian particles, we focus our attention on the dependence of the peak values of the effective diffusion coefficient and the corresponding threshold f_c on the shape parameter. To achieve this, Fig. 13 has been plotted. In Fig. 13a, the maximum effective diffusion coefficient of Brownian particles D_{th}, as a function of the shape parameter r, is plotted, while the corresponding threshold f_c, as a function of the shape parameter r, is presented in Fig. 13b. By looking at Fig. 13a, we remark that in the deformable potential, the threshold values of the effective diffusion as a function of the shape parameter have an almost parabolic behaviour. Thus, we can write

$$D_{th} \propto | r |^{\alpha}, \tag{22}$$

with $\alpha \simeq 2$. For $r > 0$, corresponding to the potential with broad barriers and narrow wells, the maximum effective diffusion coefficient increases. The more the deformable potential wells get shrink, the more the thermal energy of the system dissipates, which reduces the transition leading a giant enhancement diffusion. However, for $r < 0$, the maximum effective diffusion coefficient increases when the potential wells get large, showing that the trays effect also favours the diffusion of Brownian particles. In general, the critical force f_c is a decreasing function of the negative values of the shape parameter, as illustrated in Fig. 13b. For the positive values of the shape parameter r, the critical force is an increasing function of the shape parameter r. This indicates that the increase of the effective diffusion is accompanied of the increase of the critical force. Finally, in Fig. 14, we plot the effective diffusion coefficient as a function of the shape parameter r, for some values of the external force f. We observe that regardless the value of the external force, the effective diffusion coefficient grows for several orders of magnitude for $r > 0$. We also notice that for each value of the external force f, the effective diffusion coefficient grows, and is centred at some specific values of the shape parameter corresponding to the values for which the giant enhancement diffusion occurs. Hence, for $f = 0.72$, $D_{th} = 6.635 \times 10^3$, $r_c \simeq 0.6$, for $f = 0.74$, $D_{th} = 1.3862 \times 10^4$, $r_c \simeq 0.64$. However, for $f = 0.98$, there are two values of the shape parameter r for which the effective diffusion gets its maximums i.e., $r_{c1} = -0.5$ and $r_{c2} = 0.75$. The threshold diffusion for these two values of the shape parameter are given by $D_{th} = 1.2181 \times 10^3$ and $D_{th} = 3.922 \times 10^4$ for $r_{c1} = -0.5$ and $r_{c2} = 0.75$, respectively. $f = 0.98$ represents the critical force for $r = -0.5$ and 0.75. The result obtained in Fig. 14 further agrees with what has been said before, namely the geometry of the system induces a giant enhancement diffusion no matter the temperature of the system.

4. Conclusion

In this work, we have studied the underdamped Brownian motion in a tilted deformable potential represented by a modified RP potential with the shape parameter r, which is obviously more realistic and flexible for possible applications in condensed matter physics and biology, in the presence of white thermal noise source. We have investigated the transport of Brownian particles under the influence of the shape parameter and have shown that it undergoes a qualitative change upon the variation of the shape parameter of the system, in the presence of an external load. Based on the dynamics of the system described by the Fokker–Planck equation, we have numerically computed the effective diffusion coefficient via the dynamic structure factor of the system using the matrix-continued-fraction method. It has been proven that due to the geometry of the system, many new effects occur in the transport process of Brownian particles. Results have also shown that for the positive values of the shape parameter ($r > 0$), representing the deformable potential with narrow wells and broad barriers, the transport of Brownian particles is affected by some radiations coming from the phonon bath associated with the friction of the system, leading to a slow down of Brownian particle motion. This slows down of the motion goes with a difficult jump of Brownian particles from one well to the adjacent ones and requires an extra thermal energy to favour the transport of Brownian particles. However, for $r < 0$, corresponding to the deformable potential with broad wells and narrow barriers, the transport of Brownian particles are optimized. The distribution of the long-time velocity shows that for $r < 0$, there are more running solutions when the mean thermal energy and the

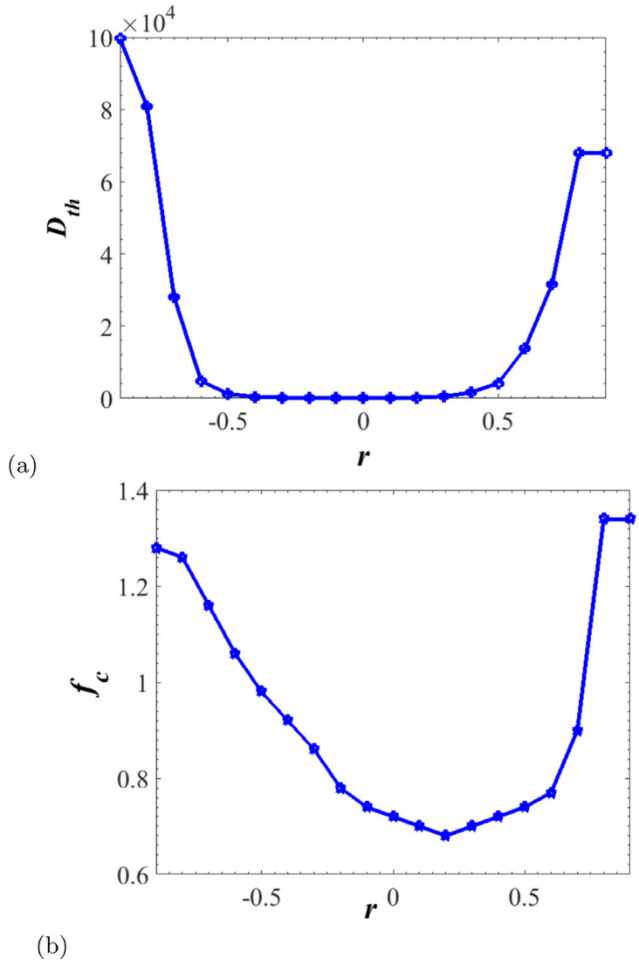

Fig. 13. (a) Maximum values of the effective diffusion coefficient vs the shape parameter r. (b) Critical force of the system as a function of the shape parameter. Other parameter values: $K_BT = 0.094$, $\omega_0 = 1.0$, $\gamma = 0.4$.

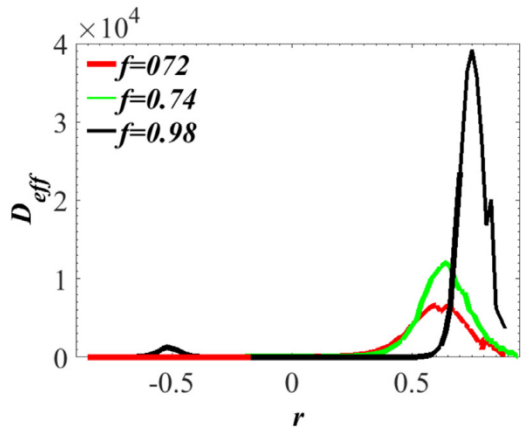

Fig. 14. The effective diffusion coefficient as a function of the shape parameter r for some values of the external force: $f = 0.72$, 0.74 and 0.98. Other parameter values: $K_BT = 0.094$, $\omega_0 = 1.0$, $\gamma = 0.4$.

external force are increased. The general dependence of the diffusion coefficient versus tilting force obeys, as a rule, the typical behaviour found earlier. However, in the present case, the acceleration of diffusion is strongly influenced by the

geometry of the system and is enhanced in a finite range of forces that is also well within the region of bistability of the deterministic velocity dynamics independently from the temperature. For $r > 0$, the diffusion coefficient intensifies and is more pronounced than when $r = 0$ and $r < 0$, stemming from the fact that the transition between locked and running states are reduced in the potential with narrow wells and broad barriers.

Acknowledgements

Thanks to Electronical Journal Delivery Service of the International Centre of Theoretical Physics (ICTP) for providing valuable reference used in this study. CBT acknowledges financial support from BIUST, Botswana under grant DVG/RDI/2/1/16I (25).

References

[1] P. Hänggi, F. Marchesoni, Rev. Modern Phys. 81 (2009).
[2] P. Reimann, Phys. Rep. 361 (2002) 57.
[3] B. Lindner, M. Kostur, L. Schimansky-Geier, Fluctuation Noise Lett. 1 (2001) 1.
[4] B. Lindner, I.M. Sokolov, Phys. Rev. E 93 (2016) 042106.
[5] P. Fulde, L. Pietronero, W.R. Schneider, S. Strässler, Phys. Rev. Lett. 35 (1975) 26.
[6] P. Maass, M. Meyer, A. Bunde, W. Dieterich, Phys. Rev. Lett. 77 (8) (1996).
[7] H. Risken, The Fokker–Planck Equation, Springer, Berlin, 1984.
[8] L. Longobardi, D. Massarotti, G. Rotoli, D. Stornaiuolo, G. Papari, A. Kawakami, G.P. Pepe, A. Barone, F. Tafuri, Phys. Rev. B 84 (2011) 184504.
[9] A. Asaklil, Y. Boughaleb, M. Mazroui, M. Chhib, L. El Arroum, Solid State Ion. 159 (2003) 331–343.
[10] E. Heinsalu, T. Örd, R. Tammelo, Phys. Rev. E 70 (2004) 041104.
[11] Jind-Dong Bao, Yan Zhan, Kun Lü, Phys. Rev. E 74 (2006) 041125.
[12] C. Cattuto, F. Marchesoni, Phys. Rev. Lett. 79 (1997) 5070.
[13] Xingfeng He, Yizhou Zhu, Yifei Mo, Nature Commun. 8 (2017).
[14] W.D. Richards, et al., Nature Commun. 7 (2016).
[15] M. Remoissenet, M. Peyrard, J. Phys. C 14 (1981) L481.
[16] M. Peyrard, M. Remoissenet, Phys. Rev. B 26 (1982) 2886.
[17] M.F. Kepnang Pebeu, R.L. Woulache, T.C. Kofane, Phys. Rev. E 98 (2018) 052107.
[18] R.L. Woulache, F.M. Kepnang Pebeu, T.C. Kofane, Physica A 460 (2016) 326.
[19] Lahcen Arfa, Mehdi Ouahmane, Lahcen El Arroum, Physica A 492 (2017) 781.
[20] C.M. Varma, Phys. Rev. B 14 (1976) 1.
[21] G. Costantini, F. Marchesoni, M. Borromeo, Phys. Rev. E 65 (2002) 051103.
[22] C.J. Reid, Mol. Phys. 49 (1983) 331.
[23] G.T. Evans, J. Chem. Phys. 78 (1983) 4963.
[24] W. Dieterich, I. Perschel, W.R. Schneider, Z. Phys. B 27 (1977) 177.
[25] J.H. Weiner, R.E. Forman, Phys. Rev. B 10 (1977) 315.
[26] Léon Van Hove, Phys. Rev. 95 (1954) 1.
[27] C.T. Chudley, R.J. Elliot, Proc. Phys. Soc. LXXVII 2 (1960).
[28] R. Ferrando, R. Spadacini, G.E. Tommei, G. Caratti, Physica A 195 (1993) 506.
[29] D.E. Knuth, The Art of Computer Programming, Vol. 2, Addison-Wesley, 1969, Reading, MA.
[30] M.S. Suñé, J.M. Sancho, K. Lindenberg, Eur. Phys. J. B 87 (2014) 201.
[31] H.D. Vollmer, H. Risken, Z. Physik B 34 (1979) 313.
[32] B. Lindner, E.M. Nicola, Phys. Rev. Lett. 101 (2008) 190603.
[33] K. Lindenberg, J.M. Sancho, A.M. Lacasta, I.M. Sokolov, Phys. Rev. Lett. 98 (2007) 020602.
[34] G. Costantini, F. Marchesoni, Europhys. Lett. 88 (1999) 491.
[35] P. Reimann, C. Van den Broeck, H. Linke, P. Hänggi, J.M. Rubi, A. Pérez-Madrid, Phys. Rev. Lett. 87 (2001) 1.
[36] B. Lindner, E.M. Nicola, Eur. Phys. J. Spec. Top. 157 (2008) 43.